

**Quantum control of dynamics of quasiparticles in periodic  
and disordered lattice potentials**

by

Ping Xiang

Bachelor of Science, Nankai University, 2007

A THESIS SUBMITTED IN PARTIAL FULFILLMENT  
OF THE REQUIREMENTS FOR THE DEGREE OF

**Doctor of Philosophy**

in

THE FACULTY OF GRADUATE AND POSTDOCTORAL  
STUDIES  
(Chemistry)

The University Of British Columbia  
(Vancouver)

June 2014

© Ping Xiang, 2014

# Abstract

This thesis describes research on controlling the dynamics of quasiparticles in periodic and disordered lattice potentials. Working with model systems of arrays of atoms and molecules trapped in optical lattices, I focus on, but not limited to, the rotational excitons of polar molecules and propose to use external fields to control the binding and propagation of quasiparticles.

First, we study the binding of rotational excitons in a periodic potential. We show that non-linear interactions of such excitons can be controlled by an electric field. The exciton-exciton interactions can be tuned to induce exciton pairing, leading to the formation of biexcitons and three-body bound states of excitons. In addition, we propose a non-optical way to create biexcitons by splitting a high-energy exciton into two low-energy excitons.

Second, we present schemes to control the propagation of a collective excited state in ordered and disordered aggregates of coupled particles. We demonstrate that the dynamics of these excitations can be controlled by applying a transient external potential which modifies the phase of the quantum states of the individual particles. The method is based on an interplay of adiabatic and sudden time scales in the quantum evolution of the many-body states. We show that specific phase transformations can be used to accelerate or decelerate quantum energy transfer and spatially focus delocalized excitations onto different parts of arrays of quantum particles. For the model systems of atoms and molecules trapped in an optical lattice, we consider possible experimental implementations of the proposed technique and study the effect of disorder, due to the presence of impurities, on its fidelity. We further show that the proposed technique can allow control of energy transfer in completely disordered systems.

Finally, in an effort to refine the theoretical tools to study dynamics of quasiparticles, I extend calculations of lattice Green's functions to disordered systems. We develop a generic algorithm that can be easily adapted to systems with long-range interactions and high dimensionalities. As an application of the method, we propose to use the Green's function to study the tunneling of biexciton states through impurities.

# Preface

Part of the material in Chapter 3 was published in the article: P. Xiang, M. Litinskaya and R. V. Krems, *Tunable exciton interactions in optical lattices with polar molecules*, Phys. Rev. A **85**, 061401(R) (2012). The project was identified and designed by Roman Krems, Marina Litinskaya and the author. The author performed all the numerical calculations and derived all the analytical expressions, except the expression for the biexciton wavefunction, which is the work of Marina Litinskaya. Marina Litinskaya also contributed to the numerical calculations in an indirect way by providing analytical results that were used to check the results of numerical computation.

Part of the material in Chapter 4 was published in the paper: P. Xiang, M. Litinskaya, E. A. Shapiro, and R. V. Krems, *Non-adiabatic control of quantum energy transfer in ordered and disordered arrays*, New J. Phys. **15**, 063015 (2013). The project was designed by E. A. Shapiro, M. Litinskaya, R. V. Krems and the author. The idea of phase kicking was initially proposed by E. A. Shapiro and the idea of controlling the group velocity of exciton wavepackets by external fields came from Marina Litinskaya. The author performed all the numerical calculations and analytical derivations, except the derivations in Section 4.3.1 and Section 4.3.3, which are the work of Marina Litinskaya, and the estimates in Section 4.4.1, which was done by Evgeny Shapiro.

Chapter 5 is unpublished work by the author. The project was designed by the author under the guidance of Roman Krems. We are preparing a research publication based on these results.

# Table of Contents

<b>Abstract</b> . . . . .	<b>ii</b>
<b>Preface</b> . . . . .	<b>iv</b>
<b>Table of Contents</b> . . . . .	<b>v</b>
<b>List of Figures</b> . . . . .	<b>viii</b>
<b>Acknowledgments</b> . . . . .	<b>xvi</b>
<b>1 Introduction</b> . . . . .	<b>1</b>
1.1 Implications of ultracold temperatures . . . . .	1
1.2 External field control of ultracold molecules . . . . .	4
1.3 Ultracold polar molecules on optical lattices . . . . .	5
1.4 Thesis outline . . . . .	8
<b>2 Background material</b> . . . . .	<b>11</b>
2.1 Review of angular momentum theory . . . . .	11
2.1.1 Symmetry groups . . . . .	11
2.1.2 Rotation operators and spherical harmonics . . . . .	12
2.1.3 Rotation matrices . . . . .	17
2.1.4 Properties of rotation matrices . . . . .	19
2.1.5 Coupling of angular momenta . . . . .	21
2.1.6 Clebsch-Gordan series . . . . .	24
2.1.7 Spherical tensor operators . . . . .	26

2.1.8	Coupling of spherical tensors . . . . .	30
2.1.9	Matrix elements of tensor operators . . . . .	32
2.2	Application of angular momentum theory . . . . .	35
2.2.1	Diatomc molecule in external field . . . . .	35
2.2.2	Dipole-dipole interaction . . . . .	37
2.3	Introduction to excitons in molecular crystals . . . . .	43
2.3.1	Commutation relation . . . . .	44
2.3.2	Exciton Hamiltonian in second quantization . . . . .	48
2.3.3	Eigenstates of the exciton Hamiltonian in the Heitler-London approximation . . . . .	51
<b>3</b>	<b>Tunable exciton interactions in optical lattices with polar molecules</b>	<b>56</b>
3.1	Introduction . . . . .	56
3.2	Exciton-exciton interactions in an optical lattice . . . . .	58
3.3	Biexcitons . . . . .	60
3.3.1	Method to calculate biexciton energies . . . . .	60
3.3.2	Analytical derivation of the biexciton wavefunction . . . . .	68
3.3.3	Properties of biexciton states . . . . .	76
3.4	Non-optical creation of biexcitons . . . . .	79
3.5	Extension to exciton trimers . . . . .	84
3.6	Discussion . . . . .	88
<b>4</b>	<b>Quantum energy transfer in ordered and disordered arrays</b>	<b>90</b>
4.1	Introduction . . . . .	90
4.2	Sudden phase transformation . . . . .	93
4.2.1	Group velocity of wave packet . . . . .	94
4.2.2	Phase kicking in quasimomentum space . . . . .	96
4.3	Focusing of a delocalized excitation . . . . .	101
4.3.1	Focusing to a single site . . . . .	102
4.3.2	Focusing a broad wavepacket in coordinate space . . . . .	104
4.3.3	Focusing a plane wave in coordinate space . . . . .	108
4.3.4	Numerical results . . . . .	110
4.4	Experimental feasibility of phase transformation . . . . .	113

4.4.1	Suppressing spontaneous emission in system of ultracold atoms . . . . .	113
4.4.2	Phase kicking of collective excitation in arrays of ultracold molecules . . . . .	115
4.4.3	Focusing in system of ultracold molecules . . . . .	120
4.5	Control of energy transfer in dipolar systems . . . . .	123
4.5.1	The effect of long-range interaction . . . . .	124
4.5.2	Anisotropy of dipolar interaction . . . . .	125
4.5.3	Computation details . . . . .	127
4.6	Energy transfer in the presence of vacancies . . . . .	137
4.7	Focusing in the presence of strong disorder . . . . .	139
4.8	Conclusion . . . . .	145
<b>5</b>	<b>Green's function for two particles on a lattice . . . . .</b>	<b>148</b>
5.1	Introduction . . . . .	148
5.2	Equation of motion for Green's function . . . . .	149
5.3	Recursive calculation of Green's function . . . . .	152
5.3.1	With the nearest neighbor approximation . . . . .	152
5.3.2	Extension to long-range interactions . . . . .	157
5.3.3	Extension to high-dimensional systems . . . . .	161
5.3.4	Comparison with other methods . . . . .	162
5.4	Application to the problem of biexciton scattering . . . . .	166
5.5	Summary . . . . .	171
<b>6</b>	<b>Conclusion . . . . .</b>	<b>173</b>
6.1	Summary of the thesis . . . . .	173
6.2	Limitations and possible extension . . . . .	175
6.3	Future research directions . . . . .	177
6.3.1	Influence of exciton-exciton interaction on polariton lasing	177
6.3.2	Parallel computation of Green's functions . . . . .	179
<b>Bibliography . . . . .</b>		<b>183</b>

# List of Figures

Figure 3.1	(a) The parameters $D$ and $J$ (in units of $V_{dd} = d^2/a^3$ ) as functions of the electric field strength. (b) The ratio $D/J$ as a function of the electric field strength. The field is perpendicular to the intermolecular axis. For LiCs molecules possessing the dipole moment $d=5.529$ Debye, the value $\mathcal{E}_f d/B_e = 1$ corresponds to $\mathcal{E}_f = 2.12$ kV/cm. (c) Schematic depiction of the angle $\theta$ between the field (represented by blue arrows) and the molecular array (represented by red dots). (d) $D$ and $J$ for a 1D array of LiCs molecules separated by 400 nm as functions of $\theta$ for $\mathcal{E}_f = 6$ kV/cm. . . . .	77
Figure 3.2	(a) and (b): Two-excitation spectra of a 1D array of LiCs molecules on an optical lattice: NNA (dashed lines) and exact solutions (solid lines). The shaded regions encapsulate the bands of the continuum two-exciton states. (c) $\theta$ -dependence of the biexciton binding energy $\Delta$ . The electric field magnitude is 6.88 kV/cm, $\theta_0 = \arccos \sqrt{2/3}$ , $\theta^* = \arccos \sqrt{1/3}$ . (d) Biexciton wave function vs the lattice site separation $ r  =  n - m $ of the two excitations for $K = 0$ . Inset: Mean width of the biexciton wave function $\langle r \rangle$ calculated as the width of $\psi_K^2(r)$ at half maximum. Numbers on each curve indicate the value of $D/2J$ . . . . .	78
Figure 3.3	The rotational energies of a closed-shell polar molecule as a function of the strength of a DC field. The dashed lines represent other rotational states with $M_N \neq 0$ . . . . .	81

Figure 3.4	Population dynamics for the transition from $ g\rangle \rightarrow  f\rangle$ exciton (middle panel) and from an $f$ state localized on a single molecule (lower panel) to coherent $ g\rangle \rightarrow  e\rangle$ excitons and biexcitons. The green dashed curves denote the population accumulated in the pairs of non-bound $ g\rangle \rightarrow  e\rangle$ exciton states, the red solid curves the biexciton state and the blue dot-dashed curves the $f$ state. The shaded region in the upper panel encapsulates the band of the continuum two-exciton states. The calculation is for a 1D ensemble of $N_{mol} = 501$ LiCs molecules on an optical lattice with lattice separation $a = 400$ nm. The electric field of magnitude 6.88 kV/cm is perpendicular to the molecular array. . . . .	83
Figure 3.5	Three-excitation spectra of a 1D array of molecules on an optical lattice. The calculation is done for a system of 20 lattice sites with the hopping interaction $J = 10$ kHz and the dynamic interaction $D = 30$ kHz. The black dots represent energies of all three-exciton states, the red curves denote the boundaries of energy continuum of three free excitons, and the blue curves represent the boundaries of energy continuum for a biexciton plus a free exciton. . . . .	88
Figure 4.1	The dispersion curve of an exciton. The interaction between site $m$ and site $n$ is proportional to $1/ n - m ^3$ . . . . .	96

Figure 4.2 Example of controlled energy transfer in a one-dimensional array of quantum monomers subjected to a linear phase transformation. The graph illustrates the evolution of the exciton wave packet centered at  $k = 0$  and initially positioned at the center of the array. The phase of the wave function is shown by color. The brightness of color corresponds to the amplitude of the excitation with white color corresponding to zero amplitude. The calculation is for a one-dimensional array of 201 monomers with  $\alpha = 22.83$  kHz and  $\Delta E_{e-g} = 12.14$  GHz, and the linear phase transformation  $\Phi_n \simeq \Phi_0 - 1.29n$ . The corresponding experimental setup is illustrated in Fig. 4.6 . . . . . 99

Figure 4.3 “Bloch oscillation” of the exciton wave packet in the momentum and coordinate spaces. The phase of the wave function is shown by color as in Fig. 4.2. A low laser intensity of  $10^6$  W/cm<sup>2</sup> is used and all other parameters are the same as in Fig. 4.2. Part (a) shows that the wave packet moves in  $k$  space in response to the linear laser field. However, since the wave vector is limited in the first Brillouin zone, when the wave packet reaches  $-\pi$  or  $\pi$ , it disappears at the boundary and reappears at the other boundary. Part (b) presents the motion of the wave packet in coordinate space in accordance with the phase kicking in  $k$  space. Note that the wave packet spreads in both the momentum and coordinate spaces because the laser intensity profile along the molecular array is not perfect and this is amplified over an extended time period. . . . . . 100

Figure 4.4	Focusing of a completely delocalized collective excitation (panels a and b) and a broad Gaussian wave packet of Frenkel excitons (panels c and d) in a one-dimensional array using the quadratic phase transformations at $t = 0$ as described in Section 4.3.2 and Section 4.3.3. In panels (b) and (d), the excitation probability distribution is displayed by color. The dashed lines show the initial distribution magnified by 20 and 5 respectively in (a) and (c). The solid curves in panels (a) and (c) correspond to two different phase transformations focusing the same wave packet onto different parts of the array. The calculations are performed with the same parameters $\alpha$ , $a$ , and $\Delta E_{e-g}$ as in Fig. 4.2. The results are computed with all couplings accounted for. . . . .	111
Figure 4.5	Focusing of a delocalized excitation in a 2D array shown at $t = 0$ in panel (a) onto different parts of the lattice (panels b–d). For better visualization, the probability distribution in panel (a) is magnified by a factor of 60. The calculations are performed with the same parameters $\alpha$ , $a$ , and $\Delta E_{e-g}$ as in Fig. 4.2 and the quadratic phase transformation at $t = 0$ . . . . .	112
Figure 4.6	The experimental setup for the calculation corresponding to Fig. 4.2. A 1D array of LiCs molecules trapped on an optical lattice with lattice constant $a = 400$ nm is subjected to a homogeneous DC field of 1 kV/cm directed perpendicular to the intermolecular axis. The kicking potential leading to the phase transformation presented by Eq. (4.54) can be provided by a $\lambda = 1064$ nm Gaussian laser beam that is linearly polarized in the direction of the DC field, with the propagation direction along the array axis, focused to a radius of 5 $\mu\text{m}$ , with the intensity at the focus equal to $10^7 \text{ W/cm}^2$ . The laser pulse is on between 0 and 3 $\mu\text{s}$ . . . . .	118

Figure 4.7 An illustration to show the orientations of 1D and 2D molecular arrays inside the Gaussian beam. (a) the 1D lattice lies along the $x$ -axis of the $z = 0$ plane and the DC field is at some angle with the $x$ -axis such that the coupling $\alpha$ between molecules is negative. (b) the 2D square lattice is at the center of the $z = 0$ plane and the DC field is at $45^\circ$ degree with the $x$ -axis. In both cases, the laser is linearly polarized along the direction of the DC field. . . . .	120
Figure 4.8 Control of excitation transfer in a 1D many-body system with dipolar interactions by varying the direction of an external electric field. (a) Exciton dispersion curves for a 1D ensemble of diatomic molecules on an optical lattice for different angles $\theta$ between the direction of the external DC electric field and the axis of the molecular array. In 1D, the coupling $\alpha \propto (1/3 - \cos^2 \theta)$ . (b) Propagation of a wave packet centered at $ak = -\pi/3$ controlled by tuning the electric field direction. The thin dotted line depicts the corresponding angle variations with time. The brightness of the color corresponds to the probability of the excitation. . . . .	126
Figure 4.9 Control of excitation transfer in a 2D many-body system with dipolar interactions by varying the direction of an external electric field. Panels (a) and (b) show the trajectories of the center of an exciton wave packet in a 2D lattice during the time from 0 to 3 ms; Panels (c) and (d) represent the changing of the dressing DC field orientation ( $\theta, \phi$ ) associated with (a) and (b) respectively. The initial wave packet is a 2D Gaussian distribution centered around $ak_x = ak_y = \pi/2$ and has a width of $\sim 60$ lattice sites in coordinate space. The magnitude of the DC field is fixed to 6 kV/cm while its direction is changing. The calculations are done for a 2D array of LiCs molecules in a lattice with $a = 400$ nm. . . . .	128

Figure 4.10 The orientations of the DC field and molecular arrays in the coordinate systems. (a) The DC field is along the $z$ -axis and the 1D molecular array is in the direction represented by $\theta_R$ and $\phi_R$ . (b) The 2D molecular array is on the $XY$ plane and the orientation of the DC field is represented by $(\theta, \phi)$ . For clarity, we have only drawn the molecules (as blue dots) along a particular axis which is at angle $\gamma$ with respect to the $X$ -axis. It is to be understood that there are also other intermolecular axes at different angles with the $X$ -axis. Note part (a) and part (b) have different coordinate systems and the meaning of $(\theta_R, \phi_R)$ is different from that of $(\theta, \phi)$ . In fact, the angle $\theta_R$ between the DC field and the molecular array in (b) is related to $\theta$ and $\phi$ by $\cos \theta_R = \cos \theta \cos(\phi - \gamma)$ .	130
Figure 4.11 Enhancement factors $\eta$ (red symbols) and $\chi$ (blue symbols) as functions of vacancy percentage in a 2D lattices. See text for the definitions of $\eta$ and $\chi$ . The error bars are for 95% of confidence interval.	138
Figure 4.12 Time snapshots of a collective excitation in a 2D array with a vacancy concentration of 10 % (a) The distribution of the vacant sites; (b) The initial probability distribution of the excited state; (c) The probability distribution of the excitation at the focusing time when the focusing scheme is applied. The focusing time is found numerically as the time when the probability at the target molecule (71, 71) reaches maximum for a given phase transformation. (d) The probability distribution of the wave function at the focusing time when the focusing scheme is not applied. The calculations are performed with the same parameters as in Fig. 4.5. The probabilities in (b) and (d) are magnified by 16 and 6, respectively.	140

- Figure 4.13 Focusing of a collective excitation in a strongly disordered system with 60% of lattice sites unoccupied. Panel (a) shows different phases applied to different blocks of the lattice before the time evolution. (b) The initial probability distribution of the excited state. (c) The probability distribution of the excited state at the focusing time  $T = 3$  ms with the phase transformation depicted in panel (a) before the time evolution. (d) The probability distribution of the excited state at the focusing time  $T = 3$  ms with no phase transformation applied. The calculations are performed with the same parameters as in Fig. 4.5. The probabilities in (b) and (d) are magnified by 60 and 5, respectively. . . . . 143
- Figure 4.14 Efficiency of focusing collective excitations in strongly disordered 2D lattices. The molecular array is divided into 400 blocks as shown in Fig.4.13(a). The focusing time  $t_*$  is arbitrarily set to 4 ms. For each realization of disorder, we use Eq.(4.99) with  $T = t_*$  to find the phase mask applied to different blocks. Shown are the enhancement factors  $\eta$  (red symbols) defined in Eq.(4.90), as a function of the vacancy percentage. The error bars are for 95% confidence interval. . . . . 144
- Figure 5.1 Green's function  $G(10, 71, 50, 51, E + i\eta)$  with  $\eta = 0.1$  as a function of energy  $E$ . The calculation was done for a finite ordered 1D crystal of 101 lattice sites with the nearest-neighbor approximation. The energies of the particles  $e_n$  were set to zero, and the dynamic interaction and the hopping interaction were set to 5. The upper panel shows the real part of the Green's function and the lower panel shows the imaginary part. The results calculated by the brute-force method are marked with empty circles while the results obtained by our recursive method are marked by "X". This figure clearly demonstrates that the recursive method produces the same results as the brute-force method. . . . . 164



# Acknowledgments

First of all, I would like to thank my supervisor, Prof. Roman Krems for accepting me into his group and giving me helpful guidance throughout my PhD study. Also I want to thank Prof. Yan Alexander Wang, Prof. Mark Thachuk and Prof. Gren Patey for their help during my time in Vancouver.

I truly appreciate fruitful discussions and collaborations with Marina Litinskaya, Evgeny Shapiro and Felipe Herrera. In addition, I want to thank Yu Zhang, Yakun Chen and Zhiying Li for their useful advice on life and career.

Especially, I am grateful to my wife for her love, support and encouragement. She brings a lot of happiness to my life and I am very lucky to have such a lovely and smart life partner. And last but not least, I thank my father for inspiring my interest in science since my childhood, and my mother for being supportive all these years. I owe too much to my parents for their everlasting love and support.

*To my parents and my wife.*

# Chapter 1

## Introduction

This thesis is a theoretical study on controlling the quantum dynamics of quasiparticles in periodic and disordered lattice potentials. Although some work presented in the thesis is quite general and can be applied to any system with a periodic or disordered lattice potential, the main systems considered here are ultracold atoms and molecules, as their experimental manipulation is relatively easy. The control schemes proposed in the thesis are also related closely to recent developments in the laser cooling and trapping of atoms and molecules. Therefore, to give the reader a broad context in which to understand the thesis, this chapter presents an introductory overview of the field of ultracold atoms and molecules. In Section 1.1, I briefly introduce ultracold atoms and molecules and discuss the unique features of ultracold ensembles. After that, in Section 1.2, I discuss the controllability of ultracold molecules. In Section 1.3, I introduce a particular ultracold system with polar molecules trapped on optical lattices. Finally, I outline the research presented in the thesis in Section 1.4.

### 1.1 Implications of ultracold temperatures

Cooling gaseous ensembles of atoms and molecules to extremely low temperatures has revolutionized the field of atomic, molecular and optical physics. The development of experimental techniques for cooling atoms to ultracold temperatures has led to many ground-breaking applications[1, 2], including the fundamental studies

of Bose–Einstein condensation of weakly interacting particles[3], nonlinear and quantum atom optics[4], collisions at ultracold temperatures[5], the development of all-optical atomic clock[6], and quantum information processing with atoms and photons[7]. Inspired by this success with ultracold atoms, researchers are now aiming to extend the experimental methods to cooling molecules. The experimental work with ultracold molecules is likewise expected to have a great impact on different areas of science and technology, which is covered by numerous review articles[8–17]. By convention, a distinction is made between two ranges of temperature  $T$ : cold  $1 \text{ mK} < T < 1 \text{ K}$ , and ultracold  $T < 1 \text{ mK}$ . At ultracold temperatures, the translational motion of particles has a velocity that can be as low as a few cm/s, in sharp contrast with the speed of a few hundred m/s at room temperatures. The small kinetic energies associated with the ultra-slow translational motion have some important consequences, summarized below.

First, ultracold temperatures allow for novel macroscopic quantum states of matter. A particle in the gaseous phase behaves as a quantum-mechanical wavepacket with the extension on the order of its de Broglie wavelength, given by

$$\Lambda = \frac{\hbar}{mv} . \quad (1.1)$$

For the ultra-slow velocity  $v$  at ultracold temperatures, the corresponding de Broglie wavelength is larger than at room temperatures by several orders of magnitude, and is comparable to or larger than the mean distance between particles in the gas phase. Under these conditions, the particles in a gaseous ensemble become indistinguishable and their wavefunctions overlap heavily, leading to the formation of a macroscopic coherent matter wave, that is, a Bose-Einstein condensate[3, 18] for bosonic particles in which all particles occupy the lowest quantum state, and a quantum degenerate Fermi gas[19, 20] for fermionic particles of same kind in which every accessible energy level is occupied by exactly one particle due to the Pauli exclusion principle.

Second, ultracold temperatures lead to new collision phenomena. Because of the large de Broglie wavelengths of ultracold particles, their low-energy collision is qualitatively different from the collision at thermal temperatures. At ultracold temperatures, particles do not have well-defined trajectories in phase space, the

spherical harmonics  $Y_{lm}(\theta, \phi)$ , also called partial waves with  $l = 0, 1, 2, \dots$  that represent the angular momenta of the rotational motion of the collision complex, are commonly used to describe the collisions. In the absence of external fields, as  $T \rightarrow 0$ , the quantum threshold regime is reached and only the lowest allowed partial wave contributes to the collision[21, 22]. For collisions between reactive particles at ultracold temperatures, the quantum phenomena are even more dramatic. As the kinetic energy is so small, the tunneling under reaction barriers becomes the dominant mechanism of chemical reactions, giving temperature-independent reaction rate constants that can be very large at zero Kelvin[23–26]. Moreover, quantum statistics governs reactive collisions at ultracold temperatures. For example, depending on whether the colliding molecules are in the same internal quantum state, the collisions can be dominated by *s*-wave collisions or *s*-wave and *p*-wave collisions, giving very different reaction rates[27].

Third, ultracold temperatures enable numerous control possibilities. It has been a long-sought goal to control atomic and molecular dynamics by utilizing their interactions with external fields. However, at normal temperatures, the thermal motion of atoms and molecules randomizes their encounters and diminishes the effect of external fields. As the temperature approaches a few  $\mu\text{K}$ , the kinetic energy of ultracold molecules becomes so small that it is even less than the energy splittings of hyperfine structures of molecules. In this case, an external field of moderate strength can produce a perturbation in energy that is larger than the translational energy of molecules, creating dramatic changes in the collisions properties of molecules[22]. Normally, ultracold particles are obtained by first cooling them to cold temperatures and then loading them into a trap for further evaporative cooling[28]. This inspired the development of a variety of traps, such as electrostatic traps[29], AC electric traps[30], optical and microwave traps[31, 32], and magnetic and magneto-optical traps[33–35]. Within the traps, the thermal motion of particles is restricted, so their interaction with external fields can be more precisely controlled. This leads to unprecedented precision of spectroscopic measurement because of the much longer interrogation time[36–38]. Because the shapes of the traps can be changed, the trapped ultracold atoms and molecules can be confined in restricted geometries. This may be used for quantum simulations of fundamental many-body systems[17] and various setups for quantum computing[39–45].

## 1.2 External field control of ultracold molecules

Perhaps the most important feature of ultracold atoms and molecules is their controllability via interactions with external fields. Since the corresponding research field is so vast, as reviewed by Ref.[46], we limit the discussion to ultracold molecules as they are more relevant for our research. Compared with atoms, molecules have additional vibrational and rotational degrees of freedom, which leads to rich control possibilities. In the following, I briefly outline the possibilities from the aspect of single molecule and from the aspect of intermolecular interaction separately.

First of all, the internal states of ultracold molecules can be selected by their interaction with external fields. This is very important because it enables the production of a near quantum degenerate gas of molecules in their rovibronic ground state[47, 48], which provides a basis for other research that requires a supply of ultracold molecules. Recently, it has been demonstrated that a rovibronic ground-state molecular quantum gas can be prepared in a single hyperfine state or in an arbitrary coherent superposition of hyperfine states[27] by using a two-photon microwave transition in the presence of a magnetic field. This control over hyperfine structures, together with the manipulation of electronic, vibrational, and rotational states, provides the full control over all internal degrees of freedom of molecules. As quantum information can be encoded into the internal states of molecules, the ability to manipulate the internal states constitutes the basis of quantum computation. For instance, as presented in Ref.[49], universal quantum gates can be implemented using the hyperfine levels of ultracold heteronuclear polar molecules in their electronic, vibrational, and rotational ground state. These high-fidelity logic gates, driven by microwave pulses between hyperfine states, offer versatile encoding possibilities as a consequence of the richness of the energy structures and the state mixing of molecules in external fields. The precise control of internal states also facilitates quantum simulation of many-body systems using ultracold molecules. For example, it has been shown that hyperfine structures of polar molecules in an one-dimensional lattice can be controllably accessed and manipulated as a resource for generating complex quantum dynamics [50].

Moreover, the permanent electric dipole moment of polar molecules enables the tuning of long-range intermolecular interactions. The electric dipole moment

describes the separation of positive and negative electrical charges in a molecule and is given by

$$\boldsymbol{\mu} = \sum_n q_n \mathbf{r}_n , \quad (1.2)$$

where  $\mathbf{r}_n$  gives the positions of charges  $q_n$  and the sum is over all charges in the molecule including the electrons and nuclei. For molecules in a particular electronic and vibrational state, it is convenient to define the dipole operator as  $\mathbf{d} = \langle \psi | \boldsymbol{\mu} | \psi \rangle$  by integrating over the electronic and vibrational wavefunction  $\psi$ . The dipole moment operator only couples states with different parity. Take a simple  ${}^1\Sigma$  molecule for example, its rotational eigenstate  $|J, M\rangle$  has a well-defined parity determined by the angular momentum quantum number  $J$  in the following way:

$$P|J, M\rangle = (-1)^J |J, M\rangle , \quad (1.3)$$

where  $P$  is the parity operator. It follows that molecules in a rotational eigenstate have no net dipole moment as  $\langle J, M | \mathbf{d} | J, M \rangle = 0$  in the laboratory frame. If molecules are prepared in their electronic, vibrational and rotational ground state, they possess no net dipole moment and interact at large intermolecular distances via a van der Waals attraction which falls off as  $\frac{1}{r^6}$  with respect to the interparticle separation  $r$ . With the application of electric fields that mix rotational states of different parity, static or oscillating dipoles are induced in molecules, leading to nonzero interaction – dipole-dipole interaction, which falls off as  $\frac{1}{r^3}$  and dominates over the van der Waals interaction at long range. The dipole-dipole interaction can be modified by external fields to change the strength and shape of the interaction potential between polar molecules[44, 51]. This tunability, combined with the anisotropy characteristic of the dipole-dipole interaction, has inspired a large body of research on the condensed matter theory of dipolar quantum gases[17, 52–54].

### 1.3 Ultracold polar molecules on optical lattices

In the past few years, our group has been interested in ensembles of ultracold polar molecules trapped on optical lattices. Optical lattices are periodic potentials formed by the standing wave patterns of laser beams[55, 56]. The simplest optical lattice is an one-dimensional lattice created by superimposing two counter-

propagating laser beams with the same frequency, intensity and polarization. If the two laser beams propagate in the  $+z$  and  $-z$  directions respectively, the resulting total electric field is given by

$$\begin{aligned}\mathbf{E}(z,t) &= E_0 \cos(kz - \omega t) \hat{\mathbf{e}} + E_0 \cos(-kz - \omega t) \hat{\mathbf{e}} \\ &= 2E_0 \cos(\omega t) \cos(kz) \hat{\mathbf{e}},\end{aligned}\quad (1.4)$$

where  $\hat{\mathbf{e}}$  is the polarization vector. This oscillating electric field induces an oscillating dipole moment in a particle and at the same time interacts with the dipole moment, creating a time-averaged periodic potential  $V(z) \propto E_0^2 \cos^2(kz)$  whose troughs can be used as microtraps in the  $z$  direction. The depth of those microtraps is proportional to the light intensity and their effective sizes can be as small as several tens of nm. If the two laser beams are Gaussian beams, their Gaussian intensity profiles in the  $xy$  plane will provide an additional weak radial confinement potential. This can be combined with the periodic standing wave pattern to form an one-dimensional array of disk-like trapping potentials. Optical lattices with higher dimensions can be created by using additional pairs of laser beams. For example, adding a pair of counter-propagating laser beams along the  $x$  direction to the current one-dimensional lattice can produce a two-dimensional array of traps, each of which looks like a tube in the  $y$  direction. These tube-like potentials can be broken into small segments along the  $y$  direction by adding a third pair of laser beams in that direction. This leads to a three-dimensional periodic potential. In addition to dimensionality, the geometry of optical lattices can also be changed by adjusting the angles between different pair of laser beams. For instance, if three pairs of laser beams are arranged in the  $xy$  plane with an angle  $2\pi/3$  with respect to each other and they are all polarized along the  $z$  direction, the resulting lattice potential  $V(x,y) \propto 3 + 4 \cos(3kx/2) \cos(\sqrt{3}ky/2) + 2 \cos(\sqrt{3}ky)$  is a triangular lattice in two dimensions. Apart from dimensionality and geometry, the trap depths and the lattice separations of optical lattices can also be controlled by changing the laser intensities and wavelengths. This kind of flexibility doesn't exist in natural solid state crystals. Moreover, compared with natural solid state crystals with the lattice constants on the order of a few angstroms, optical lattices have much larger lattice site separations on the order of an optical wavelength (micron), which open

the possibility to address individual sites in optical lattices[57, 58]. Due to all the above features, optical lattices with polar molecules trapped inside, provide a very versatile platform for studying controllable many-body phenomena[17] and for implementing new schemes of quantum computing[59–61].

The low-energy physics of particles trapped in an optical lattice can be described by the Hubbard Hamiltonian

$$H = - \sum_{i,j,\sigma} J_{ij}^\sigma b_{i,\sigma}^\dagger b_{j,\sigma} + \sum_{i,j,\sigma,\sigma'} \frac{U_{ij}^{\sigma\sigma'}}{2} b_{i,\sigma}^\dagger b_{i,\sigma} b_{j,\sigma'}^\dagger b_{j,\sigma'} , \quad (1.5)$$

where  $b_{i,\sigma}^\dagger$  ( $b_{i,\sigma}$ ) are the creation (annihilation) operators for a particle at site  $i$  in the internal state  $\sigma$ ,  $J_{ij}^\sigma$  describes the hopping of a particle from site  $j$  to site  $i$ , and  $U_{ij}^{\sigma\sigma'}$  is the onsite ( $i = j$ ) or offsite ( $i \neq j$ ) interaction between the particle at site  $i$  in state  $\sigma$  and the particle at site  $j$  in state  $\sigma'$ . By tuning the trap depth, the ratio between  $J$  and  $U$  can be controlled. When the particle number is commensurate with the number of lattice sites and the trap depth is deep enough such that  $J \ll U$ , a phase transition from a superfluid phase or a Fermi liquid to a Mott insulator can be observed[62–66]. In the Mott insulator phase, the tunneling of particles between sites is suppressed and the number of particles at a site is an integer value. For the system that our group is interested – ensembles of polar molecules trapped on optical lattices, a lot of effort has been devoted to exploring exotic quantum phases (see Ref.[17] and the references therein) because of the long-range and anisotropic character of the dipole-dipole interaction between trapped polar molecules. In those studies, many novel phase diagrams, associated with different rates of particle tunneling and various types of interparticle interactions, have been discovered.

We instead focus on the Mott insulator phase and explore the tunability of the system of ultracold molecules in the context of collective excitations. The form of the relevant Hamiltonian is still the same as Eq. (1.5), but the creation and annihilation operators are defined with respect to the quasiparticles – the molecular excitations rather than the real particles. So  $J$  now describes the propagation of the excitation energy in the crystal and  $U$  represents the interaction between two or more molecular excitations. This is a new line of research which may be ex-

ploited to study collective excitations in new interaction regimes. For example, previous work by our group members has demonstrated that the artificial crystals of polar molecules in the Mott insulator phase can be used to investigate controllable exciton-impurity interactions[67], to control collective spin excitations[68], to engineer open quantum systems with tunable coupling to the bath[69], and to study new polaron models[70].

## 1.4 Thesis outline

The current thesis extends the work on collective excitations in several new directions. Here is the overview for the whole thesis.

Chapter 2 introduces the background material that can help the reader to understand the thesis. I first give a review of angular momentum theory, and then apply the theory to obtain the rotational levels of a diatomic molecule in external fields and to calculate the dipole-dipole interaction. After that, I present a brief introduction to the exciton theory. More specifically, I explain the commutation relations for excitons, derive the exciton Hamiltonian in second quantization, and introduce the Heitler-London approximation.

Chapter 3 investigates the interactions between multiple collective excitations, and in particular the binding mechanism of these excitations. We study a particular kind of quasiparticles – rotational Frenkel excitons in a periodic lattice potential. These quasiparticles are the collective excitonic modes of polar molecules trapped on an optical lattice in the Mott insulator phase, and are induced by the dipole-dipole interaction which couples the rotational states of different molecules. We show that the application of a moderate electric field, through mixing rotational states of different parity, can give rise to a non-linear dynamic interaction  $D$  between the rotational excitons. The dynamic interaction is always attractive and its strength can be tuned by the external DC field. This leads to controllable formation of biexciton states with tunable binding energy, as demonstrated numerically for a 1D array of LiCs molecules on an optical lattice. We also obtain the two-excitation spectra of the rotational excitons and derive analytical expressions for the wavefunction of biexciton states using the nearest-neighbor approximation. In an effort to extend the theoretical model of exciton binding, we calculate three-

excitation spectra of rotational excitons and observe the three-body bound states of the excitons. To make our theoretical study of biexciton states more relevant to experiments, we propose an nonoptical way to create the rotational biexciton states, avoiding the difficulty involved in direct excitation. This method makes use of the resonance between the high-energy ( $N = 2$ ) excitonic states and the biexciton states of low-energy ( $N = 1$ ) excitons and can produce biexcitons with high efficiency.

Chapter 4 focuses on the propagation properties of excitations. This chapter proposes a new scheme to control the energy transfer in ordered and disordered crystals. We show that the energy transfer through an array of coupled quantum monomers can be controlled by applying a transient external potential which modifies the phase of the quantum states of the individual monomers. The success of the method relies on two very different time scales in the quantum evolution of the many-body states, namely the fast time scale corresponding to the excitation of a single monomer and the slow one associated with the excitation hopping between monomers. Because of these two different time scales, it is possible to find a suitable local perturbation to a single monomer that is adiabatic with respect to the monomer excitation but is sudden with respect to the excitation hopping. In an ordered crystal, if such perturbations are applied to give different phases to different monomers, the momentum of the collective excitation is modified and its propagation behavior is influenced as well. Our work shows that different phase transformations can accelerate or decelerate quantum energy transfer and spatially focus delocalized excitations onto different parts of those ordered arrays. On the other hand, for a completely disordered array, random scattering at numerous lattice sites disturbs the above phase transformations. In this case, inspired by the “transfer matrix” methods for focusing a collimated light beam in an opaque medium[71–80], we develop another scheme of phase transformation that can achieve effective focusing of a delocalized excitation in the presence of strong disorder. To make connection with the current study of ultracold molecules, we also consider possible experimental implementations of the proposed technique in an array of ultracold atoms or molecules trapped on an optical lattice, and demonstrate the feasibility of the phase transformations.

Chapter 5 extends the method[81–83] for computing the Green’s functions for particles in periodic potentials to calculate two-particle Green’s functions in dis-

ordered crystals. This provides a powerful tool to study the quantum dynamics of quasiparticles in a disordered potential. This chapter shows that by grouping Green's functions into different set of vectors, the equation of motion of Green's function can be rewritten as a recursion relation that links three consecutive vectors. Provided that certain boundary conditions are assumed, the recursion relation enables the recursive calculations of Green's functions. I present the recursive method in the form of a generic algorithm which can be easily adapted to systems with long-range interactions and high dimensionalities, and describe its advantage over the conventional methods to calculate Green's functions. As an application of the method, I propose to use the Green's function to study the tunneling of biexciton states through impurities.

Chapter 6 concludes the thesis. This chapter gives a summary of the conclusions of the thesis, points out the limitations of the current research, and comments on future research directions.

# Chapter 2

## Background material

This chapter briefly outlines the background material that is directly related to the research in later chapters.

### 2.1 Review of angular momentum theory

In this section, we briefly review the theory of angular momentum. Instead of giving a comprehensive picture as various books[84–92] have already done, we take a pragmatic approach that is more concerned with intuitive understanding, discussing only the concepts and ideas that are relevant to research in this thesis.

#### 2.1.1 Symmetry groups

The theory of angular momentum is essentially the study of symmetry under rotations in quantum mechanics. As group theory is an important tool that is used to determine symmetry, we introduce the concepts of group theory in this subsection.

A set of operations  $\{A, B, C, \dots\}$  is called a group if it satisfies the following properties:

- there is an identity operation  $I$  in the set such that  $AI = A$
- each operation  $A$  has an inverse operation  $A^{-1}$  in the same set such that  $AA^{-1} = A^{-1}A = I$
- the multiplication of two operations is also an operation in the same set

- operations are associative such that  $(AB)C = A(BC)$

### 2.1.2 Rotation operators and spherical harmonics

As the theory of angular momentum concerns symmetry under rotations, we start by defining the rotation operator in quantum mechanics. Given a rotation  $R$ , we associate a rotation operator  $D(R)$  that transforms a state from the original system to the rotated system

$$|\psi\rangle_R = D(R)|\psi\rangle . \quad (2.1)$$

To construct the rotation operator, we denote the rotation operator  $D(\hat{\mathbf{n}}, d\phi)$  for infinitesimal rotation by angle  $d\phi$  about an axis  $\hat{\mathbf{n}}$ . Because  $D(\hat{\mathbf{n}}, d\phi)$  must be linear in  $d\phi$  for small rotation angle and becomes the identity operator when  $d\phi = 0$ , it is useful to define the angular momentum operator  $J_{\hat{\mathbf{n}}}$  for rotations about the axis  $\hat{\mathbf{n}}$  as

$$J_{\hat{\mathbf{n}}} \equiv i\hbar \lim_{\phi \rightarrow 0} \frac{D(\hat{\mathbf{n}}, \phi) - 1}{\phi} , \quad (2.2)$$

such that

$$D(\hat{\mathbf{n}}, d\phi) = 1 - i \left( \frac{J_{\hat{\mathbf{n}}}}{\hbar} \right) d\phi . \quad (2.3)$$

From the above equation, we can regard  $J_{\hat{\mathbf{n}}}$  as the generator of rotation in the sense that  $J_{\hat{\mathbf{n}}}$  produces the increment of a general function  $f$  due to a rotation  $R$  by  $d\phi$  about the axis  $\hat{\mathbf{n}}$ , that is,

$$-id\phi \left( \frac{J_{\hat{\mathbf{n}}}}{\hbar} \right) f = D(\hat{\mathbf{n}}, d\phi)f - f . \quad (2.4)$$

By compounding successively infinitesimal rotations about the same axis, we can obtain the finite rotation operator

$$\begin{aligned} D(\hat{\mathbf{n}}, \alpha) &= \lim_{m \rightarrow \infty} \left[ 1 - i \left( \frac{\alpha}{m} \right) \left( \frac{J_{\hat{\mathbf{n}}}}{\hbar} \right) \right]^m \\ &= \exp \left( \frac{-i\alpha J_{\hat{\mathbf{n}}}}{\hbar} \right) \\ &= 1 - \frac{i\alpha J_{\hat{\mathbf{n}}}}{\hbar} - \frac{1}{2!} \frac{\alpha^2 J_{\hat{\mathbf{n}}}^2}{\hbar^2} + \dots . \end{aligned} \quad (2.5)$$

where in the second step the following equation,

$$\lim_{x \rightarrow \infty} \left[ 1 + \left( \frac{1}{x} \right) \right]^x = e, \quad (2.6)$$

was used. It is clear that the set of all rotation operations satisfy the four conditions of a group (see Section 2.1.1). Correspondingly, the infinite set of rotation operators also satisfy the same conditions and thus form a group which is called the full rotation group.

Rotations have the following important property: rotations about the same axis commute whereas rotations about different axes do not. This property leads to the commutation relation of the angular momentum operator  $J$  and its Cartesian components. To illustrate this point, let's consider rotations  $R_x$ ,  $R_y$ , and  $R_z$  about the  $x$ ,  $y$  and  $z$  axes respectively. In coordinate space, these rotations can be represented by  $3 \times 3$  matrices. For instance, the rotation by angle  $\phi$  about the  $z$  axis can be expressed as

$$R_z(\phi) = \begin{pmatrix} \cos \phi & -\sin \phi & 0 \\ \sin \phi & \cos \phi & 0 \\ 0 & 0 & 1 \end{pmatrix}. \quad (2.7)$$

In the case of an infinitesimal angle  $\phi \rightarrow \varepsilon$ , the above equation can be written as

$$R_z(\varepsilon) = \begin{pmatrix} 1 - \frac{\varepsilon^2}{2} & -\varepsilon & 0 \\ \varepsilon & 1 - \frac{\varepsilon^2}{2} & 0 \\ 0 & 0 & 1 \end{pmatrix}. \quad (2.8)$$

By comparing the effect of a  $y$ -axis rotation followed by an  $x$ -axis rotation with that of an  $x$ -axis rotation followed by a  $y$ -axis rotation, we can show that

$$R_x(\varepsilon)R_y(\varepsilon) - R_y(\varepsilon)R_x(\varepsilon) = R_z(\varepsilon^2) - I. \quad (2.9)$$

Assuming the corresponding rotation operators satisfy a similar equation as Eq. (2.9) and making use of Eq. (2.3), we obtain

$$[J_x, J_y] = i\hbar J_z. \quad (2.10)$$

Repeating the above analysis for other axes, we obtain the commutation relations for the components of angular momentum

$$[J_i, J_j] = i\hbar \epsilon_{ijk} J_k , \quad (2.11)$$

where  $i, j, k$  can be any one of  $x, y$  and  $z$ , and  $\epsilon_{ijk}$  is defined as

$$\epsilon_{ijk} = \begin{cases} 1 & \text{if } (i, j, k) \text{ is an even permutation of } (x, y, z) \\ -1 & \text{if } (i, j, k) \text{ is an odd permutation of } (x, y, z) \\ 0 & \text{if two or more indices are equal} \end{cases} . \quad (2.12)$$

Many important properties follow from the angular-momentum commutation relation represented by Eq. (2.11). For example, by making use of Eq. (2.11), we can show that the operator  $\mathbf{J}^2$  defined by

$$\mathbf{J}^2 \equiv J_x^2 + J_y^2 + J_z^2 , \quad (2.13)$$

commutes with any one of  $J_x, J_y$  and  $J_z$ , namely,

$$[\mathbf{J}^2, J_k] = 0, \quad (k = x, y, z) . \quad (2.14)$$

Since  $\mathbf{J}^2$  and  $J_z$  commute, the eigenstates of  $\mathbf{J}^2$  can be chosen to be also the eigenstates of  $J_z$ . We denote these states by  $|j, m\rangle$  such that

$$\begin{aligned} \mathbf{J}^2 |j, m\rangle &= j(j+1)\hbar^2 |j, m\rangle , \\ J_z |j, m\rangle &= m\hbar |j, m\rangle . \end{aligned} \quad (2.15)$$

To determine the allowed values for  $j$  and  $m$ , it is convenient to work with the non-Hermitian operators

$$J_{\pm} = J_x \pm iJ_y , \quad (2.16)$$

where  $J_+$  is called the raising operator and  $J_-$  is called the lowering operator.  $J_{\pm}$

satisfy the following commutation relations

$$\begin{aligned} [J_+, J_-] &= 2\hbar J_z, \\ [J_z, J_{\pm}] &= \pm\hbar J_{\pm}, \\ [\mathbf{J}^2, J_{\pm}] &= 0, \end{aligned} \quad (2.17)$$

all of which can easily be derived from Eq. (2.11).

As a special case of the angular momentum operator, the orbital angular momentum operator  $\mathbf{L} = \mathbf{r} \times \mathbf{p}$  has components that satisfy the same commutation relations

$$[L_i, L_j] = i\hbar\epsilon_{ijk}L_k. \quad (2.18)$$

Using the fact that momentum is the generator of translation

$$T(d\mathbf{x})|\mathbf{r}\rangle = \left[1 - i\left(\frac{\mathbf{p}}{\hbar}\right) \cdot d\mathbf{x}\right] |\mathbf{r}\rangle = |\mathbf{r} + dx\hat{\mathbf{x}}\rangle, \quad (2.19)$$

we have

$$\begin{aligned} \left[1 - i\left(\frac{d\phi}{\hbar}\right) L_z\right] |x, y, z\rangle &= \left[1 - i\left(\frac{d\phi}{\hbar}\right) (xp_y - yp_x)\right] |x, y, z\rangle \\ &= \left[1 - i\left(\frac{p_y}{\hbar}\right) xd\phi + i\left(\frac{p_x}{\hbar}\right) yd\phi\right] |x, y, z\rangle \\ &= |x - yd\phi, y + xd\phi, z\rangle. \end{aligned} \quad (2.20)$$

The above equation shows exactly the effect of an infinitesimal rotation about the  $z$  axis, as one would expect. For an arbitrary state  $|\psi\rangle$ , an infinitesimal rotation about  $z$  axis changes the wavefunction  $\langle x, y, z | \psi \rangle$  to

$$\langle x, y, z | \left[1 - i\left(\frac{d\phi}{\hbar}\right) L_z\right] |\psi\rangle = \langle x + yd\phi, y - xd\phi, z | \psi \rangle. \quad (2.21)$$

By changing to spherical coordinates  $(r, \theta, \phi)$ , the above equation can be converted

to

$$\begin{aligned} \langle r, \theta, \phi | \left[ 1 - i \left( \frac{d\phi}{\hbar} \right) L_z \right] |\psi\rangle &= \langle r, \theta, \phi - d\phi | \psi \rangle \\ &= \langle r, \theta, \phi | \psi \rangle - d\phi \frac{\partial}{\partial \phi} \langle r, \theta, \phi | \psi \rangle . \end{aligned} \quad (2.22)$$

Therefore, we obtain

$$L_z = -i\hbar \frac{\partial}{\partial \phi} . \quad (2.23)$$

In the way, we can also derive the expressions for the other orbital angular momentum operators, giving

$$\begin{aligned} L_x &= -i\hbar \left( -\sin \phi \frac{\partial}{\partial \theta} - \cot \theta \cos \phi \frac{\partial}{\partial \phi} \right) , \\ L_y &= -i\hbar \left( \cos \phi \frac{\partial}{\partial \theta} - \cot \theta \sin \phi \frac{\partial}{\partial \phi} \right) . \end{aligned} \quad (2.24)$$

The eigenfunctions of  $\mathbf{L}^2$  and  $L_z$  are known as the spherical harmonics, which are given by

$$\langle \hat{\mathbf{n}} | l, m \rangle = Y_{lm}(\theta, \phi) , \quad (2.25)$$

where  $\theta$  and  $\phi$  specify the orientation of  $\hat{\mathbf{n}}$ . The dependence of spherical harmonics on angles can be separated so that

$$Y_{lm}(\theta, \phi) = \Theta_{lm}(\theta) \Phi_m(\phi) , \quad (2.26)$$

where

$$\Phi_m(\phi) = \sqrt{\frac{1}{2\pi}} \exp(im\phi) , \quad (2.27)$$

and

$$\Theta_{lm}(\theta) = (-1)^m \left[ \frac{2l+1}{2} \frac{(l-m)!}{(l+m)!} \right]^{1/2} P_l^m(\cos \theta) , \quad (2.28)$$

for  $m \geq 0$  and  $\Theta_{lm}(\theta) = (-1)^m \Theta_{l-m}(\theta)$  for  $m < 0$ , and  $P_l^m(\cos \theta)$  are the associated Legendre polynomials. Sometimes, it is more convenient to work with modified

spherical harmonics  $C_{lm}$  defined by

$$C_{lm}(\theta, \phi) = \sqrt{\frac{4\pi}{2l+1}} Y_{lm}(\theta, \phi). \quad (2.29)$$

### 2.1.3 Rotation matrices

Since an arbitrary rotation can be decomposed into rotations about three coordinate axes ( $x$ ,  $y$ , and  $z$  axis), it is usually convenient to express the orientations of a body in terms of rotations about some fixed axes. For this to work, we have to choose an initial orientation as a reference on which the rotations are operating. For a vector described by the two spherical polar angles  $\theta$  and  $\phi$ , we use a reference orientation parallel to the space-fixed  $Z$  axis. It is obvious to see that a rotation of this reference orientation through an angle  $\theta$  about the space-fixed  $Y$  axis and a rotation by an angle  $\phi$  about the space-fixed  $Z$  axis can reproduce the orientation of the vector. For a general body, three angles  $\phi$ ,  $\theta$  and  $\chi$  are needed to describe an arbitrary rotation. We attach a second coordinate system  $(x,y,z)$  to the body and refer to it as the body-fixed axis system. This axis system is called body-fixed as by construction it moves and rotates along with the body as a whole. In contrast, the original coordinate system  $(X,Y,Z)$  is fixed in space, so it is called the space-fixed axis system. To describe the orientation of a body, we imagine that the body is initially at a position with its body-fixed axis system coincident with the space-fixed axis system, and then we carry out the following three rotations:

1. rotate by  $\chi$  about the space-fixed  $Z$  axis,
2. rotate by  $\theta$  about the space-fixed  $Y$  axis,
3. rotate by  $\phi$  about the space-fixed  $Z$  axis.

These three rotations can produce arbitrary orientation of the body. For an intuitive understanding of the Euler angles, we link the orientation of the body directly with  $\phi$ ,  $\theta$  and  $\chi$ . It can be shown that  $\theta$  and  $\phi$  can be used to define the orientation of the body-fixed  $z$  axis in the space-fixed axis system, in the same way as  $\theta$  and  $\phi$  are used to define the orientation of a vector. The angle  $\chi$  measures a rotation

about the body-fixed  $z$  axis. It is an azimuthal angle about the  $z$  axis just as  $\phi$  is an azimuthal angle about the  $Z$  axis.

Based on Eq. (2.5), the rotation operator that corresponds to the three Euler angles can be written as

$$D(\phi, \theta, \chi) = \exp\left(\frac{-i\phi J_Z}{\hbar}\right) \exp\left(\frac{-i\theta J_Y}{\hbar}\right) \exp\left(\frac{-i\chi J_Z}{\hbar}\right). \quad (2.30)$$

Because of the closure property of the full rotation group, the multiplication of three rotation operators in Eq. (2.30) is equivalent to another rotation operator

$$D(R) = \exp\left(\frac{-i\alpha \mathbf{J}_{\hat{\mathbf{n}}}}{\hbar}\right) = D(\phi, \theta, \chi), \quad (2.31)$$

which corresponds to a rotation  $R$  through an angle  $\alpha$  about an axis  $\hat{\mathbf{n}}$ .

Now we study the matrix elements of the rotation operator  $D(R)$ . As a consequence of that fact that  $\mathbf{J}^2$  commutes with any component of  $\mathbf{J}$ , the rotation operator  $D(R)$ , a function of  $J_{\hat{\mathbf{n}}}$ , also commutes with  $\mathbf{J}^2$ . Thus the eigenfunctions  $|j, m\rangle$  of  $\mathbf{J}^2$  are also eigenfunctions of the rotation operator and rotations don't change the total angular momentum. As a result, to see the effect of a rotation on a state with a definite angular momentum, we only need to calculate the matrix elements of the rotation operator between two states with the same  $j$  value, that is

$$D_{m'm}^j = \langle j, m' | \exp\left(\frac{-i\alpha \mathbf{J}_{\hat{\mathbf{n}}}}{\hbar}\right) | j, m \rangle. \quad (2.32)$$

The  $(2j+1) \times (2j+1)$  matrix formed by  $D_{m'm}^j$  in the above equation is called the rotation matrix. Making use of Eq. (2.30), we can easily show that

$$\begin{aligned} D_{m'm}^j(\phi, \theta, \chi) &= \exp(-i\phi m' - i\chi m) \langle j, m' | \exp(-i\theta J_Y/\hbar) | j, m \rangle \\ &\equiv \exp(-i\phi m' - i\chi m) d_{m'm}^j(\theta), \end{aligned} \quad (2.33)$$

where  $d_{m'm}^j(\theta)$  is the element of a reduced rotation matrix. As the above equation shows, the reduced rotation matrix can be calculated from the matrix representation

of  $J_Y$  and its expression is[87]:

$$d_{m',m}^j(\theta) = \sum_t (-1)^t \frac{[(j+m')!(j-m')!(j+m)!(j-m)!]^{1/2}}{(j+m'-t)!(j-m-t)!t!(t+m-m')!} \times \left( \cos \frac{\theta}{2} \right)^{2j+m'-m-2t} \left( \sin \frac{\theta}{2} \right)^{2t-m'+m}, \quad (2.34)$$

where the sum over  $t$  is for all integers for which the factorial arguments are non-negative. It can be shown that  $d_{m',m}^j(\theta)$  satisfies the following symmetry relations[87]:

$$d_{m',m}^j(\theta) = (-1)^{m'-m} d_{m,m'}^j(\theta) = (-1)^{m'-m} d_{-m',-m}^j(\theta). \quad (2.35)$$

To understand the physical meaning of the rotation matrix, we start from a state  $|j, m\rangle$  and rotate it. Even though the rotation  $R$  doesn't change the  $j$  value, we will generally expect the  $m$  value to be different after the rotation. Consequently, one would be interested in knowing the probability of the system being found in a state  $|j, m'\rangle$ . By using the identity relation,  $I = \sum_{j',m'} |j', m'\rangle \langle j', m'|$ , the final state can be written as

$$\begin{aligned} D(R)|j, m\rangle &= \sum_{j'} \sum_{m'} |j', m'\rangle \langle j', m'| D(R)|j, m\rangle \\ &= \sum_{m'} |j, m'\rangle \langle j', m'| D(R)|j, m\rangle \delta_{j,j'} \\ &= \sum_{m'} |j, m'\rangle \langle j, m'| D(R)|j, m\rangle \\ &= \sum_{m'} |j, m'\rangle D_{m',m}^j(R). \end{aligned} \quad (2.36)$$

From the above equation, one can see that the matrix element  $D_{m',m}^j(R)$  is simply the probability amplitude for the rotated state to be found in  $|j, m'\rangle$  when the original state is  $|j, m\rangle$ .

#### 2.1.4 Properties of rotation matrices

Let's consider some important properties of the rotation matrices. From the last subsection, we know the basis ket  $|j, m\rangle$  are orthonormal and remain so on rotation, this means that the matrices that represent rotations are unitary, that is,  $D^{-1} = D^\dagger$ .

More specifically, we have

$$D_{m',m}^j(R^{-1}) = (D^\dagger)_{m',m}^j(R) = [D_{m',m}^j(R)]^*, \quad (2.37)$$

where  $R^{-1}$  denotes the inverse of the rotation  $R$ .

From Eq. (2.34), we can see the matrix elements of reduced rotation matrices are always real. Taking this fact into account, and using Eq. (2.33) and Eq. (2.35), we arrive at

$$\begin{aligned} D_{m',m}^{j*}(R) &= \exp[-i\phi(-m') - i\chi(-m)] d_{m',m}^j(\theta) \\ &= \exp[-i\phi(-m') - i\chi(-m)] (-1)^{m-m'} d_{-m',-m}^j(\theta) \\ &= (-1)^{m-m'} D_{-m',-m}^j(R). \end{aligned} \quad (2.38)$$

As will be seen later, this equation is very useful because it helps us to deal with the complex conjugates of matrix elements of rotation matrices.

Another important property is that the rotation matrix elements  $D_{m',m}^l$  reduces to spherical harmonics when  $l$  is an integer and  $m'$  or  $m$  is zero[87], that is

$$\begin{aligned} D_{m,0}^l(\phi, \theta, \chi) &= C_{lm}^*(\theta, \phi) = \sqrt{\frac{2l+1}{4\pi}} Y_{lm}^*(\theta, \phi), \\ D_{0,m}^l(\phi, \theta, \chi) &= C_{l-m}(\theta, \phi) = \sqrt{\frac{2l+1}{4\pi}} Y_{l-m}(\theta, \phi). \end{aligned} \quad (2.39)$$

Given a general state  $|\hat{\mathbf{n}}\rangle$  with the unit vector  $\hat{\mathbf{n}}$  with the orientation specified by  $(\theta, \phi)$ , we know from previous discussion that it can be constructed from the state  $|\hat{\mathbf{z}}\rangle$  by a rotation about  $y$  axis by angle  $\theta$  and a rotation about  $z$  axis by angle  $\phi$ . Thus we obtain

$$\begin{aligned} |\hat{\mathbf{n}}\rangle &= D(\phi, \theta, \chi)|\hat{\mathbf{z}}\rangle \\ &= \sum_{l'} \sum_{m'} D(\phi, \theta, \chi) |l', m'\rangle \langle l', m' | \hat{\mathbf{z}} \rangle \end{aligned} \quad (2.40)$$

where  $\chi$  is undetermined. Multiplying both sides of the above equation by  $\langle l, m |$ , we get

$$\langle l, m | \hat{\mathbf{n}} \rangle = \sum_{m'} D_{m,m'}^l(\phi, \theta, \chi) \langle l, m' | \hat{\mathbf{z}} \rangle. \quad (2.41)$$

Based on the definition of the spherical harmonics,  $\langle l, m' | \hat{\mathbf{z}} \rangle$  is just  $Y_{lm'}^*(\theta, \phi)$  with  $\theta = 0$  and  $\phi$  undetermined. For  $\theta = 0$  the associated Legendre polynomials satisfy  $P_l^m(1) = \delta_{m,0}$ , so that the spherical harmonics of Eq. (2.26) gives rise to

$$\begin{aligned}\langle l, m' | \hat{\mathbf{z}} \rangle &= Y_{lm}^*(\theta = 0, \phi) \delta_{m,0} \\ &= \sqrt{\frac{2l+1}{4\pi}} \delta_{m,0}.\end{aligned}\quad (2.42)$$

Substituting this equation into Eq. (2.41) yields Eq. (2.39).

Finally, we consider the integral of rotation matrices. From Eq. (2.33) and Eq. (2.34), it can be shown that the integral of a rotation matrix over  $d\omega = \sin \theta d\theta d\phi d\chi$  is a product of delta functions[92], that is

$$\int D_{m',m}^j(\phi, \theta, \chi) d\omega = 8\pi^2 \delta_{j,0} \delta_{m',0} \delta_{m,0}. \quad (2.43)$$

Similarly, the integral of two rotation matrices is given by[87]

$$\int D_{m'_1, m_1}^{j_1*}(\phi, \theta, \chi) D_{m'_2, m_2}^{j_2}(\phi, \theta, \chi) d\omega = \frac{8\pi^2}{2j_1 + 1} \delta_{j_1, j_2} \delta_{m'_1, m'_2} \delta_{m_1, m_2}, \quad (2.44)$$

which describes the normalization condition for rotation matrices.

### 2.1.5 Coupling of angular momenta

Suppose a system can be divided into two parts with different angular momentum operators  $\mathbf{J}_1$  and  $\mathbf{J}_2$ , respectively. When the two parts of the system interact through some physical mechanism,  $\mathbf{J}_1$  and  $\mathbf{J}_2$  become coupled and we define the addition of the two angular momentum operator as

$$\mathbf{J} = \mathbf{J}_1 + \mathbf{J}_2. \quad (2.45)$$

It is easy to verify that  $\mathbf{J}$  also satisfies the commutation rules of angular momentum (Eq. (2.11)) and thus the sum of two angular momentum operator is also an angular momentum operator.

In quantum mechanics, the state of a system is described by the simultaneous eigenfunctions of a complete set of commuting operators. For the current system

of angular momenta, there are two complete sets of angular momentum operators. One set is  $\mathbf{J}_1^2$ ,  $\mathbf{J}_2^2$ ,  $J_{1Z}$ , and  $J_{2Z}$ , and therefore we can use their simultaneous eigenstates  $|j_1, m_1; j_2, m_2\rangle \equiv |j_1, m_1\rangle |j_2, m_2\rangle$  to describe the system. This representation is called the uncoupled representation. The other complete set of commuting angular momentum operators is  $\mathbf{J}_1^2$ ,  $\mathbf{J}_2^2$ ,  $\mathbf{J}^2$ , and  $J_Z$ . Their simultaneous eigenstates  $|(j_1 j_2)j, m\rangle$  which we sometimes write as  $|j, m\rangle$  are used to describe the system. This representation is called the coupled representation as the quantum numbers  $j$  and  $m$  of the coupled angular momentum are used. Note that the bracket “()” in  $|(j_1 j_2)j, m\rangle$  indicates the coupling of the two angular momenta  $\mathbf{J}_1$  and  $\mathbf{J}_2$  and the result of the coupling is represented by the number  $j$  immediately after the bracket.

The two representations describe the same set of states of the system so they can be related by an unitary transformation connecting two bases, that is

$$|(j_1 j_2)j, m\rangle = \sum_{m_1, m_2} |j_1, m_1; j_2, m_2\rangle \langle j_1, m_1; j_2, m_2| (j_1 j_2)j, m\rangle , \quad (2.46)$$

where  $\langle j_1, m_1; j_2, m_2| (j_1 j_2)j, m\rangle$  are called the Clebsch-Gordan coefficients. Due to symmetry considerations, it is often convenient to express the coefficients by the 3- $j$  symbols. The relation between the Clebsch-Gordan coefficients and 3- $j$  symbols is[87]

$$\begin{pmatrix} j_1 & j_2 & j_3 \\ m_1 & m_2 & m_3 \end{pmatrix} \equiv (-1)^{j_1 - j_2 - m_3} (2j_3 + 1)^{-\frac{1}{2}} \langle j_1 m_1, j_2 m_2 | j_3 - m_3 \rangle , \quad (2.47)$$

$$\langle j_1 m_1, j_2 m_2 | j_3 m_3 \rangle \equiv (-1)^{j_1 - j_2 + m_3} (2j_3 + 1)^{\frac{1}{2}} \begin{pmatrix} j_1 & j_2 & j_3 \\ m_1 & m_2 & -m_3 \end{pmatrix} . \quad (2.48)$$

The 3- $j$  symbols are more symmetric than the Clebsch-Gordan coefficients. We do not discuss the symmetry properties here as they are not important for understanding the thesis. The interested readers should refer to Zare's book[87]. The 3- $j$  symbols are subject to the selection rules of angular momentum, that is

$$\begin{pmatrix} j_1 & j_2 & j_3 \\ m_1 & m_2 & m_3 \end{pmatrix} = 0 \text{ unless } m_1 + m_2 + m_3 = 0 \text{ and } |j_1 - j_2| \leq j_3 \leq j_1 + j_2,$$

which physically means that only certain angular momenta are coupled. Many calculations in molecular spectroscopy boil down to the evaluation of 3-*j* symbols. For details on the evaluation, readers should refer to Zare's book[87], which mentions some efficient algorithms for calculating 3-*j* symbols and gives the algebraic expressions for the commonly encountered 3-*j* symbols in Table 2.5.

Different from the coupling of two angular momenta, the coupling of three angular momenta has more than one possible coupling scheme, and all these coupling schemes are related by unitary transformations. We might couple  $\mathbf{J}_1$ ,  $\mathbf{J}_2$  and  $\mathbf{J}_3$  in such a way that  $\mathbf{J}_1 + \mathbf{J}_2 = \mathbf{J}_{12}$ ,  $\mathbf{J}_{12} + \mathbf{J}_3 = \mathbf{J}$ . The eigenfunctions in this coupling scheme are given by  $|[(j_1 j_2) j_{12} j_3] j, m\rangle$ , where the brackets “[]” and “()”, indicate the coupling of two angular momenta  $j_{12}$  and  $j_3$  to produce  $j$ . We can also couple  $\mathbf{j}_2$  and  $\mathbf{j}_3$  to produce a new angular momentum  $\mathbf{j}_{23}$ , and then couple  $\mathbf{j}_{23}$  with  $\mathbf{j}_1$  to produce the total angular momentum  $\mathbf{j}$ . The corresponding eigenstates are given by  $|[j_1 (j_2 j_3) j_{23}] j, m\rangle$ . The transformation between the two different coupling schemes is

$$|(j_1 j_{23}) j, m\rangle = \sum_{j_{12}} \langle (j_{12} j_3) j, m | (j_1 j_{23}) j', m' \rangle |(j_{12} j_3) j', m' \rangle \delta_{j, j'} \delta_{m, m'}, \quad (2.49)$$

where  $|(j_1 j_{23}) j, m\rangle$  is a short-hand way to write  $|[j_1 (j_2 j_3) j_{23}] j, m\rangle$ . In the above equation, since  $\langle (j_{12} j_3) j, m | (j_1 j_{23}) j', m' \rangle$  is a scalar product, it doesn't depend on the orientation of the coordinate system and is independent of the projection quantum numbers. Thus we can drop  $m$  and  $m'$  and write it as  $\langle (j_{12} j_3) j | (j_1 j_{23}) j' \rangle$ . These recoupling coefficients can be replaced with the so-called 6-*j* symbols defined as[87]

$$\left\{ \begin{array}{ccc} j_1 & j_2 & j_{12} \\ j_3 & j & j_{23} \end{array} \right\} = (-1)^{j_1 + j_2 + j_3 + j} [(2j_{12} + 1)(2j_{23} + 1)]^{-\frac{1}{2}} \langle (j_{12} j_3) j | (j_1 j_{23}) j' \rangle. \quad (2.50)$$

Similarly, the coupling of four angular momenta also has more than one possible coupling scheme. For example,  $|[(j_1 j_2) j_{12} (j_3 j_4) j_{34}] j, m\rangle$  is associated with

the coupling scheme

$$\mathbf{J}_1 + \mathbf{J}_2 = \mathbf{J}_{12}, \quad \mathbf{J}_3 + \mathbf{J}_4 = \mathbf{J}_{34}, \quad \mathbf{J}_{12} + \mathbf{J}_{34} = \mathbf{J},$$

and  $|[(j_1 j_4) j_{14} (j_2 j_3) j_{23}] j, m\rangle$  is associated with another coupling scheme:

$$\mathbf{J}_1 + \mathbf{J}_4 = \mathbf{J}_{14}, \quad \mathbf{J}_2 + \mathbf{J}_3 = \mathbf{J}_{23}, \quad \mathbf{J}_{14} + \mathbf{J}_{23} = \mathbf{J}.$$

The relation between the states corresponding to those two coupling schemes is

$$|[(j_1 j_4) j_{14} (j_2 j_3) j_{23}] j, m\rangle = \sum_{j_{12}} \sum_{j_{34}} \langle (j_1 j_2) j_{12} (j_3 j_4) j_{34} j | (j_1 j_4) j_{14} (j_2 j_3) j_{23} j \rangle \\ \times |[(j_1 j_4) j_{14} (j_2 j_3) j_{23}] j, m\rangle, \quad (2.51)$$

and the correspondingly the 9-*j* symbol is defined by[87]

$$\langle (j_1 j_2) j_{12} (j_3 j_4) j_{34} j | (j_1 j_4) j_{14} (j_2 j_3) j_{23} j \rangle \\ = \sqrt{(2j_{12} + 1)(2j_{34} + 1)(2j_{14} + 1)(2j_{23} + 1)} \left\{ \begin{array}{ccc} j_1 & j_2 & j_{12} \\ j_3 & j_4 & j_{34} \\ j_{14} & j_{23} & j \end{array} \right\}. \quad (2.52)$$

The last column of the 9-*j* symbol is related to the first coupling scheme and the last row is associated with the second coupling scheme.

### 2.1.6 Clebsch-Gordan series

After discussing the coupling of angular momenta, we now return to the rotation matrix and further develop its properties in the context of angular momentum coupling. We consider the connection between the uncoupled  $|j_1, m_1\rangle |j_2, m_2\rangle$  and the coupled  $|j, m\rangle$  representations under a rotational transformation. Applying the rotation transformation on  $|j_1, m_1\rangle$ ,  $|j_1, m_1\rangle$  and  $|j, m\rangle$  in Eq. (2.46) individually and

using Eq. (2.36) we obtain

$$\begin{aligned} & \sum_{m'_1 m'_2} \sum D_{m'_1, m_1}^{j_1}(R) D_{m'_2, m_2}^{j_2}(R) |j_1, m'_1\rangle |j_2, m'_2\rangle \\ &= \sum_j \sum_{m'} \langle j_1, m_1; j_2, m_2 | j, m \rangle D_{m', m}^j(R) |j, m'\rangle . \end{aligned} \quad (2.53)$$

Multiplying both sides by  $\langle j_1, m'_1 | \langle j_2, m'_2 |$  and making use of Eq. (2.38), we obtain the so-called Clebsch-Gordan series:

$$\begin{aligned} D_{m'_1, m_1}^{j_1}(R) D_{m'_2, m_2}^{j_2}(R) &= \sum_j \langle j_1, m_1; j_2, m_2 | j, m \rangle \langle j_1, m'_1; j_2, m'_2 | j, m' \rangle D_{m', m}^j(R) \\ &= \sum_j (2j+1) \left( \begin{array}{ccc} j_1 & j_2 & j \\ m_1 & m_2 & m \end{array} \right) \left( \begin{array}{ccc} j_1 & j_2 & j \\ m'_1 & m'_2 & m' \end{array} \right) D_{m', m}^{j*}(R) \end{aligned} \quad (2.54)$$

Similarly, the inverse Clebsch-Gordan series are given by

$$\begin{aligned} D_{m', m}^{j*}(R) &= \sum_{m_1} \sum_{m'_1} \sum_{m_2} \sum_{m'_2} (2j+1) \left( \begin{array}{ccc} j_1 & j_2 & j \\ m_1 & m_2 & m \end{array} \right) \left( \begin{array}{ccc} j_1 & j_2 & j \\ m'_1 & m'_2 & m' \end{array} \right) \\ &\times D_{m'_1, m_1}^{j_1}(R) D_{m'_2, m_2}^{j_2}(R) . \end{aligned} \quad (2.55)$$

The Clebsch-Gordan series can help us to evaluate the integral over a product of three rotation matrix elements. Multiplying both sides of Eq. (2.54) by  $D_{m'_3, m_3}^{j_3}(R)$  we have

$$\begin{aligned} D_{m'_1, m_1}^{j_1}(R) D_{m'_2, m_2}^{j_2}(R) D_{m'_3, m_3}^{j_3}(R) &= \sum_j (2j+1) \left( \begin{array}{ccc} j_1 & j_2 & j \\ m_1 & m_2 & m \end{array} \right) \left( \begin{array}{ccc} j_1 & j_2 & j \\ m'_1 & m'_2 & m' \end{array} \right) \\ &\times D_{m', m}^j(R)^* D_{m'_3, m_3}^{j_3}(R) . \end{aligned} \quad (2.56)$$

Integrating over  $d\omega = \sin \theta d\theta d\phi d\chi$  and utilizing the normalization condition of

Eq. (2.44) then gives

$$\begin{aligned} & \int D_{m'_1, m_1}^{j_1}(\phi, \theta, \chi) D_{m'_2, m_2}^{j_2}(\phi, \theta, \chi) D_{m'_3, m_3}^{j_3}(\phi, \theta, \chi) d\omega \\ &= 8\pi^2 \begin{pmatrix} j_1 & j_2 & j_3 \\ m'_1 & m'_2 & m'_3 \end{pmatrix} \begin{pmatrix} j_1 & j_2 & j_3 \\ m_1 & m_2 & m_3 \end{pmatrix}. \end{aligned} \quad (2.57)$$

The above equation is very important because alternative ways to evaluate the integral are very laborious. We will use this equation in the derivation of the Wigner-Eckart theorem. Since the rotation matrix is proportional to the spherical harmonics under some special conditions (see Eq. (2.39)), we have

$$\begin{aligned} & \int D_{m_1, 0}^{l_1}(\phi, \theta, \chi) D_{m_2, 0}^{l_2}(\phi, \theta, \chi) D_{m_3, 0}^{l_3}(\phi, \theta, \chi) d\omega \\ &= 8\pi^2 \begin{pmatrix} l_1 & l_2 & l_3 \\ m_1 & m_2 & m_3 \end{pmatrix} \begin{pmatrix} l_1 & l_2 & l_3 \\ 0 & 0 & 0 \end{pmatrix} \\ &= \sqrt{\frac{4\pi \cdot 4\pi \cdot 4\pi}{(2l_1+1)(2l_2+1)(2l_3+1)}} \\ & \quad \times 2\pi \int Y_{l_1 m_1}^*(\phi, \theta) Y_{l_2 m_2}^*(\phi, \theta) Y_{l_3 m_3}^*(\phi, \theta) \sin \theta d\phi d\theta, \end{aligned} \quad (2.58)$$

which gives rise to

$$\begin{aligned} & \int Y_{l_1 m_1}(\phi, \theta) Y_{l_2 m_2}(\phi, \theta) Y_{l_3 m_3}(\phi, \theta) \sin \theta d\theta d\phi \\ &= \sqrt{\frac{(2l_1+1)(2l_2+1)(2l_3+1)}{4\pi}} \begin{pmatrix} l_1 & l_2 & l_3 \\ m_1 & m_2 & m_3 \end{pmatrix} \begin{pmatrix} l_1 & l_2 & l_3 \\ 0 & 0 & 0 \end{pmatrix}. \end{aligned} \quad (2.59)$$

### 2.1.7 Spherical tensor operators

We have seen how the angular momentum wavefunction  $|j, m\rangle$  transforms under a rotation. Specifically, based on Eq. (2.36), a general state  $|\alpha\rangle$  is changed under a rotation  $R$  according to

$$|\alpha\rangle \rightarrow D(R)|\alpha\rangle. \quad (2.60)$$

Now we study how an operator transforms under a rotation. Let's consider a so-called vector operator, for example  $\mathbf{J}$ , which is composed of operators  $J_X$ ,  $J_Y$  and  $J_Z$ . We know a vector in classical physics with three components transforms like  $V_j \rightarrow \sum_j R_{i,j} V_i$  under a rotation  $R$ . It is reasonable to expect that the expectation value of a vector operator  $\mathbf{V}$  transforms like a classical vector, that is

$$\langle \alpha | V_i | \alpha \rangle \rightarrow \langle \alpha | D^\dagger(R) V_i D(R) | \alpha \rangle = \sum_j R_{i,j} \langle \alpha | V_j | \alpha \rangle , \quad (2.61)$$

where Eq. (2.60) has been used. From the above equation, it follows that the transformed operator in the original basis is given by

$$D^\dagger(R) V_i D(R) = \sum_j R_{i,j} V_j . \quad (2.62)$$

By generalizing the definition of a vector  $V_j \rightarrow \sum_j R_{i,j} V_i$ , we define a tensor as a quantity which transforms like

$$T_{ijk\dots} \rightarrow \sum_{i'} \sum_{j'} \sum_{k'} \dots R_{i,i'} R_{j,j'} R_{k,k'} \dots T_{i'j'k'\dots} . \quad (2.63)$$

The number of indices is called the rank of a tensor. Such a tensor is called a Cartesian tensor because its components  $T_{ijk\dots}$  are defined with respect to the Cartesian axes.

The problem with a Cartesian tensor is that it is reducible meaning it contains parts that transform differently under rotations. Take for example a Cartesian tensor  $\mathbf{T}$  formed from the product of two vectors  $\mathbf{U}$  and  $\mathbf{V}$

$$T_{ij} \equiv U_i V_j . \quad (2.64)$$

It can be shown that the tensor can be decomposed into the following parts:

$$U_i V_j = \frac{\mathbf{U} \cdot \mathbf{V}}{3} \delta_{i,j} + \frac{U_i V_j - U_j V_i}{2} + \left( \frac{U_i V_j + U_j V_i}{2} - \frac{\mathbf{U} \cdot \mathbf{V}}{3} \delta_{i,j} \right) . \quad (2.65)$$

The first term on the right hand side is a scalar and has 1 independent component. The second term looks like a cross product of two vectors and has 3 independent

components. The third term is more complicated and we can rewrite it as

$$(1 - \delta_{i,j}) \frac{U_i V_j - U_j V_i}{2} + \delta_{i,j} \left( U_i V_i - \frac{\mathbf{U} \cdot \mathbf{V}}{3} \right),$$

where the first term represents the off-diagonal part of the  $3 \times 3$  tensor and the second term represent the diagonal part. Now, it can be easily seen that this term is symmetric and its trace is zero. So it contains 5 independent components. The number of independent components associated with the three terms in Eq. (2.65) is 1, 3, and 5 respectively, which are precisely the multiplicities of angular momenta with  $l = 0$ ,  $l = 1$ , and  $l = 2$  respectively. This suggests that the tensor  $\mathbf{T}$  can be decomposed into tensors that can transform like spherical harmonics with  $l = 0, 1$ , and 2.

From the above example, it seems like the spherical harmonics can be used as irreducible tensors to represent any reducible tensor. This motivates us to define irreducible spherical tensors based on the spherical harmonics. Before presenting the definition of a spherical tensor, let's first investigate how the spherical harmonics transform under rotations. For a direction eigenket  $|\hat{\mathbf{n}}\rangle$ , a rotation transforms it to another direction eigenket  $|\hat{\mathbf{n}}'\rangle$ , that is

$$|\hat{\mathbf{n}}'\rangle = D(R)|\hat{\mathbf{n}}\rangle. \quad (2.66)$$

By taking the hermitian adjoint of the above equation and then multiplying by  $|lm\rangle$  on the right, we obtain

$$Y_{lm}(\hat{\mathbf{n}}') = \sum_{m'} Y_{lm'}(\hat{\mathbf{n}}) (D^\dagger)_{m'm}^l(R). \quad (2.67)$$

The spherical harmonics can be used as both functions and operators just like the coordinates  $x, y, z$  can also be used as position operators. Treating the spherical harmonics as operators,  $Y_{lm}(\hat{\mathbf{n}}')$  on the left hand side of Eq. (2.67) are the operators after the rotation transformation, which can be written in terms of the original operator  $D^\dagger(R)Y_{lm}(\hat{\mathbf{n}})D(R)$  based on Eq. (2.62). So that Eq. (2.67) becomes

$$D^\dagger(R)Y_{lm}(\hat{\mathbf{n}})D(R) = \sum_{m'} Y_{lm'}(\hat{\mathbf{n}})D_{mm'}^{l*}(R). \quad (2.68)$$

Similarly, we define an irreducible spherical tensor operator of rank  $k$  with  $(2k+1)$  components as

$$D^\dagger(R)T_q^{(k)}(\hat{\mathbf{n}})D(R) = \sum_{q'=-k}^k D_{qq'}^{k*}(R)T_{q'}^{(k)}(\hat{\mathbf{n}}). \quad (2.69)$$

Replacing the rotation  $R$  by its inverse  $R^{-1}$  and using Eq. (2.37), the above definition can be recast as

$$D(R)T_q^{(k)}(\hat{\mathbf{n}})D^\dagger(R) = \sum_{q'=-k}^k T_{q'}^{(k)}(\hat{\mathbf{n}})D_{q'q}^k(R). \quad (2.70)$$

Note that  $T_q^{(k)}$  and  $T_{q'}^{(k)}$  here are defined with respect to the same axis system. Because the spherical harmonics and the irreducible spherical tensors transform in the same way under rotations, they are proportional to each other, that is[87]

$$T_q^{(k)}(\hat{\mathbf{n}}) = \left( \frac{4\pi k!}{(2k+1)!!} \right)^{1/2} Y_{kq}(\hat{\mathbf{n}}), \quad (2.71)$$

where

$$n!! = \begin{cases} n \cdot (n-2) \cdots 5 \cdot 3 \cdot 1 & \text{if } n \text{ is odd and positive} \\ n \cdot (n-2) \cdots 6 \cdot 4 \cdot 2 & \text{if } n \text{ is even and positive} \\ 1 & \text{if } n \text{ is } -1 \text{ or } 0 \end{cases} \quad (2.72)$$

From Eq. (2.71), it follows that the first-rank irreducible spherical tensor is just the modified spherical harmonics, namely

$$T_q^{(1)} = C_{1q}. \quad (2.73)$$

In quantum mechanics, operators are usually written in terms of Cartesian vectors, like the position vector  $\mathbf{r}$  and the electric dipole moment operator  $\mathbf{d}$ , and we want to know their corresponding spherical tensor operators. In such cases, the definition of the spherical tensors is not very useful and we need to find alternative ways. It turns out that the irreducible spherical tensors can be written in terms of Cartesian coordinates. For example the first-rank irreducible spherical tensor is

given by

$$T_1^{(1)} = -\frac{1}{\sqrt{2}}(\hat{X} + i\hat{Y}), \quad (2.74)$$

$$T_0^{(1)} = \hat{Z}, \quad (2.75)$$

$$T_{-1}^{(1)} = \frac{1}{\sqrt{2}}(\hat{X} - i\hat{Y}), \quad (2.76)$$

where  $\hat{X}$ ,  $\hat{Y}$ , and  $\hat{Z}$  represents the units lengths for the Cartesian coordinate system. For every Cartesian vector  $\mathbf{V}$ , there is one corresponding first-rank spherical tensor  $T^{(1)}(\mathbf{V})$ . Similar to the irreducible spherical tensor,  $T^{(1)}(\mathbf{V})$  can also be written in terms of Cartesian vectors  $\mathbf{V}$ , that is

$$T_1^{(1)}(\mathbf{V}) = -\frac{1}{\sqrt{2}}(V_X \hat{X} + iV_Y \hat{Y}), \quad (2.77)$$

$$T_0^{(1)}(\mathbf{V}) = V_Z \hat{Z}, \quad (2.78)$$

$$T_{-1}^{(1)}(\mathbf{V}) = \frac{1}{\sqrt{2}}(V_X \hat{X} - iV_Y \hat{Y}). \quad (2.79)$$

### 2.1.8 Coupling of spherical tensors

As we have seen, the spherical tensors behave like spherical harmonics. As a result, the spherical tensors couple in the same way as angular momenta. For example, two spherical tensors  $\mathbf{R}^{k_1}$  and  $\mathbf{S}^{k_2}$  can be combined to form a tensor of rank  $K$ ,

$$T_P^{(K)}(\mathbf{R}^{k_1}, \mathbf{S}^{k_2}) = \sum_{p_1, p_2} \langle k_1, p_1; k_2, p_2 | K, P \rangle T_{p_1}^{(k_1)}(\mathbf{R}) T_{p_2}^{(k_2)}(\mathbf{S}). \quad (2.80)$$

In practice, we can regard the above equation as the coupling of two angular momenta  $\mathbf{j}_1$  and  $\mathbf{j}_2$  to form  $\mathbf{j}$ . Comparing Eq. (2.46) with Eq. (2.80), we can easily see that  $j_1$  corresponds to  $k_1$ ,  $p_1$  to  $m_1$ ,  $j_2$  to  $k_2$ ,  $p_2$  to  $m_2$ ,  $j$  to  $K$ , and  $m$  to  $P$ . Similarly,  $K$  can only takes the values from  $|k_1 - k_2|$  to  $k_1 + k_2$ . We call  $T_P^{(K)}$  the tensor product of  $\mathbf{R}^{k_1}$  and  $\mathbf{S}^{k_2}$  and sometimes denote it as

$$T_P^{(K)}(\mathbf{R}^{k_1}, \mathbf{S}^{k_2}) = [\mathbf{R}^{(k_1)} \otimes \mathbf{S}^{(k_2)}]_P^{(K)}.$$

For later reference, the two most important cases of Eq. (2.80) are[87]

$$\left[ \mathbf{A}^{(k)} \otimes \mathbf{B}^{(k)} \right]_0^{(0)} = (2k+1)^{-\frac{1}{2}} \sum_q (-1)^{k-q} T_q^{(k)}(\mathbf{A}) T_{-q}^{(k)}(\mathbf{B}), \quad (2.81)$$

$$\begin{aligned} \left[ \mathbf{A}^{(1)} \otimes \mathbf{B}^{(1)} \right]_q^{(2)} &= \sum_{q_A, q_B} \langle 1, q_A; 1, q_B | 2, q \rangle T_{q_A}^{(1)}(\mathbf{A}) T_{q_B}^{(1)}(\mathbf{B}) \\ &= \sum_{q_A, q_B} (-1)^q \sqrt{5} \begin{pmatrix} 1 & 1 & 2 \\ q_A & q_B & -q \end{pmatrix} T_{q_A}^{(1)}(\mathbf{A}) T_{q_B}^{(1)}(\mathbf{B}). \end{aligned} \quad (2.82)$$

It is helpful to examine further the meaning of  $\left[ A^{(1)} \otimes B^{(1)} \right]_0^{(0)}$ . Based on Eq. (2.81)) we obtain

$$\left[ \mathbf{A}^{(1)} \otimes \mathbf{B}^{(1)} \right]_0^{(0)} = \frac{1}{\sqrt{3}} \left[ T_1^{(1)}(\mathbf{A}) T_{-1}^{(1)}(\mathbf{B}) - T_0^{(1)}(\mathbf{A}) T_0^{(1)}(\mathbf{B}) + T_{-1}^{(1)}(\mathbf{A}) T_1^{(1)}(\mathbf{B}) \right]. \quad (2.83)$$

Substituting Eqs. (2.77), (2.78) and (2.79) into the above equation gives

$$\left[ \mathbf{A}^{(1)} \otimes \mathbf{B}^{(1)} \right]_0^{(0)} = -\frac{1}{\sqrt{3}} (A_X B_X + A_Y B_Y + A_Z B_Z) = -\frac{1}{\sqrt{3}} \mathbf{A} \cdot \mathbf{B}. \quad (2.84)$$

Therefore, the rank-zero tensor product of two rank-one tensors is equivalent to the scalar product of the corresponding vectors except for a factor. Similarly, it can be shown that the tensor product of rank  $k = 1$  is related to the cross product by

$$\left[ A^{(1)} \otimes B^{(1)} \right]_q^{(k)} = (\mathbf{A} \times \mathbf{B}) \cdot \hat{\mathbf{e}}_q, \quad (2.85)$$

where

$$\begin{aligned} \hat{\mathbf{e}}_{+1} &= -\frac{1}{\sqrt{2}} (\hat{\mathbf{X}} + i\hat{\mathbf{Y}}), \\ \hat{\mathbf{e}}_0 &= \hat{\mathbf{Z}}, \\ \hat{\mathbf{e}}_{-1} &= \frac{1}{\sqrt{2}} (\hat{\mathbf{X}} - i\hat{\mathbf{Y}}). \end{aligned} \quad (2.86)$$

It is worthwhile mentioning that all the results so far assume that the spherical tensor operators are defined with respect to one specific fixed axis system. However, in practice, this assumption is usually not valid. Some tensor operators are naturally described in body-fixed coordinates, for example the molecular dipole moment operator, and other operators are more conveniently expressed in space-fixed coordinates, for instance the external field operator. This leads to the question, “How the spherical harmonics defined in the space-fixed axis system be related to those in body-fixed axis system?”. Suppose the molecule-fixed axes can be obtained by a rotation  $R$  of the space-fixed axes. Equation (2.70) will still be valid. Now, the tensor operators are all defined in the space-fixed axis system and the body-fixed axes can be obtained by rotation  $R$  of the space-fixed axes. We recall that a transformation  $S$  turns a wavefunction  $\psi$  into  $S\psi$  and turns an operator  $T$  into  $STS^{-1}$  in the transformed basis set. In the case of the rotation transformation  $D$ , the new operator in the rotated basis set is given by  $DTD^{-1} = DTD^\dagger$ . Therefore, the left hand side of Eq. (2.70) can be interpreted as new tensor operator in the rotated axis system (or body-fixed axis system), and Eq. (2.70) can be written as

$$T_b^{(k)}(\mathbf{T}) = \sum_{s=-k}^k D_{sb}^k(R) T_s^{(k)}(\mathbf{T}), \quad (2.87)$$

where  $T_b^{(k)}$  is the tensor operator defined in body-fixed axis system and  $T_s^{(k)}$  is the tensor operator defined in space-fixed axis system. Note that  $s$  labels space-fixed components and  $q$  labels body-fixed components. Replacing  $R$  with its inverse  $R^{-1}$ , using Eq. (2.37) and exchanging  $b$  and  $s$ , we obtain the inverse of Eq. (2.87), namely

$$T_s^{(k)}(\mathbf{T}) = \sum_{s=-k}^k D_{sb}^k(R)^* T_b^{(k)}(\mathbf{T}). \quad (2.88)$$

### 2.1.9 Matrix elements of tensor operators

We now consider the evaluation of matrix elements of tensor operators with respect to angular-momentum eigenstates. Given a matrix element  $\langle \eta, j, m | T_q^{(k)}(\mathbf{A}) | \eta', j', m' \rangle$  where  $\eta$  and  $\eta'$  denotes quantum numbers other than rotational quantum numbers, we can rotate the bra, operator and ket using Eq. (2.36) and Eq. (2.87), the result

must be the same. Therefore we obtain

$$\begin{aligned} & \langle \eta, j, m | T_q^{(k)}(\mathbf{A}) | \eta', j', m' \rangle \\ &= \sum_{n, n', p} D_{nm}^j(R)^* D_{pq}^k(R) D_{n'm'}^{j'}(R) \langle \eta, j, n | T_p^{(k)}(\mathbf{A}) | \eta', j', n' \rangle . \end{aligned} \quad (2.89)$$

Integrating over  $d\omega = \sin \theta d\theta d\phi d\chi$ , we obtain on the left hand side  $8\pi^2 \times$  “original term” as the matrix element is a scalar and independent of any angles, and we have on the right hand side the integral over three rotation matrices, that is

$$\int d\omega D_{nm}^{j*}(R) D_{pq}^k(R) D_{n'm'}^{j'}(R) . \quad (2.90)$$

Rewriting  $D_{nm}^{j*}(R)$  in terms of  $D_{-n-m}^j(R)$  using Eq. (2.38) and evaluating the integral using Eq. (2.57) gives the value as

$$(-1)^{n-m} 8\pi^2 \begin{pmatrix} j & k & j' \\ -m & q & m' \end{pmatrix} \begin{pmatrix} j & k & j' \\ -n & p & n' \end{pmatrix} , \quad (2.91)$$

which then used in Eq. (2.89) gives

$$\begin{aligned} & \langle \eta, j, m | T_q^{(k)}(\mathbf{A}) | \eta', j', m' \rangle \\ &= (-1)^{j-m} \begin{pmatrix} j & k & j' \\ -m & q & m' \end{pmatrix} \left\{ \sum_{n, n', p} (-1)^{j-n} \begin{pmatrix} j & k & j' \\ -n & p & n' \end{pmatrix} \right. \\ & \quad \left. \times \langle \eta, j, n | T_p^{(k)}(\mathbf{A}) | \eta', j', n' \rangle \right\} . \end{aligned} \quad (2.92)$$

The term in the braces is independent of the projection quantum numbers and we write it as  $\langle \eta, j || T_p^{(k)}(\mathbf{A}) || \eta', j' \rangle$ . Thus, we have[92]

$$\langle \eta, j, m | T_q^{(k)}(\mathbf{A}) | \eta', j', m' \rangle = (-1)^{j-m} \begin{pmatrix} j & k & j' \\ -m & q & m' \end{pmatrix} \langle \eta, j || T^{(k)}(\mathbf{A}) || \eta', j' \rangle . \quad (2.93)$$

This is the Wigner-Eckart theorem and states that the matrix element of a tensor operator in angular-momentum eigenstates can be separated into a part which describes all the angular dependence and another part which is independent of pro-

jection quantum numbers and hence of orientation.

To make the Wigner-Eckart theorem useful, we need to know how to evaluate the reduced matrix element  $\langle \eta, j || T_p^{(k)}(\mathbf{A}) || \eta', j' \rangle$ . The usual approach is to calculate the matrix element for some special cases and then derive the reduced matrix element from the result. For example, if we want to calculate the matrix elements associated with the tensor operator of the modified spherical harmonics  $C_{kq}(\theta, \phi)$ ,  $\langle l_1, m_1 | C_{kq}(\theta, \phi) | l_2, m_2 \rangle$ , we can consider the special case when  $q = 0$ ,  $m_1 = 0$  and  $m_2 = 0$ . The corresponding matrix element can be converted to an integral over a product of three spherical harmonics, that is

$$\langle l_1, 0 | C_{k0}(\theta, \phi) | l_2, 0 \rangle = \sqrt{\frac{4\pi}{2k+1}} \langle Y_{l_1 0} | Y_{k0} | Y_{l_2 0} \rangle ,$$

which gives rise to

$$[(2l_1 + 1)(2l_2 + 1)]^{1/2} \begin{pmatrix} l_1 & k & l_2 \\ 0 & 0 & 0 \end{pmatrix}^2 , \quad (2.94)$$

based on Eq. (2.59). Alternatively, from the Wigner-Eckart theorem we have

$$\langle l_1, 0 | C_{k0}(\theta, \phi) | l_2, 0 \rangle = (-1)^{l_1} \begin{pmatrix} l_1 & k & l_2 \\ 0 & 0 & 0 \end{pmatrix} \langle l_1 || C^{(k)} || l_2 \rangle . \quad (2.95)$$

Comparing Eq. (2.94) with Eq. (2.95) gives

$$\langle l_1 || C^{(k)} || l_2 \rangle = (-1)^{l_1} [(2l_1 + 1)(2l_2 + 1)]^{1/2} \begin{pmatrix} l_1 & k & l_2 \\ 0 & 0 & 0 \end{pmatrix} . \quad (2.96)$$

From this reduced matrix element, any matrix elements can be calculated using the Wigner-Eckart theorem, so that Eq. (2.93) gives

$$\begin{aligned} \langle l_1, m_1 | C_{kq}(\theta, \phi) | l_2, m_2 \rangle &= (-1)^{m_1} [(2l_1 + 1)(2l_2 + 1)]^{1/2} \begin{pmatrix} l_1 & k & l_2 \\ 0 & 0 & 0 \end{pmatrix} \\ &\times \begin{pmatrix} l_1 & k & l_2 \\ -m_1 & q & m_2 \end{pmatrix} . \end{aligned} \quad (2.97)$$

## 2.2 Application of angular momentum theory

We have reviewed the theory of angular momentum in Section 2.1. To lay the foundation for later chapters, we apply the theory of angular momentum to solve some problems closely related to the research in this thesis.

### 2.2.1 Diatomic molecule in external field

The first problem involves calculating the dressed rotational states of molecules in an external field. For simplicity, we only consider  ${}^1\Sigma$  molecules with a permanent dipole momentum and no spins. Since only rotational states are relevant here, the total Hamiltonian can be written as

$$H = H_{\text{rot}} + H_I , \quad (2.98)$$

where  $H_{\text{rot}}$  describes the rotational states of the system without any external field and  $H_I$  describes the interaction with the external field. For  ${}^1\Sigma$  molecules,

$$H_{\text{rot}} = B\hat{N}^2 , \quad (2.99)$$

where  $\hat{N}$  is the rotational angular momentum operator and  $B$  is the rotational constant obtained by averaging over all quantum states other than rotational states. To obtain the eigenstate of the total Hamiltonian, we can use the bare rotational states  $|N, M\rangle$  as a basis set. We want to know the matrix representation of  $H$  and calculate its eigenvalues and eigenvectors. The rotational part of the Hamiltonian only contributes to the diagonal part of the matrix and is given by

$$\langle N, M | H_{\text{rot}} | N', M' \rangle = \delta_{N,N'} \delta_{M,M'} B N(N+1) . \quad (2.100)$$

The evaluation of the contribution from the interaction part is more involved and we discuss it in the following two cases.

First, consider a static electric (DC) field for which

$$H_I = -\mathbf{d} \cdot \mathbf{E} = d\mathcal{E}_{\text{DC}} \cos \theta , \quad (2.101)$$

where  $\mathbf{d}$  is the permanent dipole,  $\mathbf{E}$  is the external field, and  $\theta$  is the angle between

**d** and **E**. To evaluate the corresponding matrix elements, we need to calculate  $\langle N, M | \cos \theta | N', M' \rangle$ . Because  $\cos \theta$  can be expressed in terms of a spherical harmonic

$$\cos \theta = \sqrt{\frac{4\pi}{3}} Y_{10}(\theta, \phi) = C_{10} , \quad (2.102)$$

Eq. (2.97) gives

$$\begin{aligned} \langle N, M | H_I | N', M' \rangle &= Ed \langle N, M | C_{10} | N', M' \rangle \\ &= (-1)^M d \mathcal{E}_{DC} \sqrt{(2N+1)(2N'+1)} \begin{pmatrix} N & 1 & N' \\ 0 & 0 & 0 \end{pmatrix} \begin{pmatrix} N & 1 & N' \\ -M & 0 & M' \end{pmatrix} . \end{aligned} \quad (2.103)$$

Second, we consider a laser (AC) field which is off-resonant with any vibrational or electronic states of the molecule. The strength of the AC field is given by

$$\mathcal{E}_{AC}(t) = \mathcal{E}_{AC,0} \cos(\omega t) , \quad (2.104)$$

where  $\omega$  is the frequency of the laser field. In this case, the interaction Hamiltonian is given by [93]

$$H_I(t) = -d \mathcal{E}_{AC}(t) \cos \theta_{AC} - \frac{1}{2} \mathcal{E}_{AC}^2(t) (\alpha_{||} \cos^2 \theta_{AC} + \alpha_{\perp} \sin^2 \theta_{AC}) , \quad (2.105)$$

where  $\theta_{AC}$  is the angle between the dipole moment of the molecule and the AC field, and  $\alpha_{||}$  and  $\alpha_{\perp}$  are the parallel and perpendicular polarizabilities of the molecule, respectively. The interaction Hamiltonian is a function of time, and changes very fast as  $\mathcal{E}_{AC}(t)$  oscillates at optical frequency. During one period of rotational motion of the molecule, the interaction Hamiltonian has oscillated many times. Therefore, we can average  $H_I(t)$  over one oscillation period of the light and obtain the effective interaction Hamiltonian

$$H_I = -\frac{1}{4} \mathcal{E}_{AC,0}^2 (\Delta \alpha \cos^2 \theta_{AC} + \alpha_{\perp}) , \quad (2.106)$$

where  $\Delta \alpha = \alpha_{||} - \alpha_{\perp}$ . As we did in the case of the DC field, to calculate the matrix elements of the interaction Hamiltonian, we rewrite  $\cos^2 \theta_{AC}$  in terms of spheri-

cal harmonics and express the matrix elements in terms of those of the modified spherical harmonics. Doing this and using Eq. (2.97) gives

$$\begin{aligned}
& \langle N, M | H_I | N', M' \rangle \\
&= -\frac{1}{4} \mathcal{E}_{AC,0}^2 \langle N, M | (\Delta\alpha \cos^2 \theta_{AC} + \alpha_{\perp}) | N', M' \rangle \\
&= -\frac{1}{4} \mathcal{E}_{AC,0}^2 \langle N, M | \left[ \Delta\alpha \left( \frac{2}{3} C_{20} + \frac{1}{3} \right) + \alpha_{\perp} \right] | N', M' \rangle \\
&= -\frac{\mathcal{E}_{AC,0}^2}{12} \left[ (-1)^M 2\Delta\alpha \sqrt{(2N+1)(2N'+1)} \begin{pmatrix} N & 2 & N' \\ 0 & 0 & 0 \end{pmatrix} \begin{pmatrix} N & 2 & N' \\ -M & 0 & M' \end{pmatrix} \right. \\
&\quad \left. + (\Delta\alpha + 3\alpha_{\perp}) \delta_{N,N'} \delta_{M,M'} \right]. \tag{2.107}
\end{aligned}$$

### 2.2.2 Dipole-dipole interaction

The second problem we consider calculates the matrix elements of the dipole-dipole interaction between two molecules by using the theory of angular momentum. Consider two molecules A and B, in rotational states  $|N_A M_A\rangle$  and  $|N_B M_B\rangle$ , respectively. In free space, one molecule can rotate around the other and the state of the two molecules can be expressed as

$$|N_A M_A\rangle |N_B M_B\rangle |lm\rangle ,$$

where  $l$  is the orbital angular momentum of A around B. However, in the solid state or optical lattices, the position of molecules are fixed to a good approximation, and they cannot rotate around each other. In this case, their states are given by  $|N_A M_A\rangle |N_B M_B\rangle$  if there is no interaction between them. If we consider the interaction between the two molecules, we can always use  $|N_A M_A\rangle |N_B M_B\rangle$  as basis set. By expanding the Hamiltonian in this basis set and diagonalizing it, we can get the new eigenstates.

As the first step, we have to know the interaction between the two molecules. If A has a permanent dipole  $\mathbf{d}_A$  and B has a permanent dipole  $\mathbf{d}_B$  and the vector connecting their centers of mass is  $\mathbf{R}$ , then the dipole-dipole interaction between A

and  $\mathbf{B}$  is given by

$$\hat{V}_{dd} = \left( \frac{1}{R^3} \right) [\mathbf{d}_A \cdot \mathbf{d}_B - 3(\mathbf{d}_A \cdot \hat{\mathbf{R}})(\mathbf{d}_B \cdot \hat{\mathbf{R}})] . \quad (2.108)$$

Here we only consider the dipole moment. There also exists quadrupole, octopole, and higher order moments, but their magnitudes are so small that we can ignore them at large distances, say, 400 nm. Our final goal is to evaluate the matrix element  $\langle N_A M_A | \langle N_B M_B | \hat{V}_{dd} | N'_A M'_A \rangle | N'_B M'_B \rangle$  by rewriting  $\hat{V}_{dd}$  in terms of spherical harmonics, and then in terms of 3-j symbols which can be calculated numerically.

The first term in the square bracket of Eq. (2.108), can be expressed in terms of a tensor product using Eq. (2.84), that is

$$\mathbf{d}_A \cdot \mathbf{d}_B = -\sqrt{3} \left[ \mathbf{d}_A^{(1)} \otimes \mathbf{d}_B^{(1)} \right]_0^{(0)} . \quad (2.109)$$

The second term in the square bracket of Eq. (2.108) is the product of two scalars  $(\mathbf{d}_A \cdot \hat{\mathbf{R}})(\mathbf{d}_B \cdot \hat{\mathbf{R}})$ , which we consider as a special case of the dot product of two vectors in one-dimensional space. So that according to Eq. (2.109), we can write

$$(\mathbf{d}_A \cdot \hat{\mathbf{R}})(\mathbf{d}_B \cdot \hat{\mathbf{R}}) = 3 \left[ \left[ \mathbf{d}_A^{(1)} \otimes \hat{\mathbf{R}}^{(1)} \right]_0^{(0)} \otimes \left[ \mathbf{d}_B^{(1)} \otimes \hat{\mathbf{R}}^{(1)} \right]_0^{(0)} \right]^{(0)} . \quad (2.110)$$

There is a simple understanding of the above equation: an angular momentum  $\mathbf{d}_A$  with  $j_1 = 1$  couples another angular momentum  $\hat{\mathbf{R}}$  with  $j_2 = 1$  to give rise to a new angular momentum, and an angular momentum  $\mathbf{d}_B$  with  $j_3 = 1$  couples with another angular momentum  $\hat{\mathbf{R}}$  with  $j_4 = 1$  to give rise to another new angular momentum, and then these two new angular momenta couple with each other.

The form of Eq. (2.110) is not convenient for calculations. We know only  $\mathbf{d}_A$  and  $\mathbf{d}_B$  operate on the rotational states  $|N_A, M_A\rangle |N_B, M_B\rangle$ , but they are coupled with  $\hat{\mathbf{R}}$ , which makes the calculation of the matrix element associated with Eq. (2.110) cumbersome. Therefore, it is necessary to regroup these operators so that the dipole operators are separated from the position operators. Let us expand  $\left[ \left[ \mathbf{d}_A^{(1)} \otimes \hat{\mathbf{R}}^{(1)} \right]_0^{(0)} \otimes \left[ \mathbf{d}_B^{(1)} \otimes \hat{\mathbf{R}}^{(1)} \right]_0^{(0)} \right]^{(0)}$  in terms of another coupling scheme, where  $\mathbf{d}_A$  couples with  $\mathbf{d}_B$  and  $\hat{\mathbf{R}}$  couples with  $\hat{\mathbf{R}}$ . This involves the definition of

$9-j$  symbols. Based on Eq. (2.51) and Eq. (2.52) we have

$$(\mathbf{d}_A \cdot \hat{\mathbf{R}})(\mathbf{d}_B \cdot \hat{\mathbf{R}}) = 3 \sum_k (2k+1) \left\{ \begin{array}{ccc} 1 & 1 & k \\ 1 & 1 & k \\ 0 & 0 & 0 \end{array} \right\} \left[ [\mathbf{d}_A^{(1)} \otimes \mathbf{d}_B^{(1)}]^{(k)} \otimes [\hat{\mathbf{R}}^{(1)} \otimes \hat{\mathbf{R}}^{(1)}]^{(k)} \right]_0^{(0)}. \quad (2.111)$$

The  $9-j$  symbols in the above equation can be expressed in terms of  $6-j$  symbols (related to the coupling of 3 angular momenta). In the special case where the final angular momentum  $j_9 = 0$ , we have[87]

$$\left\{ \begin{array}{ccc} j_1 & j_2 & j_3 \\ j_4 & j_5 & j_6 \\ j_7 & j_8 & j_9 \end{array} \right\} = (-1)^{j_2+j_3+j_4+j_7} [(2j_3+1)(2j_7+1)]^{-\frac{1}{2}} \times \left\{ \begin{array}{ccc} j_1 & j_2 & j_3 \\ j_5 & j_4 & j_7 \end{array} \right\} \delta_{j_3 j_6} \delta_{j_7 j_8}, \quad (2.112)$$

so that

$$\left\{ \begin{array}{ccc} 1 & 1 & k \\ 1 & 1 & k \\ 0 & 0 & 0 \end{array} \right\} = (-1)^{k+2} (2k+1)^{-\frac{1}{2}} \left\{ \begin{array}{ccc} 1 & 1 & k \\ 1 & 1 & 0 \end{array} \right\} = (-1)^{k+2} (2k+1)^{-\frac{1}{2}} \left\{ \begin{array}{cc} \frac{1}{3}(-1)^{-k} & 0 \leq k \leq 2 \\ 0 & \text{otherwise} \end{array} \right. . \quad (2.113)$$

Because  $k$  results from the coupling of  $j_1 = 1$  and  $j_2 = 1$ , it is in the range of  $|j_1 - j_2|, \dots, |j_1 + j_2|$ , and the above equation can be simplified as

$$\left\{ \begin{array}{ccc} 1 & 1 & k \\ 1 & 1 & k \\ 0 & 0 & 0 \end{array} \right\} = \frac{(2k+1)^{-\frac{1}{2}}}{3}. \quad (2.114)$$

Substituting Eq. (2.114) into Eq. (2.111) and using Eq. (2.81) gives

$$(\mathbf{d}_A \cdot \hat{\mathbf{R}})(\mathbf{d}_B \cdot \hat{\mathbf{R}}) = \sum_{k=0,1,2} \sum_q (-1)^{k-q} \left[ \mathbf{d}_A^{(1)} \otimes \mathbf{d}_B^{(1)} \right]_q^{(k)} \left[ \hat{\mathbf{R}}^{(1)} \otimes \hat{\mathbf{R}}^{(1)} \right]_{-q}^{(k)}. \quad (2.115)$$

Since the tensor product of rank 1 is related to the cross product (see Eq. (2.85)),  $\left[ \hat{\mathbf{R}}^{(1)} \otimes \hat{\mathbf{R}}^{(1)} \right]_{-q}^{(k=1)}$  is associated with  $\hat{\mathbf{R}} \times \hat{\mathbf{R}} = 0$  and is zero. So that Eq. (2.115) simplifies to

$$\begin{aligned} (\mathbf{d}_A \cdot \hat{\mathbf{R}})(\mathbf{d}_B \cdot \hat{\mathbf{R}}) &= \left[ \mathbf{d}_A^{(1)} \otimes \mathbf{d}_B^{(1)} \right]_0^{(0)} \left[ \hat{\mathbf{R}}^{(1)} \otimes \hat{\mathbf{R}}^{(1)} \right]_0^{(0)} \\ &\quad + \sum_{|q|=0,1,2} (-1)^q \left[ \mathbf{d}_A^{(1)} \otimes \mathbf{d}_B^{(1)} \right]_q^{(2)} \left[ \hat{\mathbf{R}}^{(1)} \otimes \hat{\mathbf{R}}^{(1)} \right]_{-q}^{(2)} \\ &= \left( -\frac{1}{\sqrt{3}} \mathbf{d}_A \cdot \mathbf{d}_B \right) \left( -\frac{1}{\sqrt{3}} \hat{\mathbf{R}} \cdot \hat{\mathbf{R}} \right) \\ &\quad + \sum_q (-1)^q \left[ \mathbf{d}_A^{(1)} \otimes \mathbf{d}_B^{(1)} \right]_q^{(2)} \left[ \hat{\mathbf{R}}^{(1)} \otimes \hat{\mathbf{R}}^{(1)} \right]_{-q}^{(2)} \\ &= \frac{\mathbf{d}_A \cdot \mathbf{d}_B}{3} + \sum_q (-1)^q \left[ \mathbf{d}_A^{(1)} \otimes \mathbf{d}_B^{(1)} \right]_q^{(2)} \left[ \hat{\mathbf{R}}^{(1)} \otimes \hat{\mathbf{R}}^{(1)} \right]_{-q}^{(2)}. \end{aligned} \quad (2.116)$$

Substituting Eq. (2.116) into Eq. (2.108) yields

$$\hat{V}_{dd}(\mathbf{R}) = \frac{-3}{R^3} \sum_{q=-2}^2 (-1)^q \left[ \mathbf{d}_A^{(1)} \otimes \mathbf{d}_B^{(1)} \right]_q^{(2)} \left[ \hat{\mathbf{R}}^{(1)} \otimes \hat{\mathbf{R}}^{(1)} \right]_{-q}^{(2)}. \quad (2.117)$$

In the above equation,  $\hat{\mathbf{R}}$  can be viewed as a first-order irreducible spherical tensor, therefore the contraction of two  $\hat{\mathbf{R}}$  gives rise to the second-order irreducible spherical tensor

$$\left[ \hat{\mathbf{R}}^{(1)} \otimes \hat{\mathbf{R}}^{(1)} \right]_{-q}^{(2)} = T_{-q}^{(2)}(\hat{\mathbf{R}}). \quad (2.118)$$

Based on Eq. (2.71) we obtain

$$\left[ \hat{\mathbf{R}}^{(1)} \otimes \hat{\mathbf{R}}^{(1)} \right]_{-q}^{(2)} = \sqrt{\frac{8\pi}{15}} Y_{2-q}(\theta_R, \phi_R), \quad (2.119)$$

where  $\theta_R$  and  $\phi_R$  describe the orientation of  $\hat{\mathbf{R}}$  in the space-fixed axis system, and

then the dipole-dipole operator becomes:

$$\hat{V}_{dd}(\mathbf{R}) = -2\sqrt{\frac{6\pi}{5}} \frac{1}{R^3} \sum_{q=-2}^2 (-1)^q Y_{2-q}(\theta_R, \phi_R) \left[ \mathbf{d}_A^{(1)} \otimes \mathbf{d}_B^{(1)} \right]_q^{(2)}. \quad (2.120)$$

To calculate the matrix elements of the dipolar operator, we now only need to consider the tensor product  $\left[ \mathbf{d}_A^{(1)} \otimes \mathbf{d}_B^{(1)} \right]_q^{(2)}$ . Using Eq. (2.82), we can express the tensor product in terms of the tensor components in some axis system

$$\left[ \mathbf{d}_A^{(1)} \otimes \mathbf{d}_B^{(1)} \right]_q^{(2)} = \sum_{q_A, q_B} (-1)^q \sqrt{5} \begin{pmatrix} 1 & 1 & 2 \\ q_A & q_B & -q \end{pmatrix} T_{q_A}^{(1)}(\mathbf{d}_A) T_{q_B}^{(1)}(\mathbf{d}_B). \quad (2.121)$$

The rotational states  $|N_A, M_A\rangle |N_B, M_B\rangle$  are defined in the space-fixed axis system, so only tensor operators defined in the same axis system can operate on them directly. Therefore, for the convenience of calculation, the tensor components in Eq. (2.121) should also be in the space-fixed axis system. However, the dipole moment of a molecule is most conveniently expressed in the body-fixed axis system. In the case of a diatomic polar molecule, we can choose the body-fixed  $z$ -axis to be in the same direction as the dipole moment. So that the only nonzero body-fixed  $b$  component is given by

$$T_{b=0}^{(1)}(\mathbf{d}) = d\hat{z}, \quad (2.122)$$

where  $d$  is the magnitude of the dipole moment. Now the problem is obtaining the space-fixed dipole moment component from the body-fixed component. From Eq. (2.88), we have

$$\begin{aligned} T_s^{(1)}(\mathbf{d}) &= \sum_{b=-1}^1 D_{sb}^{1*} T_b^{(1)}(\mathbf{d}) \\ &= D_{s0}^{1*} d \\ &= d_0 C_{1s}, \end{aligned} \quad (2.123)$$

where  $T_s^{(1)}$  is the tensor component in space-fixed axis system and the last equality

comes from Eq. (2.39). Substituting Eq. (2.123) into Eq. (2.121) then gives

$$\left[ \mathbf{d}_A^{(1)} \otimes \mathbf{d}_B^{(1)} \right]_s^{(2)} = \sum_{s_A, s_B} (-1)^s \sqrt{5} d_A d_B \begin{pmatrix} 1 & 1 & 2 \\ s_A & s_B & -s \end{pmatrix} C_{1s_A} C_{1s_B}. \quad (2.124)$$

Using Eq. (2.97), the corresponding matrix elements are given by

$$\begin{aligned} & \langle N_A, M_A | \langle N_B, M_B | \left[ \mathbf{d}_A^{(1)} \otimes \mathbf{d}_B^{(1)} \right]_s^{(2)} | N'_A, M'_A \rangle | N'_B, M'_B \rangle \\ &= (-1)^{s+M_A+M_B} d_A d_B \sqrt{5} \sqrt{(2N_A+1)(2N_B+1)(2N'_A+1)(2N'_B+1)} \\ & \quad \times \begin{pmatrix} N_A & 1 & N'_A \\ 0 & 0 & 0 \end{pmatrix} \begin{pmatrix} N_B & 1 & N'_B \\ 0 & 0 & 0 \end{pmatrix} \\ & \quad \times \sum_{s_A, s_B} \begin{pmatrix} N_A & 1 & N'_A \\ -M_A & s_A & M'_A \end{pmatrix} \begin{pmatrix} N_B & 1 & N'_B \\ -M_B & s_B & M'_B \end{pmatrix} \begin{pmatrix} 1 & 1 & 2 \\ s_A & s_B & -s \end{pmatrix}. \end{aligned} \quad (2.125)$$

Finally, after considering every possible value of  $q$  in Eq. (2.120) and making use of Eq. (2.120), we arrive at

$$\begin{aligned} & \langle N_A, M_A | \langle N_B, M_B | \hat{V}_{dd}(\mathbf{R}) | N'_A, M'_A \rangle | N'_B, M'_B \rangle \\ &= -\frac{F}{2R^3} \left\{ 3 \sin^2 \theta_R e^{-2i\phi_R} D_-^A D_-^B - 6 \sin \theta_R \cos \theta_R e^{-i\phi_R} [D_0^A D_-^B + D_-^A D_0^B] \right. \\ & \quad + 3 \sin^2 \theta_R e^{2i\phi_R} D_+^A D_+^B + 6 \sin \theta_R \cos \theta_R e^{i\phi_R} [D_0^A D_+^B + D_+^A D_0^B] \\ & \quad \left. + \sqrt{6}(3 \cos^2 \theta_R - 1) [D_+^A D_-^B + D_-^A D_+^B + D_0^A D_0^B] \right\}, \end{aligned} \quad (2.126)$$

where

$$\begin{aligned} F &= (-1)^{M_A+M_B} d_A d_B \sqrt{5} \sqrt{(2N_A+1)(2N_B+1)(2N'_A+1)(2N'_B+1)} \\ & \quad \times \begin{pmatrix} N_A & 1 & N'_A \\ 0 & 0 & 0 \end{pmatrix} \begin{pmatrix} N_B & 1 & N'_B \\ 0 & 0 & 0 \end{pmatrix}, \end{aligned} \quad (2.127)$$

and  $D_{\pm,0}^A D_{\pm,0}^B$  are defined using

$$f_{AB}(s_A, s_B) = \begin{pmatrix} N_A & 1 & N'_A \\ -M_A & s_A & M'_A \end{pmatrix} \begin{pmatrix} N_B & 1 & N'_B \\ -M_B & s_B & M'_B \end{pmatrix} \begin{pmatrix} 1 & 1 & 2 \\ s_A & s_B & -s \end{pmatrix}, \quad (2.128)$$

in the following way

$$\begin{aligned} D_+^A D_+^B &= f_{AB}(1,1), \\ D_+^A D_0^B &= f_{AB}(1,0), \\ D_+^A D_-^B &= f_{AB}(1,-1), \\ D_0^A D_-^B &= f_{AB}(1,-1), \\ D_0^A D_+^B &= f_{AB}(0,1), \\ D_0^A D_0^B &= f_{AB}(0,0), \\ D_0^A D_-^B &= f_{AB}(0,-1), \\ D_-^A D_+^B &= f_{AB}(-1,1), \\ D_-^A D_0^B &= f_{AB}(-1,0), \\ D_-^A D_-^B &= f_{AB}(-1,-1). \end{aligned} \quad (2.129)$$

The factor  $F$  describes the selection rule of rotational quantum number  $N$  for the dipole-dipole interaction, which says that only two consecutive rotational levels are coupled.  $D_{\pm,0}^A D_{\pm,0}^B$  describes the change of the projection quantum number  $M$  by the dipole-dipole interaction. It can be easily seen from Eq. (2.128) that  $D_X^A D_Y^B$  is nonzero only if the projection quantum numbers change in a certain way. For example,  $D_+^A D_+^B$  is nonzero if only  $M_A - M'_A = 1$  and  $M_B - M'_B = 1$ .

### 2.3 Introduction to excitons in molecular crystals

In this section, we aim to give a very brief introduction to excitons. For simplicity, we consider a 1D molecular crystal with every lattice site occupied by one

molecule. The Hamiltonian is given by

$$H = \sum_n H_n + \frac{1}{2} \sum_n \sum_{m \neq n} V_{nm}, \quad (2.130)$$

where  $n$  is the molecule index,  $H_n$  is the Hamiltonian for an isolated molecule  $n$ , and  $V_{nm}$  describes the interaction between the two molecules labeled  $n$  and  $m$ . The extension to 2D and 3D molecular arrays is straightforward: one only needs to replace the number index  $n$  by a vector index  $\mathbf{n}$  in the 2D or 3D dimensional space.

### 2.3.1 Commutation relation

In a molecular crystal, there are a large number of identical interacting molecules. To study the excited states of the system, it is suitable to use the second-quantization formalism which is convenient for describing many-particle systems.

The second-quantization representation uses a basis that describes the number of particles occupying each state in a complete orthonormal set of single-particle states. Assuming the distance between any two molecules is large such that their wavefunctions hardly overlap, we can choose the single-particle states to be the eigenfunctions  $\psi_n^f$  of the isolated molecule Hamiltonian  $H_n$ . The basis set for the second-quantization formalism is then given by the wavefunction that describes a crystal formed by non-interacting molecules, that is

$$|N_{1f'} N_{2f''} \dots N_{nf'} \dots \rangle,$$

where  $N_{nf}$  represents the occupation number of state  $f$  in molecule  $n$  and it is either 0 or 1. Accordingly, the occupation number operator is defined as

$$\hat{N}_{nf} |...N_{nf} \dots \rangle = N_{nf} |...N_{nf} \dots \rangle. \quad (2.131)$$

For the crystal formed by interacting molecules, its eigenstates can be expressed in terms of linear combinations of the above basis set.

The molecule at site  $n$  must be in some state, therefore the occupation operators

of all states sum up to the identity operator:

$$\sum_f \hat{N}_{nf} = 1 , \quad (2.132)$$

where  $f$  denotes any (ground or excited) states of molecule  $n$ . It is convenient to introduce two operators  $b_{nf}^\dagger$  and  $b_{nf}$  associated with molecule  $n$  and state  $f$  such that

$$\begin{aligned} b_{nf}^\dagger |...N_{nf}...\rangle &= (1 - N_{nf}) |...(N_{nf} + 1)... \rangle , \\ b_{nf} |...N_{nf}...\rangle &= N_{nf} |...(N_{nf} - 1)... \rangle , \end{aligned} \quad (2.133)$$

and express the occupation number operator as the product of these two operators,

$$\hat{N}_{nf} = b_{nf}^\dagger b_{nf} . \quad (2.134)$$

The physical meaning of the two operators is clear:  $b_{nf}^\dagger$  creates the state  $f$  in molecule  $n$  and  $b_{nf}$  destroys the state  $f$  in molecule  $n$ . It follows from Eq. (2.133) that the commutation relation of the  $b$  operators for the same energy level of the same molecule is given by

$$\begin{aligned} b_{nf} b_{nf}^\dagger &+ b_{nf}^\dagger b_{nf} = 1 , \\ b_{nf} b_{nf} &= b_{nf}^\dagger b_{nf}^\dagger = 0 . \end{aligned} \quad (2.135)$$

Because an operator for a specific molecule  $n$  and state  $f$  does not operate on other molecules and other states, any two operators that correspond to different molecules  $n$  and  $m$  or different states  $f$  and  $f'$  commute.

The  $b$  operators defined above are not very convenient as they are associated with both the ground and excited states. Since we want to focus on the excited states, we define the so-called excitation creation and annihilation operators as

$$P_{ne}^\dagger = b_{ne}^\dagger b_{ng} , \quad P_{ne} = b_{ng}^\dagger b_{ne} , \quad (2.136)$$

where  $g$  denotes the ground state and  $e$  represents any excited state. Based on the physical meaning of  $b_{nf}^\dagger$  and  $b_{nf}$ , it is clear that  $P_{ne}^\dagger$  creates an excited state from the

vacuum state  $|0\rangle$  and  $P_{ne}$  does the reverse. Making use of Eq. (2.135), we obtain from the above definitions that

$$\begin{aligned} P_{ne}^\dagger P_{ne} &= b_{ne}^\dagger b_{ng} b_{ng}^\dagger b_{ne} \\ &= b_{ne}^\dagger (1 - b_{ng}^\dagger b_{ng}) b_{ne} \\ &= \hat{N}_{ne}, \end{aligned} \quad (2.137)$$

$$\begin{aligned} P_{ne} P_{ne}^\dagger &= b_{ng}^\dagger b_{ne} b_{ne}^\dagger b_{ng} \\ &= b_{ng}^\dagger (1 - b_{ne}^\dagger b_{ne}) b_{ng} \\ &= \hat{N}_{ng}. \end{aligned} \quad (2.138)$$

Note that the above derivations are valid because  $b_{ng} b_{ne}$  and  $b_{ne} b_{ng}$  produce zero when operating on any states. Based on Eq. (2.132), the subtraction and addition of Eq. (2.137) and Eq. (2.138) yield:

$$P_{ne} P_{ne}^\dagger - P_{ne}^\dagger P_{ne} = 1 - \sum_{f \neq g} \hat{N}_{nf} - \hat{N}_{ne}, \quad (2.139)$$

$$P_{ne} P_{ne}^\dagger + P_{ne}^\dagger P_{ne} = 1 - \sum_{f \neq g} \hat{N}_{nf} + \hat{N}_{ne}. \quad (2.140)$$

Because  $P_{nf}$  and  $P_{nf}^\dagger$  don't operate on a different molecule  $n'$ , any exciton operators corresponding to different molecules or different states commute with each other, so that Eq. (2.139) can be extended as

$$P_{ne} P_{n'e'}^\dagger - P_{n'e'}^\dagger P_{ne} = \delta_{nn'} \delta_{ee'} \left( 1 - \sum_{f \neq g} \hat{N}_{nf} - \hat{N}_{ne} \right). \quad (2.141)$$

Eq. (2.140) and Eq. (2.141) describe the exact statistics of excitons. Unfortunately, it is cumbersome to take into account the exact statistics in most cases. Usually, only a small number of molecules in a crystal is excited, so the following inequality

$$\langle N_{ne} \rangle \ll 1 \quad (2.142)$$

holds for any excited state  $e$ . This means we can ignore the operators  $\hat{N}_{ne}$  in prac-

tice. However, we cannot ignore all  $\hat{N}_{ne}$  in both Eq. (2.139) and Eq. (2.140) as it will lead to contradictory results, that is

$$P_{ne}P_{ne}^\dagger - P_{ne}^\dagger P_{ne} = 1 , \quad (2.143)$$

which describes two bosons at the same site, and

$$P_{ne}P_{ne}^\dagger + P_{ne}^\dagger P_{ne} = 1 , \quad (2.144)$$

which describes two fermions at the same site. The above two equations cannot be satisfied at the same time, so we have to choose either one of them. Considering the fact that two excitations cannot reside at the same site as a molecule cannot be excited twice, it seems more reasonable to choose Eq. (2.144) to be valid. In addition, in the Heitler-London approximation where only the ground and first excited states are considered, Eq. (2.144) becomes exact as  $\hat{N}_{ng} + \hat{N}_{ne} = 1$ . As the Heitler-London approximation is usually a good approximation, it also makes sense to choose Eq. (2.144). Therefore, we usually approximate the exact statistics of Eq. (2.140) and Eq. (2.141) by the following commutation relations:

$$P_{ne}P_{ne}^\dagger + P_{ne}^\dagger P_{ne} = 1 , \quad (2.145)$$

$$P_{n'e'}P_{ne}^\dagger - P_{n'e'}^\dagger P_{ne} = 0 \quad \text{for } n \neq n' \text{ or } e \neq e' . \quad (2.146)$$

This is called the Pauli commutation relation as Eq. (2.145) looks like the commutation relation for fermions and Eq. (2.146) looks like the commutation relation for bosons. For the convenience of calculations, the commutation relation is rewritten as

$$\begin{aligned} \{P_{ne}, P_{me}^\dagger\} &= \delta_{m,n} + (1 - \delta_{m,n})2P_{me}^\dagger P_{ne} , \\ [P_{ne}, P_{me}] &= [P_{ne}^\dagger, P_{me}^\dagger] = 0 , \\ [P_{ne}, P_{ne'}] &= [P_{ne}^\dagger, P_{ne'}^\dagger] = 0 , \\ P_{ne}P_{ne} &= P_{ne}^\dagger P_{ne}^\dagger = 0 , \end{aligned} \quad (2.147)$$

where  $n$  and  $m$ ,  $e$  and  $e'$  are assumed to be different,  $\{A, B\} = AB + BA$ , and  $[A, B] =$

$AB - BA$ .

### 2.3.2 Exciton Hamiltonian in second quantization

The Hamiltonian in Eq. (2.130) can be rewritten in terms of the exciton creation and annihilation operators. Here, we first derive the Hamiltonian in the two-level approximation and then give the Hamiltonian for the most general case.

In the first step, we express the Hamiltonian in terms of the  $b$  operators. The result is[87]

$$H = \sum_i \epsilon_i b_{if}^\dagger b_{if} + \frac{1}{2} \sum_{i,j \neq i} \sum_{f,f',l,l'} b_{if'}^\dagger b_{jl'}^\dagger b_{if} b_{jl} \langle f' l' | V_{ij} | f l \rangle , \quad (2.148)$$

where  $i$  and  $j$  are site indices,  $f, f', l$  and  $l'$  represent any molecular state, and  $\langle f' l' | V_{ij} | f l \rangle$  is a shorthand for  $\langle f' |_i \langle l' |_j V_{ij} | f \rangle_i | l \rangle_j$ .

Now we consider the two-level approximation where each molecule has only two energy levels: the ground state  $g$  and one excited state  $e$  such that  $f, f', l$  and  $l'$  in Eq. (2.148) can only take  $g$  or  $e$ . Making use of the definitions of exciton creation and annihilation operators(Eq. (2.136)), we can easily show that Eq. (2.148) can be written as

$$\begin{aligned} H = & \sum_i \left( \epsilon_g b_{ig}^\dagger b_{ig} + \epsilon_e b_{ie}^\dagger b_{ie} \right) + \sum_{i,j \neq i} \left[ \frac{1}{2} b_{ig}^\dagger b_{ig} b_{jg}^\dagger b_{jg} \langle gg | V_{ij} | gg \rangle \right. \\ & + \left( P_{ie}^\dagger + P_{ie} \right) b_{jg}^\dagger b_{jg} \langle eg | V_{ij} | gg \rangle + P_{ie}^\dagger P_{je}^\dagger \langle ee | V_{ij} | gg \rangle \\ & + b_{ie}^\dagger b_{ie} b_{jg}^\dagger b_{jg} \langle eg | V_{ij} | eg \rangle + P_{ie}^\dagger P_{je} \langle eg | V_{ij} | ge \rangle \\ & + b_{ie}^\dagger b_{ie} \left( P_{je}^\dagger + P_{je} \right) \langle eg | V_{ij} | ee \rangle \\ & \left. + \frac{1}{2} b_{ie}^\dagger b_{ie} b_{je}^\dagger b_{je} \langle ee | V_{ij} | ee \rangle \right] . \end{aligned} \quad (2.149)$$

There are terms like  $b_{ig}^\dagger b_{ig}$  and  $b_{ie}^\dagger b_{ie}$  in the above equation. We want to get rid of those terms. Noticing that

$$b_{ie}^\dagger b_{ie} = P_{ie}^\dagger P_{ie} = \hat{N}_{ie} , \quad (2.150)$$

and

$$b_{ig}^\dagger b_{ig} = \hat{N}_{ig} = 1 - \hat{N}_{ie} = 1 - P_{ie}^\dagger P_{ie} , \quad (2.151)$$

we can rewrite the Hamiltonian as

$$H = H_0 + H_1 + H_2 + H_3 + H_4 + H_5 + H_6 , \quad (2.152)$$

where

$$H_0 = \epsilon_g N_{\text{mol}} + \frac{1}{2} \sum_{i,j \neq i} \langle gg | V_{ij} | gg \rangle , \quad (2.153)$$

$$H_1 = \sum_i \left\{ (\epsilon_e - \epsilon_g) + \sum_{j \neq i} \left[ \langle eg | V_{ij} | eg \rangle - \langle gg | V_{ij} | gg \rangle \right] \right\} P_{ie}^\dagger P_{ie} , \quad (2.154)$$

$$H_2 = \sum_{i,j \neq i} \langle eg | V_{ij} | ge \rangle P_{ie}^\dagger P_{je} , \quad (2.155)$$

$$H_3 = \frac{1}{2} \sum_{i,j \neq i} \langle eg | V_{ij} | ge \rangle \left( P_{ie}^\dagger P_{je}^\dagger + P_{ie} P_{je} \right) , \quad (2.156)$$

$$H_4 = \frac{1}{2} \sum_{i,j \neq i} \left[ \langle ee | V_{ij} | ee \rangle + \langle gg | V_{ij} | gg \rangle - 2 \langle eg | V_{ij} | eg \rangle \right] P_{ie}^\dagger P_{ie} P_{je}^\dagger P_{je} , \quad (2.157)$$

$$H_5 = \sum_{i,j \neq i} \langle eg | V_{ij} | gg \rangle \left( P_{ie}^\dagger + P_{ie} \right) , \quad (2.158)$$

$$H_6 = \sum_{i,j \neq i} \left[ \langle eg | V_{ij} | ee \rangle - \langle eg | V_{ij} | gg \rangle \right] \left( P_{ie}^\dagger + P_{ie} \right) P_{je}^\dagger P_{je} . \quad (2.159)$$

For the general case with multiple energy levels, the derivation of the Hamiltonian in terms of exciton operators is very similar but tedious. So I choose to use the

Mathematica software[94] to write a symbolic program to handle the derivations. For reference, the result is given below. The Hamiltonian can be divided as

$$H = H^{(0)} + H^{(1)} + H^{(2)} + H^{(3)} + H^{(4)}, \quad (2.160)$$

where the superscripts “ $(n)$ ” mean that the corresponding term contains  $n$  exciton operators. In the following, we use capital characters  $L$ ,  $L'$ ,  $M$  and  $M'$  to represent any excited state of molecule, and  $G$  to denote the ground state. The first two term can be expressed as

$$H^{(0)} = \varepsilon_G N_{\text{mol}} + \frac{1}{2} \sum_{i,j \neq i} \langle GG|V_{ij}|GG\rangle, \quad (2.161)$$

$$H^{(1)} = \sum_{i,j \neq i} \sum_M \left[ \langle GG|V_{ij}|GM\rangle P_{jM} + \langle GM|V_{ij}|GG\rangle P_{jM}^\dagger \right], \quad (2.162)$$

neither of which doesn't conserve particle numbers.  $H^{(2)}$  can be further divided into a part that conserves particle numbers and a part that doesn't, that is

$$H^{(2)} = H_{\text{conserving}}^{(2)} + H_{\text{non-conserving}}^{(2)}, \quad (2.163)$$

where

$$\begin{aligned} H_{\text{conserving}}^{(2)} &= \sum_i \sum_M \left\{ (\varepsilon_M - \varepsilon_G) + \sum_{j \neq i} \left[ \langle MG|V_{ij}|MG\rangle - \langle GG|V_{ij}|GG\rangle \right] \right\} P_{iM}^\dagger P_{iM} \\ &\quad + \sum_{i,j \neq i} \sum_{L,M} \langle GL|V_{ij}|MG\rangle P_{iM} P_{jL}^\dagger \\ &\quad + \sum_{i,j \neq i} \sum_{L,M} (1 - \delta_{M,L}) \langle LG|V_{ij}|MG\rangle P_{iL}^\dagger P_{iM}, \end{aligned} \quad (2.164)$$

$$H_{\text{non-conserving}}^{(2)} = \frac{1}{2} \sum_{i,j \neq i} \sum_{L,M} \left[ \langle GG|V_{ij}|ML\rangle P_{iM} P_{jL} + \langle ML|V_{ij}|GG\rangle P_{iM}^\dagger P_{jL}^\dagger \right]. \quad (2.165)$$

$H^{(3)}$  doesn't conserve particle numbers and is given by

$$H^{(3)} = \sum_{i,j \neq i} \sum_{M,M',L} \left\{ \left[ \langle MG|V_{ij}|M'L\rangle - \delta_{M,M'} \langle GG|V_{ij}|GL\rangle \right] P_{iM}^\dagger P_{iM'} P_{jL} + \left[ \langle ML|V_{ij}|M'G\rangle - \delta_{M,M'} \langle GL|V_{ij}|GG\rangle \right] P_{iM}^\dagger P_{iM'} P_{jL} \right\}. \quad (2.166)$$

$H^{(4)}$  conserves particle numbers and is given by

$$H^{(4)} = \frac{1}{2} \sum_{i,j \neq i} \sum_{M,M',L,L'} \left[ \delta_{M,M'} \delta_{L,L'} \langle GG|V_{ij}|GG\rangle + \langle ML|V_{ij}|M'L'\rangle - 2\delta_{L,L'} \langle MG|V_{ij}|M'G\rangle \right] P_{iM}^\dagger P_{iM'} P_{jL}^\dagger P_{jL'}. \quad (2.167)$$

### 2.3.3 Eigenstates of the exciton Hamiltonian in the Heitler-London approximation

The Heitler-London approximation was first used by Frenkel in his study [95, 96] of electronic excitations in molecular crystals. Considering only two levels of a molecule, the ground state  $g$  and excited state  $e$ , the approximation assumes the following:

- the ground-state wavefunction of the crystal is the product of the ground-state wavefunction of individual molecules that constitute the crystal
- an excited state of the crystal is a superposition of products  $\cdots |g\rangle_i |e\rangle_j |g\rangle_k \cdots$  in which only one molecule  $j$  is excited and all other molecules are in the ground state

From the above two statements, we see that the Heitler-London approximation is expected to be good when the intermolecular interaction is weak and the molecules in the crystal preserve a large part of their individuality.

We now consider the lowest excited state of a crystal, which corresponds to the basis set  $\{ \cdots |g\rangle_i |e\rangle_j |g\rangle_k \cdots \}$  with only one molecule excited. In this case, the number of excitations is conserved, so that only the parts of the Hamiltonian in

Eq. (2.152) that conserve particle numbers need to be included, and we can rewrite the Hamiltonian as

$$H = H_0 + H_1 + H_2 + H_4 . \quad (2.168)$$

To understand the problem better, we analyze this Hamiltonian.  $H_0$  is a constant and thus we can set it as zero energy and ignore it.  $H_1$  can be written as

$$H_1 = \sum_i (\Delta\epsilon_e + \mathcal{D}_e) P_{ie}^\dagger P_{ie} , \quad (2.169)$$

where

$$\Delta\epsilon_e = \epsilon_e - \epsilon_g \quad (2.170)$$

is the excitation energy of an isolated molecule, and

$$\mathcal{D}_e = \sum_{j \neq i} \left[ \langle eg | V_{ij} | eg \rangle - \langle gg | V_{ij} | gg \rangle \right] \quad (2.171)$$

is the difference of the two interactions: one for the excited molecule with all remaining ground-state molecules in the crystal, and the other for the same nonexcited molecule with all remaining ground-state molecules.  $\mathcal{D}_e$  is also called the gas-condensed matter shift and it exists when the molecules in the crystal are interacting with each other.  $H_2$ , as given by

$$H_2 = \sum_{i,j \neq i} \langle eg | V_{ij} | ge \rangle P_{ie}^\dagger P_{je} , \quad (2.172)$$

destroys an excitation in molecule  $j$  and then creates an excitation in molecule  $i$ . Therefore, it describes the propagation of an excitation in the crystal and we call it the hopping term. The strength of the hopping interaction is given by the matrix elements  $\langle eg | V_{ij} | ge \rangle$ . Usually, the interaction between two nearest molecules is strongest and it decays fast with respect to the separation of two molecules, so sometimes it is justified to consider only the interaction between two nearest neighbors. We call this the nearest-neighbor approximation.  $H_4$  is the so-called the dynamic interaction, which describes the interaction between two excitations. It

can be written as

$$H_4 = \frac{1}{2} \sum_{i,j \neq i} \Phi_{ij} P_{ie}^\dagger P_{ie} P_{je}^\dagger P_{je} , \quad (2.173)$$

and its strength is determined by the matrix elements

$$\Phi_{ij} = \langle ee | V_{ij} | ee \rangle + \langle gg | V_{ij} | gg \rangle - 2 \langle eg | V_{ij} | eg \rangle .$$

In molecular crystals, the dipole-dipole interaction is an important kind of interaction  $V_{ij}$  between molecules. For molecules with a center of inversion, their eigenstates (for example  $|e\rangle$  and  $|g\rangle$ ) have well-defined parity, and the above matrix elements are zero. Under these circumstance, the dynamic interaction is zero and  $H_4$  can be ignored. In the case studied in this thesis, when we are concerned with the one-excitation subspace, we can safely ignore the dynamic interaction because it requires two excitations in the crystal. From another perspective, we can ignore the dynamic interaction because its matrix elements in the one-excitation subspace vanish. For illustration purposes, we give the derivation here. Based on Eq. (2.147), it can be shown that the matrix element of  $H_4$  is given by

$$\begin{aligned} & \langle e_n, g_m | \frac{1}{2} \sum_{i,j \neq i} \Phi_{ij} P_{ie}^\dagger P_{ie} P_{je}^\dagger P_{je} | g_n, e_m \rangle \\ &= \frac{1}{2} \sum_{i,j \neq i} \Phi_{ij} \langle 0 | P_{ne} P_{ie}^\dagger P_{ie} P_{je}^\dagger P_{je} P_{me}^\dagger | 0 \rangle \\ &= \frac{1}{2} \sum_{i,j \neq i} \Phi_{ij} \langle 0 | \left[ \delta_{i,n} + (1 - 2\delta_{i,n}) P_{ie}^\dagger P_{ne} \right] P_{je}^\dagger P_{je} \left[ \delta_{j,m} + (1 - 2\delta_{j,m}) P_{je}^\dagger P_{me} \right] | 0 \rangle . \end{aligned} \quad (2.174)$$

Without proceeding further, we can easily see that the above equation gives 0 as it consists of terms in which either  $P^\dagger$  operates on  $\langle 0 |$  or  $P$  operates on  $| 0 \rangle$ .

The above analysis shows that Eq. (2.160) can be simplified to

$$H = \sum_n (\Delta\epsilon_e + \mathcal{D}_e) P_{ne}^\dagger P_{ne} + \sum_{n,m \neq n} \langle eg | V_{nm} | ge \rangle P_{ne}^\dagger P_{me} , \quad (2.175)$$

if one is only interested in the lowest-energy excited state of the crystal. Eq. (2.175) gives the exciton Hamiltonian in the Heitler-London approximation. The corresponding eigenstates are called Frenkel excitons, which are many-body excited states of the whole crystal.

The Hamiltonian in the Heitler-London approximation can be diagonalized analytically. Before showing this, we first introduce the concepts of site representation and quasimomentum representation. Previously, the excitation creation and annihilation operators  $P_{nf}$  and  $P_{nf}^\dagger$  were defined with respect to the lattice site  $n$ . These operators form the site representation. Due to the periodicity of the crystal, we can use the quasimomentum representation, to represent excitations by taking the Fourier transforms of  $P_{nf}$  and  $P_{nf}^\dagger$ , that is

$$\begin{aligned} P_f(k) &= \frac{1}{\sqrt{N}} \sum_n e^{-ikn} P_{nf} , \\ P_f^\dagger(k) &= \frac{1}{\sqrt{N}} \sum_n e^{ikn} P_{nf}^\dagger , \end{aligned} \quad (2.176)$$

where  $N$  is the number of molecules in the crystal. Accordingly, the inverse Fourier transforms are

$$\begin{aligned} P_{nf} &= \frac{1}{\sqrt{N}} \sum_k e^{ikn} P_f(k) , \\ P_{nf}^\dagger &= \frac{1}{\sqrt{N}} \sum_k e^{-ikn} P_f^\dagger(k) . \end{aligned} \quad (2.177)$$

The conversion between the site representation and the quasimomentum representation usually involves the equalities

$$\begin{aligned} \frac{1}{N} \sum_k e^{ik(n-m)} &= \delta_{n,m} , \\ \frac{1}{N} \sum_n e^{in(k-k')} &= \delta_{k,k'} . \end{aligned} \quad (2.178)$$

These two equalities are very important and we will use them frequently in later derivations.

Substituting Eq. (2.177) into Eq. (2.175) gives

$$\begin{aligned}
H &= \sum_n (\Delta\epsilon_e + \mathcal{D}_e) \frac{1}{N} \sum_k e^{-ikn} P_f^\dagger(k) \sum_{k'} e^{ik'n} P_f(k') \\
&\quad + \sum_n \sum_{m \neq n} \langle eg | V_{nm} | ge \rangle \frac{1}{N} \sum_k e^{-ikm} P_f^\dagger(k) \sum_{k'} e^{ik'n} P_f(k') \\
&= \sum_{k,k'} \left( \frac{1}{N} \sum_n e^{in(k'-k)} \right) P_f^\dagger(k) P_f(k') \\
&\quad + \sum_n \sum_{l=n-m} \langle eg | V_{n,n-l} | ge \rangle e^{ikl} \left( \frac{1}{N} e^{in(k'-k)} \right) P_f^\dagger(k) P_f(k') . 
\end{aligned} \tag{2.179}$$

Because of the periodicity of the crystal, the interaction  $V_{n,m}$  only depends on the separation of the two molecules at site  $n$  and  $m$ . Thus  $\langle eg | V_{n,n-l} | ge \rangle$  in the above equation is independent of the index  $n$ , so we rewrite it as  $\langle eg | V(l) | ge \rangle$ . After that, making use of Eq. (2.178), we can easily show that the diagonal form of the Hamiltonian is

$$H = \sum_k E_f(k) P_f^\dagger(k) P_f(k) , \tag{2.180}$$

where  $E_f(k)$  is the eigenenergy of the system and is given by

$$E_f(k) = \Delta\epsilon_e + \mathcal{D}_e + \sum_l \langle eg | V(l) | ge \rangle e^{ikl} , \tag{2.181}$$

and thus the eigenstates of the Hamiltonian are

$$|k\rangle = P_f^\dagger(k) |0\rangle = \frac{1}{\sqrt{N}} \sum_n e^{ikn} |n\rangle , \tag{2.182}$$

where  $|0\rangle$  is the vacuum state and  $|n\rangle$  represents the single-excitation state in which molecule  $n$  is in the excited state and all other molecules are in the ground state. The state  $|k\rangle$  is a Frenkel exciton with quasimomentum (or wavevector)  $k$ .

## Chapter 3

# Tunable exciton interactions in optical lattices with polar molecules

The rotational excitation of polar molecules trapped in an optical lattice gives rise to rotational excitons. Here we show that non-linear interactions among such excitons can be controlled by an electric field. The exciton–exciton interactions can be tuned to induce exciton pairing, leading to the formation of biexcitons. Tunable non-linear interactions between excitons can be used for many applications ranging from the controlled preparation of entangled quasiparticles to the study of polaron interactions and the effects of non-linear interactions on quantum energy transport in molecular aggregates.

### 3.1 Introduction

The absorption of photons by a solid-state crystal gives rise to quasiparticles called excitons. There are two limiting models of excitons: Wannier-Mott excitons and Frenkel excitons. Wannier-Mott excitons occur in crystals with band structure leading to collective excitations with an effective radius much greater than the lattice constant, while Frenkel excitons are typical for molecular crystals, where collective excitations are superpositions of elementary excitations localized on different lat-

tice sites. These properties lead to important differences in the non-linear exciton interactions for the two models. The interactions between Wannier-Mott excitons are determined by Coulomb interactions and phase space filling [97, 98], while the interactions of Frenkel excitons are determined by shorter range dynamical couplings [99]. Multiple experiments have demonstrated that Wannier-Mott excitons can form two-exciton bound states called biexcitons [100–106]. By contrast, despite many theoretical studies [107–110], Frenkel biexcitons have eluded experimental observation, with one notable exception [111, 112]. In the present work, we show that the rotational excitation of ultracold molecules trapped on an optical lattice gives rise to Frenkel excitons with controllable non-linear interactions. We demonstrate that the exciton–exciton interactions can be tuned to induce the formation of Frenkel biexcitons and that the biexciton binding energy can be controlled by an external electric field.

Several experiments have recently demonstrated that ultracold molecules can be trapped in the periodic potential of an optical lattice [113–115]. Such systems can be used for the study of quantum energy transfer [67, 116], non-linear photon–photon interactions [117], novel quantum memory devices [118, 119] and, most notably, for quantum simulation of lattice models [43, 50, 120–127]. Although describing different phenomena, the Hamiltonians presented in these references, and in the present work, can be cast in the same form. For example, the exciton Hamiltonian discussed here can be mapped onto the  $t$ - $V$  model, which is a special case of the Heisenberg-like models studied in the context of ultracold molecules in Refs. [43, 121, 122, 126, 127]. The key difference between the present work and that in Refs. [43, 121, 122, 126, 127] is that we explore phenomena associated with the excitation spectrum of the many-body system in the limit of a small number of excitations. Because we consider a simpler Hamiltonian, our scheme is conceptually simpler, requiring fewer molecular states and external field parameters. We use the rotational states of molecules as a probe of the collective interactions, i.e. the experiments proposed here can be carried out by measuring site-selective populations of the rotational states. This can be achieved by applying a gradient of an electric field and detecting resonant transitions from Stark-shifted levels, as described in Ref. [59].

### 3.2 Exciton-exciton interactions in an optical lattice

We consider an ensemble of polar diatomic molecules in the  ${}^1\Sigma$  electronic state trapped on an optical lattice in the ro-vibrational ground state. The rotational states of the molecules  $|NM_N\rangle$  are described by the rotational angular momentum  $\hat{N}$  and its projection on the quantization axis  $M_N$ . We assume that the molecules are in the Mott-insulator phase [113–115] and that each lattice site contains only one molecule. We consider the rotational excitation  $|N=0, M_N=0\rangle \rightarrow |N=1, M_N=0\rangle$  of molecules in the lattice [128]. For simplicity, we denote the ground state of the molecule in site  $n$  by  $|g_n\rangle$  and the excited state by  $|e_n\rangle$ . Because the molecules are coupled by the dipole-dipole interaction, the rotational excitation gives rise to a rotational Frenkel exciton [67], which is an eigenstate of the Hamiltonian

$$\hat{H}_{\text{exc}} = E_0 \sum_{n=1}^{N_{\text{mol}}} \hat{P}_n^\dagger \hat{P}_n + \sum_{n,m \neq n}^{N_{\text{mol}}} J(n-m) \hat{P}_n^\dagger \hat{P}_m, \quad (3.1)$$

where  $J(n-m) = \langle e_n, g_m | \hat{V}_{dd}(n-m) | g_n, e_m \rangle$  with  $\hat{V}_{dd}(n-m)$  representing the dipole-dipole interaction between molecules in sites  $n$  and  $m$ ,  $E_0$  is the energy difference between the states  $|g\rangle$  and  $|e\rangle$ , and the operators  $\hat{P}_n^\dagger$  and  $\hat{P}_n$  are defined by the relations  $\hat{P}_n^\dagger |g_m\rangle = \delta_{nm} |e_n\rangle$  and  $\hat{P}_n |e_m\rangle = \delta_{nm} |g_n\rangle$ . The  $\hat{P}_n$  and  $\hat{P}_m$  operators satisfy the Pauli commutation relation, as shown by Eq. (2.145) and Eq. (2.146). More specifically, by omitting the subscript “ $e$ ” in these two equations, we have the fermionic commutation

$$\hat{P}_n \hat{P}_m^\dagger + \hat{P}_m^\dagger \hat{P}_n = 1, \quad (3.2)$$

if  $n = m$ , and the bosonic commutation

$$\hat{P}_n \hat{P}_m^\dagger - \hat{P}_m^\dagger \hat{P}_n = \delta_{n,m} = 0, \quad (3.3)$$

if  $n \neq m$  [99]. It is useful to combine the two commutation relations as

$$\hat{P}_n \hat{P}_m^\dagger + \hat{P}_m^\dagger \hat{P}_n = \delta_{m,n} + (1 - \delta_{m,n}) 2 \hat{P}_m^\dagger \hat{P}_n, \quad (3.4)$$

which gives rise to

$$\hat{P}_n \hat{P}_m^\dagger = \delta_{m,n} + (1 - 2\delta_{m,n}) \hat{P}_m^\dagger \hat{P}_n. \quad (3.5)$$

We will make frequent usage of Eq. (3.5) when evaluating the matrix elements of Hamiltonians.

Multiple excitations lead to dynamical exciton–exciton interactions described by [99]

$$\hat{H}_{\text{dyn}} = \frac{1}{2} \sum_{n,m \neq n}^{N_{\text{mol}}} D(n-m) \hat{P}_n^\dagger \hat{P}_m^\dagger \hat{P}_n \hat{P}_m \quad (3.6)$$

where

$$\begin{aligned} D(n-m) &= \langle e_n, e_m | \hat{V}_{dd}(n-m) | e_n, e_m \rangle + \langle g_n, g_m | \hat{V}_{dd}(n-m) | g_n, g_m \rangle \\ &\quad - 2 \langle e_n, g_m | \hat{V}_{dd}(n-m) | e_n, g_m \rangle, \end{aligned} \quad (3.7)$$

and the factor 1/2 is there to cancel the effect of double counting of the pairs  $(n, m)$ . In the above summations, we have the restriction that  $m$  cannot equal to  $n$  because two excitations cannot sit at the same lattice site (or in other words a molecule can't be excited twice to the same excited state). The dipole - dipole interaction operator  $\hat{V}_{dd}(n-m)$  can only couple states of different parity [92]. If  $|g\rangle$  and  $|e\rangle$  are states of well-defined parity, such as the rotational states  $|N, M_N\rangle$ , the matrix elements  $D(n-m)$  must be zero.

The inversion symmetry (parity) of molecules on an optical lattice can be broken by applying an external dc electric field. In an electric field,  $|g_n\rangle$  and  $|e_n\rangle$  are eigenstates of the Hamiltonian  $\hat{H}_n^{\text{mol}} = B_e \hat{N}_n^2 - \mathbf{d}_n \cdot \mathcal{E}_f$ , where  $\mathbf{d}_n$  is the dipole moment of molecule in site  $n$  and  $\mathcal{E}_f$  is the electric field vector. They can be expressed as  $|g\rangle = \sum_N a_N |N, M_N = 0\rangle$  and  $|e\rangle = \sum_N b_N |N, M_N = 0\rangle$ , where  $a_N$  and  $b_N$  are determined by the electric field strength. Note that we choose  $M_N = 0$  states because they adiabatically connect to nondegenerate rotational bare states as the external field goes to zero, leading to a single isolated exciton band. For other  $M_N \neq 0$  states, for example  $M_N = 1$  states, there will be two crossing exciton bands corresponding to the excitation from the dressed state  $|0, 1\rangle$  to  $|1, 1\rangle$  (See figure 2 in Ref. [67]).

As shown in Section 2.3.3, the Hamiltonian of Eq. (3.1) can be diagonalized by the Fourier transforms:  $\hat{P}^\dagger(k) = \frac{1}{\sqrt{N_{\text{mol}}}} \sum_n e^{ikn} \hat{P}_n^\dagger$  and  $\hat{P}(k) = \frac{1}{\sqrt{N_{\text{mol}}}} \sum_n e^{-ikn} \hat{P}_n$ , where  $k$  is the wave vector of the exciton. This transformation leads to  $\hat{H}_{\text{exc}} =$

$\sum_k E(k) \hat{P}^\dagger(k) \hat{P}(k)$ , where  $E(k) = E_0 + J(k)$  with  $J(k) = \sum_n J(n) e^{-ikn}$ , and  $\hat{P}^\dagger(k)$  and  $\hat{P}(k)$  create and annihilate Frenkel excitons with energies  $E(k)$ . The interaction of Eq. (3.6) in the momentum representation is

$$\hat{H}_{\text{dyn}} = \frac{1}{N_{\text{mol}}} \sum_{k_1, k_2, q} \tilde{D}(q) \hat{P}^\dagger(k_1 + q) \hat{P}^\dagger(k_2 - q) \hat{P}(k_1) \hat{P}(k_2), \quad (3.8)$$

where

$$\tilde{D}(q) = \sum_n D(n) e^{-iqn}. \quad (3.9)$$

### 3.3 Biexcitons

The exciton–exciton interactions generally have little effect on the energy spectrum of two-particle continuum states  $E(k_1) + E(k_2)$ . However, under certain conditions discussed below, non-linear interactions may result in the formation of a bound two-exciton complex, a biexciton. The biexciton state is split from the two-particle continuum. The splitting is the biexciton binding energy.

#### 3.3.1 Method to calculate biexciton energies

In the following, we discuss how to calculate the energy of a biexciton. We start from the Hamiltonian

$$\begin{aligned} \hat{H} &= \hat{H}_{\text{exc}} + \hat{H}_{\text{dyn}} \\ &= \underbrace{E_0 \sum_{n=1}^{N_{\text{mol}}} \hat{P}_n^\dagger \hat{P}_n}_{(1)} + \underbrace{\sum_{n,m} J(n-m) \hat{P}_n^\dagger \hat{P}_m}_{(2)} + \underbrace{\frac{1}{2} \sum_{n,m} D(n-m) \hat{P}_n^\dagger \hat{P}_m^\dagger \hat{P}_n \hat{P}_m}_{(3)}, \end{aligned} \quad (3.10)$$

where the constraint that  $m \neq n$  is removed by assuming  $J(0) = 0$  and  $D(0) = 0$ . The task is to find the eigenvalues and eigenfunctions of the above Hamiltonian in the two-excitation basis sets

$$|\psi\rangle = \sum_{n,m} C_{n,m} \hat{P}_n^\dagger \hat{P}_m^\dagger |0\rangle. \quad (3.11)$$

Normally, we would exclude the terms in which  $n = m$  from the above expansion. But in the current case, we assume  $C_{n,n} = 0$  and keep those terms so that the Fourier transformation for the coefficients  $C_{n,m}$  to a quasimomentum space

$$C_{n,m} = \frac{1}{N_{\text{mol}}} \sum_{k_1, k_2} C_{k_1, k_2} e^{i(k_1 n + k_2 m)} \quad (3.12)$$

is well-defined. More importantly, by doing so we can derive an equation that will correspond to the case of two noninteracting bosons. This will become evident later. Based on the physical meaning of the coefficients  $C_{n,m}$ , we conclude that  $C_{n,m}$  satisfy the symmetry relation

$$C_{n,m} = C_{m,n} , \quad (3.13)$$

and are to be normalized by

$$\sum_{n,m} |C_{n,m}|^2 = 1 . \quad (3.14)$$

Assuming the wavefunction  $\psi$  satisfies the Schrödinger equation

$$\hat{H}|\psi\rangle = E|\psi\rangle , \quad (3.15)$$

we can obtain the equations for the coefficients  $C_{n,m}$ . Since the terms  $C_{n,n}$  are added into Eq. (3.12) for artificial purposes, their values are not determined by the Schrödinger equation. To derive the equations for  $C_{n,m}$ , we let the Hamiltonian  $\hat{H}$  operate on the wavefunction term by term. The first term in Eq. (3.10) gives

$$\begin{aligned} \textcircled{1} |\psi\rangle &= E_0 \sum_{n',n,m} C_{n,m} \hat{P}_{n'}^\dagger \hat{P}_{n'} \hat{P}_n^\dagger \hat{P}_m^\dagger |0\rangle \\ &= E_0 \sum_{n',n,m} C_{n,m} \hat{P}_{n'}^\dagger [\delta_{n',n} + (1 - 2\delta_{n',n}) \hat{P}_n^\dagger \hat{P}_{n'}] \hat{P}_m^\dagger |0\rangle \\ &= E_0 \sum_{n',n,m} C_{n,m} [\delta_{n',n} \hat{P}_{n'}^\dagger \hat{P}_m^\dagger + (1 - 2\delta_{n',n}) \hat{P}_{n'}^\dagger \hat{P}_n^\dagger \hat{P}_{n'}^\dagger \hat{P}_m^\dagger] |0\rangle \\ &= E_0 \sum_{n',n,m} C_{n,m} [\delta_{n',n} \hat{P}_n^\dagger \hat{P}_m^\dagger + (1 - 2\delta_{n',n}) \hat{P}_n^\dagger \hat{P}_m^\dagger \delta_{n',m}] |0\rangle \\ &= E_0 \sum_{n,m} C_{n,m} [\hat{P}_n^\dagger \hat{P}_m^\dagger + (1 - 2\delta_{m,n}) \hat{P}_m^\dagger \hat{P}_n^\dagger] |0\rangle , \end{aligned} \quad (3.16)$$

where  $|0\rangle$  is the vacuum state where every particle is in the ground state. In the above derivation, Eq. (3.5) and  $\hat{P}_n|0\rangle = 0$  has been used. Similarly, the second term and the third term in Eq. (3.10) give rise to

$$\textcircled{2}|\psi\rangle = \sum_{n,m} \left[ \sum_{n'} J(n' - n) C_{n',m} \hat{P}_n^\dagger \hat{P}_m^\dagger + \sum_{n'} J(n' - m) C_{n,n'} (1 - 2\delta_{n',n}) \hat{P}_m^\dagger \hat{P}_n^\dagger \right] |0\rangle \quad (3.17)$$

and

$$\textcircled{3}|\psi\rangle = \frac{1}{2} \sum_{n,m} [D(n - m) C_{n,m} \hat{P}_m^\dagger \hat{P}_n^\dagger + D(n - m) C_{n,m} (1 - 2\delta_{m,n}) \hat{P}_n^\dagger \hat{P}_m^\dagger] |0\rangle \quad (3.18)$$

respectively. The right hand side of Eq. (3.15) is

$$E|\psi\rangle = E \sum_{n,m} C_{n,m} \hat{P}_n^\dagger \hat{P}_m^\dagger |0\rangle . \quad (3.19)$$

Given the fact that  $\hat{P}_n^\dagger \hat{P}_m^\dagger$  and  $\hat{P}_m^\dagger \hat{P}_n^\dagger$  are equivalent, a comparison of both sides of the Schrödinger equation yields the following equation for  $C_{n,m}$  when  $n \neq m$

$$(E - 2E_0)C_{n,m} - \sum_{n'} J(n' - n) C_{n',m} - \sum_{n'} J(n' - m) C_{n,n'} = D(n - m) C_{n,m} . \quad (3.20)$$

When  $n = m$ , the above equation becomes

$$\begin{aligned} & (E - 2E_0)C_{n,m} - \sum_{n'} J(n' - n) C_{n',m} - \sum_{n'} J(n' - m) C_{n,n'} \\ &= (E - 2E_0)C_{n,n} - 2 \sum_{n'} J(n - n') C_{n,n'} . \end{aligned} \quad (3.21)$$

Note the two sides of Eq. (3.21) are equivalent, so we cannot obtain the value of  $C_{n,n}$  from it. This is consistent with the previous assumption that  $C_{n,n} = 0$  because Eq. (3.21) allows us to take an arbitrary value for  $C_{n,n}$ . By combining Eq. (3.20)

for  $n \neq m$  and Eq. (3.21) for  $n = m$ , we obtain a new equation

$$\begin{aligned}
& \underbrace{(E - 2E_0)C_{n,m}}_{(4)} - \underbrace{\sum_{n'} J(n' - n)C_{n',m}}_{(5)} - \underbrace{\sum_{n'} J(n' - m)C_{n,n'}}_{(6)} \\
&= \underbrace{\delta_{n,m}(E - 2E_0)C_{n,m}}_{(7)} - \underbrace{2\delta_{n,m} \sum_{n'} J(n - n')C_{n,n'}}_{(8)} + \underbrace{D(n - m)C_{n,m}}_{(9)}, \quad (3.22)
\end{aligned}$$

which is valid for all coefficients  $C_{n,m}$ . The left hand side of Eq. (3.22) now corresponds to the case of two noninteracting bosons since the summations include terms like  $C_{m,m}$  and  $C_{n,n}$ . On the right hand side, the first two terms describe the kinematic interaction of excitons due to Eq. (3.4) and Eq. (3.5), and the last term represents the dynamical interaction of excitons.

The dimension of the system of coupled equations (3.22) is about  $N_{\text{mol}} \times N_{\text{mol}}$ , which is large even for a lattice with moderate size. To reduce the number of equations that we need to solve, we make use of the translational symmetry of the lattices and convert Eq. (3.22) into the quasimomentum representation. Since the conversion involves some nontrivial derivations, we give the details for (8) in

Eq. (3.22) which are characteristic for the whole calculations, namely

$$\begin{aligned}
(8) &= \delta_{n,m} \left[ \sum_{n'} J(n' - n) C_{n',m} + \sum_{n'} J(n' - m) C_{n,n'} \right] \\
&= \frac{\delta_{n,m}}{N_{\text{mol}}} \left[ \sum_{n'} J(n' - n) \sum_{k_1, k_2} C_{k_1, k_2} e^{i(k_1 n' + k_2 m)} + \sum_{n'} J(n' - m) \sum_{k_1, k_2} C_{k_1, k_2} e^{i(k_1 n + k_2 n')} \right] \\
&= \frac{\delta_{n,m}}{N_{\text{mol}}} \left[ \sum_{k_1, k_2} C_{k_1, k_2} e^{i(k_2 m + k_1 n)} \sum_{n'} J(n' - n) e^{ik_1(n' - n)} \right. \\
&\quad \left. + \sum_{k_1, k_2} C_{k_1, k_2} e^{i(k_1 n + k_2 m)} \sum_{n'} J(n' - m) e^{ik_2(n' - m)} \right] \\
&= \frac{\delta_{n,m}}{N_{\text{mol}}} \left[ \sum_{k_1, k_2} C_{k_1, k_2} e^{i(k_2 m + k_1 n)} \sum_{n' - m} J(n' - n) e^{ik_1(n' - n)} \right. \\
&\quad \left. + \sum_{k_1, k_2} C_{k_1, k_2} e^{i(k_1 n + k_2 m)} \sum_{n' - m} J(n' - m) e^{ik_2(n' - m)} \right] \\
&= \frac{\delta_{n,m}}{N_{\text{mol}}} \sum_{k_1, k_2} e^{i(k_1 n + k_2 m)} C_{k_1, k_2} [\tilde{J}(k_1) + \tilde{J}(k_2)] \\
&= \frac{1}{N_{\text{mol}}^2} \sum_{k_3} e^{ik_3(n-m)} \sum_{k_1, k_2} e^{i(k_1 n + k_2 m)} C_{k_1, k_2} [\tilde{J}(k_1) + \tilde{J}(k_2)] \\
&= \frac{1}{N_{\text{mol}}^2} \sum_{k_1, k_2, k_3} e^{i(k_1 + k_3)n} e^{i(k_2 - k_3)m} C_{k_1, k_2} [\tilde{J}(k_1) + \tilde{J}(k_2)] \\
&= \frac{1}{N_{\text{mol}}^2} \sum_{k'_1 = k_1 + k_3, k'_2 = k_2 - k_3} e^{i(k'_1 n + k'_2 m)} C_{k'_1 - k_3, k'_2 + k_3} \sum_{k_3} [\tilde{J}(k'_1 - k_3) + \tilde{J}(k'_2 + k_3)] \\
&= \frac{1}{N_{\text{mol}}^2} \sum_{k_1, k_2} e^{i(k_1 n + k_2 m)} C_{k_1 - k_3, k_2 + k_3} \sum_{k_3} [\tilde{J}(k_1 - k_3) + \tilde{J}(k_2 + k_3)] . \tag{3.23}
\end{aligned}$$

In the above derivation, we have made use of Eq. (3.12), the definition of  $\tilde{J}(k)$ :

$$\tilde{J}(k) \equiv \sum_n e^{ikn} J(n) \tag{3.24}$$

and the normalization relation of plane wave:

$$\frac{1}{N} \sum_k e^{ik(n-m)} = \delta_{n,m} . \tag{3.25}$$

In the last step of Eq. (3.23), since  $k'_1$  and  $k'_2$  have the same range as  $k_1$  and  $k_2$ , we have dropped their prime superscripts. Similar derivations like the above yield

$$\textcircled{4} = \frac{(E - 2E_0)}{N_{\text{mol}}} \sum_{k_1, k_2} C_{k_1, k_2} e^{i(k_1 n + k_2 m)}, \quad (3.26)$$

$$\textcircled{5} = \frac{1}{N_{\text{mol}}} \sum_{k_1, k_2} C_{k_1, k_2} e^{i(k_1 n + k_2 m)} \tilde{J}(k_1), \quad (3.27)$$

$$\textcircled{6} = \frac{1}{N_{\text{mol}}} \sum_{k_1, k_2} C_{k_1, k_2} e^{i(k_1 n + k_2 m)} \tilde{J}(k_2), \quad (3.28)$$

$$\textcircled{7} = \frac{(E - 2E_0)}{N_{\text{mol}}^2} \sum_{k_1, k_2} e^{i(k_1 n + k_2 m)} \sum_{k_3} C_{k_1 - k_3, k_2 + k_3}, \quad (3.29)$$

and

$$\textcircled{9} = \frac{1}{N_{\text{mol}}^2} \sum_{k_1, k_2} e^{i(k_1 n + k_2 m)} \sum_{k_3} \tilde{D}(k_3) C_{k_1 - k_3, k_2 + k_3}. \quad (3.30)$$

With all these results, Eq. (3.22) reduces to an equation for  $C_{k_1, k_2}$ , namely

$$\begin{aligned} [E - \varepsilon(k_1) - \varepsilon(k_2)] C_{k_1, k_2} &= \sum_{k_3} \frac{E - \varepsilon(k_1 - k_3) - \varepsilon(k_2 + k_3)}{N_{\text{mol}}} C_{k_1 - k_3, k_2 + k_3} \\ &+ \frac{1}{N_{\text{mol}}} \sum_{k_3} \tilde{D}(k_3) C_{k_1 - k_3, k_2 + k_3}, \end{aligned} \quad (3.31)$$

where  $\varepsilon(k)$  is the energy of an exciton and is given by

$$\varepsilon(k) = E_0 + \sum_n J(n) e^{ikn}. \quad (3.32)$$

There is an additional constraint for  $C_{k_1, k_2}$  which is due to the assumption that

$C_{n,n} = 0$ , that is

$$\begin{aligned}
\sum_{k_1+k_2=K} C_{k_1,k_2} &= \sum_{k_1,k_2} \frac{1}{N} \sum_{n,m} C_{n,m} e^{-i(k_1 n + k_2 m)} \\
&= \sum_{k_1} \frac{1}{N} \sum_{n,m} C_{n,m} e^{-i[k_1 n + (K - k_1)m]} \\
&= \sum_{n,m} C_{n,m} e^{iKm} \frac{1}{N} \sum_{k_1} e^{-ik_1(n-m)} \\
&= \sum_{n,m} C_{n,m} e^{iKm} \delta_{n,m} \\
&= \sum_n C_{n,n} e^{iKn} = 0.
\end{aligned} \tag{3.33}$$

Because of Eq. (3.33), we can eliminate  $E$  terms in the first summation on the right hand side of Eq. (3.31) and obtain

$$[E - \varepsilon(k_1) - \varepsilon(k_2)] C_{k_1,k_2} = \frac{1}{N_{\text{mol}}} \sum_{k_3} [\tilde{D}(k_3) - \varepsilon(k_1 - k_3) - \varepsilon(k_2 + k_3)] C_{k_1-k_3, k_2+k_3}. \tag{3.34}$$

Note in the above equation, the range of the wavevectors  $k_1$ ,  $k_2$  and  $k_3$  is  $[-\pi, \pi]$  so that the range of  $k_1 - k_3$  and  $k_2 + k_3$  is  $(-\pi, \pi)$  which is outside the first Brillouin zone. However, due to the symmetry property of the lattice, we can always bring  $k_1 - k_3$  or  $k_2 + k_3$  back to the first Brillouin zone by adding or subtracting  $2\pi$ . Thus, we define two new wavevectors

$$k'_1 = k_1 - k_3 \pm 2\pi, \tag{3.35}$$

and

$$k'_2 = k_2 + k_3 \pm 2\pi, \tag{3.36}$$

in which  $+$  or  $-$  is used to make sure the values of  $k'_1$  and  $k'_2$  are within the first Brillouin zone. With this change, Eq. (3.34) becomes

$$[E - \varepsilon(k_1) - \varepsilon(k_2)] C_{k_1,k_2} = \frac{1}{N_{\text{mol}}} \sum_{k'_1+k'_2=k_1+k_2} [\tilde{D}(k_1 - k'_1) - \varepsilon(k'_1) - \varepsilon(k'_2)] C_{k'_1, k'_2}. \tag{3.37}$$

To avoid double counting exciton pairs  $(k_1, k_2)$ , we restrict the summation to  $k_1 \geq$

$k_2$  and  $k'_1 \geq k'_2$ , reducing the dimension of Eq. (3.37) by half, leading to

$$\begin{aligned} [E - \varepsilon(k_1) - \varepsilon(k_2)] C_{k_1, k_2} &= \frac{1}{N_{\text{mol}}} \sum_{\substack{k'_1 \geq k'_2 \\ k'_1 + k'_2 = k_1 + k_2}} \left\{ \tilde{D}(k_1 - k'_1) + (1 - \delta_{k'_1, k'_2}) \tilde{D}(k_1 - k'_2) \right. \\ &\quad \left. - (2 - \delta_{k'_1, k'_2}) [\varepsilon(k'_1) + \varepsilon(k'_2)] \right\} C_{k'_1, k'_2}. \end{aligned} \quad (3.38)$$

As can be seen from the above equation, each coefficient  $C_{k_1, k_2}$  is only coupled to other coefficients  $C_{k'_1, k'_2}$  when  $k_1 + k_2 = k'_1 + k'_2$ . Therefore we can separate Eq. (3.38) into different sets and solve them independently. This will reduce the number of equations by a factor of  $N_{\text{mol}}$ , which is the reason that we want to convert Eq. (3.22) from the site representation to the quasimomentum representation. For each set of equations, the summation of wavevectors  $k_1 + k_2 = K$  is fixed for all pairs, so Eq. (3.38) can be written in the form of an eigenvalue equation

$$\mathbf{A}(K)\mathbf{C} = E(K)\mathbf{C}(K), \quad (3.39)$$

where the elements of the matrix  $\mathbf{A}(K)$  are given by

$$\begin{aligned} \mathbf{A}_{(k_1, k_2), (k'_1, k'_2)} &= \frac{1}{N_{\text{mol}}} \left\{ \tilde{D}(k_1 - k'_1) + (1 - \delta_{k'_1, k'_2}) \tilde{D}(k_1 - k'_2) \right. \\ &\quad \left. - (2 - \delta_{k'_1, k'_2}) [\varepsilon(k'_1) + \varepsilon(k'_2)] \right\} \\ &\quad + \delta_{k_1, k'_1} \delta_{k_2, k'_2} [\varepsilon(k_1) + \varepsilon(k_2)], \end{aligned} \quad (3.40)$$

and  $\mathbf{C}$  is a vector composed of all the relevant coefficients  $C_{k_1, k_2}$

$$\mathbf{C} = \begin{pmatrix} \vdots \\ C_{k_1, k_2} \\ \vdots \\ C_{k'_1, k'_2} \\ \vdots \end{pmatrix}. \quad (3.41)$$

By solving Eq. (3.39) under the constraint presented in Eq. (3.33), we can obtain all the eigenvalues and eigenvectors of the two-exciton system. Under some

conditions, a set of eigen-energies is split from the energy continuum of two free excitons and correspond to the biexciton states.

### 3.3.2 Analytical derivation of the biexciton wavefunction

To gain a deeper understanding of the biexciton state, we aim to derive the biexciton wavefunction in site representation using the nearest neighbor approximation. In this section, I will sketch the entire derivation and give some details of the difficult part.

To begin, let's examine the coefficients  $C_{n,m}$  in the most general two-exciton wavefunction of Eq. (3.11). These  $C_{n,m}$ 's are related to  $C_{k_1,k_2}$  by Eq. (3.12). From the analysis in Section 3.3.1, we know the sum of wavevectors of two excitons is a good quantum number for a biexciton state. Thus, it makes sense to define two new wavevectors in terms of  $k_1$  and  $k_2$ , namely

$$K = k_1 + k_2 , \quad (3.42)$$

$$k = \frac{k_1 - k_2}{2} . \quad (3.43)$$

Substituting the above two equations into Eq. (3.12), and using the Fourier transform

$$C_k^K = \frac{1}{\sqrt{N_{\text{mol}}}} \sum_l C^K(l) e^{-ikl} , \quad (3.44)$$

and

$$C^K(l) = \frac{1}{\sqrt{N_{\text{mol}}}} \sum_k C_k^K e^{ikl} , \quad (3.45)$$

we arrive at

$$\begin{aligned} C_{n,m} &= \frac{1}{N_{\text{mol}}} \sum_{k_1,k_2} C_{k_1,k_2} e^{i(K/2+k)n} e^{i(K/2-k)m} \\ &= \frac{1}{N_{\text{mol}}} \sum_{K,k} C_k^K e^{i(K/2+k)n} e^{i(K/2-k)m} \\ &= \frac{1}{\sqrt{N_{\text{mol}}}} \sum_K C^K(n-m) e^{iK(n+m)/2} . \end{aligned} \quad (3.46)$$

The two-exciton wavefunction (Eq. (3.11)) can then be written as

$$|\psi\rangle = \frac{1}{\sqrt{N_{\text{mol}}}} \sum_{n,m} \sum_K C^K(n-m) e^{iK(n+m)/2} \hat{P}_n^\dagger \hat{P}_m^\dagger |0\rangle . \quad (3.47)$$

The above equation inspires us to introduce a wavefunction that corresponds to a particular  $K$

$$|\psi_b^K\rangle = \frac{1}{\sqrt{N_{\text{mol}}}} \sum_{n,m} C^K(n-m) e^{iK(n+m)/2} \hat{P}_n^\dagger \hat{P}_m^\dagger |0\rangle , \quad (3.48)$$

and we are expecting it to be the wavefunction for a biexciton state. To verify our guess, we check the orthonormality of the wavefunction. The calculation of the overlap between two  $K$ -wavefunctions gives rise to

$$\langle \psi_b^Q | \psi_b^K \rangle = 2\delta_{Q,K} \sum_l |C^K(l)|^2 . \quad (3.49)$$

This indicates that the wavefunctions for different  $K$ 's are orthogonal and the normalization of the wavefunction can be satisfied as long as

$$2 \sum_l |C^K(l)|^2 = 1 . \quad (3.50)$$

Now the problem of finding the biexciton wavefunction becomes the problem of finding the values of  $C^K(l)$  that satisfy Eq. (3.50). As usual, wavefunctions can be obtained by solving the Schrödinger equation, so we work with Eq. (3.37) which is equivalent to the Schrödinger equation for the biexciton states. The main idea is to substitute Eq. (3.44) into Eq. (3.37) and get rid of the individual wavevector  $k_1$ ,  $k_2$ ,  $k'_1$  and  $k'_2$ . In this way, we will finally obtain an equation for  $C^K(l)$  that depends on the summation of the wavevectors  $K = k_1 + k_2$  rather than the individual wavevectors. However before doing that, we need to introduce the Green's function

$$G_{k_1,k_2}^K = \frac{1}{E - \epsilon(k_1) - \epsilon(k_2)} , \quad (3.51)$$

and its fourier transform

$$\begin{aligned} G^K(n) &= \frac{1}{N_{\text{mol}}} \sum_q \frac{e^{iqn}}{E - \varepsilon(K/2 + q) - \varepsilon(K/2 - q)} \\ &= \frac{1}{N_{\text{mol}}} \sum_{k_1+k_2=K} \frac{e^{i(k_1-k_2)n/2}}{E - \varepsilon(k_1) - \varepsilon(k_2)}. \end{aligned} \quad (3.52)$$

In the nearest neighbor approximation where only the interaction between the nearest sites is considered, the energy  $\varepsilon(k_1)$  of an exciton with wavevector  $k_1$  is given by

$$\varepsilon(k_1) = E_0 + 2J \cos(k_1), \quad (3.53)$$

and Eq. (3.52) reduces to

$$\begin{aligned} G^K(n) &= \frac{1}{N_{\text{mol}}} \sum_q \frac{e^{iqn}}{(E - 2E_0) - 2J \cos(K/2 + q) - 2J \cos(K/2 - q)} \\ &= \frac{1}{N_{\text{mol}}} \sum_q \frac{e^{iqn}}{(E - 2E_0) - 2J_K \cos(q)}, \end{aligned} \quad (3.54)$$

where  $J_K$  can be understood as the half bandwidth of the two free excitons with wavevector  $K/2 + q$  and  $K/2 - q$ , and is given by

$$J_K = 2J \cos(K/2). \quad (3.55)$$

When the number of sites  $N_{\text{mol}}$  becomes very large, Eq. (3.54) can be approximated by the integral

$$G^K(n) = \frac{1}{2\pi} \int_{-\pi}^{\pi} dq \frac{e^{iqn}}{(E - 2E_0) - 2J_K \cos(q)}, \quad (3.56)$$

which can be transformed into another integral over the complex variable  $w = e^{iq}$  along the unit circle

$$G^K(n) = \frac{1}{2\pi i |J_K|} \oint dw \frac{w^{|n|}}{w^2 + 2xw + 1}, \quad (3.57)$$

where  $x = E/2J_K$ . Equation (3.56) can be calculated using the Residue theorem.

In the case of a biexciton state, its energy  $E_b^K$  is outside the energy continuum of two free excitons  $\varepsilon(K/2 + q) + \varepsilon(K/2 - q)$ . There are two scenarios: first, when  $E - 2E_0 > 2J_K > 0$ ,  $G^K(n)$  is given by

$$G^K(n) = \frac{1}{\sqrt{(E - 2E_0)^2 - (2J_K)^2}} \left[ -\frac{E - 2E_0}{2J_K} + \sqrt{\left(\frac{E - 2E_0}{2J_K}\right)^2 - 1} \right]^{|n|}; \quad (3.58)$$

second, when  $E - 2E_0 < 2J_K < 0$ ,  $G^K(n)$  is given by

$$G^K(n) = \frac{1}{\sqrt{(E - 2E_0)^2 - (2J_K)^2}} \left[ -\frac{E - 2E_0}{2J_K} - \sqrt{\left(\frac{E - 2E_0}{2J_K}\right)^2 - 1} \right]^{|n|}. \quad (3.59)$$

For the derivations of the above two equations, please refer to page 88 of Economou's book on Green's function [129]. Since the analysis for the two scenarios are very similar, we will only concern ourselves with the first one in the following discussions.

The reason we want to calculate  $G^K(n)$  before working with Eq. (3.37) is that Eq. (3.37) contains  $G_{k_1, k_2}^K$  and  $G_{k_1, k_2}^K$ , the Fourier transform of  $G^K(n)$ , that is

$$G_{k_1, k_2}^K = \sum_m G^K(m) e^{-i(k_1 - k_2)m/2}. \quad (3.60)$$

To utilize the known analytical expression of  $G^K(n)$ , we divide both sides of Eq. (3.37) by  $[E - \varepsilon(k_1) - \varepsilon(k_2)]$  and rewrite  $\tilde{D}(k)$  in terms of  $D(n)$  using Eq. (3.9). The result is then given by

$$\begin{aligned}
\underbrace{C_{k_1, k_2}}_{(10)} &= \underbrace{\frac{1}{N_{\text{mol}}} G_{k_1, k_2}^K \sum_{k'_1 + k'_2 = k_1 + k_2} \sum_n D(n) e^{i(k_1 - k'_1)n} C_{k'_1, k'_2}}_{(11)} \\
&\quad - \underbrace{\frac{1}{N_{\text{mol}}} G_{k_1, k_2}^K \sum_{k'_1 + k'_2 = k_1 + k_2} \varepsilon(k'_1) C_{k'_1, k'_2}}_{(12)} \\
&\quad - \underbrace{\frac{1}{N_{\text{mol}}} G_{k_1, k_2}^K \sum_{k'_1 + k'_2 = k_1 + k_2} \varepsilon(k'_2) C_{k'_1, k'_2}}_{(13)}. \tag{3.61}
\end{aligned}$$

This is the equation we work with to derive an equation for  $C^K(n)$ . Since the derivation is not straightforward, we illustrate some difficult points by dealing with the equation term by term.

Substituting Eq. (3.44) and Eq. (3.60) into Eq. (3.61) gives for each term:

$$(10) = \frac{1}{\sqrt{N_{\text{mol}}}} \sum_l C^K(l) e^{-i(k_1 - k_2)l/2}, \tag{3.62}$$

$$\begin{aligned}
(11) &= \frac{1}{N_{\text{mol}}} \sum_m G^K(m) e^{-i(k_1 - k_2)m/2} \sum_{k'_1 + k'_2 = k_1 + k_2} \sum_n D(n) e^{i(k_1 - k'_1)n} \\
&\quad \times \frac{1}{\sqrt{N_{\text{mol}}}} \sum_l C^K(l) e^{-i(k'_1 - k'_2)l/2} \\
&= \frac{1}{N_{\text{mol}} \sqrt{N_{\text{mol}}}} \sum_{m,n,l} \sum_{k'_1 + k'_2 = k_1 + k_2} G^K(m) e^{-i(k_1 - k_2)m/2} D(-n) e^{-i(k_1 - k'_1)n} \\
&\quad \times C^K(l) e^{-i[k'_1 - (k_1 + k_2 - k'_1)]l/2} \\
&= \frac{1}{(N_{\text{mol}})^{3/2}} \sum_{m,n,l} G^K(m) e^{-i(k_1 - k_2)m/2} D(n) e^{-ik_1 n} C^K(l) e^{i(k_1 + k_2)l/2} \sum_{\substack{k'_1 + k'_2 \\ = k_1 + k_2}} e^{ik'_1(n-l)} \\
&= \frac{1}{\sqrt{N_{\text{mol}}}} \sum_{m,n,l} G^K(m) e^{-i(k_1 - k_2)m/2} D(n) e^{-ik_1 n} C^K(l) e^{i(k_1 + k_2)l/2} \delta_{n,l} \\
&= \frac{1}{\sqrt{N_{\text{mol}}}} \sum_{m,l} G^K(m) e^{-i(k_1 - k_2)m/2} D(l) C^K(l) e^{-i(k_1 - k_2)l/2}, \tag{3.63}
\end{aligned}$$

$$\begin{aligned}
(12) &= \frac{1}{N_{\text{mol}}} \sum_m G^K(m) e^{-i(k_1 - k_2)m/2} \sum_{k'_1 + k'_2 = k_1 + k_2} \left[ E_0 + \sum_n J(n) e^{ik'_1 n} \right] \\
&\quad \times \frac{1}{\sqrt{N_{\text{mol}}}} \sum_l C^K(l) e^{-i(k'_1 - k'_2)l/2} \\
&= \frac{1}{\sqrt{N_{\text{mol}}}} \sum_{m,n,l} G^K(m) e^{-i(k_1 - k_2)m/2} e^{i(k_1 + k_2)l/2} \\
&\quad \times \left[ E_0 C^K(l) \frac{1}{N_{\text{mol}}} \sum_{k'_1 + k'_2 = k_1 + k_2} e^{-ik'_1 l} + J(l) C^K(l) \frac{1}{N_{\text{mol}}} \sum_{k'_1 + k'_2 = k_1 + k_2} e^{ik'_1(n-l)} \right] \\
&= \frac{1}{\sqrt{N_{\text{mol}}}} \sum_{m,n,l} G^K(m) e^{-i(k_1 - k_2)m/2} e^{i(k_1 + k_2)l/2} [E_0 C^K(l) \delta_{l,0} + J(l) C^K(l) \delta_{l,n}] \\
&= \frac{1}{\sqrt{N_{\text{mol}}}} \sum_{m,l} G^K(m) e^{-i(k_1 - k_2)m/2} J(l) C^K(l) e^{iKl/2} \tag{3.64}
\end{aligned}$$

and

$$\textcircled{13} = \frac{1}{\sqrt{N_{\text{mol}}}} \sum_{m,l} G^K(m) e^{-i(k_1-k_2)m/2} J(l) C^K(l) e^{-iKl/2}. \quad (3.65)$$

A comparison between the left hand side and the right hand side of Eq. (3.61) indicates that we can eliminate the exponent  $e^{-i(k_1-k_2)m/2}$  from  $\textcircled{12}$  and  $\textcircled{13}$  by exchanging the index  $l$  with  $m$ . However, term  $\textcircled{11}$  will cause a problem because after exchanging  $l$  with  $m$  it becomes

$$\textcircled{11} = \frac{1}{\sqrt{N_{\text{mol}}}} \sum_{m,l} G^K(l) e^{-i(k_1-k_2)l/2} D(m) C^K(m) e^{-i(k_1-k_2)m/2}. \quad (3.66)$$

After dividing both sides of Eq. (3.61) by the common factor  $e^{-i(k_1-k_2)l/2}$ , the exponent  $e^{-i(k_1-k_2)m/2}$  will still remain in term  $\textcircled{13}$ . As mentioned before, we want to obtain an equation for  $C^K(n)$  that has only dependence on the summation of wavevectors  $K = k_1 + k_2$ , so we don't want  $e^{-i(k_1-k_2)m/2}$  to appear. It turns out this problem can be resolved by making use of the periodicity of the lattices. Due to the translational symmetry of the lattices,  $l - m$  takes the same range  $(-\infty, \infty)$  as  $l$  for a crystal with infinite size, so we can replace the summation over  $l$  with the summation over  $l - m$ , that is

$$\begin{aligned} \sum_l G^K(l) e^{-i(k_1-k_2)l/2} &= \sum_{l-m} G^K(l-m) e^{-i(k_1-k_2)(l-m)/2} \\ &= \sum_l G^K(l-m) e^{-i(k_1-k_2)(l-m)/2}. \end{aligned} \quad (3.67)$$

Although this equation is only strictly valid for a lattice with infinite number of sites, we can still use it for the case of sufficiently large lattices with a large  $N_{\text{mol}}$ . Substituting Eq. (3.67) into Eq. (3.66), we obtain

$$\textcircled{11} = \frac{1}{\sqrt{N_{\text{mol}}}} \sum_{m,l} G^K(l-m) D(m) C^K(m) e^{-i(k_1-k_2)l/2}, \quad (3.68)$$

so that Eq. (3.61) reduces to

$$C^K(l) = \sum_m C^K(m) [G^K(l-m) D(m) - 2G^K(l) J(m) \cos(Km/2)]. \quad (3.69)$$

In the nearest neighbor approximation, the above equation for  $C^K(m)$  can be simplified as

$$C^K(l) = C^K(1) \{ D(1) [G^K(l-1) + G^K(l+1)] - 2G^K(l)J_K \} , \quad (3.70)$$

where  $G^K(l)$  can be calculated from Eq. (3.58) and  $J_K$  is defined by Eq. (3.55).

Substituting Eq. (3.58) into Eq. (3.70) and taking  $l$  to be 1, we obtain an equation for the biexciton energy  $E_b^K$  which can be solved to give

$$E_b^K = 2E_0 + D + \frac{J_K^2}{D} . \quad (3.71)$$

Substituting this solution into Eq. (3.58), we can obtain an expression for  $G^K(n)$  in terms of  $D$  and  $J$

$$G^K(n) = \frac{D}{D^2 - J_K^2} \left( \frac{J_K}{D} \right)^{|n|} . \quad (3.72)$$

Up to this point, everything except  $C^K(l)$  in Eq. (3.70) has been known, therefore every other  $C^K(l)$  can be written in terms of  $C^K(1)$ , so that the normalization condition for  $C^K(l)$ , i.e., Eq. (3.50), becomes an equation for  $C^K(1)$  only. We can easily solve Eq. (3.50) by assuming  $N_{\text{mol}}$  is sufficiently large and  $D > J_K$  to obtain

$$C^K(n) = \frac{\sqrt{D^2 - J_K^2}}{2D} \left( \frac{J_K}{D} \right)^{|n|-1} . \quad (3.73)$$

So the biexciton wave function in the site representation in the nearest neighbor approximation because

$$\begin{aligned} |\Psi_b(K)\rangle &= \sum_{n,m \neq n} e^{iK(n+m)/2} \psi_K(|n-m|) |\hat{P}_n^\dagger \hat{P}_m^\dagger\rangle, \\ \psi_K(r) &= \frac{\sqrt{D^2 - 4J^2 \cos^2(K/2)}}{2D\sqrt{N_{\text{mol}}}} \left( \frac{2J \cos(K/2)}{D} \right)^{|r|-1}, \end{aligned} \quad (3.74)$$

where  $r = |n-m|$  is the distance between two excitations. Since  $J_K = 2J \cos(K/2) < D$ , we can see from the biexciton wavefunction that the amplitude  $\psi_K(r)$  for two excitations to appear at two sites decays exponentially with the distance between the two sites, which indicates that biexciton states are indeed bound states.

### 3.3.3 Properties of biexciton states

Reference [107] shows that biexcitons can generally form in 1D and 2D crystals if

$$|D| \geq 2|J| , \quad (3.75)$$

where  $D$  and  $J$  are the coupling constants  $D(n-m)$  and  $J(n-m)$  for  $n-m=1$ . In 3D crystals, biexcitons can form if  $|D| > 6|J|$  [110]. For 1D crystals, the biexciton energy in the nearest neighbor approximation (NNA) is

$$E_b(K) = 2E_0 + D + \frac{4J^2 \cos^2(aK/2)}{D} , \quad (3.76)$$

where  $K$  is the total wave vector for two interacting excitons and  $a$  is the lattice constant, and the biexciton binding energy is  $\Delta = (D - 2J)^2/D$ . The maximum number of exciton-exciton bound states is equal to the dimensionality of the crystal, i.e. one biexciton state for 1D, two for 2D and three for 3D [107, 130].

For molecules in an optical lattice, the magnitudes of  $J$  and  $D$  depend on the strength of the applied electric field and the angle between the field and the molecular array ( $\theta$ ), as seen in Fig. 3.1 (c). We calculate these parameters for a 1D array of  ${}^1\Sigma$  polar molecules (such as alkali metal dimers produced in ultracold molecule experiments) trapped on an optical lattice with the lattice separation  $a = 400$  nm. Fig. 3.1 (b) shows that for a fixed angle  $\theta$  the ratio  $D/J$  increases as the electric field magnitude increases. For LiCs molecules, the condition of Eq. (3.75) is satisfied for electric fields  $> 3.6$  kV/cm. Note that the ratio  $D/J$  is independent of  $\theta$ .

Frenkel excitons are quasiparticles characterized by an effective mass,  $m_{\text{eff}}$ . The sign of  $J$  determines the sign of the effective mass [67]: negative  $J$  corresponds to positive  $m_{\text{eff}}$  and vice versa, as seen in Fig. 3.1 (d). Due to the linearity of the Schrödinger equation, a positive potential is attractive for particles with negative mass, just like a negative potential is attractive for particles with positive mass. Because the signs of  $J$  and  $D$  are the same (and consequently the signs of  $D$  and  $m_{\text{eff}}$  are opposite), the dynamical interaction of Eq. (3.6) between excitons in this system is attractive.

To demonstrate the formation of the biexciton and calculate the biexciton en-

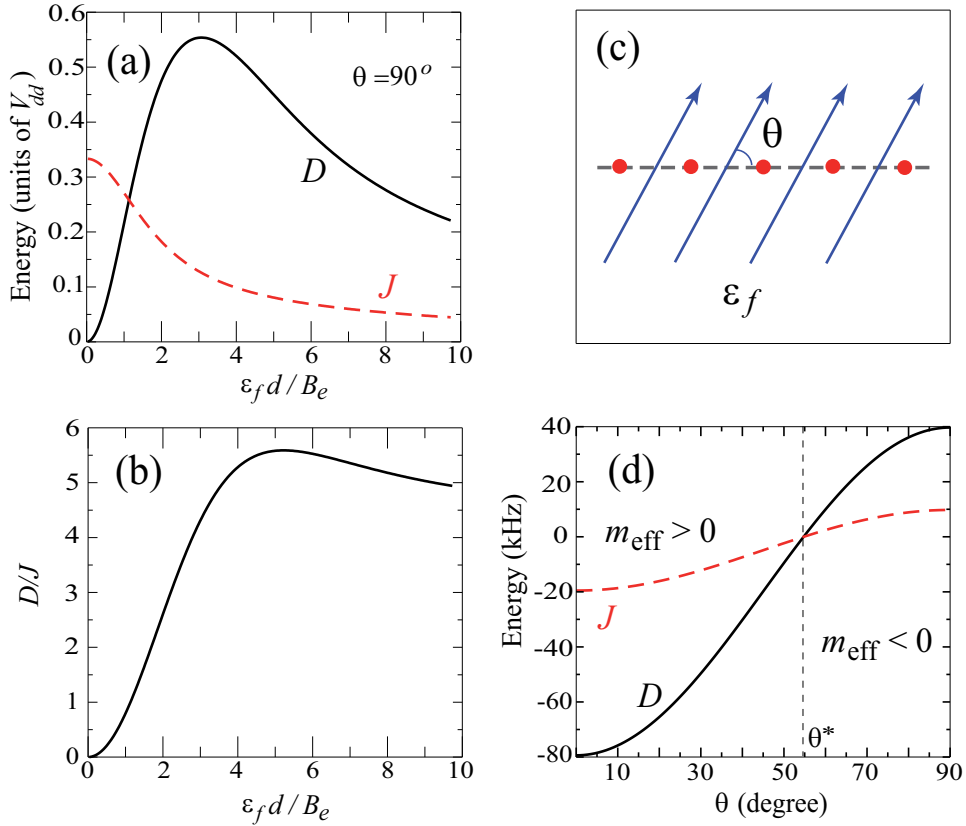


**Figure 3.1:** (a) The parameters  $D$  and  $J$  (in units of  $V_{dd} = d^2/a^3$ ) as functions of the electric field strength. (b) The ratio  $D/J$  as a function of the electric field strength. The field is perpendicular to the intermolecular axis. For LiCs molecules possessing the dipole moment  $d=5.529$  Debye, the value  $\epsilon_f d/B_e = 1$  corresponds to  $\epsilon_f = 2.12$  kV/cm. (c) Schematic depiction of the angle  $\theta$  between the field (represented by blue arrows) and the molecular array (represented by red dots). (d)  $D$  and  $J$  for a 1D array of LiCs molecules separated by 400 nm as functions of  $\theta$  for  $\epsilon_f = 6$  kV/cm.

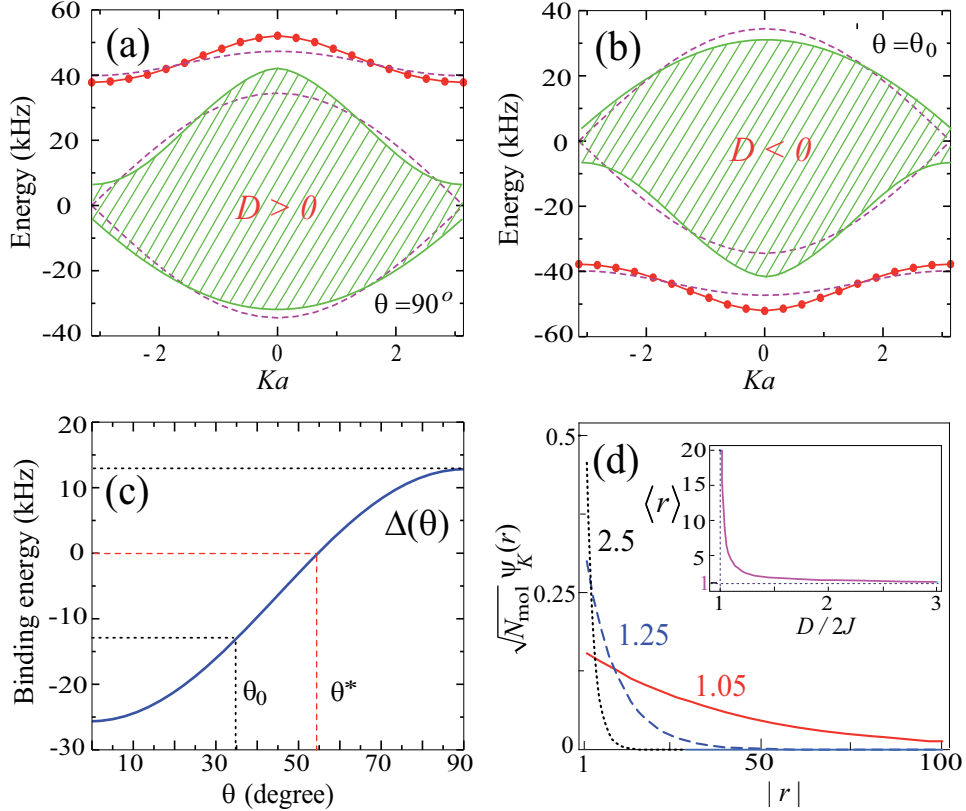


**Figure 3.2:** (a) and (b): Two-excitation spectra of a 1D array of LiCs molecules on an optical lattice: NNA (dashed lines) and exact solutions (solid lines). The shaded regions encapsulate the bands of the continuum two-exciton states. (c)  $\theta$ -dependence of the biexciton binding energy  $\Delta$ . The electric field magnitude is 6.88 kV/cm,  $\theta_0 = \arccos \sqrt{2/3}$ ,  $\theta^* = \arccos \sqrt{1/3}$ . (d) Biexciton wave function vs the lattice site separation  $|r| = |n - m|$  of the two excitations for  $K = 0$ . Inset: Mean width of the biexciton wave function  $\langle r \rangle$  calculated as the width of  $\psi_K^2(r)$  at half maximum. Numbers on each curve indicate the value of  $D/2J$ .

ergy, we diagonalize the Hamiltonian  $\hat{H}_{\text{exc}} + \hat{H}_{\text{dyn}}$  for a one-dimensional array of  $N_{\text{mol}} = 501$  LiCs molecules. The matrix of the Hamiltonian is evaluated by expanding the biexciton states as

$$\begin{aligned} |\Psi_b(K)\rangle &= \sum_{\substack{k_1+k_2=K \\ k_1 \geq k_2}} C_{k_1,k_2} |k_1, k_2\rangle \\ &= \sum_{k \geq 0} C_k^K |\hat{P}^\dagger(K/2+k) \hat{P}^\dagger(K/2-k)\rangle, \end{aligned} \quad (3.77)$$

where  $K = k_1 + k_2$  and  $k = (k_1 - k_2)/2$ , and  $k_1$  and  $k_2$  denote the wavevectors of the interacting excitons. The Hamiltonian matrix is diagonalized numerically for fixed values of  $K$ , which is conserved. Figure 3.2 (c) shows that for  $\theta = 90^\circ > \theta^* = \arccos(1/\sqrt{3})$  the biexciton energy is above the two-exciton continuum (binding for particles with negative mass), and for  $\theta = \arccos \sqrt{2/3} < \theta^*$  below it (binding for particles with positive mass). The binding energy of the biexciton changes sign at  $\theta = \theta^*$ . The biexciton wave function  $\psi_K(r)$  is plotted in Fig. 3.2 (d). Figure 3.1 and Fig. 3.2 thus illustrate that the biexciton binding energy and size can be tuned by varying the strength and orientation of the electric field.

### 3.4 Non-optical creation of biexcitons

The possibility of forming Frenkel biexcitons has been proposed quite a long time ago[110]. However, in contrast to the well-known Wannier-Mott biexcitons in semiconductors, Frenkel biexcitons in solid-state molecular crystals are very difficult to observe. We now explain the reasons. First, many molecular crystals, such as anthracene or naphthalene, possess inversion symmetry. In these crystals, the constant  $D$  as defined in the line after Eq. (3.6) must vanish and Eq. (3.75) is not satisfied. Second, it is difficult to excite biexciton states optically: it was shown in Ref.[108] that the oscillator strength for the photon-induced transitions to the biexciton state must decrease with the increasing binding energy of the biexcitons. Therefore, two-photon excitation can only produce unstable weakly bound biexcitons. Third, excitons in molecular crystals decay via bimolecular annihilation processes into higher-energy states and subsequent relaxation accompanied by emission of phonons. This process is prohibited by conservation of energy in an optical

lattice with diatomic molecules. Figure 3.1 demonstrates that the first obstacle can be removed by tuning the electric field. To overcome the second obstacle, we propose a non-optical method of populating deeply bound biexciton states based on the unique structure of  ${}^1\Sigma$  polar molecules. At zero electric field, the rotational states  $|g\rangle$  and  $|e\rangle$  are separated by the energy  $\Delta\epsilon_{e-g} = 2B_e$ , while the energy separation between state  $|e\rangle$  and the next rotationally excited state  $|f\rangle \equiv |N=2, M_N=0\rangle$  is equal to  $\Delta\epsilon_{e-f} = 4B_e$ . As the electric field increases,  $\Delta\epsilon_{e-g}$  increases faster than  $\Delta\epsilon_{e-f}$ , as shown in Fig. 3.3. When  $\mathcal{E}_f d/B_e \simeq 3.24$  (corresponding to  $\mathcal{E}_f \simeq 6.88$  kV/cm for LiCs),  $\Delta\epsilon_{f-g} = 2\Delta\epsilon_{e-g}$ . At electric fields near this magnitude, two  $|g\rangle \rightarrow |e\rangle$  excitons can undergo the transition to the  $|f\rangle$  state, and, inversely, the  $|g\rangle \rightarrow |f\rangle$  excitation can produce a pair of  $|g\rangle \rightarrow |e\rangle$  excitons or a biexciton state depicted in Fig. 3.2. The coupling between states  $|e\rangle$  and  $|f\rangle$  is  $\hat{H}_{12} = \sum_{n \neq m} M(n-m) \hat{R}_n \hat{P}_n^\dagger \hat{P}_m^\dagger$ , where  $M(n-m) = \langle e_n, e_m | V_{dd}(n-m) | f_n, g_m \rangle$ , and the operator  $\hat{R}_n$  annihilates the  $|f\rangle$  excitation in lattice site  $n$ . The total Hamiltonian describing this three-level system is

$$\hat{H}_{g-e-f} = \hat{H}_{\text{exc}} + \hat{H}_{\text{dyn}} + \hat{H}_2 + \hat{H}_{12}, \quad (3.78)$$

where

$$\hat{H}_2 = E_f \sum_n \hat{R}_n^\dagger \hat{R}_n + \sum_{n,m \neq n} J_{g-f}(n-m) \hat{R}_n^\dagger \hat{R}_m \quad (3.79)$$

and

$$J_{g-f}(n-m) = \langle g_n, f_m | V_{dd}(n-m) | f_n, g_m \rangle. \quad (3.80)$$

In order to calculate the probability of the population transfer from state  $f$  to the biexciton state, we solve the time-dependent Schrödinger equation with the Hamiltonian  $\hat{H}_{g-e-f}$  evaluated in the basis of products of the eigenstates of  $\hat{H}_{\text{exc}} + \hat{H}_{\text{dyn}}$  and the eigenstates of  $\hat{H}_2$ . This leads to coupled differential equations

$$i\hbar \dot{\mathbf{C}} = \mathbf{H}\mathbf{C}, \quad (3.81)$$

where  $\mathbf{C}$  is a vector that represents a wavefunction in the basis set and  $\dot{\mathbf{C}}$  is its derivative with respect to time. Since the total Hamiltonian  $\mathbf{H}$  is time-independent,

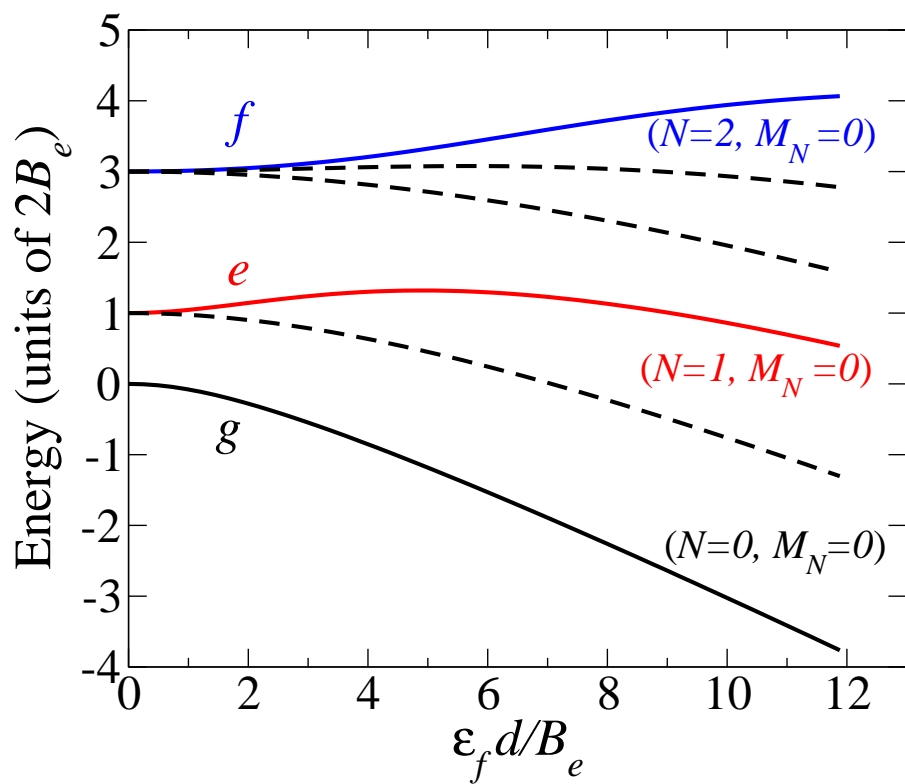


**Figure 3.3:** The rotational energies of a closed-shell polar molecule as a function of the strength of a DC field. The dashed lines represent other rotational states with  $M_N \neq 0$ .

we can make a basis-set transformation to diagonalize  $\mathbf{H}$

$$\mathbf{U}^T \mathbf{H} \mathbf{U} = \mathbf{D}, \quad (3.82)$$

so that  $\mathbf{C}$  in the new basis set can then be solved by direct integration and then  $\mathbf{C}$  in the original basis set can be found by the inverse basis-set transformation. Multiplying both sides of Eq. (3.81) by  $\mathbf{U}^T$ , we obtain

$$i\hbar \mathbf{U}^T \dot{\mathbf{C}} = \mathbf{U}^T \mathbf{H} \mathbf{U} \mathbf{U}^T \mathbf{C}, \quad (3.83)$$

where  $\mathbf{U} \mathbf{U}^T = \mathbf{I}$  has been used. Let's define

$$\mathbf{A} \equiv \mathbf{U}^T \mathbf{C}, \quad (3.84)$$

then

$$\dot{\mathbf{A}} = \mathbf{U}^T \dot{\mathbf{C}} \quad (3.85)$$

because  $\mathbf{H}$  is time-independent and  $\mathbf{U}^T$  must be time-independent too. So Eq. (3.81) can be rewritten as

$$i\hbar \dot{\mathbf{A}} = \mathbf{D} \mathbf{A}, \quad (3.86)$$

which can solved formally by direct integration to give

$$\mathbf{A}(t) = e^{-\frac{i}{\hbar} \mathbf{D} t} \mathbf{A}(0). \quad (3.87)$$

Substituting Eq. (3.84) into Eq. (3.87), we get

$$\mathbf{C}(t) = \mathbf{U} e^{-\frac{i}{\hbar} \mathbf{D} t} \mathbf{U}^T \mathbf{C}(0), \quad (3.88)$$

where  $\mathbf{D}$  is a diagonal matrix whose non-zero elements are the eigenvalues of  $\mathbf{H}$ , and each column of  $\mathbf{U}$  is an eigenvector of  $\mathbf{H}$ . Therefore, given the eigenvalues and eigenvectors of the total Hamiltonian and the initial wavefunction  $\mathbf{C}(0)$ , the wavefunction  $\mathbf{C}(t)$  at any time  $t$  can be calculated from Eq. (3.88). In our numerical calculations, we use subroutines from the LAPACK library[131] to calculate the eigenvalues and eigenvectors of the matrix.

The magnitude of  $J_{g-f}$  is about ten times smaller than  $J$ . In the absence of de-

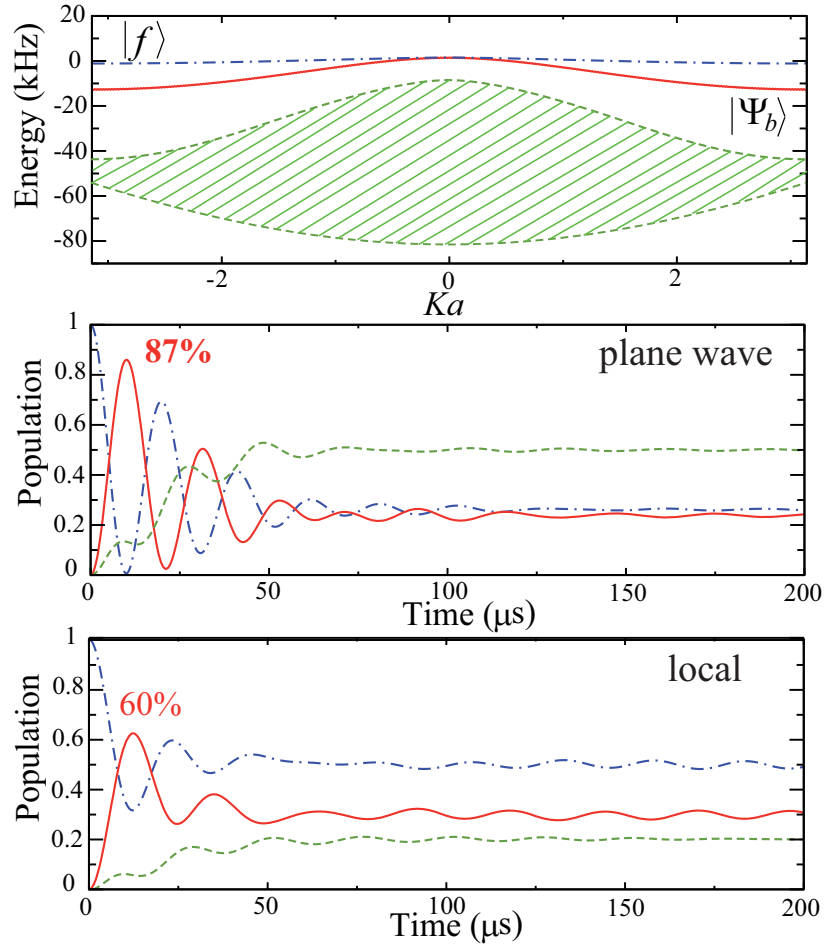


**Figure 3.4:** Population dynamics for the transition from  $|g\rangle \rightarrow |f\rangle$  exciton (middle panel) and from an  $f$  state localized on a single molecule (lower panel) to coherent  $|g\rangle \rightarrow |e\rangle$  excitons and biexcitons. The green dashed curves denote the population accumulated in the pairs of non-bound  $|g\rangle \rightarrow |e\rangle$  exciton states, the red solid curves the biexciton state and the blue dot-dashed curves the  $f$  state. The shaded region in the upper panel encapsulates the band of the continuum two-exciton states. The calculation is for a 1D ensemble of  $N_{mol} = 501$  LiCs molecules on an optical lattice with lattice separation  $a = 400$  nm. The electric field of magnitude 6.88 kV/cm is perpendicular to the molecular array.

coherence, the  $|g\rangle \rightarrow |f\rangle$  excitation gives rise to the Frenkel exciton and the transition from the  $f$  states to the biexciton state is a coherent exciton–exciton transition. In the presence of decoherence, the exciton states become localized. If the decoherence rate is larger than  $J_{g-f}/h$ , but smaller than  $J/h$ , the  $|g\rangle \rightarrow |f\rangle$  excitation is localized, while the biexciton states remain coherent. Figure 3.4 presents the calculations of the population transfer probabilities for both scenarios. The results show that the biexciton states can be populated with high efficiency. The equilibrium populations (in the limit of large  $t$ ) depend on the relative energies of the  $f$  state, the biexciton bound state and exciton–exciton continuum states, which can be tuned by varying the electric field magnitude. The efficiency of the population transfer can be maximized if the electric field is detuned far away from resonance when the biexciton population oscillations reach the first maximum. Detuning the electric field to low magnitudes effectively decouples the  $f$  state from the states in the  $\{g,e\}$  subspace and interrupts the population dynamics. This corresponds to switching off the channel for bimolecular annihilation of excitons, which is one of the reasons of the biexciton population depletion in solids. We have confirmed that the calculations with electric fields  $< 5.0$  kV/cm yield no noticeable population transfer.

### 3.5 Extension to exciton trimers

In Section 3.3, it was shown that Frenkel rotational biexcitons exist under some conditions in optical lattices. The question arises naturally, ‘‘If two excitons can bind together, what about three excitons?’’. In this section, we extend the method to handle the three-exciton case and answer the question about exciton trimers.

Similar to the case for biexcitons, we define a three-exciton wavefunction in the site representation as

$$|\Psi\rangle = \sum_{n_1, n_2, n_3} C_{n_1, n_2, n_3} \hat{P}_{n_1}^\dagger \hat{P}_{n_2}^\dagger \hat{P}_{n_3}^\dagger |0\rangle , \quad (3.89)$$

and start from the Schrödinger equation with the same Hamiltonian  $\hat{H} = \hat{H}_{\text{exc}} + \hat{H}_{\text{dyn}}$

$$\hat{H}|\Psi\rangle = E_{\text{trimer}}|\Psi\rangle . \quad (3.90)$$

Since two excitations can't exist at the same molecule, we have the constraint on  $C_{n_1,n_2,n_3}$  that

$$C_{n_1,n_2,n_3} = 0 \text{ if } n_1 = n_2 \text{ or } n_2 = n_3 \text{ or } n_1 = n_3 . \quad (3.91)$$

After derivations similar to those used for the biexciton case, Eq. (3.90) and Eq. (3.91) lead to

$$\begin{aligned} & [3E_0D(n_1 - n_2) + D(n_1 - n_3) + D(n_2 - n_3) - E_{\text{trimer}}] C_{n_1,n_2,n_3} \\ & + \sum_n [J(n - n_1)C_{n,n_2,n_3} + J(n - n_2)C_{n_1,n,n_3} + J(n - n_3)C_{n_1,n_2,n}] \\ & = 2\delta_{n_1,n_2} \sum_n J(n_1 - n)C_{n,n_2,n_3} + 2\delta_{n_2,n_3} \sum_n J(n_2 - n)C_{n_1,n,n_3} \\ & + 2\delta_{n_1,n_3} \sum_n J(n_3 - n)C_{n_1,n_2,n} . \end{aligned} \quad (3.92)$$

Note that this equation can't be used to determine the values of  $C_{n_1,n_2,n_3}$  when any two of  $n_1$ ,  $n_2$ , and  $n_3$  are equal. Using the Fourier transform

$$C_{n_1,n_2,n_3} = \frac{1}{(\sqrt{N_{\text{mol}}})^3} \sum_{k_1,k_2,k_3} C(k_1, k_2, k_3) e^{i(k_1 n_1 + k_2 n_2 + k_3 n_3)} , \quad (3.93)$$

we can transform Eq. (3.92) to

$$\begin{aligned} & \frac{1}{N_{\text{mol}}} \sum_q \tilde{D}(q) [C(k_1 - q, k_2 + q, k_3) + C(k_1 - q, k_2, k_3 + q) + C(k_1, k_2 - q, k_3 + q)] \\ & + [\epsilon(k_1) + \epsilon(k_2) + \epsilon(k_3) - E_{\text{trimer}}] C(k_1, k_2, k_3) \\ & = \frac{2}{N_{\text{mol}}} \sum_q [\tilde{J}(k_1 - q)C(k_1 - q, k_2 + q, k_3) + \tilde{J}(k_2 - q)C(k_1, k_2 - q, k_3 + q) \\ & + \tilde{J}(k_3 - q)C(k_1 + q, k_2 + q, k_3 - q)] , \end{aligned} \quad (3.94)$$

which can be written as an eigenvalue problem

$$\sum_{k'_1+k'_2+k'_3=K} \mathbf{A}_{k_1 k_2 k_3; k'_1 k'_2 k'_3} C(k'_1, k'_2, k'_3) = E_{\text{trimer}} C(k_1, k_2, k_3) , \quad (3.95)$$

where

$$\begin{aligned}
\mathbf{A}_{k_1 k_2 k_3; k'_1 k'_2 k'_3} &= \delta_{k_1, k'_1} \delta_{k_2, k'_2} \delta_{k_3, k'_3} [\varepsilon(k_1) + \varepsilon(k_2) + \varepsilon(k_3)] \\
&\quad + \frac{1}{N_{\text{mol}}} \left\{ \delta_{k_1, k'_1} [\tilde{D}(k_2 - k'_2) - 2\tilde{J}(k'_2)] \right. \\
&\quad \quad + \delta_{k_2, k'_2} [\tilde{D}(k_3 - k'_3) - 2\tilde{J}(k'_3)] \\
&\quad \quad \left. + \delta_{k_3, k'_3} [\tilde{D}(k_1 - k'_1) - 2\tilde{J}(k'_1)] \right\}. \quad (3.96)
\end{aligned}$$

The above equations clearly show that only those coefficients  $C(k_1, k_2, k_3)$  whose wavevectors add up to a fixed  $K$  are coupled to each other. Therefore, the eigenvalues for each value of  $K$  can be calculated independently. However, since we assumed that  $C_{n_1, n_2, n_3} = 0$  when any two of  $n_1, n_2, n_3$  are equal, we need to take care of this constraint when solving Eq. (3.95).

Let's examine the effect of the constraint on  $C_{n_1, n_2, n_3}$ . Assuming  $k_3$  is fixed, we have

$$\begin{aligned}
\sum_{k_1+k_2=K-k_3} C(k_1, k_2, k_3) &= \sum_{k_1} \sum_{n_1, n_2, n_3} \frac{1}{(\sqrt{N_{\text{mol}}})^3} e^{i(k_1 n_1 + k_2 n_2 + k_3 n_3)} C_{n_1, n_2, n_3} \\
&= \sum_{n_1, n_2, n_3} \frac{1}{\sqrt{N_{\text{mol}}}} \left( \frac{1}{N_{\text{mol}}} \sum_{k_1} e^{ik_1(n_1 - n_2)} \right) e^{i(K - k_3)n_2} e^{ik_3 n_3} C_{n_1, n_2, n_3} \\
&= \sum_{n_1, n_2, n_3} \frac{1}{\sqrt{N_{\text{mol}}}} \delta_{n_1, n_2} e^{i(K - k_3)n_2} e^{ik_3 n_3} C_{n_1, n_2, n_3} \\
&= \sum_{n_2, n_3} \frac{1}{\sqrt{N_{\text{mol}}}} e^{i(K - k_3)n_2} e^{ik_3 n_3} C_{n_2, n_2, n_3} \\
&= 0. \quad (3.97)
\end{aligned}$$

Since the fixed wavevector  $k_3$  can be chosen arbitrarily, a condition similar to Eq. (3.97) will hold for a fixed  $k_1$  and a fixed  $k_2$  as well. This means for a particular  $K$ , summing all the  $C(k'_1, k'_2, k'_3)$  whose first (second or third) wavevector

$k'_1$  ( $k'_2$  or  $k'_3$ ) is equal to a fixed  $k$ , will give zero. Thus, we can add the zero

$$\frac{1}{N_{\text{mol}}} \sum_{k'_1, k'_2, k'_3} \left[ -2\tilde{J}(k_2)\delta_{k'_1, k_1} C(k'_1, k'_2, k'_3) - 2\tilde{J}(k_3)\delta_{k'_2, k_2} C(k'_1, k'_2, k'_3) - 2\tilde{J}(k_1)\delta_{k'_3, k_3} C(k'_1, k'_2, k'_3) \right] = 0 , \quad (3.98)$$

to the left hand side of Eq. (3.95) to produce a new equation

$$\sum_{k'_1 + k'_2 + k'_3 = K} \mathbf{B}_{k_1 k_2 k_3; k'_1 k'_2 k'_3} C(k'_1, k'_2, k'_3) = E_{\text{trimer}} C(k_1, k_2, k_3) , \quad (3.99)$$

where

$$\begin{aligned} \mathbf{B}_{k_1 k_2 k_3; k'_1 k'_2 k'_3} &= \delta_{k_1, k'_1} \delta_{k_2, k'_2} \delta_{k_3, k'_3} [\varepsilon(k_1) + \varepsilon(k_2) + \varepsilon(k_3)] \\ &\quad + \frac{1}{N_{\text{mol}}} \left\{ \delta_{k_1, k'_1} \left[ \tilde{D}(k_2 - k'_2) - 2\tilde{J}(k_2) - 2\tilde{J}(k'_2) \right] \right. \\ &\quad \left. + \delta_{k_2, k'_2} \left[ \tilde{D}(k_3 - k'_3) - 2\tilde{J}(k_3) - 2\tilde{J}(k'_3) \right] \right. \\ &\quad \left. + \delta_{k_3, k'_3} \left[ \tilde{D}(k_1 - k'_1) - 2\tilde{J}(k_1) - 2\tilde{J}(k'_1) \right] \right\} \end{aligned} \quad (3.100)$$

The advantage of Eq. (3.99) over Eq. (3.95) is that the matrix  $\mathbf{B}$  is symmetric, which leads to easier diagonalization.

The energies of three-exciton states can be obtained by diagonalizing the matrix  $\mathbf{B}$  in Eq. (3.99) and filtering out the eigenvalues whose corresponding eigenvectors don't satisfy Eq. (3.97). As a proof-of-principle example, we have solved Eq. (3.99) for a small lattices under the nearest-neighbor approximation and present the results in Fig. 3.5. As can be seen from the figure, three excitons may form a three-body bound state or a biexciton plus a free exciton. Since the energies of three-body bound states are located outside the energy continuum of a biexciton plus a free exciton, an interesting question arise, “Do three-body bound states of excitons exist when two-body bound states don't form, that is, does the Efimov effect occur in the current case?”. Unfortunately, numerical investigation shows that the three-body and two-body bound states always occur at the same time when  $D/J$  reaches 2, indicating no Efimov effect. However, this is not a conclusive result as

only the interaction between nearest neighbors are included in the calculation and the effect of long-range interactions needs to be examined.

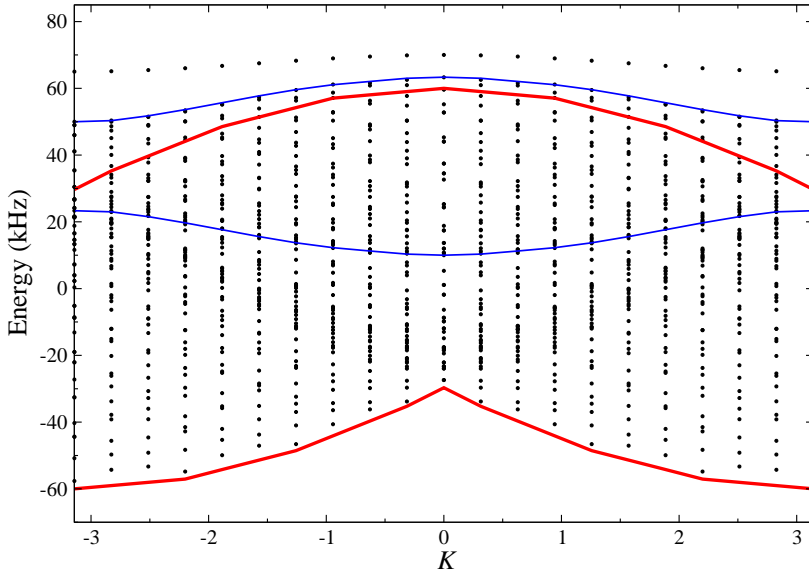


**Figure 3.5:** Three-excitation spectra of a 1D array of molecules on an optical lattice. The calculation is done for a system of 20 lattice sites with the hopping interaction  $J = 10$  kHz and the dynamic interaction  $D = 30$  kHz. The black dots represent energies of all three-exciton states, the red curves denote the boundaries of energy continuum of three free excitons, and the blue curves represent the boundaries of energy continuum for a biexciton plus a free exciton.

### 3.6 Discussion

We have shown that rotational excitation of molecules trapped on an optical lattice gives rise to rotational excitons whose interactions can be controlled by an external electric field. The exciton–exciton interactions can be tuned to produce two-exciton bound states. A biexciton is an entangled state of two Frenkel exci-

tons. The creation of biexcitons and tuning of the electric field to the regime of zero binding energy can thus be used for the controlled preparation of entangled pairs of non-interacting excitons. In order to observe the biexcitons, one could measure correlations between the populations of the rotationally excited states of molecules on different lattice sites by applying a gradient of an electric field and detecting resonant transitions from Stark-shifted levels, as proposed in Ref. [59].

The present work suggests several interesting questions. For example, it was recently shown that Frenkel excitons in shallow optical lattices can be coupled to lattice phonons, leading to polarons [69]. Coupling a Frenkel biexciton to phonons would produce strongly interacting polarons. It would be interesting to explore whether these interactions lead to the formation of bipolarons.

We have repeated the calculations presented here for a system of three excitons and similarly observed the formation of three-exciton bound states. It would be interesting to explore the effect of tunable exciton–exciton interactions on excitation correlations, both as a function of  $D/J$  and the density of excitations, to understand fundamental limits of exciton clustering [132].

The creation of biexcitons with tunable binding energy and measuring quantum energy transport for different ratios  $D/J$  can be used to study the effects of exciton–exciton entanglement on energy transfer in molecular aggregates [133–135]. The ability to tune exciton–exciton interactions can be used to explore the role of multiple excitation correlations on energy transfer in disordered systems (the confining lattice potential can be tilted or the molecules can be perturbed by a disorder potential produced by an inhomogeneous electric field).

## Chapter 4

# Quantum energy transfer in ordered and disordered arrays

An elementary excitation in an aggregate of coupled particles generates a collective excited state. We show that the dynamics of these excitations can be controlled by applying a transient external potential which modifies the phase of the quantum states of the individual particles. The method is based on an interplay of adiabatic and sudden time scales in the quantum evolution of the many-body states. We show that specific phase transformations can be used to accelerate or decelerate quantum energy transfer and spatially focus delocalized excitations onto different parts of arrays of quantum particles. We consider possible experimental implementations of the proposed technique and study the effect of disorder due to the presence of impurities on its fidelity. We further show that the proposed technique can allow control of energy transfer in completely disordered systems.

### 4.1 Introduction

The experiments with ultracold atoms and molecules trapped in optical lattices have opened a new frontier of condensed-matter physics research[8–17]. The unique properties of these systems – in particular, large ( $> 400$  nm) separation of lattice sites, the possibility of tuning the tunneling amplitude of particles between lattice sites by varying the trapping field and the possibility of controlling

interparticle interactions with external electric or magnetic fields – offer many exciting applications ranging from quantum simulation of complex lattice models [43, 50, 66, 120–127, 136–138] to the study of novel quasi-particles [139] that cannot be realized in solid-state crystals. In the limit of strong trapping field, each site of an optical lattice is populated by a fixed number of ultracold atoms or molecules. Such states can be produced with either bosonic or fermionic particles [62, 138]. Here, we consider an optical lattice fully or partially filled with one particle per lattice site, and assume that tunneling between lattice sites is completely suppressed. Such an array can be thought of as a prototype of a system, in which a single lattice site (or a small number of lattice sites) can be individually addressed by an external field of a focused laser beam. This can be exploited for engineering the properties of quantum many-body systems by changing the energy of particles in individual lattice sites [140].

In the present chapter, we consider the generic problem of energy transfer – i.e. the time evolution of an elementary quantum excitation – in such a system. In particular, we explore the possibility of controlling energy transfer through an array of coupled quantum monomers by applying monomer-specific external perturbations. This is necessary for several applications. First, collective excitations in molecular arrays in optical lattices have been proposed as high-fidelity candidates for quantum memory [118, 119]. The ability to manipulate collective excitations is necessary for building scalable quantum computing networks [141]. Second, ultracold atoms and molecules in optical lattices can be perturbed by a disorder potential with tunable strength [142]. Engineering localized and delocalized excitations in such systems can be used to investigate the role of disorder-induced perturbations on quantum energy transfer, a question of central importance for building efficient light-harvesting devices [143]. Third, the possibility of controlling energy transfer in an optical lattice with ultracold atoms or molecules can be used to realize inelastic scattering processes with both spatial and temporal control. Finally, control over energy transfer in quantum systems can be used for studying condensed-matter excitations and energy transport without statistical averaging.

An excitation of a coupled many-body system generates a wave packet representing a coherent superposition of single-particle excitations. The method proposed here is based on shaping such many-body wave packets by a series of sudden

perturbations, in analogy with the techniques developed for strong-field alignment and orientation of molecules in the gas phase [144]. Alignment is used in molecular imaging experiments and molecular optics [144–147], and is predicted to provide control over mechanical properties of molecular scattering [148, 149]. Here, we consider the use of similar techniques for controlling quantum energy transfer in an interacting many-body system. When applied to a completely ordered system, the proposed method is reminiscent of the techniques used to move atoms in optical lattices, where a uniform force is applied for a short period of time [150]. The conceptual difference comes from the fact that in the present case the momentum is acquired by a quasi-particle – a collective excitation distributed over many monomers. During the subsequent evolution, the particles do not move – rather, the excitation is transferred from one monomer to another. In order to control such excitations, we exploit an interplay of the adiabatic and sudden time scales, which correspond to single-monomer and multi-monomer evolution. We also exploit the wave-like nature of the excitation wave function to draw on the analogy with wave optics. This analogy, too, is not complete due to the discrete nature of the lattice.

In order to emphasize the generality of the proposed method, we formulate the problem in terms of the general Hamiltonian parameters. We then describe in detail how the required external perturbations can be realized in experiments with ultracold atoms and molecules. The possibility of using rotational excitations in molecular arrays is particularly interesting due to the long lifetime of rotationally excited states. Electronic excitations of atoms in an optical lattice may also give rise to collective excitations [151]. However, the lifetime of these excited states is limited by fast spontaneous emission [152, 153]. We propose a mechanism for suppressing spontaneous decay by tailoring the properties of the excitation wave packets.

The chapter has the following structure. Section 4.2 and Section 4.3 present the results in terms of the general Hamiltonian parameters. Section 4.4 addresses the particular case of ultracold atoms and molecules. Section 4.5 discusses controlled energy transfer in systems with, specifically, dipole - dipole interactions. Section 4.6 considers the effects of lattice vacancies on the possibility of controlling energy transfer and Section 4.7 extends the proposed technique to control of excitation dynamics in strongly disordered arrays with a large concentration of im-

purities. Section 4.8 presents the conclusions.

## 4.2 Sudden phase transformation

Consider, first, an ensemble of  $N$  coupled identical monomers possessing two internal states arranged in a one-dimensional array with translational symmetry. The Hamiltonian for such a system is given by

$$H_{\text{exc}} = \Delta E_{e-g} \sum_n |e_n\rangle\langle e_n| + \sum_{n,m} \alpha(n-m) |e_n, g_m\rangle\langle g_n, e_m|, \quad (4.1)$$

where  $|g_n\rangle$  and  $|e_n\rangle$  denote the ground and excited states in site  $n$ ,  $\Delta E_{e-g}$  is the monomer excitation energy and  $\alpha(n-m)$  represents the coupling between two monomers at sites  $n$  and  $m$ . Any singly excited state of the system is given by

$$|\psi_{\text{exc}}\rangle = \sum_{n=1}^N C_n |e_n\rangle \prod_{i \neq n} |g_i\rangle. \quad (4.2)$$

In general, the expansion coefficients  $C_n$  are complicated functions of  $n$  determined by the properties of the system, in particular, the translational invariance or lack thereof as well as the strength of the disorder potential. If an ideal, periodic system with lattice constant  $a$  is excited by a single-photon transition, the expansion coefficients are  $C_n = e^{iakn}/\sqrt{N}$  and  $|\psi_{\text{exc}}\rangle \Rightarrow |k\rangle$  represents a quasi-particle called Frenkel exciton, characterized by the wave vector  $k$  [99]. The magnitude of the wave vector  $k$  is determined by the conservation of the total (exciton plus photon) momentum. The energy of the exciton is given by

$$E(k) = \Delta E_{e-g} + \alpha(k), \quad (4.3)$$

with  $\alpha(k) = \sum_n \alpha(n) e^{-iakn}$ . In the nearest neighbor approximation

$$E(k) = \Delta E_{e-g} + 2\alpha \cos ak, \quad (4.4)$$

where  $\alpha = \alpha(1)$ .

With atoms or molecules on an optical lattice, it is also possible to generate a localized excitation placed on a single site (or a small number of sites) by apply-

ing a gradient of an external electric or magnetic field and inducing transitions in selected atoms by a pulse of resonant electromagnetic field [59]. The presence of a disorder potential, whether coming from jitter in external fields or from incomplete population of lattice sites, also results in spatial localization. Similar to how Eq. (4.2) defines the collective excited states in the basis of lattice sites, the same excitation state  $|\psi_{\text{exc}}\rangle$  can be generally written as a coherent superposition of the exciton states  $|k\rangle$  with different  $k$ :

$$|\psi\rangle = \sum_k G_k |k\rangle, \quad (4.5)$$

where  $G_k$ 's are the Fourier transforms of  $C_n$ 's in Eq. (4.2).

Control over energy transfer in an ordered array can be achieved by (i) shifting the exciton wave packets in the momentum representation (which modifies the group velocity and the shape evolution of the wave packets) and (ii) focusing the wave packets in the coordinate representation to produce localized excitations in an arbitrary part of the lattice. To achieve this, we propose to apply a series of site-dependent perturbations that modify the phases of the quantum states of spatially separated monomers. These phase transformations change the dynamics of the time evolution of the collective excitations. Here we consider the transformations leading to acceleration or deceleration of collective excitations, while the focusing phase transformations are described in Section 4.3.

### 4.2.1 Group velocity of wave packet

Before we discuss how to accelerate or decelerate the motion of collective excitations, we first clarify what determines their propagation behavior. The propagation dynamics of an exciton wave packet is determined by the exciton dispersion curve. More specifically, the first derivative of the dispersion curve gives approximately the propagation speed of a wave packet in real space. This can be easily shown by simple derivations.

In a perfect crystal, the eigenstates of the system are characterized by a wavevec-

tor  $k$  and their time evolution is determined by  $E(k)$  through

$$\begin{aligned} |k(t)\rangle &= e^{-i\frac{E(k)}{\hbar}t}|k(t=0)\rangle \\ &= \frac{1}{\sqrt{N}} \sum_n e^{i[kan - \frac{E(k)}{\hbar}t]} |n(t=0)\rangle , \end{aligned} \quad (4.6)$$

where  $N$  is the number of sites in the crystal and  $|n(t=0)\rangle$  represents the state of system in which only site  $n$  is in the excited state. It can be seen from Eq. (4.6) that the probability of excitation at each site is always  $1/N$  for state  $|k\rangle$ , so the plane wave  $|k\rangle$  doesn't move in real space, as expected. Different from a plane wave state, a wave packet composed of different  $|k(t)\rangle$  states is not stationary in real space. This is because different  $|k(t)\rangle$  components correspond to different energy  $E(k)$ , so they will have different time evolutions, leading to a time-dependent interference pattern in real space. To illustrate this point, we consider a Gaussian wave packet in  $k$  space

$$\begin{aligned} |\psi(t)\rangle &= A \sum_k e^{-\frac{(k-k_0)^2}{2\sigma_k^2}} |k(t)\rangle \\ &= \frac{A}{\sqrt{N}} \sum_k e^{-\frac{(k-k_0)^2}{2\sigma_k^2}} \sum_n e^{i[kan - \frac{E(k)}{\hbar}t]} |n(t=0)\rangle , \end{aligned} \quad (4.7)$$

where  $A$  is the normalization constant. Expanding  $E(k)$  around the point  $k = k_0$  and ignoring terms with second and higher-order powers of  $(k - k_0)$ , and replacing the summation over  $k$  by integration, an equation describing the time-evolution of the wave packet in real space is obtained, that is

$$|\psi(t)\rangle = A' \sum_n e^{-\frac{(n-v_{gt})^2}{2(1/\sigma_k)^2}} |n(t=0)\rangle , \quad (4.8)$$

where  $A'$  is some factor that has nothing to do with the shape of the wavepacket in real space. The group velocity

$$v_g = \frac{1}{\hbar} \left. \frac{dE(k)}{dk} \right|_{k=k_0} \quad (4.9)$$

determines how fast the center of the wave packet moves in real space. There-

fore, once the exciton dispersion curve is known, the propagation speed of a wave packet centered around  $k_0$  in momentum space can be calculated from the slope of dispersion curve at  $k_0$ .

#### 4.2.2 Phase kicking in quasimomentum space

As an example, Fig. 4.1 presents an exciton dispersion curve. It can be seen that different regions of the dispersion curve have different slopes, corresponding to different group velocities. Direct optical excitation can create an exciton wave packet which centers around  $k \approx 0$  in the  $k$  space. However, such a wave packet hardly travels in real space as a whole since its group velocity is zero. Based on Fig. 4.1, if we want to accelerate a wave packet centered around  $k = 0$ , a sensible way is to move the wave packet to the region of the Brillouin zone near  $k = \pi/2$  where the slope of the dispersion curve is steep. Similarly, to decelerate a wave packet we should move it to a place where the slope is more shallow. Now the problem of accelerating/decelerating an exciton wave packet becomes the problem of moving the wave packet as a whole in  $k$  space.

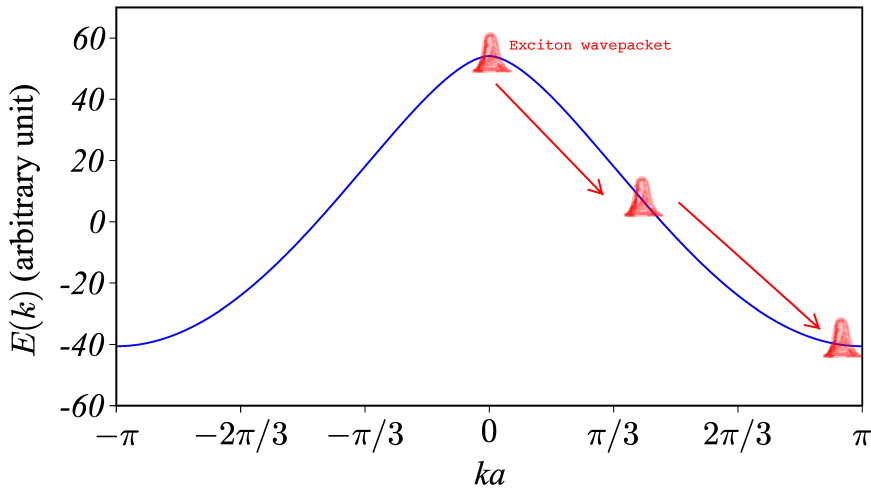


**Figure 4.1:** The dispersion curve of an exciton. The interaction between site  $m$  and site  $n$  is proportional to  $1/|n - m|^3$ .

But how do we move an exciton wave packet in  $k$  space without changing its shape? We can get a hint from the expression of the plane wave state

$$|k(t)\rangle = \frac{1}{\sqrt{N}} \sum_n e^{ikan} |n(t)\rangle . \quad (4.10)$$

This equation suggests that we can change  $|k\rangle$  to  $|k + \delta\rangle$  by adding a factor  $e^{i\delta an}$  to each term in the expansion. Since the increment  $\delta$  is independent of the  $|k\rangle$  state, each  $|k\rangle$  component in a wave packet (Eq. (4.2)) can be transformed into  $|k + \delta\rangle$  in this way. This transformation shifts the wave packets by  $\delta$  in  $k$ -space while preserving their shape. As a result, one can engineer wave packets to probe any part of the dispersion  $E(k)$  leading to different group velocities and shape evolution.

Knowing that adding the proper phases is a key step, we now study how to add those phases. There are two different time scales involved: one is related to the evolution of the free monomer states,  $T_m = \hbar/\Delta E_{e-g}$ , and the other is related to the excitation population transfer between monomers,  $T_e = \hbar/\alpha$ . Usually,  $T_m$  is smaller than  $T_e$  by several orders of magnitude. This huge difference in magnitude enables us to work with the adiabatic and sudden time scales at the same time as described below. Consider the  $n$ -th monomer subjected to an external field  $\mathcal{E}_n(t)$  which varies from 0 to some value and then back to 0 in time  $T$ . If the variation is adiabatic with respect to the evolution of the free monomer states,  $T \gg T_m$ , each eigenstate  $|f\rangle$  of the monomer acquires a state-dependent phase shift [154]

$$|f_n(T)\rangle = e^{i\phi_n^f} |f_n(0)\rangle , \quad (4.11)$$

where

$$\phi_n^f = -\frac{1}{\hbar} \int_0^T E_n^f(t) dt , \quad (4.12)$$

and  $E_n^f(t)$  is the instantaneous eigenenergy and  $f$  can be  $e$  or  $g$ . Now consider the action of such a phase change on the collective excitation state of Eq. (4.2). If  $T \ll T_e$ , the change is sudden with respect to the excitation transfer between monomers, so during the time  $T$  the excitation probability doesn't have enough time to propagate between different monomers and the  $C_n$ 's in Eq. (4.2) remain almost the same. Since the  $G_k$ 's are just Fourier transforms of  $C_n$ 's,  $G_k$  will remain

the same as well, conserving the shape of the wave packet  $|\psi_{\text{exc}}\rangle$  in  $k$  space. The wave packet  $|\psi_{\text{exc}}\rangle$  then acquires a site-dependent phase  $\Phi_n = \phi_n^e - \phi_n^g$  that will influence each  $|k\rangle$  component in the same way. If  $\Phi_n = \Phi_0 + na\delta$ , then the momentum  $\delta$  is imparted onto the excitonic wavefunction without changing its shape. By analogy with the “pulsed alignment of molecules” [144], we call this transformation a “phase kick” or “momentum kick”. Its action is also similar to that of a thin prism on a wavefront of a monochromatic laser beam.

In order to illustrate the shifting of exciton wave packets in the momentum space, we solve numerically the time-dependent Schrödinger equation with the unperturbed Hamiltonian of Eq. (4.1), subjected to a transient site-dependent external perturbation that temporarily modulates  $\Delta E_{e-g}$ . We choose the parameters  $\Delta E_{e-g} = 12.14$  GHz,  $\alpha = 22.83$  kHz and the lattice constant  $a = 400$  nm that correspond to an array of polar molecules trapped in an optical lattice, as described in detail in Section 4.4. The time-dependent perturbation has the form of a short pulse with the duration  $T = 3$   $\mu$ s. The phase acquired by the particles during this time is given by  $\Phi_n \simeq \Phi_0 - 1.29n$ , which can be achieved with a focused laser beam, as described in Section 4.4.

The excitation at  $t = 0$  is described by a Gaussian wave packet of the exciton states  $|\psi_{\text{exc}}(k)\rangle$ , with the central wavevector  $k = 0$ . Figure 4.2 shows that the entire wave packet acquires momentum during the external perturbation pulse (left panels). This is manifested as a phase variation in the coordinate representation, and as a shift of the central momentum in the  $k$ -representation. After the external perturbation is gone, the wave packet does not evolve in the  $k$ -representation but moves with the acquired uniform velocity in the coordinate representation.

As a side note, if the laser intensity remains the same after reaching the maximum, the wave packet oscillates in momentum and coordinate spaces (see Fig. 4.3). This phenomenon is analogous to conventional Bloch oscillations although here the force is acting on a quasi-particle rather than on real particles[155]. This suggests the possibility of studying condensed-matter excitations and energy transport without statistical averaging.

The results presented in Fig. 4.2 and all subsequent results of this work are for a single collective excitation in an interacting many-particle system. A general experimental implementation may result in multiple excitations, leading to non-

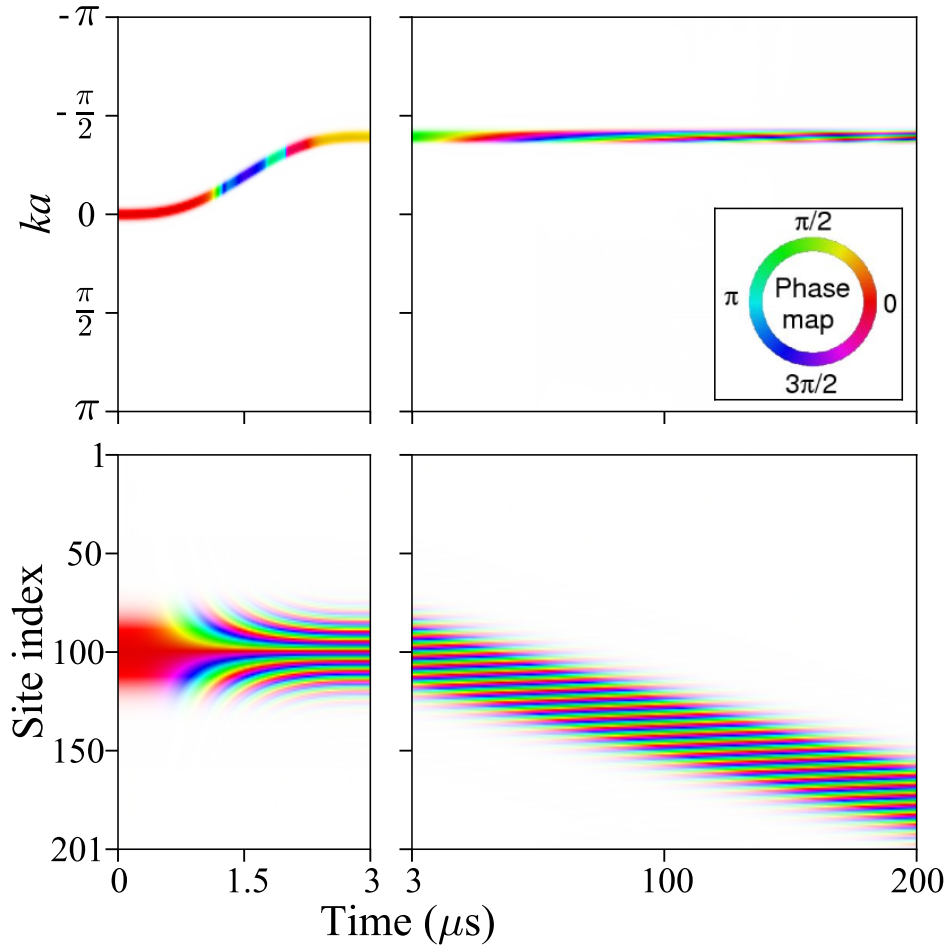


**Figure 4.2:** Example of controlled energy transfer in a one-dimensional array of quantum monomers subjected to a linear phase transformation. The graph illustrates the evolution of the exciton wave packet centered at  $k = 0$  and initially positioned at the center of the array. The phase of the wave function is shown by color. The brightness of color corresponds to the amplitude of the excitation with white color corresponding to zero amplitude. The calculation is for a one-dimensional array of 201 monomers with  $\alpha = 22.83$  kHz and  $\Delta E_{e-g} = 12.14$  GHz, and the linear phase transformation  $\Phi_n \simeq \Phi_0 - 1.29n$ . The corresponding experimental setup is illustrated in Fig. 4.6

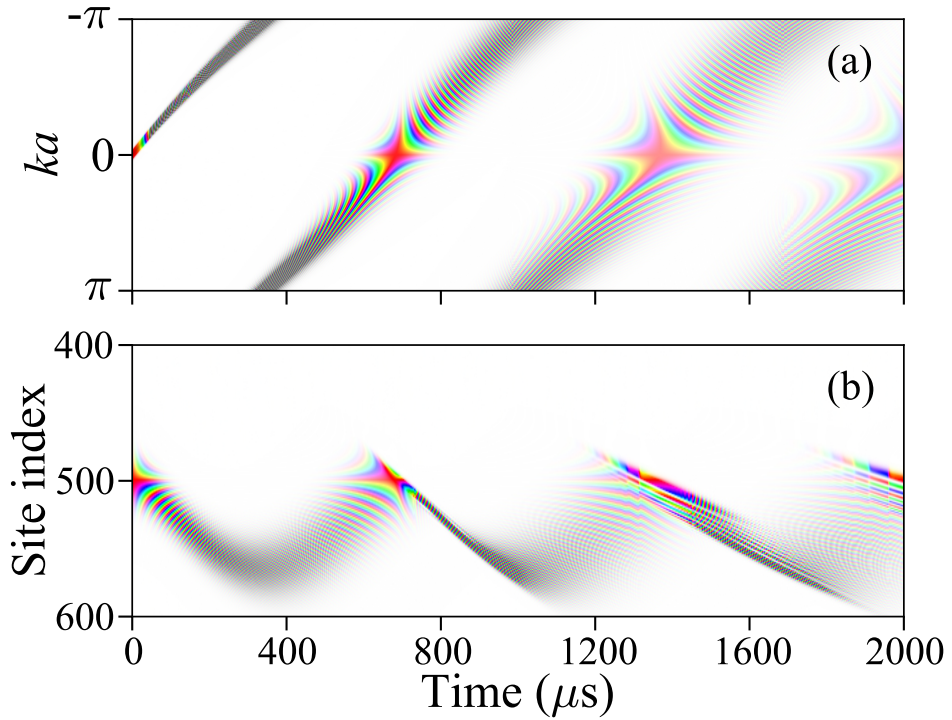


**Figure 4.3:** “Bloch oscillation” of the exciton wave packet in the momentum and coordinate spaces. The phase of the wave function is shown by color as in Fig. 4.2. A low laser intensity of  $10^6 \text{ W/cm}^2$  is used and all other parameters are the same as in Fig. 4.2. Part (a) shows that the wave packet moves in  $k$  space in response to the linear laser field. However, since the wave vector is limited in the first Brillouin zone, when the wave packet reaches  $-\pi$  or  $\pi$ , it disappears at the boundary and reappears at the other boundary. Part (b) presents the motion of the wave packet in coordinate space in accordance with the phase kicking in  $k$  space. Note that the wave packet spreads in both the momentum and coordinate spaces because the laser intensity profile along the molecular array is not perfect and this is amplified over an extended time period.

linear exciton interactions. There are two mechanisms for exciton - exciton interactions: kinematic interactions arising from the statistical properties of excitons and dynamical interactions determined by the matrix elements of the inter-particle interactions in the Hilbert sub-space of binary excitations [99, 156]. The effects of the kinematic interactions on energy transfer in molecular crystals have never been observed so these interactions are considered to be weak, especially in the limit of a small number of excitations easily achievable in experiments [157]. For molecules on an optical lattice, the dynamical interactions are important in the presence of strong external electric fields where molecular states of different parity are strongly mixed [67, 139]. At weak parity-mixing fields considered here, the exciton-exciton interactions insignificantly mix different  $k$  states of the individual excitons, contributing weakly to localization. These effects are expected to be much smaller than the disorder-induced perturbations, discussed in Section 4.6 and Section 4.7.

### 4.3 Focusing of a delocalized excitation

In order to achieve full control over excitation transfer, it is desirable to find a particular phase transformation that focuses a delocalized many-body excitation onto a small part of the lattice, ideally a single lattice site. In optics, a thin lens focuses a collimated light beam by shifting the phase of the wavefront, thus converting a plane wave to a converging spherical wave. Similarly, a phase kick can serve as a time domain “lens” for collective excitations: an excitation initially delocalized over a large number of monomers can be focused onto a small region of the array after some time. By analogy with optics, a concave or convex symmetric site-dependent phase  $\Phi(n)$  applied simultaneously to all monomers may turn a broad initial distribution  $C_n(t = 0)$  into a narrow one.

The dynamics of the excitation state in the lattice is determined by the time dependence of the coefficients  $C_n(t)$  in Eq. (4.2). In order to find the expression for  $C_n(t)$ , we expand the amplitudes at  $t = 0$  in a Fourier series

$$C_n(t = 0) = \sum_q \frac{e^{iqn}}{\sqrt{N}} C(q; t = 0) , \quad (4.13)$$

and apply the propagator  $e^{-iE(q)t/\hbar}$  to each  $q$ -component with  $E(q)$  representing the exciton energy given by Eq. (4.4). Transforming the amplitudes  $C(q)$  back to the site representation then yields

$$C_m(t) = \frac{1}{N} \sum_{n,k} C_n(t=0) e^{i[\Phi(n)+ka(m-n)-E(k)t/\hbar]}, \quad (4.14)$$

where  $\Phi(n)$  is a site-dependent phase applied at  $t = 0$ , as described in the previous section. Note that the phase  $\Phi(n)$  does not have to be applied instantaneously. The phase  $\Phi(n,t)$  can be applied continuously over an extended time interval as long as the accumulated phase gives the desired outcome  $\int_0^T \Phi(n,t) dt = \Phi(n)$ .

### 4.3.1 Focusing to a single site

As Eq. (4.14) shows, the focusing efficiency is determined by the phase transformation and the shape of the dispersion curve  $E(k)$ . Given the cosine dispersion of excitons in Eq. (4.4), is it possible to focus a delocalized excitation onto a single lattice site? To answer this question, we assume an initial condition where the excitation is localized to the site  $n_0$ , that is

$$C_n(t=0) = \delta_{n,n_0}, \quad (4.15)$$

and run a backward-in-time evolution to calculate the coefficients  $C_m(t)$  at  $t = -\tau$ : using the expansion of an exponent in Bessel functions (Jacobi-Anger expansion, see Ref. [158])

$$e^{iacosx} = \sum_n e^{-i(x-\pi/2)n} J_n(a), \quad (4.16)$$

we obtain

$$\begin{aligned}
C_m(-\tau) &= \frac{1}{N} \sum_{n,k} C_n(t=0) e^{i[ka(m-n)-E(k)(-\tau)/\hbar]} \\
&= \frac{1}{N} \sum_{n,k} C_n(t=0) e^{ika(m-n)} \sum_{n'} e^{-i(ka-\pi/2)n'} J_{n'}(2\alpha\tau/\hbar) \\
&= \frac{1}{N} \sum_{n,k} \delta_{n,n_0} e^{ika(m-n)} \sum_{n'} e^{-i(ka-\pi/2)n'} J_{n'}(2\alpha\tau/\hbar) \\
&= \frac{1}{N} \sum_k e^{ika(m-n_0)} \sum_{n'} e^{-i(ka-\pi/2)n'} J_{n'}(2\alpha\tau/\hbar) \\
&= \sum_{n'} e^{i\pi n'} J_{n'}(2\alpha\tau/\hbar) \left( \frac{1}{N} \sum_k e^{ika(m-n_0-n')} \right) \\
&= \sum_{n'} e^{i\pi n'} J_{n'}(2\alpha\tau/\hbar) \delta_{n',m-n_0} \\
&= e^{i\pi(m-n_0)/2} J_{m-n_0}(2\alpha\tau/\hbar), \tag{4.17}
\end{aligned}$$

where  $J_n$  are Bessel functions of the first kind. This calculation shows that a wavepacket in the site representation,  $C_m(0) = e^{i\pi(m-n_0)/2} J_{m-n_0}(2\alpha t/\hbar)$ , will focus onto the lattice site  $n_0$  after evolving for time  $t$ . We can easily verify the result by running a forward-in-time evolution starting with the initial wave packet and making use of the orthonormality of the Bessel functions

$$\sum_n J_n(x) J_{n-m}(x) = \delta_{m,0}. \tag{4.18}$$

Eq. (4.17) shows that the focusing of a wave packet onto a single site would require not only adding the phase  $\Phi(n) = \text{Arg}[C_m(-\tau)]$ , but also the amplitude modulations of the coefficients equal to the absolute values of  $C_m(-\tau)$ . This second task is beyond the manipulation tools considered here. Creating such a wave packet may require multiple and complicated phase transformations, which may be difficult to realize in experiments.

### 4.3.2 Focusing a broad wavepacket in coordinate space

A simpler procedure can be implemented if the phase transformations are restricted to a particular part of the exciton dispersion. From wave optics, waves with quadratic dispersion can be focused, while those with linear dispersion propagate without changing the wave packet shape [159, 160]. It is this interplay of the quadratic (at low  $k$ ) and linear (at  $k \approx \pm\pi/2a$ ) parts of the cosine-like exciton dispersion (Eq. (4.4)) that precludes perfect focusing of a general collective excitation. In order to avoid the undesirable amplitude modulations, it may be possible to focus delocalized excitations by a phase transformation that constrains the wave packet of Eq. (4.5) to the quadratic part of the dispersion  $E(k)$ . For such wave packets, adding a quadratic phase  $\Phi(n) = \Phi_0(n - n_0)^2$  must lead to focusing around site  $n_0$ . Below we illustrate the effect of the quadratic phase transformation for a broad wave packet in coordinate space. In the next subsection (Section 4.3.3), we continue to explore the case of a plane wave.

Consider a Gaussian wave packet with a narrow width  $\sigma_{k,0}$  centered around  $k = 0$  in  $k$  space with

$$C_k = A e^{-\frac{a^2 k^2}{2\sigma_{k,0}^2}}, \quad (4.19)$$

where  $A$  is some normalization factor. Since the normalization factor doesn't matter for the discussion here, we will ignore it in the following derivations. The wave packet represented by Eq. (4.19) is also a Gaussian wave packet in coordinate space. This can be verified by the transformation from  $k$  space to coordinate

space , that is

$$\begin{aligned}
C_n &= \frac{1}{\sqrt{N}} \sum_k C_k(t=0) e^{ikan} \\
&\approx \frac{A}{\sqrt{N}} \int_{-\infty}^{\infty} dk e^{-\frac{a^2 k^2}{2\sigma_{k,0}^2} + ikan} \\
&= \frac{A}{\sqrt{N}} e^{-\frac{n^2}{2\sigma_{k,0}^2}} \int_{-\infty}^{\infty} dk e^{-\frac{1}{2\sigma_{k,0}^2}(ka - in\sigma^2)^2} \\
&= \frac{A}{\sqrt{N}} \frac{\sigma_{k,0} \sqrt{2\pi}}{a} e^{-\frac{n^2 \sigma_{k,0}^2}{2}} \\
&\propto e^{-\frac{n^2}{2(1/\sigma_{k,0})^2}}, \tag{4.20}
\end{aligned}$$

where in the second step the integration approximates the summation over  $k$  in the first Brillouin zone with its range extended from  $(-\pi/a, \pi/a]$  to  $(-\infty, \infty)$  since the width  $\sigma_k$  is very small. Eq. (4.20) also shows that the width of the wave packet in coordinate space is the inverse of its width in  $k$  space, that is,  $\sigma_{x,0} = 1/\sigma_{k,0}$ .

To focus the wave packet, we apply an inhomogeneous phase  $\Phi(n) = \Phi_0(n - n_0)^2$  at  $t = 0$  so that the wave packet becomes

$$C_n(t=0) \propto e^{-\frac{n^2}{2(1/\sigma_{k,0})^2}} e^{i\Phi_0(n-n_0)^2}, \tag{4.21}$$

which upon a transformation from coordinate space to  $k$  space gives

$$\begin{aligned}
C_k(t=0) &= \frac{1}{\sqrt{N}} \sum_n C_n(t=0) e^{-ikan} \\
&\approx \frac{1}{\sqrt{N}} \int_{-\infty}^{\infty} dn C_n(t=0) e^{-ikan} \\
&\propto e^{\frac{-a^2 k^2 + 4akn_0\Phi_0 + 2in_0^2\sigma_{k,0}^2\Phi_0}{2(\sigma_{k,0}^2 - 2i\Phi_0)}}. \tag{4.22}
\end{aligned}$$

The exponent in Eq. (4.22) can be separated into a real part and an imaginary part. Since the imaginary part contributes only a trivial phase to the wavefunction and

doesn't change the shape of the wave packet, we can ignore it and obtain

$$C_k(t=0) \propto e^{-\frac{\sigma_{k,0}^2(ka-2n_0\Phi_0)^2}{2(\sigma_{k,0}^4+4\Phi_0^2)}}. \quad (4.23)$$

So the width of the wave packet after adding the phase is

$$\sigma_k(t=0) = \sqrt{\sigma_{k,0}^2 + \frac{4\Phi_0^2}{\sigma_{k,0}^2}}, \quad (4.24)$$

which is obviously larger than the initial width  $\sigma_{k,0}$ . This indicates that the phase applied for focusing cannot be too large. Otherwise the wave packet will be broadened beyond the quadratic region of the dispersion curve where the focusing scheme doesn't work. Note that the phase does not affect the width of the wave packet in coordinate space since it only adds some phase to the coefficients  $C_n(t=0)$  in Eq. (4.20).

To see how the wave packet evolves after the phases are added, we can apply the propagator  $e^{-iE(k)t/\hbar}$  to Eq. (4.23) and convert the wavefunction into coordinate space. Assuming the width  $\sigma_k(t=0)$  is very small so that a large proportion of the wave packet is within the quadratic region of the dispersion curve, then the eigen energy of the  $|k\rangle$  state can be approximated as

$$E(k) \approx E_0 + \beta a^2 k^2. \quad (4.25)$$

Using this equation, we obtain the wavefunction of the wave packet after time  $t$

$$\begin{aligned} C_n(t) &= \frac{1}{\sqrt{N}} \sum_k e^{ikan} e^{-iE(k)t/\hbar} C_k(0) \\ &\propto \sum_k e^{ikan} e^{-iE(k)t/\hbar} e^{-\frac{\sigma_{k,0}^2(ka-2n_0\Phi_0)^2}{2(\sigma_{k,0}^4+4\Phi_0^2)}} \\ &\propto e^{-\frac{(n+4t\beta\Phi_0\eta_0)^2}{2\sigma_k^2(t)}}, \end{aligned} \quad (4.26)$$

where  $\sigma_x(t)$  is a time-dependent width given by

$$\sigma_x(t) = \sigma_{x,0} \sqrt{(1+4t\beta\Phi_0)^2 + \frac{4t^2\beta^2}{\sigma_{x,0}^4}}. \quad (4.27)$$

Taking the derivative of  $\sigma_x(t)$  with respect to time and setting it to zero, we can find the time at which the wave packet is most focused, namely

$$T_F = -\frac{\Phi_0 \sigma_{x,0}^4}{\beta \left(1+4\Phi_0^2 \sigma_{x,0}^4\right)}. \quad (4.28)$$

At time  $T_F$ , the minimum width is

$$\sigma_{x,F} = \frac{\sigma_{x,0}}{\sqrt{1+4\Phi_0^2 \sigma_{x,0}^4}}, \quad (4.29)$$

and the center of the wave packet is at

$$n_c = 4T_F \beta \Phi_0 n_0 = \frac{4\Phi_0^2}{\sigma_{k,0}^4 + 4\Phi_0^2} n_0 \approx n_0. \quad (4.30)$$

Eq. (4.29) shows that the wave packet will become more focused at site  $n_0$  at  $T_F$  since  $\sigma_{x,F} < \sigma_{x,0}$  and that a larger phase  $\Phi_0$  will lead to a better focusing effect. However, as we discussed before, large values of  $\Phi_0$  may take the wave packet outside the quadratic part of the dispersion making Eq. (4.25) invalid. Therefore, the best focusing effect can only be achieved by balancing the two factors.

In the case of excitons with the cosine dispersion curve represented by Eq. (4.4),  $\beta = -\alpha a^2$ . To find the optimal phase  $\Phi_0^*$  that keeps the wave packet within the quadratic dispersion while focusing it, we use the condition  $\sigma_{k,0} \lesssim 1$ , which yields  $\Phi_0^* = \pm 1/2\sigma_{x,0}$  for the optimal focusing. At time

$$t_* \approx 1/4\alpha\Phi_0^*, \quad (4.31)$$

the wave packet is most focused and has a width

$$a\sigma_{x,F}(\Phi_0^*) = \frac{a\sigma_{x,0}}{\sqrt{1+4\Phi_0^{*2}\sigma_{x,0}^4}} \sim a. \quad (4.32)$$

For the time  $t_*$  in Eq. (4.31) to be positive,  $\alpha$  and  $\Phi_0^*$  must have the same sign. Therefore, a convex quadratic phase profile  $\Phi(n)$  with  $\Phi_0 > 0$  must focus collective excitations in a system with repulsive couplings between particles in different lattice sites ( $\alpha > 0$ ), and a concave quadratic phase profile  $\Phi(n)$  with  $\Phi_0 < 0$  must focus excitations in a system with attractive couplings ( $\alpha < 0$ ).

### 4.3.3 Focusing a plane wave in coordinate space

Consider a completely delocalized excitation of Eq. (4.2) with  $C_n(k; t=0) = e^{iakn}/\sqrt{N}$  describing an eigenstate of an ideal system of  $N$  coupled monomers. Suppose  $E(k)$  in Eq. (4.14) can be approximated as  $E(k) = \Delta E_{e-g} - \alpha a^2 k^2$ . As we saw in the derivation of last section, the effect of  $E(k)$  on the wave packet is to add a phase due to time evolution, i.e.  $e^{-iE(k)t}$ . Since  $\Delta E_{e-g}$  in  $E(k)$  contributes the same phase to all  $k$  components and thus adds a trivial phase to the whole wavefunction, we can safely ignore it if only the shape of the wavefunction is concerned. Therefore, we use  $E(k) = -\alpha a^2 k^2$  instead in the following derivation. To focus the plane wave, the quadratic phase  $\Phi(n) = \Phi_0 n^2$  is applied at  $t = 0$ . This changes the initial wavefunction to

$$C_n(k; t=0) = \frac{1}{\sqrt{N}} e^{ikan} e^{i\Phi_0 n^2}, \quad (4.33)$$

which renders the wavefunction a wave packet in  $k$  space with the coefficients

$$C_q(t=0) = \frac{1}{\sqrt{N}} \sum_n e^{-iqan} C_n(k; t=0). \quad (4.34)$$

Each  $q$  component in this equation evolves according to

$$C_q(t) = e^{-iE(q)t} C_q(0) = e^{i\alpha a^2 q^2} C_q(0), \quad (4.35)$$

and the wavefunction in coordinate space after time  $t$  is given by

$$\begin{aligned}
C_m(t) &= \frac{1}{\sqrt{N}} \sum_q e^{iqam} C_q(t) \\
&= \frac{1}{N\sqrt{N}} \sum_q e^{iqam} e^{i\alpha a^2 q^2} \sum_n e^{-iqan} e^{ikan} e^{i\Phi_0 n^2} \\
&= \frac{e^{-i\alpha a^2 k^2}}{N} \sqrt{\frac{i\pi}{N\Phi_0}} \sum_q e^{i[a^2(k-q)^2(\alpha t - 1/4\Phi_0) + qa(m+2\alpha ak)]} \\
&\quad \times \Theta\left(-\frac{N\Phi_0}{a} < k - q < \frac{N\Phi_0}{a}\right), \tag{4.36}
\end{aligned}$$

where  $\Theta(z) = 1$  if  $z$  is true and zero otherwise. In order to derive Eq. (4.36), we used the approximate equality

$$\int_{-M}^M dx e^{-i(ax^2+bx)} \approx \sqrt{\frac{\pi}{ia}} e^{ib^2/4a} \Theta(-2Ma < b < 2Ma), \tag{4.37}$$

obtained by approximating the error function of a complex argument  $\text{Erf}(\sqrt{ix})$  by the sign function, which is accurate for large argument  $x$ .

At time  $t_* = 1/4\alpha\Phi_0$ , the terms quadratic in  $q$  in Eq. (4.36) are canceled, and the sum over  $q$  reduces to a delta-function, if the summation limits are from  $-\pi/a$  to  $\pi/a$ . Therefore, the choice  $\Phi_0 = \pi/N$  yields

$$C_m(t) = \sqrt{i} e^{-iNa^2k^2/4\pi} \delta_{m,-v_k}, \tag{4.38}$$

where  $v_k$  is the index of the initial wave vector  $k = 2\pi v_k/Na$ , quantized due to the discreteness of the lattice. According to the step function  $\Theta(z)$  in Eq. (4.36), the dimensionless width of the wave packet in the wave vector space is  $\Delta_k(\Phi_0) \equiv a\sigma_k(\Phi_0) \approx 2N\Phi_0$ . When  $\Phi_0 = \pi/N$ , the wave packet spreads over the entire Brillouin zone, including the linear parts of the exciton dispersion. Using Eq. (4.37) we find that for an arbitrary value of  $\Delta_k(\Phi_0)$ , the site amplitudes at the time of

focusing  $t_* = 1/4\alpha\Phi_0$  are

$$C_n(k; t = t_*) \approx \frac{e^{i\Delta(\Phi_0)n^2/2N}}{n} \sqrt{\frac{2i}{\pi\Delta_k(\Phi_0)}} \sin(n\Delta_k(\Phi_0)/2). \quad (4.39)$$

In order to keep the linear part of the dispersion spectrum unpopulated, we choose the optimal focusing phase  $\Phi_0^* \sim 1/2N$ , so that  $\Delta_k(\Phi_0^*) \sim 1$ .

#### 4.3.4 Numerical results

In Section 4.3.2 and Section 4.3.3, Eq. (4.32) and Eq. (4.39) are derived based on the cosine dispersion curve which is valid for a many-body system with nearest neighbor interactions only. In most physical systems, the energy dispersion is modified by long-range couplings. In order to confirm that the above predictions are also valid for systems with long-range interactions and illustrate the focusing of delocalized excitations, I compute the time evolution of the wave packets by solving the wave equation numerically for a system with long-range dipole-dipole interactions. In the calculations, I expanded the Hamiltonian of Eq. (4.1) in the site basis, i.e.  $\{|e_n\rangle \prod_{i \neq n} |g_i\rangle\}$ , and applied the corresponding phase to the state  $|e_n\rangle$  of each site at  $t = 0$  and then calculated the time evolution to obtain the wavefunction at each time point. To find the time for the optimal focusing, I searched for the largest probability at the target focusing site while scanning the wavefunctions at every time point. Figure 4.4 illustrates the focusing dynamics of a completely delocalized excitation (panels a and b) and a broad Gaussian wave packet (panels c and d) in a system with all (first neighbor, second neighbor, etc.) couplings explicitly included in the calculation. The results show that the collective excitations can be focused to a few lattice sites. The role of the long-range coupling will be explicitly discussed in Section 4.6.

The focusing scheme demonstrated above can be generalized to systems of higher dimensionality. To illustrate this, we repeated the calculations presented in Fig. 4.4 (c) and Fig. 4.4 (d) for a delocalized excitation placed in a square 2D lattice with an external potential that modulates the phase as a function of both  $x$  and  $y$ . Figure 4.5 shows the focusing of an initially broad wave packet onto different parts of a 2D lattice induced by the quadratic phase transformation  $\Phi(x, y) = \Phi_0[(n_x -$

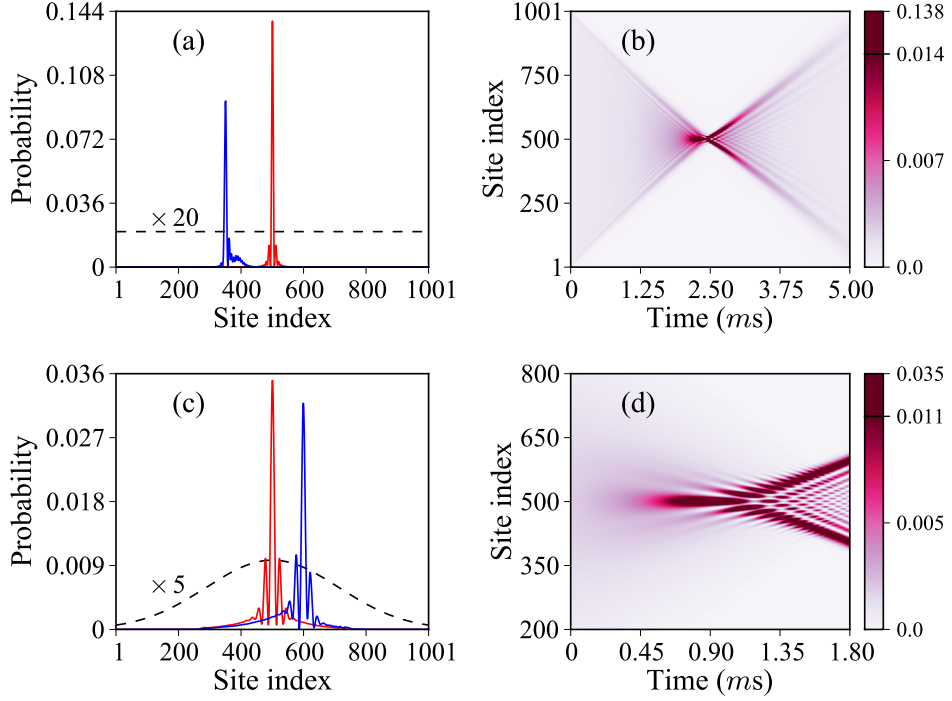


**Figure 4.4:** Focusing of a completely delocalized collective excitation (panels a and b) and a broad Gaussian wave packet of Frenkel excitons (panels c and d) in a one-dimensional array using the quadratic phase transformations at  $t = 0$  as described in Section 4.3.2 and Section 4.3.3. In panels (b) and (d), the excitation probability distribution is displayed by color. The dashed lines show the initial distribution magnified by 20 and 5 respectively in (a) and (c). The solid curves in panels (a) and (c) correspond to two different phase transformations focusing the same wave packet onto different parts of the array. The calculations are performed with the same parameters  $\alpha$ ,  $a$ , and  $\Delta E_{e-g}$  as in Fig. 4.2. The results are computed with all couplings accounted for.

$(n_{x_0})^2 + (n_y - n_{y_0})^2]$ , where  $n_x$  and  $n_y$  are the lattice site indices along the  $x$  and  $y$  directions. The calculations include all long-range couplings as in Fig. 4.4. The comparison of Fig. 4.4 and Fig. 4.5 illustrates that the focusing efficiency in 2D is greater. The results also demonstrate that the delocalized excitations can be effectively focused on different parts of the lattice simply by varying the reference site  $(n_{x_0}, n_{y_0})$  in the phase transformation.

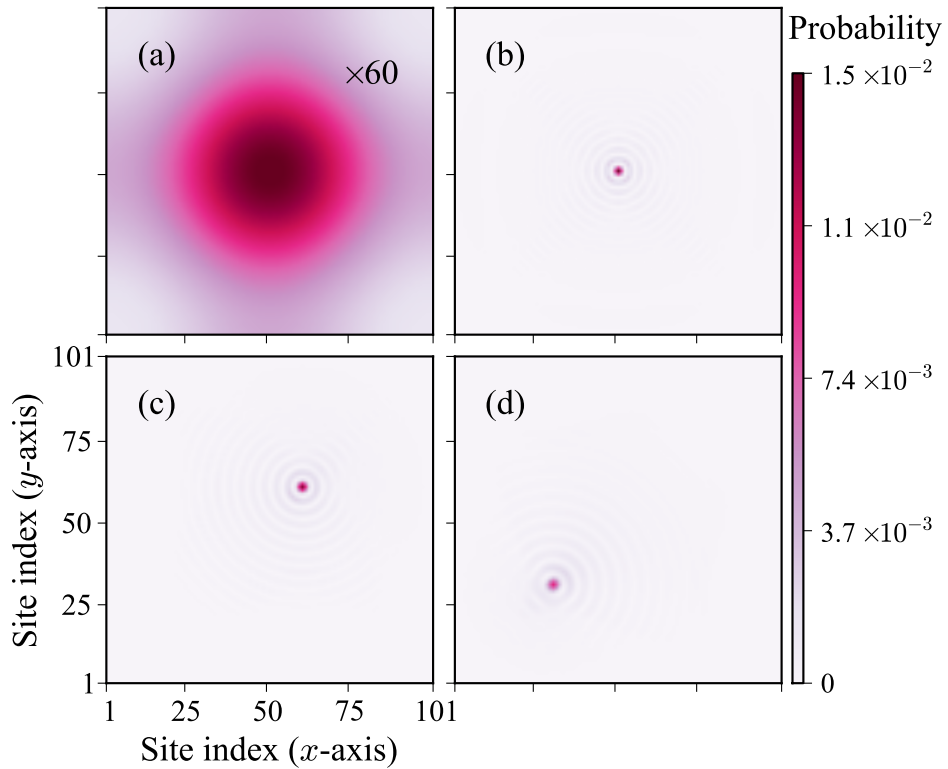


**Figure 4.5:** Focusing of a delocalized excitation in a 2D array shown at  $t = 0$  in panel (a) onto different parts of the lattice (panels b–d). For better visualization, the probability distribution in panel (a) is magnified by a factor of 60. The calculations are performed with the same parameters  $\alpha$ ,  $a$ , and  $\Delta E_{e-g}$  as in Fig. 4.2 and the quadratic phase transformation at  $t = 0$ .

## 4.4 Experimental feasibility of phase transformation

In Section 4.2 and Section 4.3, we discussed the idea of phase kicking and its application in focusing delocalized excitations, but were mainly concerned with the theoretical perspective. In this section, we focus on experimental feasibility and show that the techniques proposed in Section 4.2 and Section 4.3 can be realized with ultracold atoms or molecules trapped in an optical lattice with one particle per lattice site [57, 58, 161, 162]. Three general requirements must be satisfied:

- (i) The time required for a phase transformation must be shorter than the spontaneous decay time of the excited state.
- (ii) The overall coherence of the system must be preserved on the time scale of the excitonic evolution in the entire array, set by  $K\hbar/\alpha$ , where  $K$  is the number of monomers participating in the dynamics of the collective excitation.
- (iii) The lattice constant must be large enough to allow considerable variation of the external perturbation from site to site.

Optical lattices offer long coherence times ( $> 1$  sec) and large lattice constants ( $> 400$  nm) [31]. The lifetime of the collective excitations depends on the internal states of the particles used in the experiment and the momentum distribution of the excitonic states in the wave packet. In the following two subsections, the case of ultracold atoms and molecules are discussed, separately.

### 4.4.1 Suppressing spontaneous emission in system of ultracold atoms

For ultracold alkali metal atoms in an optical lattice, an optical excitation may generate the collective states of Eq. (4.2), as discussed in Ref. [152, 153]. The lifetime of these excited states is limited by the spontaneous emission of the electronically excited atoms and is in the range of 10 - 30 ns. However, the collective excited states can be protected from spontaneous emission if the wave vector range populated by excitons in the wave packet of Eq. (4.5) is outside of the so-called light cone, so that  $k > \Delta E_{e-g}/\hbar c$ . To understand why this is the case, we investigate the

interaction of the collective excitation state of atoms with light. A photon can excite an exciton state of ultracold atoms and the exciton can also decay as a photon. During these optical processes the energy is conserved, which leads to

$$E_{\text{ph}} = \hbar c k = \hbar c \sqrt{k_{\parallel}^2 + k_{\perp}^2} = E_{\text{ex}}(k_{\text{ex}}) , \quad (4.40)$$

where  $k$  and  $k_{\text{ex}}$  represent the magnitudes of the wave vectors of the photon and the exciton, respectively. As written in Eq. (4.40), the wave vector of the photon can be decomposed into two parts: the part ( $k_{\parallel}$ ) that is parallel to  $k_{\text{ex}}$ ; and the other part ( $k_{\perp}$ ) that is perpendicular to  $k_{\text{ex}}$ . Since only the parallel component of  $k$  is conserved in the optical excitation, we have

$$k_{\parallel} = k_{\text{ex}} < k . \quad (4.41)$$

The exciton energy  $E_{\text{ex}}(k_{\text{ex}})$  in Eq. (4.40) can be approximated by the corresponding excitation energy  $\Delta E_{e-g}$  since the interaction  $\alpha$  between atoms is much smaller than the energy gap between the ground state and the excited state of a single atom (see Eq. (4.3)). With this approximation, the wave vector of the photon can be calculated from Eq. (4.40) as

$$k_* = \frac{\Delta E_{e-g}}{\hbar c} . \quad (4.42)$$

Since  $k_{\text{ex}}$  is just the parallel component of  $k_*$ , only the excitonic states with  $k_{\text{ex}} \leq k_*$  can satisfy both the energy conservation (Eq. (4.40)) and the momentum conservation (Eq. (4.41)) at the same time, and thus interact with light. By comparing  $k_*$  and the largest value of  $k_{\text{ex}}$  in the first Brillouin zone  $(-\pi/a, \pi/a]$ , we can obtain the number of excitonic  $k$ -states in the bright and dark regions. For Frenkel excitons originating from electronic transitions in solid-state crystals, the wavelength of excitation light  $\lambda_0$  ( $\sim$  several hundred nm) is much bigger than the lattice constant  $a$  ( $\sim$  a few Å), so the bright region is narrow:  $k_{\text{ex}} < k_* = 2\pi/\lambda_0 \approx 0$ . For atoms trapped in optical lattices, the typical values of  $\lambda_0$  are of the same magnitude as the lattice constant  $a$  (several hundred nm), and a large portion of the dispersion curve lies in the bright region and the dark region may be narrow. In an ideal infinite system those states in the dark region have infinitely long radiative lifetimes, as there is no free-space photon they can emit, assuming the conservation of both

energy and momentum [99, 152, 153, 163]. In finite and/or disordered systems, the emission of photons may occur at the array boundaries or due to perturbations breaking the translational symmetry. In this case, the time scale for spontaneous decay must depend on the size of the system (i.e. the probability of the excitation to reach the array boundary) and the disorder potential breaking the translational symmetry.

Once collective excited states are created, the phase-kicking technique introduced in Section 4.2, if implemented on a time scale faster than the radiative lifetime of a single atom, can be used to shift the excited states in the wave vector space away from the bright region (cf. Fig. 4.2) and thus protect the excited states from fast spontaneous decay. This phase transformation can be induced by a pulse of an off-resonant laser field  $\mathcal{E}_{AC}$ , detuned from the  $e \leftrightarrow g$  resonance by the value  $\delta\omega$ , leading to the AC Stark shift (see e.g. Ref.[159])

$$\Delta E_{AC} = \mathcal{E}_{AC}^2 \frac{V_{eg}^2}{4\delta\omega}, \quad (4.43)$$

where  $V_{eg}$  is the matrix element of the dipole-induced transition. By choosing  $V_{eg} = 1$  a.u.,  $\delta\omega = 3V_{eg}$ , and the laser intensity  $I = 5 \times 10^{10}$  W/cm<sup>2</sup>, we obtain that the shift  $\phi = \Delta E_{AC} \times T_{\text{pulse}} = \pi$  can be achieved in less than 1 ns. Another phase transformation can bring the excited state back to the bright region, where it can be observed via fast spontaneous emission. The experiments with ultracold atoms have demonstrated a lattice filling factor reaching 99 % [57, 58, 161]. The phase transformations proposed here can be used to stabilize excitonic states in ultracold atomic ensembles against spontaneous emission for multiple interesting applications [151, 164].

#### 4.4.2 Phase kicking of collective excitation in arrays of ultracold molecules

The spontaneous decay problem can be completely avoided by using rotational excitations in an ensemble of ultracold polar molecules trapped in an optical lattice. The rotational states are labeled by the quantum number of the rotational angular momentum  $\mathbf{J}$  and the projection  $M_J$  of  $\mathbf{J}$  on the space-fixed quantization axis Z. We choose the rotational ground state  $|J = 0, M_J = 0\rangle$  as  $|g\rangle$  and the rotational

excited state  $|J = 1, M_J = 0\rangle$  as  $|e\rangle$ . The state  $|J = 1, M_J = 0\rangle$  is degenerate with the states  $|J = 1, M_J = \pm 1\rangle$ . This degeneracy can be lifted by applying a homogeneous DC electric field, making the  $|g\rangle$  and  $|e\rangle$  states an isolated two-level system. The molecules on different lattice sites are coupled by the dipole-dipole interaction  $V_{dd}(n - m)$ . The magnitude of the coupling constant  $\alpha(n - m) = \langle e_n, g_m | V_{dd} | n - m \rangle |g_n, e_m\rangle$  between molecules with a dipole moment of 1 Debye separated by 500 nm is on the order of 1 kHz [67]. Due to the low value of  $\Delta E_{e-g}$ , the spontaneous emission time of rotationally excited molecules exceeds 1 second.

For molecules on an optical lattice, one can implement the phase kicks by modifying the molecular energy levels with pulsed AC or DC electric fields. The rotational energy levels for  $^1\Sigma$  molecules in a combination of weak AC and DC electric fields are given by [93]

$$E_{J,M_J} \approx BJ(J+1) + \frac{\mu^2 \mathcal{E}_{DC}^2}{2B} G(J, M_J) - \frac{\alpha_\perp \mathcal{E}_{AC}^2}{4} + \frac{(\alpha_{||} - \alpha_\perp) \mathcal{E}_{AC}^2}{4} F(J, M_J), \quad (4.44)$$

where  $B$  is the rotational constant,  $G(J, M_J)$  is given by

$$G(J, M_J) = \frac{J^2 - |M_J|^2}{J(2J+1)(2J-1)} - \frac{(J+1)^2 - |M_J|^2}{(J+1)(2J+1)(2J+3)}, \quad (4.45)$$

$F(J, M_J)$  is given by

$$F(J, M_J) = -\frac{1}{2} \left[ 1 - \frac{(2|M_J| - 1)(2|M_J| + 1)}{(2J-1)(2J+3)} \right], \quad (4.46)$$

$\mathcal{E}_{AC}$  is the envelope of the quickly oscillating AC field,  $\alpha_{||}$  and  $\alpha_\perp$  are the parallel and perpendicular polarizabilities, and  $\mu$  is the permanent dipole moment of the molecule.

The momentum shift of the exciton wave packets can be achieved by applying a time-varying DC electric field  $\mathcal{E}(t) = \mathcal{E}_* + \mathcal{E}(n) \sin^2(\pi t/T)$ , where  $\mathcal{E}(n)$  is linear with respect to  $n$ . Assuming  $\mathcal{E}(n) = (n - n_0)A$  and  $\mathcal{E}(n) \ll \mathcal{E}_*$ , and using Eq. (4.12) and Eq. (4.44), we obtain the phase accumulated by the excited state  $|1, 0\rangle_n$  at site

$n$  with respect to the ground state:

$$\begin{aligned}
\phi(n) &= -\frac{1}{\hbar} \int_0^T [E_n^e(t) - E_n^g(t)] dt \\
&= -\frac{1}{\hbar} \int_0^T \frac{\mu^2 \mathcal{E}_{DC}^2}{2B} [G(1,0) - G(0,0)] dt \\
&= -\frac{4\mu^2}{15\hbar B} \int_0^T [\mathcal{E}_* + A \sin^2(\pi t/T)(n-n_0)^2] dt \\
&\approx -\frac{4\mu^2}{15\hbar B} \int_0^T [\mathcal{E}_*^2 + 2\mathcal{E}_* A \sin^2(\pi t/T)(n-n_0)] dt \\
&= -\frac{4\mu^2}{15\hbar B} \int_0^T [\mathcal{E}_*^2 T + T \mathcal{E}_* A (n-n_0)] . \tag{4.47}
\end{aligned}$$

In the above equation, the term that is linear with lattice index  $n$  will give the phase kick

$$\delta = -4A\mathcal{E}_*\mu^2 T / 15\hbar Ba . \tag{4.48}$$

I have confirmed this result by a numerical computation showing that for LiCs molecules in an electric field of  $\mathcal{E}_* = 1$  kV/cm, an electric field pulse with  $A = 7.434 \times 10^{-4}$  kV/cm and  $T = 1$   $\mu$ s results in a kick of  $\delta = -\pi/2a$ , bringing an excitonic wave packet from the  $k = 0$  region to the middle of the dispersion zone.

An alternative strategy is to use a pulse of an off-resonant laser field, as for atoms. The phase transformations can be induced by a Gaussian laser beam with the intensity profile

$$I(r,z) = \frac{I_0}{1 + \frac{z^2}{z_R^2}} \exp \left[ -\frac{2r^2}{w_0^2 \left( 1 + \frac{z^2}{z_R^2} \right)} \right] , \tag{4.49}$$

where  $I_0$  is the light intensity at the beam center,  $r$  is the radial distance from the center axis of the beam,  $z$  is the axial distance from the beam center,  $z_R = \pi w_0^2 / \lambda$  is Rayleigh range,  $w_0$  is the beam waist and  $\lambda$  is the wavelength. In order for the dressed rotational states  $|J, M_J\rangle$  to have a definite space quantization axis, the laser is linearly polarized in the direction of the DC field. As shown in Fig. 4.6, we put the 1D molecular array along the  $z$ -axis of the beam so that  $r = 0$  for all the

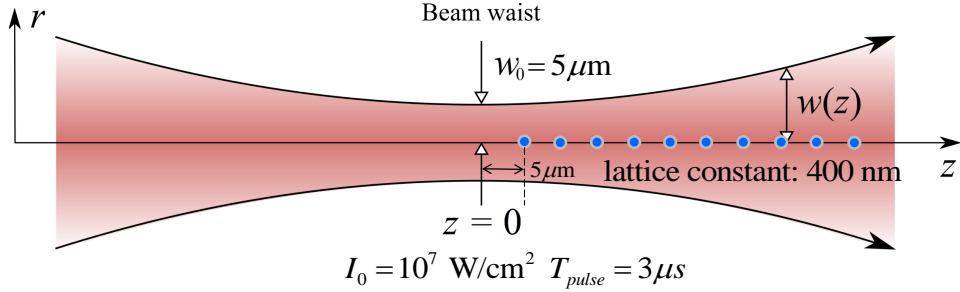


**Figure 4.6:** The experimental setup for the calculation corresponding to Fig. 4.2. A 1D array of LiCs molecules trapped on an optical lattice with lattice constant  $a = 400$  nm is subjected to a homogeneous DC field of 1 kV/cm directed perpendicular to the intermolecular axis. The kicking potential leading to the phase transformation presented by Eq. (4.54) can be provided by a  $\lambda = 1064$  nm Gaussian laser beam that is linearly polarized in the direction of the DC field, with the propagation direction along the array axis, focused to a radius of  $5 \mu\text{m}$ , with the intensity at the focus equal to  $10^7 \text{ W/cm}^2$ . The laser pulse is on between 0 and  $3\mu\text{s}$ .

molecules. Based on Eq. (4.49), the intensity for each molecule of the array is

$$I(n) = \frac{I_0}{1 + \frac{(z_0+na)^2}{z_R^2}} , \quad (4.50)$$

where  $n$  is the molecule index and  $z_0$  is the distance between the center of the wave packet and the beam center. Suppose the width of the wave packet in coordinate space is about  $S_x$  (positive integer) times of the lattice constant  $a$  and we want to use the laser gaussian beam to give the wave packet a momentum kick. For convenience, the molecule at the center of the wave packet is indexed as 0, the molecules to the left are indexed by negative integers and the molecules to the right by positive integers. In practice, we can assume that the wave packet is confined within the range  $[-S_x a, S_x a]$  for a time period much shorter than  $1/\alpha$ . To make the intensity  $I(n)$  vary linearly with  $n$ , the natural way is to put the molecular array far away from the beam center such that  $na \ll z_0$ . In this case, a Taylor series

expansion of the intensity function gives

$$I(n) = I_0 \left\{ \frac{z_R^2}{z_0^2 + z_R^2} - \frac{2an z_0 z_R^2}{(z_0^2 + z_R^2)^2} + \frac{a^2 n^2 z_R^2 (3z_0^2 - z_R^2)}{(z_0^2 + z_R^2)^3} + O(n^3) \right\}. \quad (4.51)$$

When  $z_0$  is large enough that omission of terms higher than linear is justified, the slope of the approximately linear intensity function  $I(n)$  is small, meaning a more powerful laser field is needed to give the momentum kick. This is undesirable for experiments. Instead, we find that one does not need to put the molecular array very far away from the beam center to obtain a linear intensity profile. The trick is to let  $z_0 = z_R/\sqrt{3}$  so that some higher terms (like the second-order term) in Eq. (4.51) vanish. Rather than working with the Taylor series, it is more convenient to work with the original intensity function directly. Substituting  $z_0 = z_R/\sqrt{3}$  and assuming  $1 - \frac{\sqrt{3}}{2} \frac{an}{z_R} \neq 0$  gives

$$\begin{aligned} I(n) &= \frac{I_0}{1 + \frac{(z_0 + na)^2}{z_R^2}} = \frac{I_0 \left( 1 - \frac{\sqrt{3}}{2} \frac{an}{z_R} \right)}{\left[ 1 + \left( \frac{1}{\sqrt{3}} + \frac{na}{z_R} \right)^2 \right] \left( 1 - \frac{\sqrt{3}}{2} \frac{an}{z_R} \right)} \\ &= \frac{1 - \frac{\sqrt{3}}{2} \frac{an}{z_R}}{\frac{4}{3} \left[ 1 - \frac{3\sqrt{3}}{8} \left( \frac{an}{z_R} \right)^3 \right]}. \end{aligned} \quad (4.52)$$

For  $I(n)$  to be linear within the range  $[-S_x, S_x]$ , the second term in the square brackets in Eq. (4.52) should be much less than 1. This leads to a restriction on the width of the wave packet, namely

$$S_x a \lesssim 0.5 z_R. \quad (4.53)$$

Therefore if the two conditions  $z_0 = z_R/\sqrt{3}$  and  $S_x a \lesssim 0.5 z_R$  are satisfied, we can implement the momentum kick for the wave packet. Using Eq. (4.11), Eq. (4.44) and Eq. (4.52), we carry out a calculation similar to that in Eq. (4.47) and estimate the momentum kick by such a pulse as

$$\delta = -\sqrt{3} T I_0 (\alpha_{||} - \alpha_{\perp}) / 80 z_R. \quad (4.54)$$

To demonstrate the feasibility of momentum kick by a laser pulse, a simulation

with  $z_0 = 45 \mu\text{m}$  and  $z_R = 73.8 \mu\text{m}$  was performed. The momentum kick of the wavepacket in  $k$  space, as shown in Fig. 4.2, deviates only by about 7% from the analytical estimates.

#### 4.4.3 Focusing in system of ultracold molecules

The Gaussian intensity profile of Eq. (4.49) can also be used to implement the quadratic phase transformations needed for focusing collective excitations. To achieve this, a molecular array (1D or 2D) must be arranged in the  $z = 0$  plane of the Gaussian beam. As mentioned in Section 4.4.2, an extra DC field is also needed here to lift the degeneracy of rotational states and to avoid mixing of different exciton bands. In addition, the laser is linearly polarized along the direction of the DC field in order for the system to have a well-defined space quantization axis.

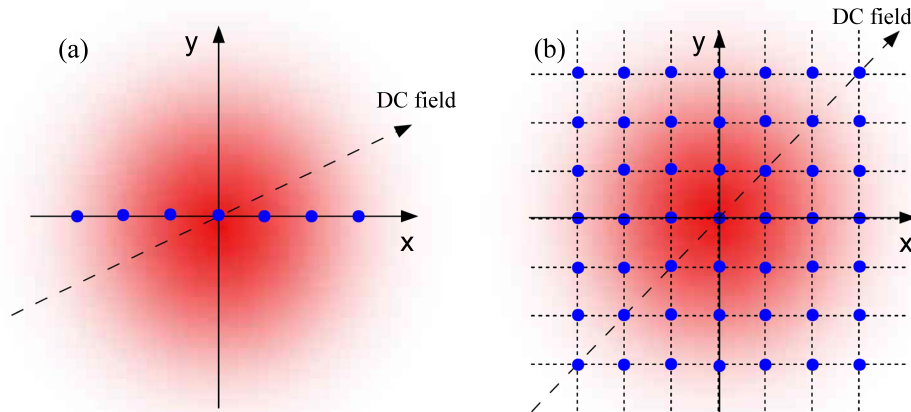


**Figure 4.7:** An illustration to show the orientations of 1D and 2D molecular arrays inside the Gaussian beam. (a) the 1D lattice lies along the  $x$ -axis of the  $z = 0$  plane and the DC field is at some angle with the  $x$ -axis such that the coupling  $\alpha$  between molecules is negative. (b) the 2D square lattice is at the center of the  $z = 0$  plane and the DC field is at  $45^\circ$  degree with the  $x$ -axis. In both cases, the laser is linearly polarized along the direction of the DC field.

First, we consider the case of a 1D molecular array. The wave packet we want to focus is a Gaussian wave packet of width  $\sigma_x$ . We put the beam center at the

center of the wave packet and define the  $x$ -axis of the  $z = 0$  plane to be along the intermolecular axis (see Fig. 4.7 (a)). Then the molecules in the lattice can be indexed by theirs  $x$  coordinates as  $n_x a$ . If the dimension of the wave packet is smaller than one third of the beam waist, the Gaussian intensity profile in Eq. (4.49) can be approximated as

$$I(x, y = 0, z = 0) \approx I_0 \left( 1 - \frac{2n_x^2 a^2}{w_0^2} \right), \quad (4.55)$$

with an accuracy of 90%. Eq. (4.55) presents a concave quadratic intensity profile which can be used to focus a wave packet with attractive coupling ( $\alpha < 0$ ) (see Section 4.3.2). This indicates that we need to make the coupling  $\alpha$  between molecules negative. A calculation of the dipole-dipole interaction between molecules in DC field shows that  $\alpha$  is proportional to  $(1/3 - \cos^2 \theta)$  where  $\theta$  is the angle between the DC field and the intermolecular axis (or  $x$ -axis). Therefore, we can orientate the DC field to a proper direction to achieve the attractive coupling between molecules. As shown in Fig. 4.8 (a),  $\theta$  must be in the range  $[0, 57.3^\circ]$  to ensure the attractive coupling.

From previous discussions in Section 4.3.2, good focusing occurs when the quadratic phase profile is  $\Phi(n) = \Phi_0 n^2$  with  $\Phi_0 = -a/2\sigma_x$  if  $\alpha < 0$ . So we will use this particular value of  $\Phi_0$  to estimate the strength of the laser field needed for the focusing. Specifically, we are proposing to use a laser pulse with a short ramp-up and ramp-down time  $T_s$  and a long steady time  $T_l$ :

$$I_0(t) = \begin{cases} I_m \sin^2 \left( \frac{\pi\tau}{2T_s} \right) & (0 \leq \tau < T_s) \\ I_m & (T_s \leq \tau \leq T_s + T_l) \\ I_m \sin^2 \left[ \frac{\pi(\tau-T_s-T_l)}{2T_s} + \frac{\pi}{2} \right] & (T_s + T_l < \tau \leq 2T_s + T_l) \end{cases} \quad (4.56)$$

Based on Eq. (4.12) and Eq. (4.44), the phase acquired by a molecule at site  $n_x$

with respect to the molecule at the beam center is given by

$$\begin{aligned}\phi(n_x) &= -\frac{2(\alpha_{||} - \alpha_{\perp})I_0 n_x^2 a^2}{15w_0^2} \left( \frac{T_s}{2} + T_l \right) \\ &\approx -\frac{2(\alpha_{||} - \alpha_{\perp})I_0 n_x^2 a^2 T_l}{15w_0^2},\end{aligned}\quad (4.57)$$

where  $T_l \ll T_s$  is assumed in the last step. Equating  $\phi(n_x)$  with the optimal phase profile  $\Phi(n_x) = \Phi_0 n_x^2 = -a/2\sigma_x n_x^2$ , and assuming the laser power is  $P$  and the initial width of the wave packet is  $\sigma_x = Sa$ , we can estimate the duration of the laser pulse to be

$$T_l \approx \frac{15\pi w_0^4}{4Sa^2(\alpha_{||} - \alpha_{\perp})P}. \quad (4.58)$$

For LiCs molecules trapped on an optical lattice with the lattice constant  $a = 400\text{nm}$ , if the initial width of the wave packet is about 100 lattice sites and the beam waist is 3 times larger than the width, the pulse duration calculated from Eq. (4.58) is about  $335\ \mu\text{s}$  for a laser Gaussian beam with the power of 10 W. To ensure the focusing works as expected, the wave packet should be exposed to the laser field for long enough time to accumulate the required phases, so the focusing time  $T_f$  for the wave packet to become most focused must be longer than the duration of the laser pulse. This is not a problem considering that  $T_f$  is inversely proportional to the coupling strength  $\alpha$

$$T_f \approx \frac{1}{4\alpha\Phi_0}, \quad (4.59)$$

and  $\alpha$  can be tuned to be very small values by changing the magnitude of the DC field [67] by only a few kV/cm or by increasing the angle  $\theta$ . For instance, when the DC field is about 1 kV/cm and orientated along the intermolecular axis, the focusing time

$$T_f \approx \frac{1}{4\alpha\Phi_0} = \frac{1}{4(-20\text{ kHz})(-\frac{1}{200})} = 2.5\ \text{ms} \quad (4.60)$$

is much longer than the duration of the laser pulse, leaving enough time for the accumulation of the phases.

Second, we consider the case of a 2D molecular array. The situation is similar

to the 1D case except the anisotropy of the dipole-dipole interaction comes into play. Instead of only considering the coupling between molecules in the  $x$ -axis, we also have to consider the dipole-dipole interactions along the  $y$ -axis and along other directions between the  $x$ -axis and  $y$ -axis. This is because the DC field will be at different angles with different chains of molecules, giving rise to different dipole-dipole interactions in different directions. For simplicity, we use the nearest neighbor approximation here and only consider the dipole-dipole interactions along the  $x$ -axis and  $y$ -axis. Assuming the dimension of the wave packet is smaller than one third of the beam waist, we can approximate the Gaussian intensity profile in Eq. (4.49) by

$$I(x, y = 0, z = 0) \approx I_0 \left[ 1 - \frac{2(n_x^2 + n_y^2) a^2}{w_0^2} \right]. \quad (4.61)$$

Similar to Eq. (4.55) in the 1D case, Eq. (4.61) is also a concave quadratic intensity profile which can be used to focus a wave packet with attractive coupling. But the difference here is that we need to make sure the couplings along both the  $x$ -axis and  $y$ -axis are negative. Since the interactions along  $x$ -axis and  $y$ -axis are independent of each other, the dependence of  $\alpha$  on  $\theta$  in the 1D case can be applied for the 2D case. Therefore, in order for the focusing scheme to work, the angle  $\theta_x$  between the DC field and the  $x$ -axis and the angle  $\theta_y$  between the DC field and the  $y$ -axis should be in the range  $[0, 57.3^\circ]$ . As an example, Fig. 4.7 shows one configuration ( $\theta_x = \theta_y = 45^\circ$ ) which will ensure attractive coupling along both axes.

## 4.5 Control of energy transfer in dipolar systems

Dipolar interactions play a central role in the study of long-range interaction effects using ultracold systems [8]. While, in general, the coupling constant  $\alpha$  in Eq. (4.1) can be determined by a variety of interactions, the dominant contribution to  $\alpha$  for atoms and molecules on an optical lattice is determined by the matrix elements of the dipole - dipole interaction. It is therefore particularly relevant to discuss the specifics of energy transfer in systems with dipolar interactions.

### 4.5.1 The effect of long-range interaction

Dipolar interactions are long-range and anisotropic. This long-range character manifests itself in the modification of the exciton dispersion. While Eq. (4.4) is valid for a system with nearest neighbor couplings only, higher-order couplings in the case of  $\alpha(n-m) \propto 1/|n-m|^3$  modify the exciton dispersion leading to a cosine-like, but non-analytic dispersion relation, both in 1D and 2D.

To see why the dispersion curve is non-analytic, we start from the expression for  $E(k)$

$$\begin{aligned} E(k) &= \Delta E_{eg} + \sum_n \alpha(n) e^{-ikan} \\ &= \Delta E_{eg} + \sum_n \frac{\alpha}{|n|^3} e^{-ikan}, \end{aligned} \quad (4.62)$$

where  $n$  is the difference between the two molecular indexes and the summation goes from  $-\infty$  to  $-1$  and from  $1$  to  $\infty$  for a crystal of infinite size. Restricting  $n$  to be a positive integer, Eq. (4.62) can be written as

$$E(k) = \Delta E_{eg} + \sum_{n=1}^{\infty} \frac{2\alpha \cos(kan)}{n^3}, \quad (4.63)$$

giving the first derivative of the dispersion curve as

$$\frac{dE(k)}{d(ka)} = - \sum_{n=1}^{\infty} \frac{2\alpha \sin(kan)}{n^2}, \quad (4.64)$$

and the second derivative as

$$\frac{d^2E(k)}{d(ka)^2} = - \sum_{n=1}^{\infty} \frac{2\alpha \cos(kan)}{n}. \quad (4.65)$$

The series in Eq. (4.63) and Eq. (4.64) converge with respect to  $n$ , but the series in Eq. (4.65) doesn't. For example, when  $ka = 0$  or  $\pi$ , the series in Eq. (4.65) becomes the harmonic series and diverges with respect to  $n$ . Therefore, the dispersion curve

cannot be Taylor series expanded as

$$E(k) = E(k_0) + \frac{dE(k)}{dk} \Big|_{k_0} (k - k_0) + \frac{d^2E(k)}{dk^2} \Big|_{k_0} (k - k_0)^2 + \dots \quad (4.66)$$

Conventionally, we only consider the interactions between nearest neighbors and take  $n = 1$  in Eq. (4.63). This might be justified if only a rough estimate of the dispersion curve is wanted because the series in Eq. (4.63) converges very fast with respect to the distance  $n$ . Given the consideration on the convergence, higher-order neighbors should be included in the summation to calculate the properties dependent on the first derivative of the dispersion curve, and all neighbors are probably needed to calculate properties determined by the second derivative.

To investigate the effect of this nonanalyticity in dispersion curve, a series of calculations were performed with the long-range couplings neglected after a certain lattice site separation  $n - m$  for the 1D system. The results become converged (to within 0.2 %) when each molecule is directly coupled with 20 nearest molecules. While the calculations with only the nearest neighbor couplings are in good agreement with the analytical predictions given by Eq. (4.31) and Eq. (4.32), the full calculations reveal that long-range couplings somewhat decrease the focusing efficiency. The long-range couplings also decrease the focusing time, by up to a factor of 2. The dynamics of collective excitations leads to interference oscillation patterns clearly visible in panels a and c of Fig. 4.4. These oscillations are much less pronounced when all but nearest neighbor couplings are omitted. Given that the analytical derivation in Section 4.3 are based on a possible invalid Taylor series expansion of the dispersion curve (Eq. (4.66)), the numerical results of Fig. 4.4 and Fig. 4.5 are particularly important because they demonstrate that the phase transformations introduced in the present work are effective for systems with dipolar interactions.

### 4.5.2 Anisotropy of dipolar interaction

The anisotropy of the dipolar interactions can be exploited for controlling energy transfer in dipolar systems by varying the *orientation* of a dressing external DC electric field. For example, for polar molecules on an optical lattice, the matrix

elements  $\alpha(n-m) = \langle e_n, g_m | V_{dd}(n-m) | g_n, e_m \rangle$  depend not only on the choice of the states  $|g\rangle$  and  $|e\rangle$ , but also on the magnitude and orientation of an external dc electric field [67, 139]. Since the value of  $\alpha$  determines the exciton dispersion, the exciton properties can be controlled by varying the angle  $\theta$  between the intermolecular axis and the applied DC field. This is illustrated in Fig. 4.8.

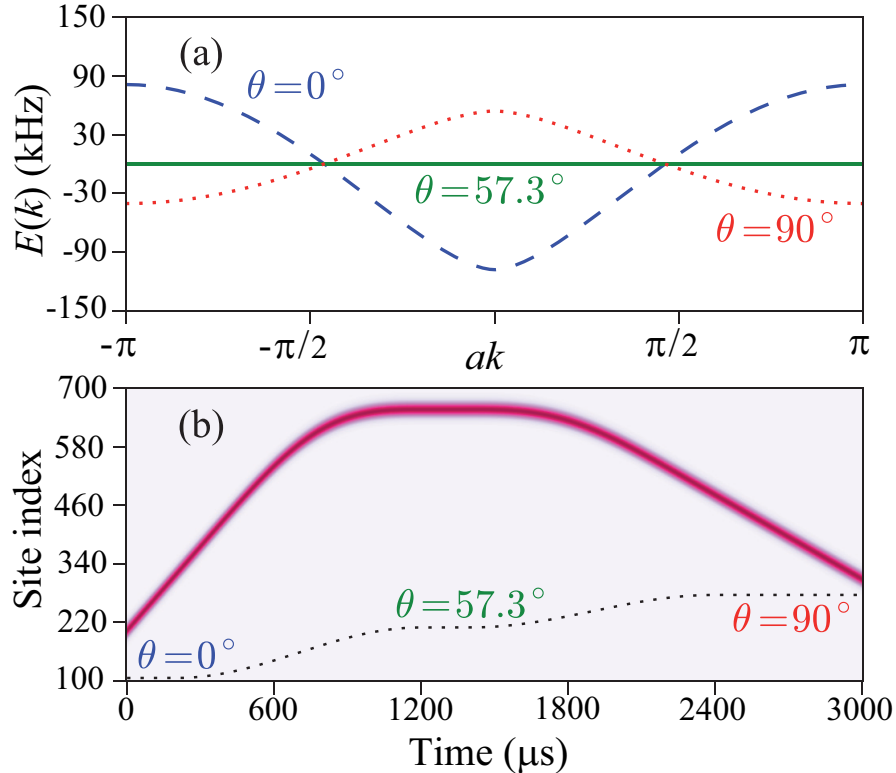


**Figure 4.8:** Control of excitation transfer in a 1D many-body system with dipolar interactions by varying the direction of an external electric field. (a) Exciton dispersion curves for a 1D ensemble of diatomic molecules on an optical lattice for different angles  $\theta$  between the direction of the external DC electric field and the axis of the molecular array. In 1D, the coupling  $\alpha \propto (1/3 - \cos^2 \theta)$ . (b) Propagation of a wave packet centered at  $ak = -\pi/3$  controlled by tuning the electric field direction. The thin dotted line depicts the corresponding angle variations with time. The brightness of the color corresponds to the probability of the excitation.

The results presented in Fig. 4.8 are for a 1D array of LiCs molecules in a lattice

with  $a = 400$  nm. As before,  $|g\rangle$  is the absolute ground state of the molecule and  $|e\rangle$  is the rotationally excited state that adiabatically correlates with the rotational state  $|J = 1, M_J = 0\rangle$  in the limit of vanishing electric field. The upper panel of Fig. 4.8 shows that the angle  $\theta$  between the electric field vector and the molecular array axis determines the sign and magnitude of  $\alpha$ , and therefore the shape of the dispersion curve. This enables control over the sign and magnitude of the group velocity of an excitonic wave packet containing contributions with  $k \neq 0$ . Dynamically tuning  $\theta$ , one can propagate a localized excitation to different parts of the lattice, as shown in Fig. 4.8 (b).

In a 2D lattice, the intermolecular interactions depend on an additional azimuthal angle  $\phi$  that describes the rotation of the electric field axis around the axis perpendicular to the lattice. The numerical calculations presented in Fig. 4.9 show that the energy flow in two dimensions can be controlled by varying both  $\theta$  and  $\phi$ . In addition to the phase transformation discussed earlier, this allows for a dynamical energy transfer in quantum many-body systems with anisotropic interparticle interactions.

### 4.5.3 Computation details

This subsection describes details of the calculations presented in Section 4.5.2. We first evaluate the dipole-dipole interaction in the 1D and 2D molecular arrays, then discuss how to form the Hamiltonian matrix in an efficient way, and finally present some approximations that can reduce the computation cost significantly.

As discussed in Section 2.2.2, the dipole-dipole operator for molecule  $A$  and molecule  $B$  connected by a vector  $\mathbf{R}$  in optical lattices is given by

$$\hat{V}_{dd}(R) = -2\sqrt{\frac{6\pi}{5}} \left(\frac{1}{R}\right)^3 \sum_q (-1)^q Y_{2,-q}(\theta_R, \phi_R) \left[ d_A^{(1)} \otimes d_B^{(1)} \right]_q^{(2)}, \quad (4.67)$$

where the angles  $(\theta_R, \phi_R)$  describe the orientation of the vector  $\mathbf{R}$  in the coordinate system whose  $z$ -axis coincides with the direction of DC field and  $Y_{2,-q}$  are the

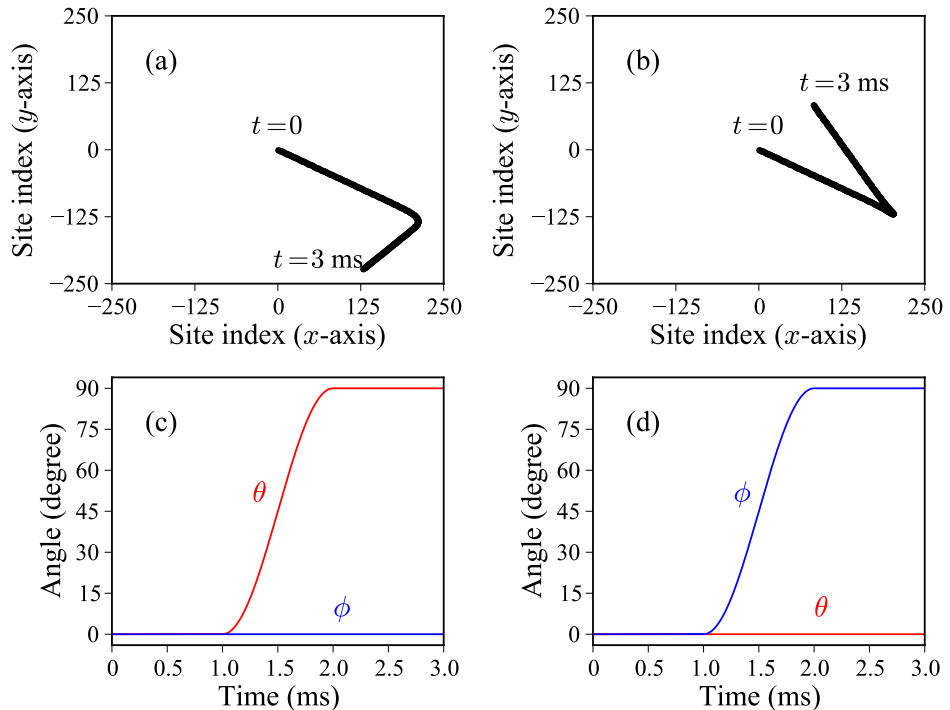


**Figure 4.9:** Control of excitation transfer in a 2D many-body system with dipolar interactions by varying the direction of an external electric field. Panels (a) and (b) show the trajectories of the center of an exciton wave packet in a 2D lattice during the time from 0 to 3 ms; Panels (c) and (d) represent the changing of the dressing DC field orientation ( $\theta, \phi$ ) associated with (a) and (b) respectively. The initial wave packet is a 2D Gaussian distribution centered around  $ak_x = ak_y = \pi/2$  and has a width of  $\sim 60$  lattice sites in coordinate space. The magnitude of the DC field is fixed to 6 kV/cm while its direction is changing. The calculations are done for a 2D array of LiCs molecules in a lattice with  $a = 400$  nm.

spherical harmonics

$$\begin{aligned}
Y_{2,-2} &= \frac{1}{4} \sqrt{\frac{15}{2\pi}} \sin^2 \theta_R e^{-2i\phi_R}, \\
Y_{2,-1} &= \frac{1}{2} \sqrt{\frac{15}{2\pi}} \sin \theta_R \cos \theta_R e^{-i\phi_R}, \\
Y_{2,0} &= \frac{1}{4} \sqrt{\frac{5}{\pi}} (3 \cos^2 \theta_R - 1), \\
Y_{2,1} &= -\frac{1}{2} \sqrt{\frac{15}{2\pi}} \sin \theta_R \cos \theta_R e^{i\phi_R}, \\
Y_{2,2} &= \frac{1}{4} \sqrt{\frac{15}{2\pi}} \sin^2 \theta_R e^{2i\phi_R}.
\end{aligned} \tag{4.68}$$

To calculate the dipole-dipole interaction, we evaluate the matrix element of the dipole-dipole operator in the basis of bare rotational states:

$$\begin{aligned}
&\langle N_A, M_A | \langle N_B, M_B | \hat{V}_{dd}(R) | N'_A, M'_A \rangle | N'_B, M'_B \rangle \\
&= -\frac{F}{2R^3} \left\{ 3 \sin^2 \theta_R e^{-2i\phi_R} D_-^A D_-^B - 6 \sin \theta_R \cos \theta_R e^{-i\phi_R} [D_0^A D_-^B + D_-^A D_0^B] \right. \\
&\quad + 3 \sin^2 \theta_R e^{2i\phi_R} D_+^A D_+^B + 6 \sin \theta_R \cos \theta_R e^{i\phi_R} [D_0^A D_+^B + D_+^A D_0^B] \\
&\quad \left. + \sqrt{6} (3 \cos^2 \theta_R - 1) [D_+^A D_-^B + D_-^A D_+^B + D_0^A D_0^B] \right\}, \tag{4.69}
\end{aligned}$$

where  $F$  and  $D_{-/0/+}^A D_{-/0/+}^B$  are given in Section 2.2.2. In Eq. (4.69), the superscript of  $D_{-/0/+}^A D_{-/0/+}^B$  denotes molecule  $X (= A$  or  $B$ ), and the subscript  $S (= +$  or  $-$  or  $0$ ) indicates that it is nonzero only if the projection of the rotational quantum number of molecule  $X$  changes in a certain way: “+” means  $M_X = M'_X + 1$ ; “-” means  $M_X = M'_X - 1$ ; 0 means  $M_X = M'_X$ . As depicted in Fig. 4.10 (a), rotating the coordinate system around its  $z$ -axis does not change the physical properties of the molecular array as the relative orientation of the DC field with respect to the intermolecular axis remains the same. Therefore we have the freedom to choose  $\phi_R = 0$  in Eq. (4.69) for the 1D molecular array. However, a 2D molecular array has many intermolecular axes that are at different angles  $(\theta_R, \phi_R)$  with the external field, which means one cannot make all  $\phi_R$  zero by rotating the coordinate system while keeping the relative orientation of the external field with respect to the molec-

ular array. So in general we have to consider both  $\theta_R$  and  $\phi_R$  when calculating the dipole-dipole interaction in a 2D molecular array.

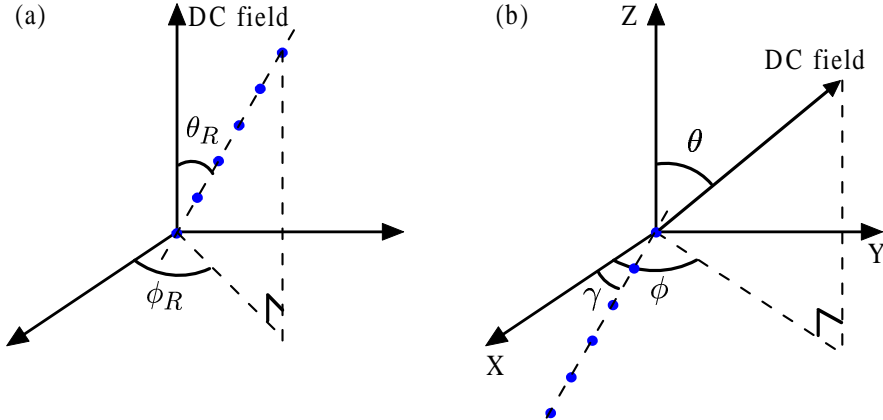


**Figure 4.10:** The orientations of the DC field and molecular arrays in the coordinate systems. (a) The DC field is along the  $z$ -axis and the 1D molecular array is in the direction represented by  $\theta_R$  and  $\phi_R$ . (b) The 2D molecular array is on the  $XY$  plane and the orientation of the DC field is represented by  $(\theta, \phi)$ . For clarity, we have only drawn the molecules (as blue dots) along a particular axis which is at angle  $\gamma$  with respect to the  $X$ -axis. It is to be understood that there are also other intermolecular axes at different angles with the  $X$ -axis. Note part (a) and part (b) have different coordinate systems and the meaning of  $(\theta_R, \phi_R)$  is different from that of  $(\theta, \phi)$ . In fact, the angle  $\theta_R$  between the DC field and the molecular array in (b) is related to  $\theta$  and  $\phi$  by  $\cos \theta_R = \cos \theta \cos(\phi - \gamma)$ .

Keeping track of both angles  $\theta_R$  and  $\phi_R$  is complicated. Fortunately, we can get rid of the dependence on  $\phi_R$  in Eq. (4.69) by choosing to deal with only certain rotational states. In a DC field or a linearly polarized laser field, the dressed rotational states  $|\tilde{N}, |M\rangle$  of the system are a linear combinations of the bare rotational states with the same projection along the direction of the DC field or along the direction of laser polarization, that is

$$|\tilde{N}, |M\rangle = \sum_N C_{N,M} |N, M\rangle \quad (4.70)$$

Note that the coefficients  $C_{N,M}$  only depend on the magnitude of the external field and have nothing to do with the angles  $\theta_R$  and  $\phi_R$ . Because those dressed states with different projections  $|M|$  have different energies, we can choose to work with the states with a particular value of  $|M|$  by tuning the excitation energy to match the corresponding energy levels. In the current study,  $|M|$  is chosen to be zero, therefore only the bare rotational states with  $M_X = 0$  are involved, so only the term associated with  $D_0^A D_0^B$  in Eq. (4.69) is nonzero, giving

$$\langle N_A, 0 | \langle N_B, 0 | \hat{V}_{dd}(R) | N'_A, 0 \rangle | N'_B, 0 \rangle = -\frac{\sqrt{6}F}{2R^3} (3 \cos^2 \theta_R - 1) D_0^A D_0^B . \quad (4.71)$$

The dipole-dipole interaction between two dressed states with  $|M| = 0$  can then be expressed as linear combinations of Eq. (4.71), that is

$$\begin{aligned} & \langle \tilde{N}_A, 0 | \langle \tilde{N}_B, 0 | \hat{V}_{dd}(R) | \tilde{N}'_A, 0 \rangle | \tilde{N}'_B, 0 \rangle \\ &= \sum_{N_A} \sum_{N_B} \sum_{N'_A} \sum_{N'_B} C_{N_A, 0}^* C_{N_B, 0}^* C_{N'_A, 0} C_{N'_B, 0} \langle N_A, 0 | \langle N_B, 0 | \hat{V}_{dd}(R) | N'_A, 0 \rangle | N'_B, 0 \rangle . \end{aligned} \quad (4.72)$$

Equation (4.71) and Eq. (4.72) show that we only need to consider the angle  $\theta_R$  between the intermolecular axis and the external field if only the dressed rotational states with  $|M| = 0$  are involved. This is valid for both the 1D and 2D cases.

Since a 1D molecular array can be treated as a limiting case of a 2D molecular array with only a single intermolecular axis, we focus on the discussion of the 2D case. As illustrated by Fig. 4.10, we suppose the 2D molecular array is in the  $XY$  plane, and the orientation of the external field is given by  $(\theta, \phi)$ . For any two molecules whose intermolecular axis is at angle  $\gamma$  with respect to the  $X$ -axis,  $\cos^2 \theta_R$  can be calculated as

$$\begin{aligned} \cos^2 \theta_R &= \left[ \cos \left( \frac{\pi}{2} - \theta \right) \cos(\phi - \gamma) \right]^2 \\ &= \sin^2 \theta (\cos \phi \cos \gamma + \sin \phi \sin \gamma)^2 . \end{aligned} \quad (4.73)$$

Therefore the dipole-dipole interaction between two molecules can be calculated from Eq. (4.71) and Eq. (4.72) provided the angle between the intermolecular axis

and the  $X$ -axis is known.

Once the dipole-dipole interaction is known, we can form the Hamiltonian matrix by expanding the Hamiltonian in the basis of individual sites. Suppose the 2D molecular array is a square lattice with  $N \times N$  sites and the coordinate system is oriented such that its  $X$ -axis and  $Y$ -axis coincide with the bottom and left edge of the 2D lattice respectively. The position of the molecule in the array can then be represented by its coordinates  $(x, y)$ . Without loss of generality, we consider only the case where the external field is oriented such that  $0 \leq \theta \leq 90^\circ$  and  $0 \leq \phi \leq 90^\circ$ , and give the indexes  $0, 1, 2, \dots, N^2 - 1$  to every molecule in the 2D array, starting from the bottom to the top of the array and from left to right in each row. Based on Eq. (4.71) and Eq. (4.72), the matrix element  $H_{i,j}$  corresponding to two sites  $i$  and  $j$  is given by

$$\begin{aligned} H_{i,j} &= \langle \tilde{0}, 0 |_i \langle \tilde{1}, 0 |_j H_0 + \hat{V}_{dd} | \tilde{1}, 0 \rangle_i | \tilde{0}, 0 \rangle_j \\ &= \sum_{N_A} \sum_{N_B} \sum_{N'_A} \sum_{N'_B} -\frac{\sqrt{6}F}{2R_{i,j}^3} (3\cos^2 \theta_R(i, j) - 1) D_0^A D_0^B C_{N_A, 0}^* C_{N_B, 0}^* C_{N'_A, 0} C_{N'_B, 0} , \end{aligned} \quad (4.74)$$

where  $R_{i,j}$  is the distance between molecules in sites  $i$  and  $j$ , and  $\theta_R(i, j)$  is the angle between the external field and the intermolecular axis. Assuming the unit length of the coordinate system is the lattice constant of the 2D array, the distance between the two sites  $i$  and  $j$  can be calculated from their coordinates

$$R_{i,j} = a \sqrt{(x_i - x_j)^2 + (y_i - y_j)^2}, \quad (4.75)$$

where

$$\begin{aligned} x_i &= i \% N \\ y_i &= i / N, \end{aligned} \quad (4.76)$$

and  $\%$  is the mod operator. Since the angle  $\gamma$  between the external field and the

intermolecular axis connecting molecules in sites  $i$  and  $j$  is given by

$$\gamma(i, j) = \arccos \left[ \frac{x_j - y_i}{\sqrt{(x_i - x_j)^2 + (y_i - y_j)^2}} \right], \quad (4.77)$$

the value of  $\cos^2 \theta_R(i, j)$  in Eq. (4.74) can be calculated from Eq. (4.73).

With the Hamiltonian matrix  $H$ , we can now run the simulations presented in Section 4.5.2. The essential problem is to solve the time-dependent Schrödinger equation

$$\dot{\Psi}(t) = \frac{1}{i\hbar} H(t) \Psi(t). \quad (4.78)$$

Solving the above differential equations involves the computation of the Hamiltonian matrix at many different time points. To make the simulation as fast as possible, I now explore how to evaluate  $H(t)$  efficiently. In the calculations, the direction of the DC field is changed adiabatically with respect to the time scale of the excitation hopping while the magnitude of the field is kept constant, therefore the coefficients  $C_{N_A,0}$ ,  $C_{N_B,0}$ ,  $C_{N'_A,0}$ , and  $C_{N'_B,0}$  in Eq. (4.74) remain the same and the time dependence of the Hamiltonian matrix is solely due to the time dependence of  $\theta_R(t)$ . Based on this observation, the Hamiltonian matrix can be separated into two parts:

$$H(t) = H_1[\theta(t), \phi(t)] * H_2, \quad (4.79)$$

where “\*” means element-wise multiplication,  $H_1$  is the time-dependent part that needs to be updated whenever  $\theta(t)$  and  $\phi(t)$  change, and  $H_2$  is the time-independent part that can be computed once and saved into memory for later retrieval. It is easy to derive from Eq. (4.74) the expression for  $H_2$ , that is

$$H_2 = \sum_{N_A} \sum_{N_B} \sum_{N'_A} \sum_{N'_B} -\frac{\sqrt{6}F}{2R_{i,j}^3} D_0^A D_0^B C_{N_A,0}^* C_{N_B,0}^* C_{N'_A,0} C_{N'_B,0}. \quad (4.80)$$

Because the angle  $\gamma$  in Eq. (4.73) is only dependent on the positions of the lattice sites, we can further separate the evaluation of  $H_1$  into different parts for the

purpose of computing efficiency. The expression for  $H_1$  is given by

$$H_1(\theta(t), \phi(t)) = 3 \cos^2[\theta(t)] * \left\{ \cos[\phi(t)] * K^{\cos} + \sin[\phi(t)] * K^{\sin} \right\} ** 2 - 1 , \quad (4.81)$$

where “\*\*2” means element-wise square, and  $K^{\cos}$  is a matrix whose elements are given by

$$K_{i,j}^{\cos} = \cos(\gamma(i, j)) , \quad (4.82)$$

and  $K^{\sin}$  is a matrix whose elements are given by

$$K_{i,j}^{\sin} = \sin(\gamma(i, j)) . \quad (4.83)$$

Since  $K^{\cos}$  and  $K^{\sin}$  are independent of time, we compute them once and save them into memory for later usage. In summary, the efficient computation of  $H(t)$  is carried out in three steps: 1. calculate  $H_2$ ,  $K^{\cos}$ , and  $K^{\sin}$  and save them into memory; 2. compute  $\theta(t)$  and  $\phi(t)$  and then use the values of  $K^{\cos}$ , and  $K^{\sin}$  in memory to calculate  $H_1$ ; 3. use the value of  $H_2$  in memory to compute  $H$ .

For the simulations, I used a complex ordinary differential equation solver called “ZVODE”[165, 166] to solve Eq. (4.78). Given an initial state  $\Psi(t = 0)$ , the derivative  $\dot{\Psi}$  of the wavefunction with respect to time, and the desired accuracy for the calculation, the solver gives the wavefunction  $\Psi(t)$  at a later time  $t$ . In my experience, the ZVODE solver is not efficient for solving a rapidly changing system of differential equations where the potential energy change is very steep. If this is the case, it is better to convert the time-dependent Schrödinger equation into a real ordinary differential equation and use the corresponding ODE solver called “DVOODE”[165, 166] that can handle rapidly changing systems much better. As a reference for future students, I show below the conversion from the time-dependent Schrödinger equation to a real ordinary differential equation. The starting point is the Schrödinger equation

$$i\hbar\dot{\mathbf{C}} = \mathbf{H}\mathbf{C} , \quad (4.84)$$

where  $\mathbf{C}$  is a vector representing the state of the system. After rewriting  $\mathbf{C}$  as

$$\mathbf{C} = \mathbf{C}_{\text{real}} + i \mathbf{C}_{\text{imag}} , \quad (4.85)$$

and  $\mathbf{H}$  as

$$\mathbf{H} = \mathbf{H}_{\text{real}} + i \mathbf{H}_{\text{imag}}, \quad (4.86)$$

and collecting the real part and imaginary part separately in Eq. (4.84), we obtain two real equation

$$\begin{aligned} \hbar \dot{\mathbf{C}}_{\text{real}} &= \mathbf{H}_{\text{imag}} \mathbf{C}_{\text{real}} + \mathbf{H}_{\text{real}} \mathbf{C}_{\text{imag}}, \\ \hbar \dot{\mathbf{C}}_{\text{imag}} &= -\mathbf{H}_{\text{real}} \mathbf{C}_{\text{real}} + \mathbf{H}_{\text{imag}} \mathbf{C}_{\text{imag}}. \end{aligned} \quad (4.87)$$

The above two equations can be written in block matrix form as

$$\hbar \begin{pmatrix} \dot{\mathbf{C}}_{\text{real}} \\ \dot{\mathbf{C}}_{\text{imag}} \end{pmatrix} = \begin{pmatrix} \mathbf{H}_{\text{imag}} & \mathbf{H}_{\text{real}} \\ -\mathbf{H}_{\text{real}} & \mathbf{H}_{\text{imag}} \end{pmatrix} \begin{pmatrix} \mathbf{C}_{\text{real}} \\ \mathbf{C}_{\text{imag}} \end{pmatrix}, \quad (4.88)$$

which leads to a real differential equation

$$\hbar \dot{\mathbf{C}}_{\text{new}} = \mathbf{H}_{\text{new}} \mathbf{C}_{\text{new}}, \quad (4.89)$$

equivalent to the original Schrödinger equation.

Finally, I discuss a few tricks and approximations that enable us to do the 2D simulations efficiently. For a 2D molecular array with  $\mathbb{N} \times \mathbb{N}$  sites, since the couplings between every two sites are included, the dimension of the Hamiltonian matrix is  $O(\mathbb{N}^2 \times \mathbb{N}^2)$ . For a medium-sized 2D array with  $\mathbb{N} = 100$ , the number of coupled differential equations is about  $10^4$ , which is close to the limit that our code can handle. As  $\mathbb{N}$  becomes larger, the number of differential equations will increase dramatically. This poses a dilemma. On one side, we want to limit the size of the crystal so that the computation is fast. On the other side, as we are studying the motion of an exciton wave packet in a DC field whose orientation is changing adiabatically with respect to the excitation hopping, the simulation time period can be long. This requires a large crystal with enough space in which the wave packet can propagate for a relatively long time without hitting the boundaries. In addition, we also want the initial size of the wave packet to be large enough so that it is narrow in  $k$ -space and doesn't spread very fast in coordinate space. After experimenting with different arrays, we found a wave packet with a width of  $\sim 60$

lattice sites in coordinate space is good for illustrative purposes. If such a wave packet is used for simulations, the crystal size must be much larger than  $100 \times 100$ , which is beyond the limit size that our code can handle. There are two ways to resolve the small-or-large-crystal dilemma. The most obvious choice is to use the nearest neighbor approximation so that each molecule will only interact with the four molecules that are closest to it. The dimension of the Hamiltonian matrix will then scale like  $O(N \times N)$ , and the number of differential equations drops significantly. However, this approach fails to account for the long-range interaction and misses some characteristics of the anisotropy of the dipole-dipole interaction as it only considers the interactions only along the  $X$ -axis and the  $Y$ -axis. In the simulation, I take another approach by treating different regions of the crystal separately. As the dipole-dipole interaction decays fast with distance, the lattice sites that are close to the position of the wave packet are most important and should be always taken into account. So I define a computation zone as the square box that encloses the wavepacket, and define the rest of the crystal as the supplement zone. At the beginning of the simulation, I choose a large enough computation zone such that the probability to find excitation at the edges of the zone is almost zero, and compute all the interactions between any two molecules inside the zone to form the Hamiltonian matrix. All the other lattice sites beyond the computation zone are ignored. In this way, the size of the Hamiltonian matrix will be determined by the smaller computation zone rather than the whole lattice and the most important part of the long-range interaction is also kept. After each time step, I find the new position of the wave packet center and shift the computation zone such that its center coincides with the wave packet center. In the process of the shifting, I lose a small portion of the wave packet because the sites near the boundaries of the computation zone will be removed out of the computation zone at the next time point and the excitation population at those sites will also be lost. However, if the computation zone is large enough, this should not be a problem. Therefore maintaining a small computation zone and dynamically moving it based on the movement of the wave packet allows for the calculation of the motion of a wave packet in a much bigger crystal. In Fig. 4.9, we have used a computation zone with the size  $101 \times 101$  and the size of the whole crystal is  $1001 \times 1001$  (not shown in the figure). During the simulation, I noticed that the wave packet spreads in coordinate space as time goes

on, but 99% of the wavepacket is still inside the computation zone. Because the wave packet spreads over time, our simulation will eventually break up at some point as more and more part of the wave packet gets lost at the boundaries of the computation zone.

## 4.6 Energy transfer in the presence of vacancies

While experiments with ultracold atoms have produced states with one atom per lattice site with 99% fidelity [57, 58, 161], the latest experiments with molecules yield lattice-site populations about 10% [162]. Multiple experiments are currently underway to trap polar molecules on an optical lattice with close to the full population of the lattice. However, lattice vacancies may be unavoidable in the best experiments. In this section, we examine the effect of vacancies on the possibility of focusing collective excitations to a desired region of the lattice by the phase transformations discussed in Section 4.3. For concreteness, we perform calculations for the system described in Section 4.4, namely a 2D array of LiCs molecules on a square optical lattice with  $a = 400$  nm.

To explore the effect of vacancy-induced interactions, we performed simulations for different vacancy numbers using the same parameters for molecule-field and inter-molecular interactions as in the calculations presented in Fig. 4.5 (b). For each vacancy concentration, we carried out 48 calculations with random distributions of empty lattice sites. The quadratic phase transformations are applied, as described in Section 4.3, in order to focus the collective excitation at time  $t_*$  to the molecule in the middle of the 2D array.

Vacancies disturb the translational symmetry of the system and produce an effective disorder potential that tends to localize collective excitations [68]. Because the natural time evolution of the wave packet in a disorder potential may lead to enhancement of the probability in certain regions of the lattice, it is necessary to distinguish the effect of the vacancy-induced localization and the effect of the focusing phase transformation. To quantify these two effects, we define two factors: the enhancement of the probability at the target molecule with respect to the initial value, that is

$$\eta = \frac{p'(t = t_*)}{p(t = 0)}, \quad (4.90)$$

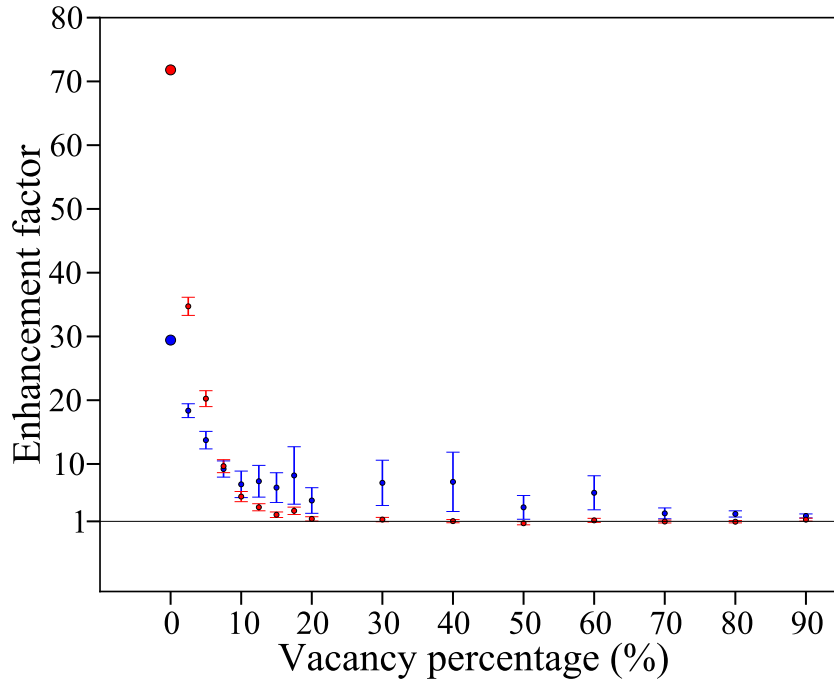


**Figure 4.11:** Enhancement factors  $\eta$  (red symbols) and  $\chi$  (blue symbols) as functions of vacancy percentage in a 2D lattices. See text for the definitions of  $\eta$  and  $\chi$ . The error bars are for 95% of confidence interval.

and the ratio of the probability to find the excitation on the target molecule with ( $p'$ ) and without ( $p$ ) the phase transformation, that is

$$\chi = \frac{p'(t = t_*)}{p(t = t_*)}. \quad (4.91)$$

The time  $t_*$  is the focusing time found numerically for the corresponding vacancy-free system. The quantity  $\eta$  illustrates the actual enhancement of the probability to focus a collective excitation, while the quantity  $\chi$  illustrates the effect of the focusing phase transformation. Figure 4.11 presents the values of  $\eta$  and  $\chi$  as functions of the vacancy concentration. It illustrates two important observations. First, the disorder potential with vacancy concentrations  $> 20\%$  renders the phase transformation ineffective. In the presence of strong disorder, the dynamics of the system

is entirely determined by the disorder potential and the energy transfer becomes highly inefficient (however, see Section 4.7). On the other hand, vacancy concentrations of less than 10 % appear to have little effect on the efficacy of the focusing phase transformation.

Our calculations indicate that the focusing time may be somewhat modified by the disorder potential, even if the concentration of vacancies is less than 10 %. Figure 4.12 depicts the excitation wave functions at the time of the maximal enhancement on the target molecule, chosen as molecule (71,71). Figure 4.12 shows that despite the presence of multiple vacancies, the focusing transformation enhances the probability to find the excitation on the target molecule by 16 times.

## 4.7 Focusing in the presence of strong disorder

Although the focusing method demonstrated in Section 4.3 and Section 4.6 appears to be robust in the presence of a disorder potential induced by a small concentration of vacancies, it is important for practical applications to also consider controlled energy transfer in quantum arrays under a strong disorder potential. To consider focusing in a strongly disordered system, we employ an analogy with the “transfer matrix” methods for focusing of a collimated light beam in opaque medium [71–80].

In optics, a collimated laser beam passing through an opaque medium results in a random pattern of speckles arising from random scattering of light inside the medium [167]. Likewise, the random distribution of empty sites in an optical lattice with molecules scatters the exciton wavepackets, resulting in a completely random excited state. However, in optics, the randomness of the scattering centers inside the opaque medium can be compensated for by shaping the incident wavefront with a spatial light modulator such that the contributions from various parts of the medium can add constructively upon exit from the medium, producing a focus. We suggest that the same can be achieved with a many-body system on a lattice by separating the entire lattice into multiple blocks and applying proper phase transformations to those individual blocks.

The initial state for an ensemble of molecules on a lattice with multiple vacan-

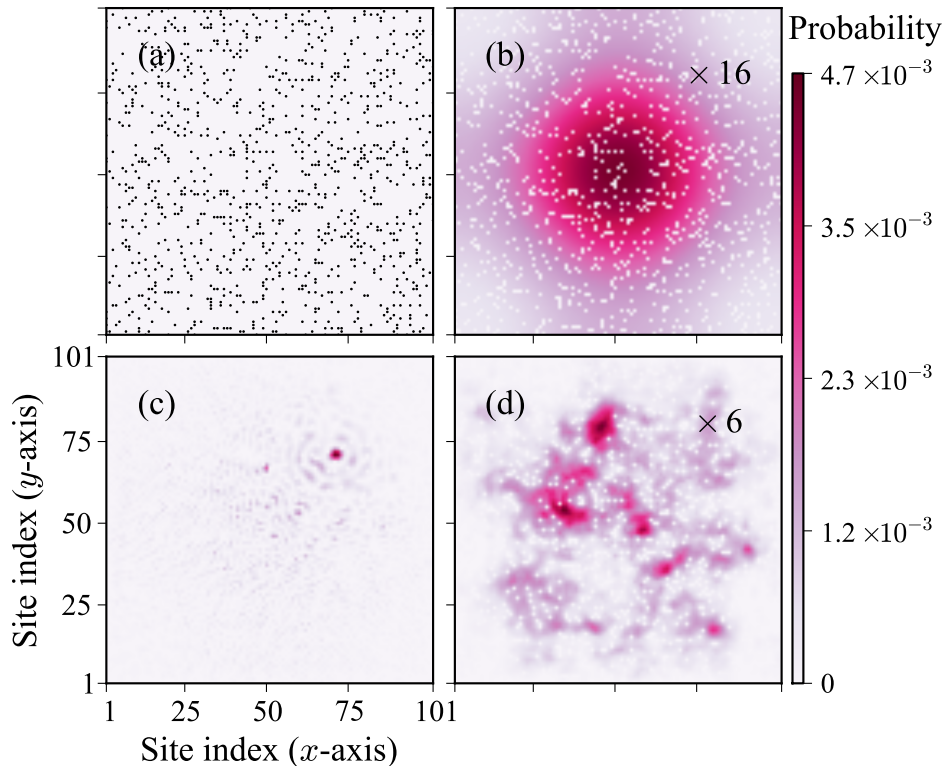


**Figure 4.12:** Time snapshots of a collective excitation in a 2D array with a vacancy concentration of 10 % (a) The distribution of the vacant sites; (b) The initial probability distribution of the excited state; (c) The probability distribution of the excitation at the focusing time when the focusing scheme is applied. The focusing time is found numerically as the time when the probability at the target molecule (71, 71) reaches maximum for a given phase transformation. (d) The probability distribution of the wave function at the focusing time when the focusing scheme is not applied. The calculations are performed with the same parameters as in Fig. 4.5. The probabilities in (b) and (d) are magnified by 16 and 6, respectively.

cies can be written as

$$|\psi(t=0)\rangle = \sum_i c_i(t=0) |i\rangle , \quad (4.92)$$

where

$$|i\rangle = |e_i\rangle \prod_{j \neq i} |g_j\rangle , \quad (4.93)$$

and the indexes  $i$  and  $j$  run over all occupied sites. After a long evolution time  $T$ , the probability amplitude for the excitation to reside on a particular target molecule is given by

$$c_o(T) = \sum_i U_{o,i}(T) c_i(t=0) \equiv \sum_i c_{oi}(T), \quad (4.94)$$

where  $U_{o,i}(t) = \langle o | \exp[-iH_{\text{exc}}t] | i \rangle$  is a matrix element of the time evolution operator. In a disordered system, the transfer coefficients  $U_{o,i}$  are not a-priori known and depend on the disorder potential. The phasors  $c_{oi}(T)$  have quasi-random amplitudes and phases. While the amplitude of each phasor cannot be controlled experimentally, their phases are controllable via the phases of the coefficients  $c_i$  at  $t = 0$ , which can be tuned using the phase-kicking transformations introduced above. To achieve the highest probability at the target molecule, it is necessary to ensure that the contribution  $c_{oi} = U_{o,i}(T)c_i(t=0)$  from every site  $i$  has the same phase so that they add up constructively.

In a practical implementation, it may be difficult to control the phase of each molecule in each individual site. It may be more desirable to work with blocks of several lattice sites. Assuming that the entire array of molecules can be divided into  $M$  blocks, each containing many molecules, and that the blocks can be perturbed individually, the excitation probability amplitude at the target molecule at time  $T$  is

$$c_o(T) = \sum_{\gamma=1}^M c_{\gamma}(T) , \quad (4.95)$$

where the contribution from block  $\gamma$  is given by

$$c_{\gamma}(T) \equiv |c_{\gamma}| e^{i\phi_{\gamma}} = \sum_{i \in \gamma} U_{o,i}(T) c_i(t=0) . \quad (4.96)$$

In Eq. (4.96), the time evolution operator  $U$  depends on the randomness of vacancy sites and thus is out of our control, but we can manipulate the initial state  $c_i(t=0)$ . It turns out that the contributions from different blocks can be made to interfere constructively by adding a phase  $\exp(-i\phi_\gamma)$  to each occupied site in block  $\gamma$ . For  $M$  blocks in the array and quasi-random evolution matrix, simply setting all the phases equal may lead to an  $\sim M$ -fold increase of the excitation probability at the target molecule, as compared to the sum of  $M$  quasi-random phasors in Eq. (4.95) [71].

Similarly to optics, the phases  $-\phi_\gamma$  which must be added in each block, can be found experimentally provided that the same (or similar) realization of disorder persists in a series of trials. A straightforward optimization would scan through the strengths of phase kicks applied to different blocks. In each experiment one would measure the excitation probability at the target molecule  $|c_o(T)|^2$ , e.g. via resonance fluorescence from the target molecule at the end of the experiment. More sophisticated optimization techniques, aimed at fast focusing multi-frequency light in optical systems, are currently under rapid development [72–80].

For a proof-of-principle calculation, we consider a 2D lattice of size  $101 \times 101$  with 60% of the sites vacant and each non-vacant site occupied by a single LiCs molecule. First, we determine the phase  $\exp(-i\phi_\gamma)$  applied to block  $\gamma$ . Due to time reversibility of the time evolution operator  $U(T)$  and Eq. (4.96), we obtain

$$|c_\gamma| \exp(-i\phi_\gamma) = \left[ \sum_{j=1}^n U_{o,j}^\gamma(T) c_j^\gamma(0) \right]^* = \left[ \sum_{j=1}^n U_{j,o}^\gamma(-T) c_j^\gamma(0) \right]^*. \quad (4.97)$$

The matrix element  $U_{j,o}^\gamma(-T)$  can be calculated by performing a backward time propagation starting from a local excitation at site “ $o$ ” and calculating the coefficient  $c_j(t)$  at time  $-T$ . Alternatively, one can propagate the evolution equations forward in time, finding  $c_j(T)$ : Since the Hamiltonian of Eq. (4.1) is real, its eigenfunctions are real, and the evolution matrix  $U$  is symmetric,  $U_{o,j} = U_{j,o}$ . Thus we find

$$c_j(T) = \sum_i U_{j,i}^\gamma(T) c_i(0) = U_{j,o}^\gamma(T), \quad (4.98)$$

since  $c_o(0) = 1$  and all other coefficients are zero. For a completely delocalized

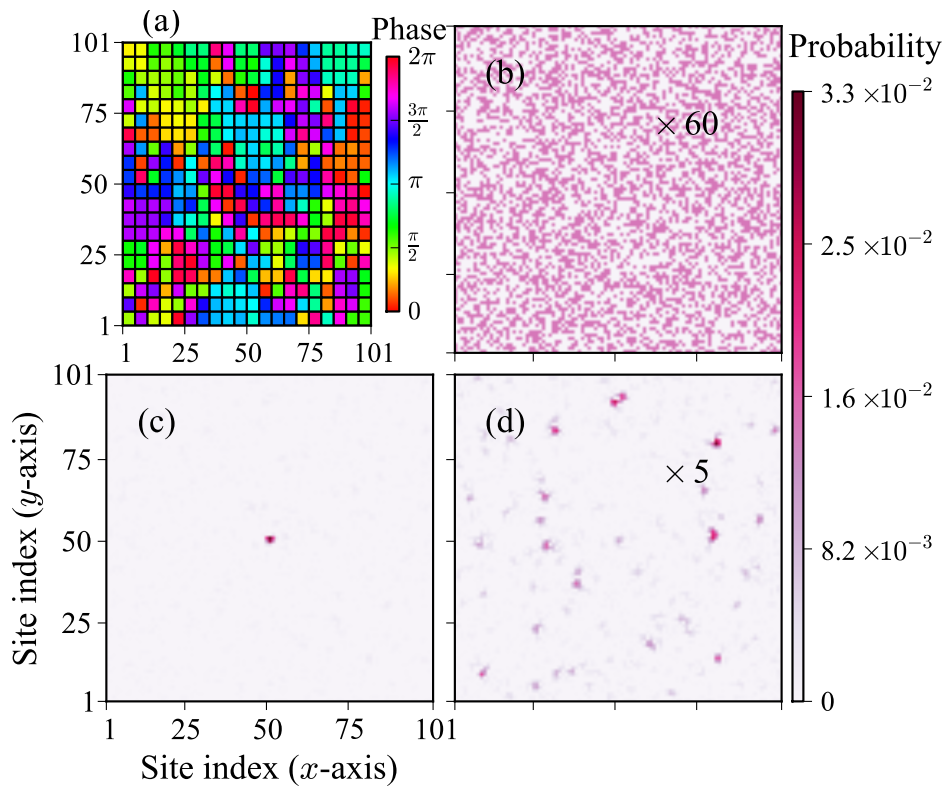


**Figure 4.13:** Focusing of a collective excitation in a strongly disordered system with 60% of lattice sites unoccupied. Panel (a) shows different phases applied to different blocks of the lattice before the time evolution. (b) The initial probability distribution of the excited state. (c) The probability distribution of the excited state at the focusing time  $T = 3$  ms with the phase transformation depicted in panel (a) before the time evolution. (d) The probability distribution of the excited state at the focusing time  $T = 3$  ms with no phase transformation applied. The calculations are performed with the same parameters as in Fig. 4.5. The probabilities in (b) and (d) are magnified by 60 and 5, respectively.

initial state, we assume that all coefficients in Eq. (4.92) are equal, so that the phases  $\phi_\gamma$  required for block  $\gamma$  are

$$|c_\gamma| \exp(-i\phi_\gamma) = \left[ \sum_j c_j(T) \right]^*, \quad (4.99)$$

where the index  $j$  runs over all occupied sites in block  $\gamma$ . Figure 4.13 shows that this choice of phases leads to effective focusing of the collective excitation in a strongly disordered system.

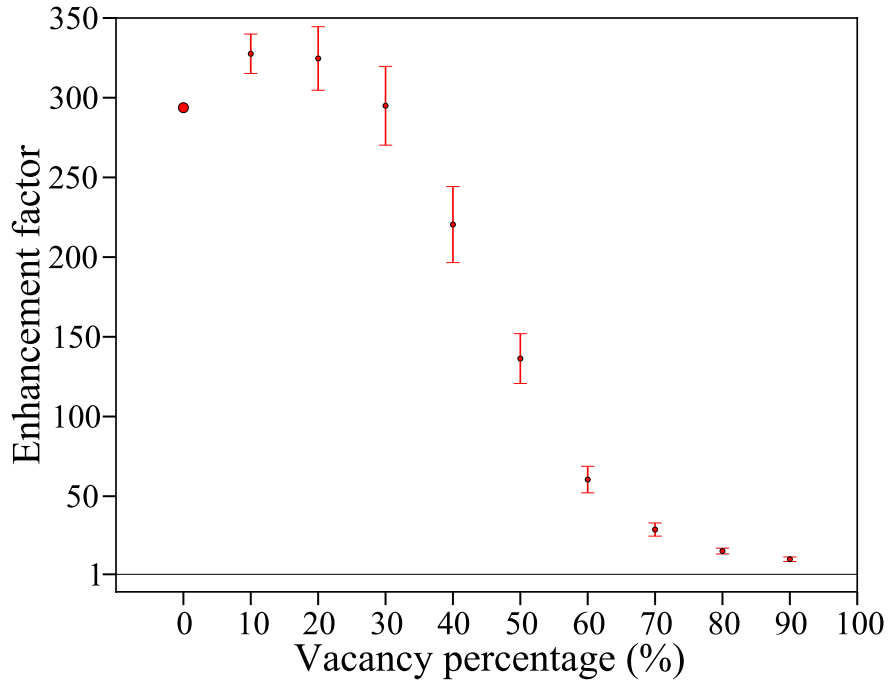


**Figure 4.14:** Efficiency of focusing collective excitations in strongly disordered 2D lattices. The molecular array is divided into 400 blocks as shown in Fig.4.13(a). The focusing time  $t_*$  is arbitrarily set to 4 ms. For each realization of disorder, we use Eq.(4.99) with  $T = t_*$  to find the phase mask applied to different blocks. Shown are the enhancement factors  $\eta$  (red symbols) defined in Eq.(4.90), as a function of the vacancy percentage. The error bars are for 95% confidence interval.

To illustrate the efficiency of the focusing method described above, we have carried out a series of calculations with different vacancy concentrations. For each vacancy concentration, we performed 48 calculations with random distributions of empty lattice sites. The phase transformations are calculated individually for each random distribution of vacancy sites as described above. The results are shown in Fig. 4.14. As can be seen, the transformations proposed above are effective for vacancy concentration  $< 70\%$ . At higher concentrations of vacancies, the excited states become strongly localized and immobile. The focusing efficiency at vacancy concentrations 10% and 20% appears to be higher than that in the absence of vacancies, which we attribute to the effect of the boundaries.

## 4.8 Conclusion

We have proposed a general method for controlling the time evolution of quantum energy transfer in ordered 1D and 2D arrays of coupled monomers. Any elementary excitation in an aggregate of coupled monomers can be represented as a coherent superposition of Frenkel exciton states. We propose shaping the exciton wave packets using nonadiabatic perturbations that temporarily modulate the energy levels of the monomers leading to monomer-dependent linear phase transformation and a displacement of the wave packets in the wave vector representation. This, combined with the possibility of focusing a collective excitation on a particular part of the lattice by a quadratic phase transformation and with the directed propagation of collective excitations, allows for control of energy transfer in the lattice. An experimental observation of the excitations described here can be achieved by measuring site-selective populations of the molecular or atomic states by applying a gradient of an electric field and detecting resonant transitions from Stark-shifted levels [59].

We have presented numerical calculations for an ensemble of polar molecules trapped on an optical lattice that demonstrate the feasibility of both momentum-shifting and focusing of collective excitations by applying external laser fields, with parameters that can be easily achieved in the laboratory. We have also investigated the effect of the disorder potential arising from incomplete population of the lattice. Our results show that the phase transformations leading to focusing of collective

excitations on different regions of a 2D lattice remain effective in the presence of vacancies with concentrations not exceeding 10 %. For systems with larger concentrations of vacancies and affected by strong disorder potentials, we propose an alternative procedure based on engineering constructive interference of the wave function contributions arising from difference parts of the lattice.

The momentum-shifting technique proposed here can be used to protect collective excitations of ultracold atoms from spontaneous emission. The spontaneous decay processes, which in the case of an ordered many-body system must satisfy both the energy and wave vector conservation rules, can be restricted by shifting the exciton wave packets to a region of the dispersion curve, where the wave vector conservation cannot be satisfied. If performed faster than the spontaneous emission time, such phase transformations should create collective excitations with much longer lifetimes, which opens a variety of new applications for ultracold atoms on an optical lattice.

As was proposed by multiple authors [168–173], molecular wavepackets can be used to encode quantum information. Similarly, collective excitations can be used for quantum memory [118, 119]. Control over excitation transfer is needed for creating networks of quantum processors where information is transmitted over large distances with photons and stored in arrays of quantum monomers via one of the quantum memory protocols [174]. Momentum kicking can be used for wave packet transport within a single array. Focusing excitonic wave packets would enable local storage of information, while directed propagation combined with controlled interactions of multiple excitons [139] or excitons with lattice impurities [175] may be used to implement logic gates. Controlled energy transfer in molecular arrays may also be used for the study of controlled chemical interactions for a class of reactions stimulated by energy excitation of the reactants. Directing energy to a particular lattice site containing two or more reagents can be used to induce a chemical interaction [176], an inelastic collision or predissociation [177] with the complete temporal and spatial control over the reaction process.

Finally, the present work may prove to be important for simulations of open quantum systems. We have recently shown [67, 70] that the rotational excitations of ultracold molecules in an optical lattice can, by a suitable choice of the trapping laser fields, be effectively coupled to lattice phonons. The exciton - phonon cou-

plings can be tuned from zero to the regime of strong interactions [67, 70]. The possibility of shaping (accelerating, decelerating and focusing) collective excitations as described in the present work combined with the possibility of coupling these excitations to the phonon bath opens an exciting prospect of detailed study of controlled energy transfer in the presence of a controllable environment. Of particular interest would be to study the effect of the transition from a weakly coupled Markovian bath to a strongly coupled non-Markovian environment on energy transfer with specific initial parameters.

We note that the effect of site-dependent phase transformations on quantum transport was independently considered in Ref. [178] from the point of view of time-reversal symmetry breaking. The authors of Ref. [178] propose an experimental realization based on ions in a linear Paul trap. Their method relies on the possibility of tuning time-dependent phases, leading to new effects. The present work and Ref. [178] should be considered complementary.

## Chapter 5

# Green's function for two particles on a lattice

### 5.1 Introduction

Calculating Green's function for particles on lattices is important in the study of condensed matter systems. Many physical quantities can be obtained or expressed in terms of lattice Green's functions, so they are used in a wide context such as, for example, the transport and diffusion properties of solids [129], band structure [179], statistical models of ferromagnetism [180–182], random walk theory [183], and analysis of infinite electric networks [184–187]. However, the numerical evaluation of the Green's function is usually a cumbersome task[81]. Berciu has recently developed a recursive method [81–83] to calculate the Green's function for particles on a lattice. This method is numerically more efficient than other existing methods and could potentially widen the application of Green's functions in more challenging problems.

In this chapter, I first extend Berciu's method to a disordered system, and then employ the Green's function to study the tunneling of biexciton states through impurities. The scattering of biexciton states is particularly interesting because they are compound particles and their transport behavior in a disordered lattice is not well-understood[188].

## 5.2 Equation of motion for Green's function

To derive the equation of motion for Green's function, we start from the Hamiltonian for the system. We are considering a 1D periodic lattice with the Hamiltonian

$$\hat{H} = \sum_l e_l \hat{P}_l^\dagger \hat{P}_l + \sum_l \sum_{r \neq 0} t_{l,l+r} \hat{P}_l^\dagger \hat{P}_{l+r} + \sum_l \sum_{r \neq 0} d_{l,l+r} \hat{P}_l^\dagger \hat{P}_{l+r}^\dagger \hat{P}_l \hat{P}_{l+r}, \quad (5.1)$$

where  $e_l$  is the energy of the particle at site  $l$ ,  $\hat{P}_l^\dagger$  creates a particle at site  $l$ ,  $t_{l,l+r}$  is the amplitude for hopping between site  $l$  and site  $l+r$ , and  $d_{l,l+r}$  represents the dynamic interaction between particles in site  $l$  and site  $l+r$ . Note that this Hamiltonian  $\hat{H}$  is very general as there is no restriction on the values of  $e_l$ ,  $t_{l,l+r}$ , and  $d_{l,l+r}$ , and thus it can describe both an ordered system and a disordered system. The Green's operator is defined in terms of the Hamiltonian, that is

$$\hat{G}(z) \equiv (z - \hat{H})^{-1}, \quad (5.2)$$

where  $z = E + i\eta$  is a complex energy with a small imaginary part  $\eta$ . From the definition of the Green's operator, it is clear that

$$(z - \hat{H})\hat{G}(z) = 1. \quad (5.3)$$

The above equation describes the system compactly.

Depending on the system under consideration, the creation and annihilation operators will satisfy different commutation rules. For instance, if the particles are fermions,  $\hat{P}_n^\dagger$  and  $\hat{P}_m$  satisfy the anticommutation relations

$$\begin{aligned} \{\hat{P}_n^\dagger, \hat{P}_m\} &= \hat{P}_n^\dagger \hat{P}_m + \hat{P}_m \hat{P}_n^\dagger = \delta_{n,m}, \\ \{\hat{P}_n^\dagger, \hat{P}_m^\dagger\} &= \{\hat{P}_n, \hat{P}_m\} = 0, \end{aligned} \quad (5.4)$$

and if the particles are bosons,  $\hat{P}_n^\dagger$  and  $\hat{P}_m$  satisfy the commutation relations

$$\begin{aligned} [\hat{P}_n^\dagger, \hat{P}_m] &= \hat{P}_n^\dagger \hat{P}_m - \hat{P}_m \hat{P}_n^\dagger = \delta_{n,m}, \\ [\hat{P}_n^\dagger, \hat{P}_m^\dagger] &= [\hat{P}_n, \hat{P}_m] = 0. \end{aligned} \quad (5.5)$$

In the current study, we are considering collective excitations of atom or molecules in a lattice. They have the characteristics of both fermions and bosons. When two excitations reside on different sites they behave like bosons, that is

$$\hat{P}_n^\dagger \hat{P}_m - \hat{P}_m \hat{P}_n^\dagger = 0 , \quad (5.6)$$

if  $n \neq m$ ; when excitations are on the same site, they behave as fermions, that is,

$$\hat{P}_n^\dagger \hat{P}_m + \hat{P}_m \hat{P}_n^\dagger = 0 , \quad (5.7)$$

if  $n = m$ . For convenience, we can combine Eq. (5.6) and Eq. (5.7) into one equation:

$$\hat{P}_m \hat{P}_n^\dagger = \delta_{m,n} + (1 - 2\delta_{m,n}) \hat{P}_n^\dagger \hat{P}_m . \quad (5.8)$$

Using the two-particle basis set  $|n, m\rangle$  (and  $n \neq m$ ), Eq. (5.3) can be rewritten as

$$\langle n, m | (z - \hat{H}) \hat{G}(z) | n', m' \rangle = \langle n, m | I | n', m' \rangle . \quad (5.9)$$

To simplify the above equation, we make use of Eq. (5.8) and evaluate the effect of the Hamiltonian operating on the basis states, giving

$$\begin{aligned} \hat{H} |n, m\rangle &= (e_n + e_m) |n, m\rangle + \sum_{r \neq 0} (1 - \delta_{n-r, m}) t_{n-r, n} |n-r, m\rangle \\ &\quad + \sum_{r \neq 0} (1 - \delta_{n, m-r}) t_{m-r, m} |n, m-r\rangle + \sum_{r \neq 0} d_{n, m} \delta_{n-m, \pm r} |n, m\rangle , \end{aligned} \quad (5.10)$$

where the factors like  $(1 - \delta_{n-r, m})$  appear because only the two-particle states  $|n, m\rangle$  with  $n \neq m$  are included in the basis set. The left-hand side of Eq. (5.9) becomes

$$\begin{aligned} &\langle n, m | (z - \hat{H}) \hat{G}(z) | n', m' \rangle \\ &= (z - e_n - e_m) G(n, m, n', m'; z) - \sum_{r \neq 0} (1 - \delta_{n-r, m}) t_{n-r, n} G(n-r, m, n', m'; z) \\ &\quad - \sum_{r \neq 0} (1 - \delta_{n, m-r}) t_{m-r, m} G(n, m-r, n', m'; z) - \sum_{r \neq 0} d_{n, m} \delta_{n-m, \pm r} G(n, m, n', m'; z) , \end{aligned} \quad (5.11)$$

where  $G(n, m, n', m'; z)$  represents the matrix element of the Green's operator in the two-particle basis set

$$G(n, m, n', m'; z) = \langle n, m | \hat{G}(z) | n', m' \rangle . \quad (5.12)$$

Similarly, substituting Eq. (5.8) into the right hand side of Eq. (5.9) gives rise to

$$\begin{aligned} \langle n, m | I | n', m' \rangle &= \langle 0 | \hat{P}_n \hat{P}_m \hat{P}_{n'}^\dagger \hat{P}_{m'}^\dagger | 0 \rangle \\ &= \langle 0 | \hat{P}_n \left[ \delta_{m, n'} + (1 - 2\delta_{m, n'}) \hat{P}_{n'}^\dagger \hat{P}_m \right] \hat{P}_{m'}^\dagger | 0 \rangle \\ &= \delta_{m, n'} \delta_{n, m'} + \delta_{n, n'} \delta_{m, m'} . \end{aligned} \quad (5.13)$$

Therefore, the equation of the motion for the Green's function is

$$\begin{aligned} &\left( z - e_n - e_m - \sum_{r \neq 0} d_{n, m} \delta_{n-m, \pm r} \right) G(n, m, n', m'; z) \\ &- \sum_{r \neq 0} (1 - \delta_{n-r, m}) t_{n-r, n} G(n - r, m, n', m'; z) \\ &- \sum_{r \neq 0} (1 - \delta_{n, m-r}) t_{m-r, m} G(n, m - r, n', m'; z) \\ &= \delta_{m, n'} \delta_{n, m'} + \delta_{n, n'} \delta_{m, m'} . \end{aligned} \quad (5.14)$$

Because two excitations cannot reside at the same lattice site, we know the Green's function  $G(n, m, n', m'; z)$  is meaningless whenever  $n = m$  or  $n' = m'$ . It is clear that Eq. (5.14) can't guarantee all the Green's functions will be physical even if we restrict the basis set to be  $|i\rangle |j\rangle$  where  $i \neq j$ . That's why factors like  $(1 - \delta_{n, m-r})$  appear.

Since all the Green's functions in Eq. (5.14) have the values of  $n'$  and  $m'$ , we define

$$\tilde{G}(n, m; z) = G(n, m, n', m'; z) \quad (5.15)$$

to simplify the notation. So that Eq. (5.14) becomes

$$\begin{aligned}
& \left( z - e_n - e_m - \sum_{r \neq 0} d_{n,m} \delta_{n-m, \pm r} \right) \tilde{G}(n, m; z) \\
& - \sum_{r \neq 0} (1 - \delta_{n-r, m}) t_{n-r, n} \tilde{G}(n-r, m; z) - \sum_{r \neq 0} (1 - \delta_{n, m-r}) t_{m-r, m} \tilde{G}(n, m-r; z) \\
& = \delta_{m, n'} \delta_{n, m'} + \delta_{n, n'} \delta_{m, m'} .
\end{aligned} \tag{5.16}$$

## 5.3 Recursive calculation of Green's function

### 5.3.1 With the nearest neighbor approximation

The equation of motion for the Green's function, Eq. (5.16), is our starting point to calculate the Green's function. In the nearest neighbor approximation, the distance between two interacting sites  $r$  can only be 1 or  $-1$ . This simplifies Eq. (5.16) to

$$\begin{aligned}
& (z - e_n - e_m - d_{n,m} \delta_{n-m, \pm 1}) \tilde{G}(n, m; z) \\
& - (1 - \delta_{n-1, m}) t_{n-1, n} \tilde{G}(n-1, m; z) - (1 - \delta_{n+1, m}) t_{n+1, n} \tilde{G}(n+1, m; z) \\
& - (1 - \delta_{n, m-1}) t_{m-1, m} \tilde{G}(n, m-1; z) - (1 - \delta_{n, m+1}) t_{m+1, m} \tilde{G}(n, m+1; z) \\
& = \delta_{m, n'} \delta_{n, m'} + \delta_{n, n'} \delta_{m, m'} .
\end{aligned} \tag{5.17}$$

As mentioned before, factors like  $(1 - \delta_{n-1, m})$  in Eq. (5.17) are used to eliminate the unphysical Green's functions like  $\tilde{G}(i, i; z)$ . For instance, when  $n = m - 1$ ,  $\tilde{G}(n+1, m; z)$  and  $\tilde{G}(n, m-1; z)$  will disappear in Eq. (5.17) because of the factors in front of them. Eq. (5.17) shows that  $\tilde{G}(n, m; z)$  only relates directly with at most four other Green's functions in the nearest neighbor approximation. This

relationship can be shown schematically as

$$\begin{aligned}
& \vdots \\
\tilde{G}(n-1, m+1; z) & \rightarrow \left\{ \tilde{G}(n-2, m+1; z), \tilde{G}(n-1, m; z), \tilde{G}(n, m+1; z), \tilde{G}(n-1, m+2; z) \right\} \\
\tilde{G}(n, m; z) & \rightarrow \left\{ \tilde{G}(n-1, m; z), \tilde{G}(n, m-1; z), \tilde{G}(n+1, m; z), \tilde{G}(n, m+1; z) \right\} \\
\tilde{G}(n+1, m-1; z) & \rightarrow \left\{ \tilde{G}(n, m-1; z), \tilde{G}(n+1, m-2; z), \tilde{G}(n+2, m-1; z), \tilde{G}(n+1, m; z) \right\} \\
& \vdots
\end{aligned} \tag{5.18}$$

For the Green's function  $\tilde{G}(i, j; z)$  on the left, the summation of parameters  $i + j = n + m$  is fixed. For the Green's functions  $\tilde{G}(i', j'; z)$  on the right, the summation of parameters  $i' + j'$  can only be either  $n + m - 1$  or  $n + m + 1$ . This inspires us to group some Green's functions into a vector  $\mathbf{V}_K$  according to their values of  $n$  and  $m$ , that is,

$$\mathbf{V}_K = \begin{pmatrix} \vdots \\ \tilde{G}(i-1, j+1; z) \\ \tilde{G}(i, j; z) \\ \tilde{G}(i+1, j-1; z) \\ \vdots \end{pmatrix}, \tag{5.19}$$

with  $K = i + j$ . So Eq. (5.17) can be written as

$$\mathbf{V}_K = \boldsymbol{\alpha}_K(z) \mathbf{V}_{K-1} + \boldsymbol{\beta}_K(z) \mathbf{V}_{K+1}, \tag{5.20}$$

if  $n' + m' \neq K$ , and as

$$\mathbf{V}_K = \boldsymbol{\alpha}_K(z) \mathbf{V}_{K-1} + \boldsymbol{\beta}_K(z) \mathbf{V}_{K+1} + \mathbf{C}, \tag{5.21}$$

if  $n' + m' = K$ . In the above two equations,  $\boldsymbol{\alpha}_K(z)$  and  $\boldsymbol{\beta}_K(z)$  are matrices and  $\mathbf{C}$  is a constant vector, and their values can be determined from Eq. (5.17). Because the two excitations are indistinguishable from each other,  $\tilde{G}(n, m; z)$  is equivalent to

$\tilde{G}(m, n; z)$ . In the following discussion, we require  $n < m$  in all  $\tilde{G}(n, m; z)$  to reduce the dimension of  $\mathbf{V}_K$  by half.

Deriving expressions for  $\boldsymbol{\alpha}_K(z)$  and  $\boldsymbol{\beta}_K(z)$  by hand is tedious. Instead we choose to do that in a programmable way using the pseudocode

```

1: Form all the vectors  $\mathbf{V}_K$  for  $K = 1$  to  $2N - 1$ 
2: Generate the index  $\mathbf{I}(n, m)$  of every  $\tilde{G}(n, m; z)$  such that the  $\mathbf{I}(n, m)$ th element
   of  $\mathbf{V}_{n+m}$  is  $\tilde{G}(n, m; z)$ , that is  $\mathbf{V}_{n+m}[\mathbf{I}(n, m)] = \tilde{G}(n, m; z)$ 
3: for every  $\tilde{G}(i, j; z)$  in  $\mathbf{V}_K$  do
4:    $n^{\text{th}} \leftarrow \mathbf{I}(i, j)$ 
5:   Set every element of  $\boldsymbol{\alpha}_K$  to 0
6:   if  $i - 1 \geq 0$  then
7:      $m^{\text{th}} \leftarrow \mathbf{I}(i - 1, j)$ 
8:      $\boldsymbol{\alpha}_K(n^{\text{th}}, m^{\text{th}}) \leftarrow \frac{t_{i-1,i}}{z - e_i - e_j - d_{i,j} \delta_{j-i,1}}$ 
9:   end if
10:  if  $j - 1 > i$  then
11:     $m^{\text{th}} \leftarrow \mathbf{I}(i, j - 1)$ 
12:     $\boldsymbol{\alpha}_K(n^{\text{th}}, m^{\text{th}}) \leftarrow \frac{t_{j-1,j}}{z - e_i - e_j - d_{i,j} \delta_{j-i,1}}$ 
13:  end if
14:  Set every element of  $\boldsymbol{\beta}_K$  to 0
15:  if  $i + 1 < j$  then
16:     $m^{\text{th}} \leftarrow \mathbf{I}(i + 1, j)$ 
17:     $\boldsymbol{\beta}_K(n^{\text{th}}, m^{\text{th}}) \leftarrow \frac{t_{i,i+1}}{z - e_i - e_j - d_{i,j} \delta_{j-i,1}}$ 
18:  end if
19:  if  $j + 1 \leq N$  then
20:     $m^{\text{th}} \leftarrow \mathbf{I}(i, j + 1)$ 
21:     $\boldsymbol{\beta}_K(n^{\text{th}}, m^{\text{th}}) \leftarrow \frac{t_{j,j+1}}{z - e_i - e_j - d_{i,j} \delta_{j-i,1}}$ 
22:  end if
23: end for
```

As we will show in the next subsection, the above algorithm is even more useful when the coupling equations like Eq. (5.17) become more complicated in the cases of longer range interaction and high-dimensional systems.

It is clear from Eq. (5.20) and Eq. (5.21) that  $\mathbf{V}_K$  relates only with  $\mathbf{V}_{K-1}$  and

$\mathbf{V}_{K+1}$ . This gives the opportunity to solve for individual  $\mathbf{V}_K$  recursively provided that a starting point is given. For example, given the values for two particular  $\mathbf{V}_K$  and  $\mathbf{V}_{K-1}$ , we can obtain  $\mathbf{V}_{K+1}$ , and then calculate  $\mathbf{V}_{K+2}$  from  $\mathbf{V}_K$  and  $\mathbf{V}_{K+1}$ , and etc. But how do we start? The hint comes from the following physical arguments:  $G(n + \delta n, m + \delta m, n, m; z)$  is expected to approach zero as  $|\delta n| \rightarrow \infty$  and  $|\delta m| \rightarrow \infty$  because its Fourier transform  $G(n + \delta n, m + \delta m, n, m; t)$  represents the amplitude for the two particles to move a distance  $\delta n$  and  $\delta m$  respectively in time  $t$  [81, 129]. To figure out which of the Green's functions can be approximated by zero, we fix the values of  $n'$  and  $m'$ . Suppose  $K_c = n' + m'$ , then we can assume that  $\mathbf{V}_K$  approaches zero when  $|K - K_c| \rightarrow \infty$ . For the purpose of numerical computations, a cutoff distance  $M$  is chosen such that  $\mathbf{V}_{K_c-M}$  and  $\mathbf{V}_{K_c+M}$  are very small. In this case, the infinite crystal is replaced by a finite crystal whose central region contains site  $n'$  and site  $m'$ . To ensure the convergence of the results, the finite crystal must be large enough such that its boundaries are far away from both site  $n'$  and site  $m'$ . Assuming the 1D finite crystal has  $N + 1$  lattice sites indexed by  $0, 1, \dots, N - 1, N$ , the starting point for the recursive calculation of the Green's function are the following two approximations

$$\begin{aligned}\mathbf{V}_{2N-1} &\approx 0, \\ \mathbf{V}_1 &\approx 0.\end{aligned}\tag{5.22}$$

Given these two approximations, we are ready to calculate the Green's functions recursively. Instead of working with the vectors  $\mathbf{V}_K$  directly, we define two quantities  $\mathbf{A}_K$  and  $\tilde{\mathbf{A}}_K$  that relate two consecutive vectors  $\mathbf{V}_K$  and  $\mathbf{V}_{K-1}$ . For  $n \geq K_c + 1$ , we have

$$\mathbf{V}_{n+1} = \mathbf{A}_{n+1} \mathbf{V}_n,\tag{5.23}$$

and for  $n \leq K_c - 1$ , we have

$$\mathbf{V}_n = \tilde{\mathbf{A}}_n \mathbf{V}_{n+1}.\tag{5.24}$$

The validity of the above two equations can be verified by substituting Eq. (5.22) into Eq. (5.20) and solving  $\mathbf{V}_K$  recursively. Because  $\mathbf{V}_{K_c}$  satisfies Eq. (5.21) rather

than Eq. (5.20), Eq. (5.23) and Eq. (5.24) are not valid for  $n = K_c$ . At the left boundary of the crystal for which  $n = 1$ , we have

$$\mathbf{V}_1 = \boldsymbol{\beta}_1(z)\mathbf{V}_2 , \quad (5.25)$$

because of Eq. (5.20), and comparing it with Eq. (5.24), we conclude

$$\tilde{\mathbf{A}}_1 = \boldsymbol{\beta}_1(z) . \quad (5.26)$$

There is a recursive relation between different  $\tilde{\mathbf{A}}_n$ . Substituting  $\mathbf{V}_{n-1} = \tilde{\mathbf{A}}_{n-1}\mathbf{V}_n$  into Eq. (5.20) gives

$$\mathbf{V}_n = [1 - \boldsymbol{\alpha}_n(z)\tilde{\mathbf{A}}_{n-1}]^{-1} \boldsymbol{\beta}_n(z)\mathbf{V}_{n+1} , \quad (5.27)$$

which upon comparison with Eq. (5.24) gives

$$\tilde{\mathbf{A}}_n = [1 - \boldsymbol{\alpha}_n(z)\tilde{\mathbf{A}}_{n-1}]^{-1} \boldsymbol{\beta}_n(z) . \quad (5.28)$$

Since this equation involves matrix inversion, which is difficult to compute numerically, we instead calculate  $\tilde{\mathbf{A}}_n$  by solving the linear equation

$$[1 - \boldsymbol{\alpha}_n(z)\tilde{\mathbf{A}}_{n-1}] \tilde{\mathbf{A}}_n = \boldsymbol{\beta}_n(z) . \quad (5.29)$$

Similarly at the right boundary of the crystal for which  $n = 2N - 1$ , we obtain the starting value of  $\mathbf{A}_K$

$$\mathbf{A}_{2N-1} = \boldsymbol{\alpha}_{2N-1}(z) , \quad (5.30)$$

and the recursive relation

$$\mathbf{A}_n = [1 - \boldsymbol{\beta}_n(z)\mathbf{A}_{n+1}]^{-1} \boldsymbol{\alpha}_n(z) . \quad (5.31)$$

To calculate the Green's functions, we start from the left boundary of the crystal and calculate  $\tilde{\mathbf{A}}_1, \tilde{\mathbf{A}}_2, \dots$ , from left to center until  $\tilde{\mathbf{A}}_{K_c-1}$  is reached. We have to stop there because Eq. (5.24) is not valid for  $\mathbf{V}_{K_c}$ . We then proceed from the right boundary to the center and calculate  $\mathbf{A}_{2N-1}, \mathbf{A}_{2N-2}, \dots$  and stop when we reach

$\mathbf{A}_{K_c+1}$  beyond which Eq. (5.23) is not valid. Knowing the value of  $\mathbf{A}_{K_c+1}$  and  $\tilde{\mathbf{A}}_{K_c-1}$ , we rewrite  $\mathbf{V}_{K_c+1}$  and  $\mathbf{V}_{K_c-1}$  in terms of  $\mathbf{V}_{K_c}$  using

$$\begin{aligned}\mathbf{V}_{K_c+1} &= \mathbf{A}_{K_c+1}\mathbf{V}_{K_c}, \\ \mathbf{V}_{K_c-1} &= \tilde{\mathbf{A}}_{K_c-1}\mathbf{V}_{K_c},\end{aligned}\quad (5.32)$$

and substitute them into Eq. (5.21) to obtain the solution for  $\mathbf{V}_{K_c}$ , that is

$$\mathbf{V}_{K_c} = [1 - \boldsymbol{\alpha}_{K_c}(z)\tilde{\mathbf{A}}_{K_c-1} - \boldsymbol{\beta}_{K_c}(z)\mathbf{A}_{K_c+1}]^{-1} \mathbf{C}. \quad (5.33)$$

Once  $\mathbf{V}_{K_c}$  is known, all  $\mathbf{V}_n$  can be calculated from Eq. (5.23) and Eq. (5.24) given the values for  $\mathbf{A}_{n+1}$  and  $\tilde{\mathbf{A}}_n$ .

In summary, the described calculation of Green's function is carried out in the following steps:

1. fix the value of  $n'$  and  $m'$  in the Green's function  $G(n, m, n', m'; z)$ , assume the two approximations in Eq. (5.22), and calculate  $\tilde{\mathbf{A}}_1$  from Eq. (5.26) and  $\mathbf{A}_{2N-1}$  from Eq. (5.30)
2. start from  $\tilde{\mathbf{A}}_1$  and calculate  $\tilde{\mathbf{A}}_2, \tilde{\mathbf{A}}_3, \dots, \tilde{\mathbf{A}}_{K_c-1}$  from Eq. (5.28)
3. start from  $\mathbf{A}_{2N-1}$  and calculate  $\mathbf{A}_{2N-2}, \mathbf{A}_{2N-3}, \dots, \mathbf{A}_{K_c+1}$  from Eq. (5.31)
4. use the values of  $\tilde{\mathbf{A}}_{K_c-1}$  and  $\mathbf{A}_{K_c+1}$  to calculate  $\mathbf{V}_{K_c}$  from Eq. (5.33)
5. start from  $\mathbf{V}_{K_c}$  and calculate  $\mathbf{V}_{K_c-1}, \mathbf{V}_{K_c-2}, \dots, \mathbf{V}_1$  from Eq. (5.24)
6. start from  $\mathbf{V}_{K_c}$  and calculate  $\mathbf{V}_{K_c+1}, \mathbf{V}_{K_c+2}, \dots, \mathbf{V}_{2N-1}$  from Eq. (5.23)

### 5.3.2 Extension to long-range interactions

As mentioned in Section 4.5.1, the dipole-dipole interaction is long-range and the nearest neighbor approximation may not represent the physical picture accurately. So it is desirable to extend the calculation method in Section 5.3.1 to the case of long-range interactions.

First, we consider a 1D lattice with the same Hamiltonian of Eq. (5.1) with both first nearest-neighbor and second nearest-neighbor interactions, for which the

equation of motion for the Green's function becomes

$$\begin{aligned}
& (z - e_n - e_m - d_{n,m}\delta_{m-n,\pm 1} - d_{n,m}\delta_{m-n,\pm 2}) \tilde{G}(n,m;z) \\
& - (1 - \delta_{n-1,m})t_{n-1,n}\tilde{G}(n-1,m;z) - (1 - \delta_{n+1,m})t_{n+1,n}\tilde{G}(n+1,m;z) \\
& - (1 - \delta_{n,m-1})t_{m-1,m}\tilde{G}(n,m-1;z) - (1 - \delta_{n,m+1})t_{m+1,m}\tilde{G}(n,m+1;z) \\
& - (1 - \delta_{n-2,m})t_{n-2,n}\tilde{G}(n-1,m;z) - (1 - \delta_{n+2,m})t_{n+2,n}\tilde{G}(n+2,m;z) \\
& - (1 - \delta_{n,m-2})t_{m-2,m}\tilde{G}(n,m-2;z) - (1 - \delta_{n,m+2})t_{m+2,m}\tilde{G}(n,m+2;z) \\
& = \delta_{m,n'}\delta_{n,m'} + \delta_{n,n'}\delta_{m,m'} . \tag{5.34}
\end{aligned}$$

The above equation shows that the Green's functions  $\tilde{G}(n',m';z)$  are only coupled with the Green's function  $\tilde{G}(i,j;z)$  whose parameters  $i$  and  $j$  sum up to  $n+m-1$  or  $n+m+1$  or  $n+m-2$  or  $n+m+2$ . As for the nearest neighbor approximation, we can group the Green's functions according to the summation of their parameters and obtain

$$\mathbf{Z}_K \mathbf{V}_K = \mathbf{M}_{K,K+1} \mathbf{V}_{K+1} + \mathbf{M}_{K,K-1} \mathbf{V}_{K-1} + \mathbf{M}_{K,K+2} \mathbf{V}_{K+2} + \mathbf{M}_{K,K-2} \mathbf{V}_{K-2} , \tag{5.35}$$

where  $\mathbf{V}_K$  has the same definition as in Eq. (5.48). Different from the NNA case where the recurrence relation links three consecutive terms  $\mathbf{V}_K$ ,  $\mathbf{V}_{K-1}$  and  $\mathbf{V}_{K+1}$ , Eq. (5.35) has two extra terms  $\mathbf{V}_{K-2}$  and  $\mathbf{V}_{K+2}$ . At first glance, adding the second nearest-neighbor interactions invalidates the method presented in Section 5.3.1 as the calculation of Green's function relies on a recurrence relation linking three consecutive terms. But if we work with combinations of  $\mathbf{V}_K$  instead of individual  $\mathbf{V}_K$ , we can obtain the proper recurrence relation. Replacing  $K$  with  $K+1$  in Eq. (5.35) gives

$$\begin{aligned}
\mathbf{Z}_{K+1} \mathbf{V}_{K+1} &= \mathbf{M}_{K+1,K+2} \mathbf{V}_{K+2} + \mathbf{M}_{K+1,K} \mathbf{V}_K + \mathbf{M}_{K+1,K+3} \mathbf{V}_{K+3} + \mathbf{M}_{K+1,K-1} \mathbf{V}_{K-1} . \tag{5.36}
\end{aligned}$$

Eq. (5.35) and Eq. (5.36) can be written as

$$\mathbf{W}_{2K+1} \begin{pmatrix} \mathbf{V}_K \\ \mathbf{V}_{K+1} \end{pmatrix} = \boldsymbol{\alpha}_{2K-3} \begin{pmatrix} \mathbf{V}_{K-2} \\ \mathbf{V}_{K-1} \end{pmatrix} + \boldsymbol{\beta}_{2K+5} \begin{pmatrix} \mathbf{V}_{K+2} \\ \mathbf{V}_{K+3} \end{pmatrix} , \tag{5.37}$$

where

$$\mathbf{W}_{2K+1} = \begin{pmatrix} \mathbf{Z}_K & -\mathbf{M}_{K,K+1} \\ -\mathbf{M}_{K+1,K} & \mathbf{Z}_{K+1} \end{pmatrix}, \quad (5.38)$$

$$\boldsymbol{\alpha}_{2K-3} = \begin{pmatrix} \mathbf{M}_{K,K-2} & \mathbf{M}_{K,K-1} \\ \mathbf{0} & \mathbf{M}_{K+1,K-1} \end{pmatrix}, \quad (5.39)$$

$$\boldsymbol{\beta}_{2K+5} = \begin{pmatrix} \mathbf{M}_{K,K+2} & \mathbf{0} \\ \mathbf{M}_{K+1,K+2} & \mathbf{M}_{K+1,K+3} \end{pmatrix}. \quad (5.40)$$

Comparing Eq. (5.37) with Eq. (5.20) shows that the method introduced in Section 5.3.1 will also work for the current case if

$$\tilde{\mathbf{V}}_{2K+1} \equiv \begin{pmatrix} \mathbf{V}_K \\ \mathbf{V}_{K+1} \end{pmatrix} \quad (5.41)$$

and use series of vectors  $\tilde{\mathbf{V}}_1, \tilde{\mathbf{V}}_5, \tilde{\mathbf{V}}_9, \dots$  is used rather than  $\mathbf{V}_1, \mathbf{V}_2, \mathbf{V}_3, \dots$ .

To further illustrate the point, we consider an even longer range interaction with the first nearest-neighbor, second nearest-neighbor, and the third nearest-neighbor couplings. Similarly, we work with a set of equations that relate different  $\mathbf{V}_K$ , that is

$$\begin{aligned} \mathbf{Z}_K \mathbf{V}_K = & \mathbf{M}_{K,K+1} \mathbf{V}_{K+1} + \mathbf{M}_{K,K-1} \mathbf{V}_{K-1} + \mathbf{M}_{K,K+2} \mathbf{V}_{K+2} + \mathbf{M}_{K,K-2} \mathbf{V}_{K-2} \\ & + \mathbf{M}_{K,K+3} \mathbf{V}_{K+3} + \mathbf{M}_{K,K-3} \mathbf{V}_{K-3}, \end{aligned} \quad (5.42)$$

$$\begin{aligned} \mathbf{Z}_{K+1} \mathbf{V}_{K+1} = & \mathbf{M}_{K+1,K+2} \mathbf{V}_{K+2} + \mathbf{M}_{K+1,K} \mathbf{V}_K + \mathbf{M}_{K+1,K+3} \mathbf{V}_{K+3} + \mathbf{M}_{K+1,K-1} \mathbf{V}_{K-1} \\ & + \mathbf{M}_{K+1,K+4} \mathbf{V}_{K+4} + \mathbf{M}_{K+1,K-2} \mathbf{V}_{K-2}, \end{aligned} \quad (5.43)$$

$$\begin{aligned} \mathbf{Z}_{K+2} \mathbf{V}_{K+2} = & \mathbf{M}_{K+2,K+3} \mathbf{V}_{K+3} + \mathbf{M}_{K+2,K+1} \mathbf{V}_{K+1} + \mathbf{M}_{K+2,K+4} \mathbf{V}_{K+4} + \mathbf{M}_{K+2,K} \mathbf{V}_K \\ & + \mathbf{M}_{K+2,K+5} \mathbf{V}_{K+5} + \mathbf{M}_{K+2,K-1} \mathbf{V}_{K-1}. \end{aligned} \quad (5.44)$$

These equations give rise to a recurrence relation that links three vectors, namely

$$\begin{aligned}
& \begin{pmatrix} \mathbf{Z}_K & -\mathbf{M}_{K,K+1} & -\mathbf{M}_{K,K+2} \\ -\mathbf{M}_{K+1,K} & \mathbf{Z}_{K+1} & -\mathbf{M}_{K+1,K+2} \\ -\mathbf{M}_{K+2,K} & -\mathbf{M}_{K+2,K+1} & \mathbf{Z}_{K+2} \end{pmatrix} \begin{pmatrix} \mathbf{V}_K \\ \mathbf{V}_{K+1} \\ \mathbf{V}_{K+2} \end{pmatrix} \\
&= \begin{pmatrix} \mathbf{M}_{K,K-3} & \mathbf{M}_{K,K-2} & \mathbf{M}_{K,K-1} \\ \mathbf{0} & \mathbf{M}_{K+1,K-2} & \mathbf{M}_{K+1,K-1} \\ \mathbf{0} & \mathbf{0} & \mathbf{M}_{K+2,K-1} \end{pmatrix} \begin{pmatrix} \mathbf{V}_{K-3} \\ \mathbf{V}_{K-2} \\ \mathbf{V}_{K-1} \end{pmatrix} \\
&+ \begin{pmatrix} \mathbf{M}_{K,K+3} & \mathbf{0} & \mathbf{0} \\ \mathbf{M}_{K+1,K+3} & \mathbf{M}_{K+1,K+4} & \mathbf{0} \\ \mathbf{M}_{K+2,K+3} & \mathbf{M}_{K+2,K+4} & \mathbf{M}_{K+2,K+5} \end{pmatrix} \begin{pmatrix} \mathbf{V}_{K+3} \\ \mathbf{V}_{K+4} \\ \mathbf{V}_{K+5} \end{pmatrix} \quad (5.45)
\end{aligned}$$

The above recurrence relation is in the form of Eq. (5.37), and a new vector can be defined as

$$\bar{\mathbf{V}}_{3K+3} \equiv \begin{pmatrix} \mathbf{V}_K \\ \mathbf{V}_{K+1} \\ \mathbf{V}_{K+2} \end{pmatrix}. \quad (5.46)$$

We can then use the series of vectors  $\bar{\mathbf{V}}_3, \bar{\mathbf{V}}_{12}, \bar{\mathbf{V}}_{21}, \dots$  in the recursive calculations.

It is clear from the above discussion that the recursive method to calculate the Green's function can be applied to any finite range interactions and the dimensions of the matrices increase linearly with respect to the number of neighbors included. As the coupling equations get more and more complicated, it becomes more difficult to derive the expressions for  $\mathbf{Z}$ 's and  $\mathbf{M}$ 's by hand. Fortunately the algorithm presented in Section 5.3.1 can be easily adapted to do this kind of computation. For example, the following algorithm can be used to calculate  $\mathbf{M}_{K,K-2}$  and  $\mathbf{M}_{K,K+2}$ :

```

1: for every  $\tilde{G}(i, j; z)$  in  $\mathbf{V}_K$  do
2:    $n^{\text{th}} \leftarrow \mathbf{I}(i, j)$ 
3:   Set every element of  $\mathbf{M}_{K,K-2}$  to 0
4:   if  $i - 2 \geq 0$  then
5:      $m^{\text{th}} \leftarrow \mathbf{I}(i - 2, j)$ 
6:      $\mathbf{M}_{K,K-2}(n^{\text{th}}, m^{\text{th}}) \leftarrow t_{i-2,i}$ 
7:   end if

```

```

8:   if  $j - 2 > i$  then
9:      $m^{\text{th}} \leftarrow \mathbf{I}(j - 2, i)$ 
10:     $\mathbf{M}_{K,K-2}(n^{\text{th}}, m^{\text{th}}) \leftarrow t_{j-2,j}$ 
11:   end if
12:   if  $j - 2 < i$  then
13:      $m^{\text{th}} \leftarrow \mathbf{I}(i, j - 2)$ 
14:      $\mathbf{M}_{K,K-2}(n^{\text{th}}, m^{\text{th}}) \leftarrow t_{j-2,j}$ 
15:   end if
16:   Set every element of  $\mathbf{M}_{K,K+2}$  to 0
17:   if  $i + 2 < j$  then
18:      $m^{\text{th}} \leftarrow \mathbf{I}(i + 2, j)$ 
19:      $\mathbf{M}_{K,K+2}(n^{\text{th}}, m^{\text{th}}) \leftarrow t_{i+2,i}$ 
20:   end if
21:   if  $i + 2 > j$  then
22:      $m^{\text{th}} \leftarrow \mathbf{I}(j, i + 2)$ 
23:      $\mathbf{M}_{K,K+2}(n^{\text{th}}, m^{\text{th}}) \leftarrow t_{i+2,i}$ 
24:   end if
25:   if  $j + 2 \leq N$  then
26:      $m^{\text{th}} \leftarrow \mathbf{I}(i, j + 2)$ 
27:      $\mathbf{M}_{K,K+2}(n^{\text{th}}, m^{\text{th}}) \leftarrow t_{j,j+2}$ 
28:   end if
29: end for

```

### 5.3.3 Extension to high-dimensional systems

In the last two subsections, we only discuss the 1D lattice. It turns out that extending the method to a high-dimensional system is straightforward. For instance, in the case of a 2D lattice, we want to calculate the Green's function

$$\tilde{G}(n_x, n_y, m_x, m_y; z) \equiv \langle n_x, n_y, m_x, m_y | \hat{G}(z) | n'_x, n'_y, m'_x, m'_y \rangle , \quad (5.47)$$

where  $|n_x, n_y\rangle$  represents the state of the particle at site  $(n_x, n_y)$  and  $n'_x, n'_y, m'_x, m'_y$  are fixed. Due to the structure of the equation of motion for the Green's function, one Green's function is only coupled with a certain set of other Green's

functions. In the nearest neighbor approximation, the Green's functions can be grouped into different vectors by defining

$$\mathbf{V}_{i_x+i_y+j_x+j_y} = \begin{pmatrix} \cdots \\ \tilde{G}(i_x-1, i_y+1, j_x, j_y; z) \\ \tilde{G}(i_x, i_y, j_x-1, j_y+1; z) \\ \tilde{G}(i_x, i_y, j_x, j_y; z) \\ \tilde{G}(i_x, i_y, j_x+1, j_y-1; z) \\ \tilde{G}(i_x+1, i_y-1, j_x, j_y; z) \\ \vdots \end{pmatrix}, \quad (5.48)$$

and the same procedure outlined in Section 5.3.1 then follows. Note that the algorithm in Section 5.3.1 can also be applied here with only a small change.

### 5.3.4 Comparison with other methods

Conventionally, Green's function can be calculated by a brute-force approach. The first step is to diagonalize the Hamiltonian  $H$  and calculate the spectrum

$$H|\phi_n(\mathbf{R})\rangle = \lambda_n|\phi_n(\mathbf{R})\rangle, \quad (5.49)$$

where  $n$  indicates the  $n^{\text{th}}$  eigenvector of the system and  $\mathbf{R}$  represents the position of the particles. From the definition of the Green's operator  $\hat{G} = (z - H)^{-1}$ , the Green's function

$$G(\mathbf{R}, \mathbf{R}'; z) = \sum'_n \frac{\phi_n(\mathbf{R})\phi_n^*(\mathbf{R}')}{z - \lambda_n}, \quad (5.50)$$

can be obtained where  $\sum'_n$  represents summation over the discrete spectrum and integration over the continuous spectrum.

This brute-force method is simple but the computational cost is large. Consider a two-particle state  $|i\rangle|j\rangle$  in a 1D lattice with  $N$  sites. The number of two-particle basis sets used to represent the system is  $O(N^2)$  and the dimension of the matrix is  $O(N^2 \times N^2)$ . As most of the algorithms for eigenvalue computations scale like  $O(n^3)$  for a  $n \times n$  matrix, the computational cost of Eq. (5.49) scales like  $O(N^6)$ . To calculate one Green's function from Eq. (5.50) requires computing the inner

product of two vectors  $N^2$  times, which costs  $O(N^6)$  operations in total. So the total cost of the brute-force approach is  $O(N^6)$ . In contrast, the recursive method is much more efficient. Of all the vectors  $\mathbf{V}_K$ ,  $\mathbf{V}_{K_c}$  has the largest size which is about  $N$ . Thus, the most time-consuming step is solving Eq. (5.33), which requires a run time that scales like  $O(N^3)$ . Since there are about  $N$  similar equations to solve, the total computational cost is  $O(N^4)$  which is much less than the cost of the brute-force approach. In addition, the recursive method yields  $N$  Green's functions at the same time.

To verify our recursive method, its results were compared with brute-force calculations for an ordered array and a disordered array for a variety of complex energies  $z$ . As shown in Fig. 5.1 and Fig. 5.2, both methods give identical results, which provides strong evidence to the correctness of the recursive method.

The brute-force approach is not often used in computations. Instead, the recursion method developed by Haydock [189, 190] is most widely used. For comparison purpose, we give a very brief description of the method and compare it with our method. The main idea of Haydock's method is to generate a series of orthonormal vectors  $|u_0\rangle, |u_1\rangle, |u_2\rangle, \dots$  from the iterations

$$H|u_n\rangle = b_n^*|u_{n-1}\rangle + a_n|u_n\rangle + b_{n+1}|u_{n+1}\rangle, \quad (5.51)$$

and calculate the values of  $a_n$  and  $b_n$  until convergence. Because the Hamiltonian matrix is tridiagonal in this basis, the Green's functions can be expressed in term of  $a_n$  and  $b_n$  as

$$\langle u_0 | \hat{G}(z) | u_0 \rangle = \frac{1}{z - a_0 - \frac{|b_1|^2}{z - a_1 - \dots}}. \quad (5.52)$$

For a tight-binding model with only nearest-neighbor interactions, the vectors  $|u_n\rangle$  are linear combinations of local states  $|\mathbf{R}\rangle$  with particles residing at  $\mathbf{R}$ . The Hamiltonian has the following useful feature:

$$H|\mathbf{R}\rangle = \mathbf{t}_{\mathbf{R},\mathbf{R}-\mathbf{1}}|\mathbf{R}-\mathbf{1}\rangle + h_{\mathbf{R},\mathbf{R}}|\mathbf{R}\rangle + \mathbf{t}_{\mathbf{R},\mathbf{R}+\mathbf{1}}|\mathbf{R}+\mathbf{1}\rangle, \quad (5.53)$$

where  $h_{\mathbf{R},\mathbf{R}}$  is the on-site energy,  $\mathbf{t}$  are the matrices related to the hopping terms, and  $|\mathbf{R}-\mathbf{1}\rangle$  and  $|\mathbf{R}+\mathbf{1}\rangle$  denote the states whose particle positions are 1 site dif-

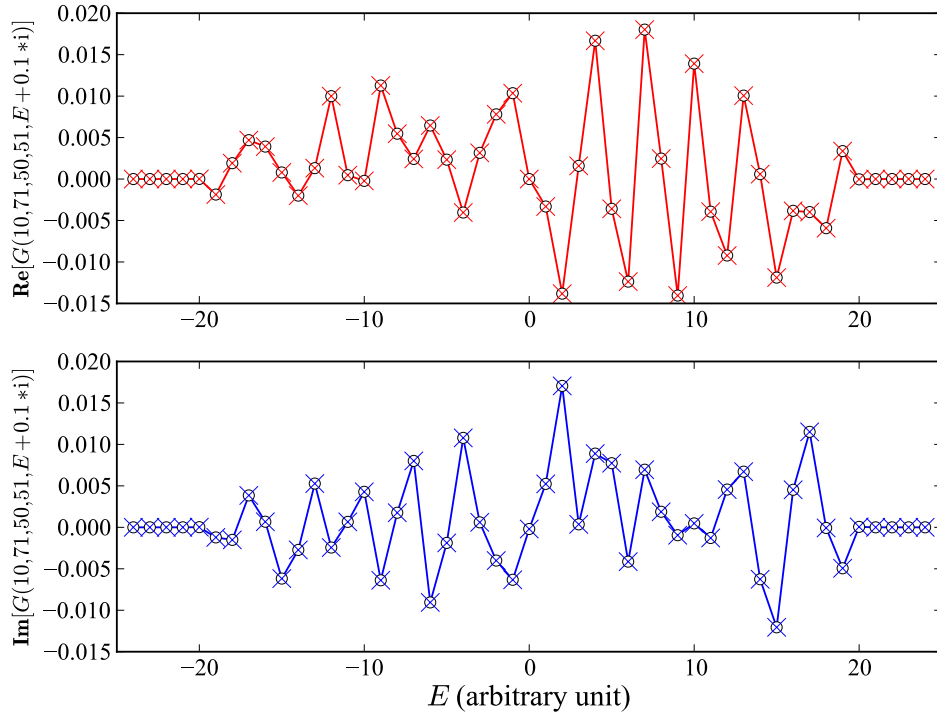


**Figure 5.1:** Green's function  $G(10, 71, 50, 51, E + i\eta)$  with  $\eta = 0.1$  as a function of energy  $E$ . The calculation was done for a finite ordered 1D crystal of 101 lattice sites with the nearest-neighbor approximation. The energies of the particles  $e_n$  were set to zero, and the dynamic interaction and the hopping interaction were set to 5. The upper panel shows the real part of the Green's function and the lower panel shows the imaginary part. The results calculated by the brute-force method are marked with empty circles while the results obtained by our recursive method are marked by “X”. This figure clearly demonstrates that the recursive method produces the same results as the brute-force method.

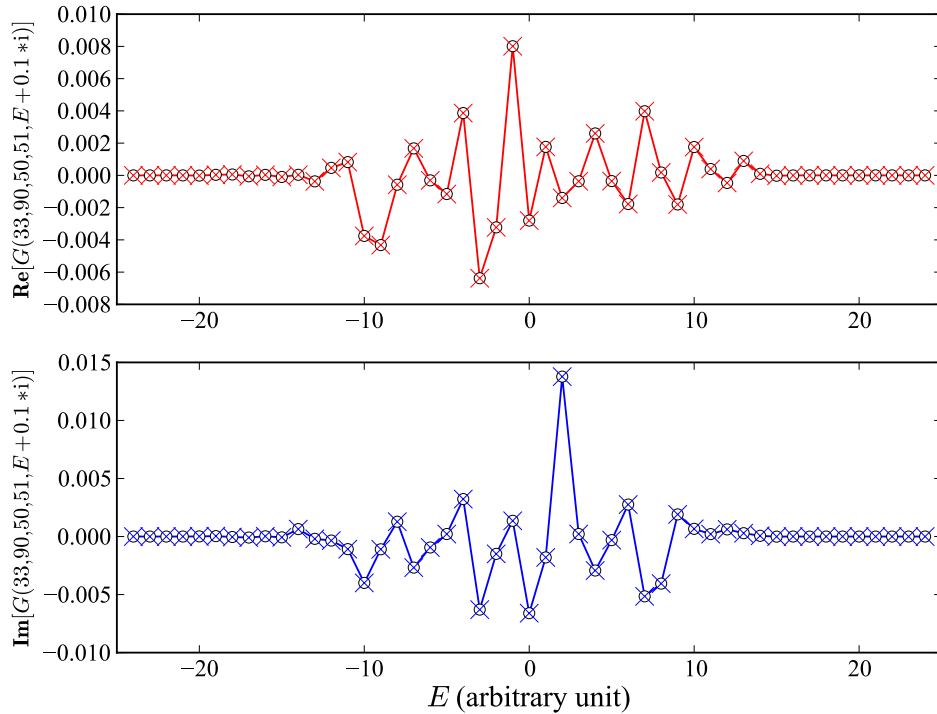


**Figure 5.2:** Green's function  $G(33,90,50,51,E+i\eta)$  with  $\eta = 0.1$  as a function of energy  $E$ . The calculation was done for a finite disordered 1D crystal of 101 lattice sites with the nearest-neighbor approximation. The dynamic interaction and the hopping interaction were set to 5, and allow the energies of the particles  $e_n$  to fluctuate in range  $[-5, 5]$  randomly. The upper panel shows the real part of the Green's function and the lower panel shows the imaginary part. The results calculated by the brute-force method are marked with empty circles while the results obtained by our recursive method are marked by “X”. This figure clearly demonstrates that the recursive method produces the same results as the brute-force method.

ferent from that of  $|\mathbf{R}\rangle$ . As a specific example, Eq. (5.10) clearly demonstrates this property of the local state  $|\mathbf{R}\rangle = |n\rangle|m\rangle$ . As a result of Eq. (5.53), to calculate  $G(\mathbf{R}, \mathbf{R}; z)$ , we can initiate the recursion by setting  $|u_0\rangle = |\mathbf{R}\rangle$  and  $b_0 = 0$ . Assuming orthonormality of local states,  $a_0$  can be obtained by taking the product of  $\langle u_0|$  with Eq. (5.51),

$$a_0 = \langle u_0|H|u_0\rangle = h_{\mathbf{R}, \mathbf{R}} . \quad (5.54)$$

Comparing Eq. (5.51) with Eq. (5.53), we can easily see that  $|u_1\rangle$  is a superposition of  $|\mathbf{R} - \mathbf{1}\rangle$  and  $|\mathbf{R} + \mathbf{1}\rangle$  and  $b_1$  can be computed by requiring  $|u_1\rangle$  to be normalized. To continue the recursion, we take  $n = 1$  in Eq. (5.51) to obtain

$$H|u_1\rangle = b_1^*|u_0\rangle + a_1|u_1\rangle + b_2|u_2\rangle , \quad (5.55)$$

and let  $H$  operate on  $|u_1\rangle$ , a superposition of  $|\mathbf{R} - \mathbf{1}\rangle$  and  $|\mathbf{R} + \mathbf{1}\rangle$ , according to Eq. (5.53), which gives rise to a linear combination of  $|\mathbf{R} - \mathbf{2}\rangle$ ,  $|\mathbf{R} - \mathbf{1}\rangle$ ,  $|\mathbf{R}\rangle$ ,  $|\mathbf{R} + \mathbf{1}\rangle$  and  $|\mathbf{R} + \mathbf{2}\rangle$  on the left hand side of Eq. (5.55). Now it is clear that  $|u_2\rangle$  will also be a superposition of  $|\mathbf{R} - \mathbf{2}\rangle$ ,  $|\mathbf{R} - \mathbf{1}\rangle$ ,  $|\mathbf{R}\rangle$ ,  $|\mathbf{R} + \mathbf{1}\rangle$  and  $|\mathbf{R} + \mathbf{2}\rangle$ , and  $b_2$  can be calculated from the normalization condition of  $|u_2\rangle$ . Follow the above analysis, we conclude that  $|u_n\rangle$  is a superposition of these local states:  $|\mathbf{R} - \mathbf{n}\rangle$ ,  $|\mathbf{R} - \mathbf{n} + \mathbf{1}\rangle$ ,  $\dots$ ,  $|\mathbf{R} + \mathbf{n} - \mathbf{1}\rangle$  and  $|\mathbf{R} + \mathbf{n}\rangle$ , which are within  $n$ -sites distance from  $\mathbf{R}$ .

Haydock's method and our method both rely on recursive calculations, but they differ a lot in numerical efficiency. Consider the calculation of the two-particle Green's function as an example. If Haydock's method terminates the recursion at step  $N$ , it has to deal with vectors of size up to  $\sim N^2$ . To employ the same number of local states as in Haydock's method, our method sets  $\mathbf{A}_{2N+1} = 0$  and  $\tilde{\mathbf{A}}_1 = 0$ , and the largest size of the vectors is about  $N$ , which is much smaller. Therefore our method involves much smaller matrices and can handle much larger crystal sizes.

## 5.4 Application to the problem of biexciton scattering

As a powerful analytical tool, Green's functions are often used to develop analytical formulations for all sorts of physical problems. However, due to difficulties in their numerical computation, these formulations often become something of theoretical merit only, and are rarely used for computations. For example, as will be

shown below, the Green's function formulation of scattering theory is quite general and elegant. It can handle all types of scattering potentials and treat single-particle scattering and multiple-particle scattering in the same way. But still the Green's functions are not used very often in scattering problems because of the numerical difficulties involved in their calculation[81]. Using the new recursive method in Section 5.3, which makes the calculation easier, the Green's function formulation of scattering will be used to develop a numerical method to calculate the tunneling of a biexciton state through disorder potentials. This method is numerically efficient and can handle multiple impurities.

We consider a periodic lattice with hopping interactions and dynamic interactions. Although the lattice is regular, disorders can still appear due to different on-site energies and different coupling strengths at different sites. We write the Hamiltonian in two parts,

$$\hat{H} = \hat{H}_0 + \hat{H}_1 , \quad (5.56)$$

where  $\hat{H}_0$  represents an ordered array and is given by

$$\hat{H}_0 = E_0 \sum_n \hat{P}_n^\dagger \hat{P}_n + \sum_{n,m \neq n} J_{n,m} \hat{P}_n^\dagger \hat{P}_m + \frac{1}{2} \sum_{n,m \neq n} D_{n,m} \hat{P}_n^\dagger \hat{P}_m^\dagger \hat{P}_n \hat{P}_m , \quad (5.57)$$

and  $\hat{H}_1$  describes the disorders and is given by

$$\begin{aligned} \hat{H}_1 &= \sum_{i \in S_0} (E_i - E_0) \hat{P}_i^\dagger \hat{P}_i + \sum_{\substack{i,j \neq i \\ (i,j) \in S_J}} (J'_{i,j} - J_{i,j}) \hat{P}_i^\dagger \hat{P}_j \\ &+ \frac{1}{2} \sum_{\substack{i,j \neq i \\ (i,j) \in S_D}} (D'_{i,j} - D_{i,j}) \hat{P}_i^\dagger \hat{P}_j^\dagger \hat{P}_i \hat{P}_j , \end{aligned} \quad (5.58)$$

where  $S_0$  is the set of sites whose energies are different from  $E_0$ ,  $S_J$  is the set of pairs of sites whose hopping terms  $J'$  are different from  $J$ , and  $S_D$  is the set of pairs of sites whose dynamic interactions  $D'$  are different from  $D$ . As shown in Chapter (3), if the dynamical interaction is 2 times larger than the hopping interaction,  $H_0$  will have a set of states with energies that are located outside the spectrum of two free exciton pairs. These states are correlated states of two excitations and are called

biexcitons. The presence of  $H_1$  in the Hamiltonian causes the eigenstates to be different from the free-biexciton state.

We are interested in the scattering of a biexciton state through disorder. For convenience, the disorder is assumed to appear at the center region of the lattice. The starting state is a biexciton state  $|\phi(K)\rangle$  which is an eigenstate of  $\hat{H}_0$ ,

$$\hat{H}_0|\phi(K)\rangle = E(K)|\phi(K)\rangle . \quad (5.59)$$

If the scattering process is elastic, we want to obtain a solution to the full-Hamiltonian Schrödinger equation with the same energy as the initial biexciton state

$$(\hat{H}_0 + \hat{H}_1)|\psi\rangle = E(K)|\psi\rangle . \quad (5.60)$$

It can be shown that the desired solution might be

$$|\psi\rangle = \frac{1}{E(K) - \hat{H}_0} \hat{H}_1 |\psi\rangle + |\phi(K)\rangle . \quad (5.61)$$

There is a problem with the above solution: the operator  $\frac{1}{E(K) - \hat{H}_0}$  will generate singular results because  $E(K)$  is an eigenenergy of  $\hat{H}_0$ . To resolve this complications, we can make the energy complex and the solution is then given by

$$|\psi^\pm\rangle = \frac{1}{E(K) \pm i\eta - \hat{H}_0} \hat{H}_1 |\psi^\pm\rangle + |\phi(K)\rangle , \quad (5.62)$$

where  $\eta$  is an infinitesimal positive number. The above equation is the Lippmann-Schwinger equation[91].  $|\psi^+\rangle$  and  $|\psi^-\rangle$  are outgoing and incoming solutions, respectively. In most cases, only  $|\psi^+\rangle$  is interesting because it corresponds to the measurement at a position far away from the scatterers. Based on the definition of Green's function, Eq. (5.62) can also be written as

$$|\psi^+\rangle = |\phi(K)\rangle + \hat{G}_0(E(K) + i\eta) \hat{H}_1 |\psi^\pm\rangle . \quad (5.63)$$

Substituting Eq. (5.63) into itself and iterating gives

$$|\psi^+\rangle = |\phi\rangle + \hat{G}_0^+ \hat{H}_1 |\phi\rangle + \hat{G}_0^+ \hat{H}_1 \hat{G}_0^+ \hat{H}_1 |\phi\rangle + \dots , \quad (5.64)$$

where

$$\hat{G}_0^+(E) = \hat{G}_0(E + i\eta) . \quad (5.65)$$

Based on Eq. (5.56), we can express the Green's operator  $\hat{G}$  for the total Hamiltonian in terms of  $\hat{G}_0$  and  $H_1$ . The derivation is presented as follows:

$$\begin{aligned} \hat{G}(z) &= (z - \hat{H}_0 - \hat{H}_1)^{-1} \\ &= \left\{ (z - \hat{H}_0) [1 - (z - \hat{H}_0)^{-1} \hat{H}_1] \right\}^{-1} \\ &= [1 - (z - \hat{H}_0)^{-1} \hat{H}_1]^{-1} (z - \hat{H}_0)^{-1} \\ &= [1 - \hat{G}_0(z) \hat{H}_1]^{-1} \hat{G}_0(z) \\ &= [1 + \hat{G}_0(z) \hat{H}_1 + \hat{G}_0(z) \hat{H}_1 \hat{G}_0(z) \hat{H}_1 + \dots] \hat{G}_0(z) \\ &= \hat{G}_0(z) + \hat{G}_0(z) \hat{H}_1 \hat{G}_0(z) + \hat{G}_0(z) \hat{H}_1 \hat{G}_0(z) \hat{H}_1 \hat{G}_0(z) + \dots . \end{aligned} \quad (5.66)$$

Substituting Eq. (5.66) into Eq. (5.64) gives

$$|\psi^+\rangle = |\phi\rangle + \hat{G}(E(K) + i\eta) \hat{H}_1 |\phi\rangle . \quad (5.67)$$

This is the equation that can be used in numerical calculations given the initial state  $|\phi\rangle$  and the Green's function  $G(z)$ .

Based on the wavefunction of a biexciton state, Eq. (3.74), derived in Section 3.3.2, we may write the biexciton state in the two-particle basis set as

$$\begin{aligned} |\phi(K)\rangle &= \sum_{n,m \neq n} e^{iK(n+m)/2} f_K(|n-m|) \hat{P}_n^\dagger \hat{P}_m^\dagger |0\rangle \\ &= \sum_{n,m \neq n} e^{iK(n+m)/2} f_K(|n-m|) |n,m\rangle , \end{aligned} \quad (5.68)$$

where  $f_K(|n-m|)$  is a function that decreases fast with increasing  $|n-m|$ . In principle, all possible two-particle states  $|n,m\rangle$  with  $n \neq m$  should be used to represent the biexciton state, but for practical purposes a cutoff distance  $L$  for  $|n-m|$  is used to greatly reduce the number of basis sets. This will hardly affect the final result as long as  $f_K(|n-m|)$  decays fast enough such that  $f_K(L) \approx 0$ . In this case the

biexciton state can be rewritten as

$$|\phi(K)\rangle \approx \sum_n \sum_{m=n\pm 1}^{n\pm L} e^{iK(n+m)/2} f_K(|n-m|) |n, m\rangle. \quad (5.69)$$

Because the two-particle states in Eq. (5.69) can effectively represent a biexciton state, they are called the biexciton basis and denoted by  $S_{\text{biexciton}}$ .

To calculate the scattering state from Eq. (5.67), let's analyze  $\hat{H}_1|\phi\rangle$  first. Expanding the disorder term in a two-particle basis set gives

$$\begin{aligned} \hat{H}_1 &= \sum_{i \in S_0} \sum_{j \neq i} (E_i - E_0) |i, j\rangle \langle i, j| + \sum_{\substack{i, j \neq i \\ (i, j) \in S_D}} \sum_{l \neq i, j} (J'_{i,j} - J_{i,j}) |j, l\rangle \langle i, l| \\ &+ \frac{1}{2} \sum_{\substack{i, j \neq i \\ (i, j) \in S_D}} (D'_{i,j} - D_{i,j}) |i, j\rangle \langle i, j|. \end{aligned} \quad (5.70)$$

The above equation can be derived by inserting the identity relation  $\sum_i |i\rangle \langle i| = I$  into the first and second terms of Eq. (5.58). Suppose the hopping disorder and the dynamic disorder only appear between two sites that are within the cutoff distance  $L$ , we can easily see that in Eq. (5.70) only the two-particle states  $|n, m\rangle$  with  $|n - m| \leq L$  will play a role, by letting  $\hat{H}_1$  operate on Eq. (5.69). Since only these two-particle states are needed to represent the effective disorder the biexciton experiences, we call them the disorder basis  $S_{\text{disorder}}$ . In the case of a small number of disorder sites,  $S_{\text{disorder}}$  is a small subset of  $S_{\text{biexciton}}$  by construction. Thus  $\hat{H}_1|\phi\rangle$  gives rise to a new wavefunction

$$|\phi_{\hat{H}_1}\rangle = \hat{H}_1|\phi\rangle = \sum_{(i,j) \in S_{\text{biexciton}}} c(i, j) |i, j\rangle, \quad (5.71)$$

where  $c(i, j)$  can be nonzero only if  $(i, j) \in S_{\text{disorder}}$ . Given  $|\phi_{\hat{H}_1}\rangle$ , we can continue to calculate the scattering state according to Eq. (5.67). Since only a small number of coefficients  $c(i, j)$  is nonzero in Eq. (5.71), only a small portion of the matrix that represents the Green's operator  $\hat{G}(E(K) + i\eta)$  is needed, that is, the matrix elements  $\langle i', j' | \hat{G}(E(K) + i\eta) | i, j \rangle$  with  $|i, j\rangle$  being states in the disorder basis. This task can be efficiently handled by the recursive method in Section 5.3 by setting

the initial particle positions  $(n', m')$  to be every site pairs  $(i, j)$  in  $S_{\text{disorder}}$ .

To prevent the processes of a biexciton breaking into two free excitons, we assume the dynamic interaction is more than 2 times larger than the hopping interaction such that the energy of a biexciton is well separated from the energy spectrum of two free excitons. During the scattering process, the energy must be conserved, and thus the scattering wavefunction has the following asymptotic behavior

$$|\psi\rangle \rightarrow \begin{cases} |\phi(K)\rangle + \mathbf{R}|\phi(-K)\rangle & \text{for } n, m \rightarrow -\infty \\ \mathbf{T}|\phi(K)\rangle & \text{for } n, m \rightarrow \infty \end{cases}, \quad (5.72)$$

if the initial biexciton state  $|\phi(K)\rangle$  incidents from the left with its eigenenergy  $E(K)$ . This asymptotic behavior can be used to calculate the transmission coefficient of a biexciton through disorder. In principle, scattering calculations usually assume a infinitely large space, but in practice, a finite crystal with sufficiently large size is used. We start the calculation from an initial biexciton state  $\phi(K)$  with eigenenergy  $E(K)$ , and then calculate the scattering state  $|\psi\rangle$  using Eq. (5.67). The transmission coefficient can then be deduced from Eq. (5.72) by choosing two sites  $n$  and  $m$  to the far right of the disorder region, that is

$$t = \frac{\langle n, m | \psi \rangle}{\langle n, m | \phi(K) \rangle}. \quad (5.73)$$

Note that the scattering wavefunction  $|\psi\rangle$  must be properly normalized with respect to the finite crystal.

## 5.5 Summary

In this chapter, a recursive method to calculate lattice Green's functions is described. The essential idea is to group Green's functions into different sets of vectors and rewrite the equation of motion of Green's function as a recursion relation linking three consecutive vectors. Based on physical reasoning, certain vectors are assumed to be zero and then substituted into the corresponding recursion relations to express one set of Green's function in terms of another set of Green's function. By iterating on the recursion relation, a chain of relationships between each two consecutive vectors can be obtained. Finally, the vector at the end of this relation-

ship chain can be calculated by solving a linear equation, and all the vectors can be calculated one by one through the relationship chain. The method can handle a system with arbitrary disorder, and can be easily extended to systems with interactions of longer (but finite) range, and to systems with high dimensionality. To show the numerical efficiency of the method, it was compared with the brute-force method and Haydock's method. Our method involves vectors of much smaller sizes. As an application, we described using the recursive method to calculate the Green's functions to study the scattering of a biexciton state by impurities.

# **Chapter 6**

## **Conclusion**

Trapping ultracold atoms and molecules in optical lattices has opened an exciting frontier of condensed matter research[17]. In the limit of strong trapping fields that completely suppress particle tunneling in optical lattices, an artificial crystal of atoms and molecules, called the Mott insulator phase, appears. These artificial crystals possess unique properties – in particular, they offer the ability to address single lattice sites[57, 58] and the possibility for controlling interparticle interactions with external electric or magnetic fields[16, 17], making them a very good platform to study collective phenomena[8, 16, 17]. The thesis, by utilizing the controllability of the artificial crystals of ultracold particles, explores theoretically the mechanisms for controlling the quantum dynamics of quasiparticles.

### **6.1 Summary of the thesis**

The control schemes presented in this thesis can be categorized into two major types: 1) mixing internal states by external fields; 2) changing the phase of internal states by temporal perturbations.

The first type of control schemes is commonly used to control the interparticle interactions in the field of ultracold atoms and molecules. For example, it has been shown that both the shape and strength of the dipole-dipole interaction between molecules can be controlled by external fields[51], which inspires numerous study on using molecules trapped on optical lattices for quantum simulation[43, 50, 120–

127]. Instead, the current thesis studied the possibility of using the external fields to control inter-quasiparticle interactions rather than interparticle interactions. In the case of the rotational excitation of polar molecules trapped in an optical lattice, the dipole-dipole operator leads to different kinds of inter-quasiparticle interactions, namely the hopping interaction that is responsible for excitation propagation, the attractive dynamic interaction that can induce exciton binding, and the conversion interaction that can split a high-energy exciton into two low-energy excitons. These interactions are associated with different dressed rotational states of molecules, which correspond to different mixing of bare rotational states in external fields. So the different inter-quasiparticle interactions respond differently to the change of external fields. This thesis showed that the ratio between the hopping and the dynamic interaction can be tuned by an electric field to induce the formation of biexciton and triexciton states with tunable binding energies, and found that the conversion interaction leads to a non-optical way to create biexciton states from the high-energy ( $N = 2$ ) excitonic states under the resonance condition when a high-energy excitonic state have the same energy as two low-energy ( $N = 1$ ) excitonic states. These results demonstrated that the physics of dipole-dipole interactions in the context of quasiparticles is also rich and opened up the possibility to control the binding and creation of collective excitation modes of polar molecules trapped on optical lattices.

The second type of control schemes is reminiscent of the techniques used for strong-field alignment and orientation of molecules in the gas phase[144]. The essential idea is to use an external field to perturb the internal states of molecules for a short time, adding phases to the wavefunctions of the internal states. This perturbation doesn't change the interparticle interactions as the internal states remain the same except that their phases are changed. Though the phase changes are seemingly unimportant, they play an important role in determining the dynamics of quasiparticles. Since a collective excitation in an array of coupled monomers is a superposition of internal states of monomers, any phase change of the internal states will translate to a change of quasimomentum of the collective excitation, and influence the excitation energy propagation in the array. The thesis showed that specific phase transformations can be used to accelerate or decelerate excitation energy transfer and spatially focus delocalized excitations in arrays of quantum

particles. The proposed control scheme is a very general as the excitations can be of any type and the array can be ordered and disordered. This thesis also demonstrated the feasibility of the control scheme in the system of ultracold atoms and molecules trapped on optical lattices. All the above results showed that the phases of individual monomer state in an array of coupled monomers can be used to manipulate the quantum energy transfer in the array, which pointed out a new way to control the dynamics of quasiparticles.

In addition, the thesis extended calculations of lattice Green's functions to disordered systems. The proposed method is numerically more efficient than conventional methods and may be used to study the dynamics of quasiparticles in strongly disordered potentials.

## 6.2 Limitations and possible extension

In this section, I discuss the limitations of the thesis and explain how the current work can be extended by going beyond those limitations.

Conventionally, the 1D and 2D crystals of ultracold atoms and molecules are created in 3D optical lattices. In a 3D optical lattice, since the intensity of every laser pair can be tuned independently, the trap depths along the  $x$ ,  $y$  and  $z$  directions can be adjusted separately. By making the trap depths along the  $x$  and  $y$  directions so deep that the particle tunneling along these two directions are completely suppressed, an effective 1D crystal can be constructed in which the trapped particles are only allowed to move in the periodic potentials along the  $z$  direction. Similarly, an effective 2D crystal can be created by suppressing the motion of trapped particles along just one direction. In this thesis, I study the excitations, rather than real particles, trapped in 1D and 2D dimensions. To confine excitations in reduced dimensionalities, it is not enough to use the effective 1D and 2D systems described previously since excitations can still propagate along a direction even if the tunneling of real particles along that direction is completely suppressed. Theoretically speaking, we need a real 1D or 2D crystal in a 3D optical lattices, where only the sites along a single line or on a single plane are occupied by atoms or molecules. The problem is that such an 1D or 2D crystal is difficult to obtain in experiments as it requires high precision to remove particles from the lattice sites that don't

belong to the required arrays. In practices, one may still use a 3D optical lattice with one polar molecule per site in the Mott insulator phase. To approximate the 1D and 2D crystals required in the thesis, the wavelengths of laser beams in some directions can be increased, producing larger lattice separations along those directions and reducing the strength of coupling between molecules in the corresponding dimensions. This leads to suppressing of the excitation propagation along those directions, creating the quasi-1D and quasi-2D arrays. However, limited by the available wavelengths of the laser beams used to form optical lattices, the ratio between the large and small lattice separations along different directions is typically about 2~3. This means that the interaction between nearest neighbors along the direction with the large lattice constant will be of the same magnitude as the interaction between next nearest neighbors or next next nearest neighbors along the direction with small lattice constant. As shown in Chapter 4, the long-range interaction between molecules can play a role in determining the dynamics of quasiparticles, therefore it is necessary to include the weak interactions along the suppressed dimension(s). In addition, because the dipole-dipole interaction is anisotropic and the relative orientation of the dipole moments with respect to the intermolecular axis are different, the weak interactions along the suppressed dimension(s) generally have different signs from the strong interaction within the 1D and 2D arrays. So it would be interesting to investigate whether the results obtained for purely 1D and 2D arrays are valid for the quasi-1D and quasi-2D crystals and especially the effect of the anisotropic weak interactions.

In the thesis, I have assumed that the optical lattices are deep and ignored the translational motion of molecules within the trap. In fact, going beyond this assumption may also lead to interesting results. Recently, Herrera showed that the rotational excitons can interact with the translational motion of molecules to form polarons[69]. The Hamiltonian for these polarons contains both breathing-mode and Su Schrieffer-Heeger couplings, leading to interesting sharp transitions in the phase diagram[70]. It might be possible to extend Herrera's work to include the dynamic interaction between excitons.

Chapter 3 has shown the existence of the two-body and three-body bound states of excitons under certain conditions. However, this does not mean that biexciton and triexciton will appear at any exciton concentrations. When more excitons are

present, the combination of biexciton and exciton might be unstable to triexciton formation and triexciton + exciton might be unstable to bigger bound complexes. So it is necessary to extend our theoretical model to handle  $n$ -body bound states and to investigate the fundamental limits of exciton clustering. References [108, 193, 194] have already studied the problem of exciton clustering under the nearest-neighbor approximation and implied the existence of excitonic  $n$ -string where  $n$  can be any positive integer. It might be worthwhile to extend their analysis to the case of long-range interactions.

The work on energy transfer presented in the thesis has so far ignored the interactions between excitons. This is justified for the case of the rotational excitations in small external fields as the exciton-exciton interaction is small compared with the hopping interaction. However as Chapter 3 shows, the dynamic interaction between excitons can be comparable and even a few times larger than the hopping interaction at certain electric field strengths. In this situation, it is important to investigate if the control scheme still works. Particularly, it would be very interesting to see whether we can control the propagation of the biexciton states.

## 6.3 Future research directions

### 6.3.1 Influence of exciton-exciton interaction on polariton lasing

The coupling between cavity photons and excitons gives rise to the half-light and half-matter quasiparticles called cavity polaritons[195]. Unlike the weakly interacting cavity photons, polaritons can strongly interact with each other due to the inherited strong-interacting characteristics from the matter (or exciton) components. This polariton-polariton interaction produces effective strong photon-photon interaction, and leads to the emerging field of quantum fluids of light[196]. One branch of the field focuses on using the Bose-Einstein condensation of cavity polaritons to create polariton laser, a new coherent source of light that may lead to new optoelectronic devices[197]. Polaritons decay in a cavity because their photonic components leak out through cavity mirrors. When polaritons form a condensation, the decay of polaritons in the macroscopic coherent state produces photons in the same coherent state. This process is similar to the conventional photon lasing but with-

out the population inversion, therefore polariton lasing has a much lower threshold energy for coherent emission[198].

In experiments with polariton lasers, both inorganic and organic semiconductors can be used as a basis for microcavities[197]. However, they have very different excitonic modes. In inorganic semiconductors, the excitons are loosely-bound electron-hole pairs called Wannier-Mott excitons, while in organic materials, the excitons are tightly-bound electron-hole pairs called Frenkel excitons. Compared with Wannier-Mott excitons, Frenkel excitons are highly stable at room temperature[199]. As a result, there is a trend towards using organic materials as the microcavities[197], with the notable achievement of room-temperature polariton lasing[200, 201].

Polariton lasers requires the Bose-Einstein condensation of polaritons. To form the polariton condensation, efficient relaxation mechanisms are required to transfer populations from other polariton states to the ground polariton state. The polariton-polariton scattering[202, 203], usually resulted from both the Coulomb interaction between excitons and the exciton saturation, is a very important relaxation mechanism. In organic materials, due to the strong screening effect, the Coulomb interaction is very weak. So the exciton saturation or the kinematic interaction (see Chapter 3), originated from the fact that two excitons cannot sit on the same lattice site, plays the dominant role and it is well investigated[204–206]. To the contrary, another type of exciton-exciton interaction, namely the dynamic interaction (see Chapter 3), is not discussed with regard to polariton lasers in organic semiconductors. In an organic crystal, if the molecules possess static dipole moments, the dynamic interaction can be as large as the width of the exciton bandwidth[99]. This strong dynamic exciton interaction can have a significant effect on the polariton-polariton interaction. It would be very interesting to investigate whether the dynamic interaction can enhance the relaxation towards the ground polariton state and further reduce the threshold energy for polariton lasing.

To simulate the polaritons in organic semiconductors, one could use a dipolar crystal of ultracold polar molecules trapped on the surface of a high-Q superconducting stripline cavity, like the setup described in Ref. [118] and Ref. [119]. The rotational excitons of the molecular array resemble the Frenkel electronic excitons in the organic crystal. The cavity photons can be provided by the microwave

stripline cavity. The rotational excitons may couple strongly with the microwave photons to form polaritons. (Note that the conventional microwave cavities like those in Ref. [207] cannot be used here because their large sizes result in very weak interaction between excitons and photons.) In the current system, an external dc field is required to induce electric dipole moments of polar molecules to maintain the dipolar crystal. This external field can be tuned to change the phonon modes and to adjust the strength of exciton-exciton interaction. Because of this tunability, it would be very interesting to study the condition of polariton lasing in the current system and to investigate the influence of exciton-exciton interaction on polariton relaxation. Recently, Cristofolini *et al.* has demonstrated polaritons with static dipole moments[208]. It is expected that the static dipole moments will reinforce polariton-polariton interactions, just like the dynamic interaction discussed before, and may leads to new effects as discussed in Ref.[209] and Ref.[210]. The current system may also be used as a platform to study the new polariton physics of the long-range dipolar interactions.

### 6.3.2 Parallel computation of Green's functions

With the advance of technology, multi-core processors are getting more powerful and less expensive, and they are expected to become the mainstream for large scientific computations. Calculating the Green's functions for multiple particles is always a computation intensive task due to the large number of degrees of freedom involved, so it is desirable to develop parallel numerical methods to speed up the computation. However, the recursive method to calculate the Green's functions, as presented in Chapter 5, can only be implemented in a sequential way. This can be easily seen from Eq. (5.28) and Eq. (5.31): the calculation of  $\tilde{\mathbf{A}}_n(\mathbf{A}_n)$  can only be done after  $\tilde{\mathbf{A}}_n(\mathbf{A}_{n+1})$  is calculated. In the following, I sketch a parallel way to calculate the Green's function as a future research direction. This method is inspired by the recursive doubling algorithm for solution of tridiagonal systems[211].

For simplicity, I only discuss the case with the nearest-neighbor coupling. It is straightforward to extend the discussion to cases with long-range interactions. Based on the analysis in Chapter 5, the equation of motion for the Green's function

can be rewritten as a set of recursive relations:

$$\mathbf{W}_K \mathbf{V}_K = \boldsymbol{\alpha}_K \mathbf{V}_{K-1} + \boldsymbol{\beta}_K \mathbf{V}_{K+1} + \boldsymbol{\gamma}_K \quad (6.1)$$

where  $\boldsymbol{\gamma}_K$  can be a zero vector or nonzero vector. For a finite crystal, the value of  $K$  is from 1 to  $K_{\max}$ . Rewriting the above recursion relation as

$$\mathbf{V}_{K+1} = \boldsymbol{\beta}_K^{-1} \mathbf{W}_K \mathbf{V}_K - \boldsymbol{\beta}_K^{-1} \boldsymbol{\alpha}_K \mathbf{V}_{K-1} - \boldsymbol{\beta}_K^{-1} \boldsymbol{\gamma}_K, \quad (6.2)$$

one can easily derive the following equation:

$$\begin{pmatrix} \mathbf{V}_{K+1} \\ \mathbf{V}_K \\ \mathbf{1} \end{pmatrix} = \begin{pmatrix} \boldsymbol{\beta}_K^{-1} \mathbf{W}_K & -\boldsymbol{\beta}_K^{-1} \boldsymbol{\alpha}_K & -\boldsymbol{\beta}_K^{-1} \boldsymbol{\gamma}_K \\ \mathbf{1} & \mathbf{0} & \mathbf{0} \\ \mathbf{0} & \mathbf{0} & \mathbf{1} \end{pmatrix} \begin{pmatrix} \mathbf{V}_K \\ \mathbf{V}_{K-1} \\ \mathbf{1} \end{pmatrix}. \quad (6.3)$$

Now define

$$\mathbf{X}_K \equiv \begin{pmatrix} \mathbf{V}_K \\ \mathbf{V}_{K-1} \\ \mathbf{1} \end{pmatrix} \quad (6.4)$$

and

$$\mathbf{B}_K \equiv \begin{pmatrix} \boldsymbol{\beta}_K^{-1} \mathbf{W}_K & -\boldsymbol{\beta}_K^{-1} \boldsymbol{\alpha}_K & -\boldsymbol{\beta}_K^{-1} \boldsymbol{\gamma}_K \\ \mathbf{1} & \mathbf{0} & \mathbf{0} \\ \mathbf{0} & \mathbf{0} & \mathbf{1} \end{pmatrix}, \quad (6.5)$$

we have

$$\mathbf{X}_{K+1} = \mathbf{B}_K \mathbf{X}_K \quad \text{for } 1 \leq K \leq K_{\max}. \quad (6.6)$$

So once  $\mathbf{X}_1$  is known, all other  $\mathbf{X}_K$  can be calculated by repeated application of Eq. (6.6):

$$\begin{aligned} \mathbf{X}_2 &= \mathbf{B}_1 \mathbf{X}_1 \\ \mathbf{X}_3 &= \mathbf{B}_2 \mathbf{X}_2 = \mathbf{B}_2 \mathbf{B}_1 \mathbf{X}_1 \\ &\dots \\ \mathbf{X}_{K_{\max}+1} &= \mathbf{B}_{K_{\max}} \mathbf{B}_{K_{\max}-1} \cdots \mathbf{B}_2 \mathbf{B}_1 \mathbf{X}_1. \end{aligned} \quad (6.7)$$

To simplify the notation, we can define the accumulative products of the **B** matrices as

$$\mathbf{C}_K = \mathbf{B}_K \mathbf{B}_{K-1} \cdots \mathbf{B}_2 \mathbf{B}_1 \mathbf{X}_1 \quad \text{for } 1 \leq K \leq K_{\max}, \quad (6.8)$$

then we have

$$\mathbf{X}_{K_{\max}+1} = \mathbf{C}_{K_{\max}} \mathbf{X}_1. \quad (6.9)$$

It can be easily shown that all the  $\mathbf{C}_K$  matrices have the following pattern:

$$\mathbf{C}_K = \begin{pmatrix} \mathbf{g}_{11}^K & \mathbf{g}_{12}^K & \mathbf{g}_{13}^K \\ \mathbf{g}_{21}^K & \mathbf{g}_{22}^K & \mathbf{g}_{23}^K \\ \mathbf{0} & \mathbf{0} & \mathbf{1} \end{pmatrix} \quad (6.10)$$

where the  $\mathbf{g}$  blocks can take zero or nonzero values. Therefore Eq. (6.9) becomes

$$\begin{pmatrix} \mathbf{V}_{K_{\max}+1} \\ \mathbf{V}_{K_{\max}} \\ \mathbf{1} \end{pmatrix} = \mathbf{C}_{K_{\max}} \begin{pmatrix} \mathbf{V}_1 \\ \mathbf{V}_0 \\ \mathbf{1} \end{pmatrix} = \begin{pmatrix} \mathbf{g}_{11} & \mathbf{g}_{12} & \mathbf{g}_{13} \\ \mathbf{g}_{21} & \mathbf{g}_{22} & \mathbf{g}_{23} \\ \mathbf{0} & \mathbf{0} & \mathbf{1} \end{pmatrix} \begin{pmatrix} \mathbf{V}_1 \\ \mathbf{V}_0 \\ \mathbf{1} \end{pmatrix}. \quad (6.11)$$

By definition,  $\mathbf{V}_{K_{\max}+1} = \mathbf{0}$  and  $\mathbf{V}_0 = \mathbf{0}$ , then from Eq. (6.11), we obtain

$$\mathbf{0} = \mathbf{g}_{11} \times \mathbf{V}_1 + \mathbf{g}_{13} \times \mathbf{1}, \quad (6.12)$$

from which  $\mathbf{V}_1$  can be solved. After that, all other  $\mathbf{V}_K$  can be calculated from Eq. (6.7).

The most time-consuming part of the above method is to calculate the accumulative products of the **B** matrices:  $\mathbf{C}_1, \mathbf{C}_2, \dots, \mathbf{C}_{K_{\max}}$ . If one can make this computation parallel, the above algorithm can be accelerated. It turns out that the computation of the series of  $\mathbf{C}_K$  matrices is very similar to the all-prefix-sums operation in parallel algorithms[212]. Given an array of objects

$$[a_1, a_2, \dots, a_n]$$

and a binary associative operator  $\oplus$ , the all-prefix-sums operation returns the ordered set

$$[a_1, (a_1 \oplus a_2), \dots, (a_1 \oplus a_2 \oplus \dots \oplus a_n)].$$

As one of the simplest and most useful building blocks in parallel algorithms[212], the all-prefix-sums operation is well studied and has been implemented in various ways[213]. However, many existing algorithms implicitly assume the computation cost of the binary operation  $\oplus$  between any two consecutive objects  $a_i$  and  $a_{i+1}$  are almost the same. This is not the case here because the dimension of the  $\mathbf{B}_K$  can vary a lot depending on the value of  $K$ . For example,  $\mathbf{B}_K$  has the largest size when  $K \approx K_{\max}/2$ . Therefore the existing algorithms might not be optimal for our case and we may need to implement an all-prefix-sums operation that is specially tailored for the current situation.

# Bibliography

- [1] K. Southwell. Ultracold matter. *Nature*, 416:205, 2002. → pages 1
- [2] S. Chu. Cold atoms and quantum control. *Nature*, 416:206, 2002. → pages 1
- [3] J. R. Anglin and W. Ketterle. Bose-Einstein condensation of atomic gases. *Nature*, 416:211, 2002. → pages 2
- [4] S. L. Rolston and W. D. Phillips. Nonlinear and quantum atom optics. *Nature*, 416:219, 2002. → pages 2
- [5] K. Burnett, P. S. Julienne, P. D. Lett, E. Tiesinga, and C. J. Williams. Quantum encounters of the cold kind. *Nature*, 416:225, 2002. → pages 2
- [6] Th. Udem, R. Holzwarth, and T. W. Hänsch. Optical frequency metrology. *Nature*, 416:233, 2002. → pages 2
- [7] C. Monroe. Quantum information processing with atoms and photons. *Nature*, 416:238, 2002. → pages 2
- [8] L. D Carr, D. DeMille, R. V. Krems, and J. Ye. Cold and ultracold molecules: science, technology and applications. *New J. Phys.*, 11:055049, 2009. → pages 2, 90, 123, 173
- [9] B. Friedrich and J. M. Doyle. Why are cold molecules so hot? *ChemPhysChem.*, 10:604, 2009. → pages 2, 90
- [10] M. Schnel and G. Meijer. Cold molecules: Preparation, applications, and challenges. *Angew. Chem. Int. Ed.*, 48:6010, 2009. → pages 2, 90
- [11] M. T. Bell and T. P. Softley. Ultracold molecules and ultracold chemistry. *Mol. Phys.*, 107:99, 2009. → pages 2, 90

- [12] R. Krems, W. C. Stwalley, and B. Friedrich, editors. *Cold molecules: theory, experiment, applications*. CRC press, 2009. → pages 2, 90
- [13] K. K. Ni, S. Ospelkaus, D. J. Nesbitt, J. Ye, and D. S. Jin. A dipolar gas of ultracold molecules. *Phys. Chem. Chem. Phys.*, 11:9626, 2009. → pages 2, 90
- [14] D. S. Jin and J. Ye. Polar molecules in the quantum regime. *Phys. Today*, 5:27, 2011. → pages 2, 90
- [15] D. S. Jin and J. Ye. Introduction to ultracold molecules: New frontiers in quantum and chemical physics. *Chem. Rev.*, 112:4801, 2012. → pages 2, 90
- [16] G. Quéméner and P. S. Julienne. Ultracold molecules under control! *Chem. Rev.*, 112:4949, 2012. → pages 2, 90, 173
- [17] M. A. Baranov, M. Dalmonte, G. Pupillo, and P. Zoller. Condensed matter theory of dipolar quantum gases. *Chem. Rev.*, 112:5012, 2012. → pages 2, 3, 5, 7, 90, 173
- [18] W. Ketterle. Nobel lecture: When atoms behave as waves: Bose-Einstein condensation and the atom laser. *Rev. Mod. Phys.*, 74:1131, 2002. → pages 2
- [19] P. Lev and S. Sandro. The quest for superfluidity in fermi gases. *Science*, 298:2144, 2002. → pages 2
- [20] G. Stefan, P. Lev, and S. Sandro. Theory of ultracold atomic fermi gases. *Rev. Mod. Phys.*, 80:1215, 2008. → pages 2
- [21] E. P. Wigner. On the behavior of cross sections near thresholds. *Phys. Rev.*, 73:1002, 1948. → pages 3
- [22] R. V. Krems. Molecules near absolute zero and external field control of atomic and molecular dynamics. *Int. Rev. Phys. Chem.*, 24:99, 2005. → pages 3
- [23] N. Balakrishnan and A. Dalgarno. Chemistry at ultracold temperatures. *Chem. Phys. Lett.*, 341:652, 2001. → pages 3
- [24] E. Bodo, F. A. Gianturco, and A. Dalgarno. F+D<sub>2</sub> reaction at ultracold temperatures. *J. Chem. Phys.*, 116:9222, 2002. → pages 3

- [25] E. Bodo, F. A. Gianturco, N Balakrishnan, and A. Dalgarno. Chemical reaction in the limit of zero kinetic energy: virtual states and ramsauer minima in  $F + H_2 \rightarrow HF + H$ . *J. Phys. B*, 37:3641, 2004. → pages 3
- [26] P. F. Weck and N. Balakrishnan. Chemical reactivity of ultracold polar molecules: investigation of  $H + HCl$  and  $H + DCl$  collisions. *Eur. Phys. J. D*, 31:417, 2004. → pages 3
- [27] S. Ospelkaus, K.-K. Ni, D. Wang, M. H. G. de Miranda, B. Neyenhuis, G. Quéméner, P. S. Julienne, J. L. Bohn, D. S. Jin, and J. Ye. Quantum-state controlled chemical reactions of ultracold potassium-rubidium molecules. *Science*, 327:853, 2010. → pages 3, 4
- [28] H. J. Metcalf and P. van der Straten. *Laser cooling and trapping*. Springer-Verlag, New York, 1999. → pages 3
- [29] H. L. Bethlem, G. Berden, F. M. H. Crompvoets, R. T. Jongma, A. J. A. van Roij, and G. Meijer. Electrostatic trapping of ammonia molecules. *Nature*, 406:491, 2000. → pages 3
- [30] J. van Veldhoven, H. L. Bethlem, and G. Meijer. ac electric trap for ground-state molecules. *Phys. Rev. Lett.*, 94:083001, 2005. → pages 3
- [31] R. Grimm, M. Weidemüller, and Y. B. Ovchinnikov. Optical dipole traps for neutral atoms. *Advances in atomic, molecular, and optical physics*, 42:95, 2000. → pages 3, 113
- [32] D. DeMille, D. R. Glenn, and J. Petricka. Microwave traps for cold polar molecules. *Eur. Phys. J. D*, 31:375, 2004. → pages 3
- [33] S. D. Hogan, A. W. Wiederkehr, H. Schmutz, and F. Merkt. Magnetic trapping of hydrogen after multistage zeeman deceleration. *Phys. Rev. Lett.*, 101:143001, 2008. → pages 3
- [34] N. Vanhaecke, W. de Souza Melo, B. Laburthe Tolra, D. Comparat, and P. Pillet. Accumulation of cold cesium molecules via photoassociation in a mixed atomic and molecular trap. *Phys. Rev. Lett.*, 89:063001, 2002. → pages 3
- [35] D. Wang, J. Qi, M. F. Stone, O. Nikolayeva, B. Hattaway, S. D. Gensemer, H. Wang, W. T. Zemke, P. L. Gould, E. E. Eyler, and W. C. Stwalley. The photoassociative spectroscopy, photoassociative molecule formation, and trapping of ultracold  $^{39}K$   $^{85}Rb$ . *Eur. Phys. J. D*, 31:165, 2004. → pages 3

- [36] S. Y. T. van de Meerakker, N. Vanhaecke, M. P. J. van der Loo, G. C. Groenenboom, and G. Meijer. Direct measurement of the radiative lifetime of vibrationally excited OH radicals. *Phys. Rev. Lett.*, 95:013003, 2005. → pages 3
- [37] J. J. Gilijamse, S. Hoekstra, S. A. Meek, M. Metsl, S. Y. T. van de Meerakker, G. Meijer, and G. C. Groenenboom. The radiative lifetime of metastable CO ( $a^3\pi, v = 0$ ). *J. Chem. Phys.*, 127:221102, 2007. → pages 3
- [38] W. C. Campbell, G. C. Groenenboom, H.-I. Lu, E. Tsikata, and J. M. Doyle. Time-domain measurement of spontaneous vibrational decay of magnetically trapped nh. *Phys. Rev. Lett.*, 100:083003, 2008. → pages 3
- [39] G. K. Brennen, C. M. Caves, P. S. Jessen, and I. H. Deutsch. Quantum logic gates in optical lattices. *Phys. Rev. Lett.*, 82:1060, 1999. → pages 3
- [40] D. Jaksch, H. J. Briegel, J. I. Cirac, C. W. Gardiner, and P. Zoller. Entanglement of atoms via cold controlled collisions. *Phys. Rev. Lett.*, 82:1975, 1999. → pages 3
- [41] J. K. Pachos and P. L. Knight. Quantum computation with a one-dimensional optical lattice. *Phys. Rev. Lett.*, 91:107902, 2003. → pages 3
- [42] A. Kay and J. K. Pachos. Quantum computation in optical lattices via global laser addressing. *New J. Phys.*, 6:126, 2004. → pages 3
- [43] A. Micheli, G. K. Brennen, and P. Zoller. A toolbox for lattice-spin models with polar molecules. *Nature Phys.*, 2:341, 2006. → pages 3, 57, 91, 173
- [44] H. P. Büchler, E. Demler, M. Lukin, A. Micheli, N. Prokof'ev, G. Pupillo, and P. Zoller. Strongly correlated 2d quantum phases with cold polar molecules: Controlling the shape of the interaction potential. *Phys. Rev. Lett.*, 98:060404, 2007. → pages 3, 5
- [45] I. Bloch. Quantum coherence and entanglement with ultracold atoms in optical lattices. *Nature*, 453:1016, 2008. → pages 3
- [46] M. Lemeshko, R. V. Krems, J. M. Doyle, and S. Kais. Manipulation of molecules with electromagnetic fields. *Mol. Phys.*, 111:1648, 2013. → pages 4
- [47] K.-K. Ni, S. Ospelkaus, M. H. G. de Miranda, Pe'er A., B. Neyenhuis, J. J. Zirbel, S. Kotchigova, P. S. Julienne, D. S. Jin, and J. Ye. A high

phase-space-density gas of polar molecules. *Science*, 322:231, 2008. → pages 4

- [48] J. G. Danzl, M. J. Mark, E. Haller, R. Gustavsson, M. Hart, J. Aldegunde, J. M. Hutson, and H.-C. Nägerl. An ultracold high-density sample of rovibronic ground-state molecules in an optical lattice. *Nature Phys.*, 6:265, 2010. → pages 4
- [49] P. Pellegrini and M. Desouter-Lecomte. Quantum gates driven by microwave pulses in hyperfine levels of ultracold heteronuclear dimers. *Eur. Phys. J. D*, 64:163, 2011. → pages 4
- [50] M. L. Wall and L. D. Carr. Hyperfine molecular hubbard hamiltonian. *Phys. Rev. A*, 82:013611, 2010. → pages 4, 57, 91, 173
- [51] A. Micheli, G. Pupillo, H. P. Büchler, and P. Zoller. Cold polar molecules in two-dimensional traps: Tailoring interactions with external fields for novel quantum phases. *Phys. Rev. A*, 76:043604, 2007. → pages 5, 173
- [52] M. A. Baranov. Theoretical progress in many-body physics with ultracold dipolar gases. *Phys. Rep.*, 464:71, 2008. → pages 5
- [53] T. Lahaye, C. Menotti, L. Santos, M. Lewenstein, and T. Pfau. The physics of dipolar bosonic quantum gases. *Rep. Prog. Phys.*, 72:126401, 2009. → pages 5
- [54] C. Trefzger, C. Menotti, B. Capogrosso-Sansone, and M. Lewenstein. Ultracold dipolar gases in optical lattices. *J. Phys. B: At. Mol. Opt. Phys.*, 44:193001, 2011. → pages 5
- [55] P. S. Jessen and I. H. Deutsch. Optical lattices. *Adv. At. Mol. Opt.*, 37:95, 1996. → pages 5
- [56] W. D. Phillips. Laser cooling and trapping of neutral atoms. *Rev. Mod. Phys.*, 70:721, 1998. → pages 5
- [57] J. F. Sherson, C. Weitenberg, M. Endres, M. Cheneau, I. Bloch, and S. Kuhr. Single-atom-resolved fluorescence imaging of an atomic mott insulator. *Nature*, 467:68, 2010. → pages 7, 113, 115, 137, 173
- [58] W. S. Bakr, A. Peng, M. E. Tai, R. Ma, J. Simon, J. I. Gillen, S. Foelling, L. Pollet, and M. Greiner. Probing the superfluid–to–mott insulator transition at the single-atom level. *Science*, 329:547, 2010. → pages 7, 113, 115, 137, 173

- [59] D. DeMille. Quantum computation with trapped polar molecules. *Phys. Rev. Lett.*, 88:067901, 2002. → pages 7, 57, 89, 94, 145
- [60] S. F. Yelin, K. Kirby, and R. Côté. Schemes for robust quantum computation with polar molecules. *Phys. Rev. A*, 74:050301, Nov 2006. → pages 7
- [61] M. Ortner, Y.L. Zhou, P. Rabl, and P. Zoller. Quantum information processing in self-assembled crystals of cold polar molecules. *Quant. Inf. Proc.*, 10:793, 2011. → pages 7
- [62] M. Greiner, O. Mandel, T. Esslinger, T. W. Hänsch, and I. Bloch. Quantum phase transition from a superfluid to a mott insulator in a gas of ultracold atoms. *Nature*, 415:39, 2002. → pages 7, 91
- [63] I. B. Spielman, W. D. Phillips, and J. V. Porto. Mott-insulator transition in a two-dimensional atomic bose gas. *Phys. Rev. Lett.*, 98:080404, Feb 2007. → pages 7
- [64] E. Haller, R. Hart, M. J. Mark, J. G. Danzl, M. Reichsöllner, L.; Gustavsson, M. Dalmonte, G. Pupillo, and H.-C. Nägerl. Pinning quantum phase transition for a luttinger liquid of strongly interacting bosons. *Nature*, 466:597, 2010. → pages 7
- [65] R. Jördens, N. Strohmaier, K. Guenter, H. Moritz, and T. Esslinger. A mott insulator of fermionic atoms in an optical lattice. *Nature*, 455:204, 2008. → pages 7
- [66] U. Schneider, L. Hackermüller, S. Will, Th. Best, and I. Bloch. Metallic and insulating phases of repulsively interacting fermions in a 3d optical lattice. *Science*, 322:1520, 2008. → pages 7, 91
- [67] F. Herrera, M. Litinskaya, and R. V. Krems. Tunable disorder in a crystal of cold polar molecules. *Phys. Rev. A*, 82:033428, 2010. → pages 8, 57, 58, 59, 76, 101, 116, 122, 126, 146, 147, 193
- [68] J. Pérez-Ríos, F. Herrera, and R. V. Krems. External field control of collective spin excitations in an optical lattice of  $2\sigma$  molecules. *New J. Phys.*, 12:103007, 2010. → pages 8, 137
- [69] F. Herrera and R. V. Krems. Tunable holstein model with cold polar molecules. *Phys. Rev. A*, 84:051401, 2011. → pages 8, 89, 176

- [70] F. Herrera, K. W. Madison, R. V. Krems, and M. Berciu. Investigating polaron transitions with polar molecules. *Phys. Rev. Lett.*, 110:223002, 2013. → pages 8, 146, 147, 176
- [71] I. M. Vellekoop and A. P. Mosk. Focusing coherent light through opaque strongly scattering media. *Opt. Lett.*, 32:2309, 2007. → pages 9, 139, 142
- [72] S. M. Popoff, G. Lerosey, R. Carminati, M. Fink, A. C. Boccara, and S. Gigan. Measuring the transmission matrix in optics: an approach to the study and control of light propagation in disordered media. *Phys. Rev. Lett.*, 104:100601, 2010. → pages 9, 139, 142
- [73] I. M. Vellekoop, A. Lagendijk, and A. P. Mosk. Exploiting disorder for perfect focusing. *Nature Photon.*, 4:320, 2010. → pages 9, 139, 142
- [74] T. Cizmar, M. Mazilu, and K. Dholakia. In situ wavefront correction and its application to micromanipulation. *Nature Photon.*, 4:388, 2010. → pages 9, 139, 142
- [75] O. Katz, E. Small, Y. Bromberg, and Y. Silberberg. Focusing and compression of ultrashort pulses through scattering media. *Nature photon.*, 5:372, 2011. → pages 9, 139, 142
- [76] D. J. McCabe, A. Tajalli, D. R. Austin, P. Bondareff, I. A. Walmsley, S. Gigan, and B. Chatel. Spatio-temporal focusing of an ultrafast pulse through a multiply scattering medium. *Nat. Commun.*, 2:447, 2011. → pages 9, 139, 142
- [77] J. Aulbach, B. Gjonaj, P. M. Johnson, A. P. Mosk, and A. Lagendijk. Control of light transmission through opaque scattering media in space and time. *Phys. Rev. Lett.*, 106:103901, 2011. → pages 9, 139, 142
- [78] E. A. Shapiro, T. M. Drane, and V. Milner. Prospects of coherent control in turbid media: Bounds on focusing broadband laser pulses. *Phys. Rev. A*, 84:053807, 2011. → pages 9, 139, 142
- [79] M. Cui. A high speed wavefront determination method based on spatial frequency modulations for focusing light through random scattering media. *Opt. Express*, 19:2989, 2011. → pages 9, 139, 142
- [80] M. Kim, Y. Choi, C. Yoon, W. Choi, J. Kim, Q-Han Park, and W. Choi. Maximal energy transport through disordered media with the implementation of transmission eigenchannels. *Nature photon.*, 6:583, 2012. → pages 9, 139, 142

- [81] M. Berciu and A. M. Cook. Efficient computation of lattice green's functions for models with nearest-neighbor hopping. *Europhys. Lett.*, 92:40003, 2010. → pages 9, 148, 155, 167
- [82] M. Berciu. Few-particle green's functions for strongly correlated system on infinite lattices. *Phys. Rev. Lett.*, 107:246403, 2011. → pages 9, 148
- [83] M. Möller, A. Mukherjee, C. P. J. Adolphs, D. J. J. Marchand, and M. Berciu. Efficient computation of lattice green functions for models with longer range hopping. *J. Phys. A: Math. Theor.*, 45:115206, 2012. → pages 9, 148
- [84] A. R. Edmonds. *Angular Momentum in Quantum Mechanics*. Princeton University Press, Princeton, 1960. → pages 11
- [85] M. E. Rose. *Elementary Theory of Angular Momentum*. John Wiley and Sons, Inc., New York, 1957. → pages 11
- [86] D. M. Brink and G. R. Satchler. *Angular Momentum*. Oxford University Press, Oxford, 1962. → pages 11
- [87] R. N. Zare. *Angular Momentum*. John Wiley and Sons, Inc., New York, 1988. → pages 11, 19, 20, 21, 22, 23, 24, 29, 31, 39, 48
- [88] B. L. Silver. *Irreducible Tensor Methods: An Introduction for Chemists*. Academic Press, New York, 1976. → pages 11
- [89] V. D. Kleinman, H. Park, R. J. Gordon, and R. N. Zare. *Companion to Angular Momentum*. Wiley Interscience, New York, 1988. → pages 11
- [90] D. A. Varshalovich, A. N. Moskalev, and V. K. Khersonskii. *Quantum Theory of Angular Momentum*. World Scientific Publications, Singapore, 1988. → pages 11
- [91] J. J. Sakurai and S. F. Tuan. *Modern quantum mechanics (Revised Edition)*. Addison Wesley, 1993. → pages 11, 168
- [92] J. M. Brown and A. Carrington. *Rotational spectroscopy of diatomic molecules*. Cambridge University Press, 2003. → pages 11, 21, 33, 59
- [93] B. Friedrich and D. Herschbach. Polarization of molecules induced by intense nonresonant laser fields. *J. Phys. Chem.*, 99:15686, 1995. → pages 36, 116

- [94] Nathan Carter. *Mathematica*. Champaign, Illinois, version 7.0 edition, 2008. → pages 50
- [95] J. Frenkel. On the transformation of light into heat in solids. i. *Phys. Rev.*, 37:17, Jan 1931. → pages 51
- [96] J. Frenkel. On the transformation of light into heat in solids. ii. *Phys. Rev.*, 37:1276, May 1931. → pages 51
- [97] J. R. Kuklinski and S. Mukamel. Optical properties of wannier excitons in the linear and weakly nonlinear regime. *Phys. Rev. B*, 42:2959, 1990. → pages 57
- [98] C. Schindler and R. Zimmermann. Analysis of the exciton-exciton interaction in semiconductor quantum wells. *Phys. Rev. B*, 78:045313, 2008. → pages 57
- [99] V. Agranovich. *Excitations in organic solids*. Oxford University Press, 2009. → pages 57, 58, 59, 93, 101, 115, 178
- [100] P. L. Gourley and J. P. Wolfe. Experimental determination of equilibrium constants for excitonic systems in stressed, ultrapure silicon. *Phys. Rev. B*, 25:6338, 1982. → pages 57
- [101] M. L. W. Thewalt and W. G. McMullan. Green and near-infrared luminescence due to the biexcitons in unperturbed silicon. *Phys. Rev. B*, 30:6232, 1984. → pages 57
- [102] J. C. Kim, D. R. Wake, and J. P. Wolfe. Thermodynamics of biexcitons in a gaas quantum well. *Phys. Rev. B*, 50:15099, 1994. → pages 57
- [103] R. C. Miller, D. A. Kleinman, A. C. Gossard, and O. Munteanu. Biexcitons in gaas quantum wells. *Phys. Rev. B*, 25:6545, 1982. → pages 57
- [104] R. Cingolani, Y. Chen, and K. Ploog. Biexciton formation in gaas/alxga1-xas multiple quantum wells: An optical investigation. *Phys. Rev. B*, 38:13478, 1988. → pages 57
- [105] R. M. Stevenson, R. J. Young, P. Atkinson, K. Cooper, D. A. Ritchie, and A. J. Shields. A semiconductor source of triggered entangled photon pairs. *Nature*, 439:179, 2006. → pages 57
- [106] Svátošlav Anatol'evič Moskalenko and David W Snoke. *Bose-Einstein condensation of excitons and biexcitons: and coherent nonlinear optics with excitons*. Cambridge University Press, 2000. → pages 57

- [107] G. Vektaris. A new approach to the molecular biexciton theory. *J. Chem. Phys.*, 101:3031, 1994. → pages 57, 76
- [108] H. Ezaki, T. Tokihiro, and E. Hanamura. Excitonic n-string in linear chains: Electronic structure and optical properties. *Phys. Rev. B*, 50:10506, 1994. → pages 57, 79, 177
- [109] F. C. Spano, V. Agranovich, and S. Mukamel. Biexciton states and two-photon absorption in molecular monolayers. *J. Chem. Phys.*, 95:1400, 1991. → pages 57
- [110] V. M. Agranovich and M. D. Galanin. Electron-excitation energy transfer in condensed media. *Moscow Izdatel Nauka*, 1, 1978. → pages 57, 76, 79
- [111] Y. Baba, G. Dujardin, P. Feulner, and D. Menzel. Formation and dynamics of exciton pairs in solid argon probed by electron-stimulated ion desorption. *Phys. Rev. Lett.*, 66:3269, 1991. → pages 57
- [112] P. Wiethoff, B. Kassühlke, D. Menzel, and P. Feulner. Biexcitons in solid neon. *Low Temperature Physics*, 29:266, 2003. → pages 57
- [113] T. Volz, N. Syassen, D. M. Bauer, E. Hansis, S. Dürr, and G. Rempe. Preparation of a quantum state with one molecule at each site of an optical lattice. *Nature Phys.*, 2:692, 2006. → pages 57, 58
- [114] J. G. Danzl, M. J. Mark, E. Haller, M. Gustavsson, R. Hart, J. Aldegunde, J. M. Hutson, and H.-C. Nägerl. An ultracold high-density sample of rovibronic ground-state molecules in an optical lattice. *Nature Phys.*, 6:265, 2010. → pages 57, 58
- [115] A. Chotia, B. Neyenhuis, S. A. Moses, B. Yan, J. P. Covey, M. Foss-Feig, A. M. Rey, D. S Jin, and J. Ye. Long-lived dipolar molecules and feshbach molecules in a 3d optical lattice. *Phys. Rev. Lett.*, 108:080405, 2012. → pages 57, 58
- [116] G. D. Scholes and G. Rumbles. Excitons in nanoscale systems. *Nature mater.*, 5:683, 2006. → pages 57
- [117] R. M. Rajapakse, T. Bragdon, A. M. Rey, T. Calarco, and S. F. Yelin. Single-photon nonlinearities using arrays of cold polar molecules. *Phys. Rev. A*, 80:013810, 2009. → pages 57
- [118] P. Rabl, D. DeMille, J. M. Doyle, M. D. Lukin, R. J. Schoelkopf, and P. Zoller. Hybrid quantum processors: molecular ensembles as quantum

memory for solid state circuits. *Phys. Rev. Lett.*, 97:033003, 2006. → pages 57, 91, 146, 178

- [119] P. Rabl and P. Zoller. Molecular dipolar crystals as high-fidelity quantum memory for hybrid quantum computing. *Phys. Rev. A*, 76:042308, 2007. → pages 57, 91, 146, 178
- [120] R. Barnett, D. Petrov, M. Lukin, and E. Demler. Quantum magnetism with multicomponent dipolar molecules in an optical lattice. *Phys. Rev. Lett.*, 96:190401, 2006. → pages 57, 91, 173
- [121] G. K. Brennen, A. Micheli, and P. Zoller. Designing spin-1 lattice models using polar molecules. *New J. Phys.*, 9:138, 2007. → pages 57, 91, 173
- [122] H. P. Büchler, A. Micheli, and P. Zoller. Three-body interactions with cold polar molecules. *Nature Phys.*, 3:726, 2007. → pages 57, 91, 173
- [123] M. L. Wall and L. D. Carr. Emergent timescales in entangled quantum dynamics of ultracold molecules in optical lattices. *New J. Phys.*, 11:055027, 2009. → pages 57, 91, 173
- [124] C. Trefzger, M. Alloing, C. Menotti, F. Dubin, and M. Lewenstein. Quantum magnetism and counterflow supersolidity of up–down bosonic dipoles. *New J. Phys.*, 12:093008, 2010. → pages 57, 91, 173
- [125] J. P. Kestner, B. Wang, J. D Sau, and S. Das Sarma. Prediction of a gapless topological haldane liquid phase in a one-dimensional cold polar molecular lattice. *Phys. Rev. B*, 83:174409, 2011. → pages 57, 91, 173
- [126] A. V. Gorshkov, S. R. Manmana, G. Chen, J. Ye, E. Demler, M. D. Lukin, and A. M. Rey. Tunable superfluidity and quantum magnetism with ultracold polar molecules. *Phys. Rev. Lett.*, 107:115301, 2011. → pages 57, 91, 173
- [127] A. V. Gorshkov, S. R. Manmana, G. Chen, E. Demler, M. D. Lukin, and A. M. Rey. Quantum magnetism with polar alkali-metal dimers. *Phys. Rev. A*, 84:033619, 2011. → pages 57, 91, 173, 174
- [128] At zero electric field, there are three degenerate states corresponding to  $N = 1$  and  $M_N = 0, \pm 1$ . In the presence of an electric field relevant for this study, the degeneracy is lifted. As shown in Ref. [67], the  $|N = 0\rangle \rightarrow |N = 1, M_N = 0\rangle$  transition is uncoupled from the  $|N = 0\rangle \rightarrow |N = 1, M_N = \pm 1\rangle$  transitions. The  $M_N = \pm 1$  states can, therefore, be ignored. → pages 58

- [129] E. N. Economou. *Green's Functions in Quantum Physics*. Springer, third edition, 2006. → pages 71, 148, 155
- [130] This analysis assumes that both  $D$  and  $J$  are isotropic. For molecules on an optical lattice, the magnitude and sign of  $D$  and  $J$  depend on the angle between the direction of the electric field and the molecular array. This may modify the properties of biexcitons in 2D and 3D systems. → pages 76
- [131] E. Anderson, Z. Bai, C. Bischof, S. Blackford, J. Demmel, J. Dongarra, J. Du Croz, A. Greenbaum, S. Hammarling, A. McKenney, and D. Sorensen. *LAPACK Users' Guide*. Society for Industrial and Applied Mathematics, Philadelphia, PA, third edition, 1999. → pages 82
- [132] A. A. Ovchinnikov. Complexes of several spins in a linear heisenberg chain. *JETP Lett.*, 5:38, 1967. → pages 89
- [133] H. van Amerongen, R. van Grondelle, and L. Valkūnas. *Photosynthetic excitons*. World Scientific, 2000. → pages 89
- [134] R. E. Blankenship. *Molecular mechanisms of photosynthesis*. Wiley, 2008. → pages 89
- [135] A. Ishizaki and G. R. Fleming. Theoretical examination of quantum coherence in a photosynthetic system at physiological temperature. *Proc. Natl. Acad. Sci.*, 106:17255, 2009. → pages 89
- [136] M. Köhl, H. Moritz, T. Stöferle, K. Günter, and T. Esslinger. Fermionic atoms in a three dimensional optical lattice: Observing fermi surfaces, dynamics, and interactions. *Phys. Rev. Lett.*, 94:080403, 2005. → pages 91
- [137] D. McKay, M. White, M. Pasienski, and B. DeMarco. Phase-slip-induced dissipation in an atomic bose–hubbard system. *Nature*, 453:76, 2008. → pages 91
- [138] R. Jördens, N. Strohmaier, K. Günter, H. Moritz, and T. Esslinger. A mott insulator of fermionic atoms in an optical lattice. *Nature*, 455:204, 2008. → pages 91
- [139] P. Xiang, M. Litinskaya, and R. V. Krems. Tunable exciton interactions in optical lattices with polar molecules. *Phys. Rev. A*, 85:061401, 2012. → pages 91, 101, 126, 146
- [140] M. Lemeshko, R. V. Krems, and H. Weimer. Nonadiabatic preparation of spin crystals with ultracold polar molecules. *Phys. Rev. Lett.*, 109:035301, 2012. → pages 91

- [141] D. P. DiVincenzo. The physical implementation of quantum computation. *Fortschr. Phys.*, 48:771, 2000. → pages 91
- [142] A. Aspect and M. Inguscio. Anderson localization of ultracold atoms. *Phys. today*, 62:30, 2009. → pages 91
- [143] B. A. Gregg. Excitonic solar cells. *J. Phys. Chem. B*, 107:4688, 2003. → pages 91
- [144] T. Seideman and E. Hamilton. Nonadiabatic alignment by intense pulses. concepts, theory, and directions. *Adv. At. Mol. Opt. Phys.*, 52:289, 2005. → pages 92, 98, 174
- [145] I. V. Litvinyuk, K. F. Lee, P. W. Dooley, D. M. Rayner, D. M. Villeneuve, and P. B. Corkum. Alignment-dependent strong field ionization of molecules. *Phys. Rev. Lett.*, 90:233003, 2003. → pages 92
- [146] S. M. Purcell and P. F. Barker. Tailoring the optical dipole force for molecules by field-induced alignment. *Phys. Rev. Lett.*, 103:153001, 2009. → pages 92
- [147] E. Gershnabel, M. Shapiro, and I. Sh. Averbukh. Stern-gerlach deflection of field-free aligned paramagnetic molecules. *J. Chem. Phys.*, 135:194310, 2011. → pages 92
- [148] U. Steinitz, Y. Prior, and I. Sh. Averbukh. Laser induced gas vortices. *Phys. Rev. Lett.*, 109:033001, 2012. → pages 92
- [149] Y. Khodorkovsky, J. R. Manson, and I. Sh. Averbukh. Modifying molecule-surface scattering by ultrashort laser pulses. *Phys. Rev. A*, 84:053420, 2011. → pages 92
- [150] J. H. Denschlag, J. E. Simsarian, H. Häffner, C. McKenzie, A. Browaeys, D. Cho, K. Helmerson, S. L. Rolston, and W. D. Phillips. A bose-einstein condensate in an optical lattice. *J. Phys. B: At. Mol. Opt. Phys.*, 35:3095, 2002. → pages 92
- [151] H. Zoubi and H. Ritsch. Excitons and cavity polaritons for ultracold atoms in an optical lattice. *Phys. Rev. A*, 76:013817, 2007. → pages 92, 115
- [152] H. Zoubi and H. Ritsch. Lifetime and emission characteristics of collective electronic excitations in two-dimensional optical lattices. *Phys. Rev. A*, 83:063831, 2011. → pages 92, 113, 115

- [153] H Zoubi and H Ritsch. Metastability and directional emission characteristics of excitons in 1d optical lattices. *Europhys. Lett.*, 90:23001, 2010. → pages 92, 113, 115
- [154] M. H. S. Amin. Consistency of the adiabatic theorem. *Phys. Rev. Lett.*, 102:220401, 2009. → pages 97
- [155] M. Raizen, C. Salomon, and Q. Niu. New light on quantum transport. *Phys. today*, 50:30, 1997. → pages 98
- [156] M. Litinskaya and R. V. Krems. Rotational excitations of polar molecules on an optical lattice: from novel exciton physics to quantum simulation of new lattice models. In K. W. Madison, Y. Wang, A. M. Rey, and K. Bongs, editors, *Annual Review of Cold Atoms and Molecules*, volume 1, page 53. World Scientific Publishing Company, Singapore, 2012. → pages 101
- [157] V. M. Agranovich, O. A. Dubovsky, D. M. Basko, G. C. La Rocca, and F. Bassani. Kinematic frenkel biexcitons. *J. Lumin.*, 85:221, 2000. → pages 101
- [158] A. Cuyt, V. Petersen, B. Verdonk, H. Waadeland, and W. B. Jones. *Handbook of continued fractions for special functions*. Springer, 2008. → pages 102
- [159] M. V. Fedorov. *Atomic and free electrons in a strong light field*. World Scientific, Singapore, 1997. → pages 104, 115
- [160] J. W. Goodman. *Introduction to Fourier optics*. McGraw-Hill, New York, 1996. → pages 104
- [161] W. S. Bakr, P. M. Preiss, M. E. Tai, R. Ma, J. Simon, and M. Greiner. Orbital excitation blockade and algorithmic cooling in quantum gases. *Nature*, 480:500, 2011. → pages 113, 115, 137
- [162] A. Chotia, B. Neyenhuis, S. A. Moses, B. Yan, J. P. Covey, M. Foss-Feig, A. M. Rey, D. S. Jin, and J. Ye. Long-lived dipolar molecules and feshbach molecules in a 3d optical lattice. *Phys. Rev. Lett.*, 108:080405, 2012. → pages 113, 137
- [163] V. M. Agranovich and O. A. Dubovskii. Effect of retarded interaction on the exciton spectrum in one-dimensional and two-dimensional crystals. *JETP Lett.*, 3:223, 1966. → pages 115

- [164] H. Zoubi and H. Ritsch. Excitons and cavity polaritons for optical lattice ultracold atoms. *Adv. At. Mol. Opt. Phys.*, 62:171, 2013. → pages 115
- [165] P. N. Brown, G. D. Byrne, and A. C. Hindmarsh. Vode, a variable-coefficient ode solver. *SIAM J. Sci. Stat. Comput.*, 10:1038, 1989. → pages 134
- [166] A. C. Hindmarsh. Odepack, a systematized collection of ode solvers. In R. S. Stepleman et al., editors, *IMACS Transactions on Scientific Computation*, volume 1, pages 55–64. North-Holland, Amsterdam, 1983. → pages 134
- [167] J. W. Goodman. *Statistical optics*. John Wiley and Sons, New York, 2000. → pages 139
- [168] Z. Amitay, R. Kosloff, and S. R. Leone. Experimental coherent computation of a multiple-input and gate using pure molecular superpositions. *Chem. Phys. Lett.*, 359:8, 2002. → pages 146
- [169] I. R. Sola, V. S. Malinovsky, and J. Santamaría. Implementing quantum gates on oriented optical isomers. *J. Chem. Phys.*, 120:10955, 2004. → pages 146
- [170] E. A. Shapiro, M. Spanner, and M. Y. Ivanov. Quantum logic in coarse grained control of wavepackets. *J. Mod. Opt.*, 52:897, 2005. → pages 146
- [171] U. Troppmann and R. de Vivie-Riedle. Mechanisms of local and global molecular quantum gates and their implementation prospects. *J. Chem. Phys.*, 122:154105, 2005. → pages 146
- [172] E. Charron and M. Raoult. Phase information revealed by interferences in the ionization of rotational wave packets. *Phys. Rev. A*, 74:033407, 2006. → pages 146
- [173] Y. Gu and D. Babikov. On the role of vibrational anharmonicities in a two-qubit system. *J. Chem. Phys.*, 131:034306, 2009. → pages 146
- [174] A. I. Lvovsky, B. C. Sanders, and W. Tittel. Optical quantum memory. *Nature Photon.*, 3:706, 2009. → pages 146
- [175] A. J. Daley, S. R. Clark, D. Jaksch, and P. Zoller. Numerical analysis of coherent many-body currents in a single atom transistor. *Phys. Rev. A*, 72:043618, 2005. → pages 146

- [176] R. V. Krems. Cold controlled chemistry. *PCCP*, 10:4079, 2008. → pages 146
- [177] A. O. G. Wallis and R. V. Krems. Rotational predissociation of extremely weakly bound atom-molecule complexes produced by feshbach resonance association. *J. Chem. Phys.*, 135:124313, 2011. → pages 146
- [178] Z. Zimboras, M. Faccin, Z. Kadar, J. Whitfield, B. Lanyon, and J. Biamonte. Quantum transport enhancement by time-reversal symmetry breaking. *Scientific Reports*, 3:2361, 2013. → pages 147
- [179] G. F. Koster and J. C. Slater. Simplified impurity calculation. *Phys. Rev.*, 96:1208, 1954. → pages 148
- [180] B. M. McCoy and T. T. Wu. Two-dimensional ising field theory for  $t < t_c$ : Green's-functions strings in  $n$ -point functions. *Phys. Rev. D*, 18:1253, 1978. → pages 148
- [181] N. W. Dalton and D. W. Wood. Critical behaviour of the simple anisotropic heisenberg model. *Proc. Phys. Soc. London*, 90:459, 1967. → pages 148
- [182] Melvin Lax. Multiple scattering of waves. II. the effective field in dense systems. *Phys. Rev.*, 85:621, 1952. → pages 148
- [183] E. W. Montroll and G. H. Weiss. Random walks on lattices. II. *J. Math. Phys.*, 6:167, 1965. → pages 148
- [184] J. Cserti. Application of the lattice greens function for calculating the resistance of infinite networks of resistors. *Am. J. Phys.*, 68:896, 2000. → pages 148
- [185] J. Cserti. Perturbation of infinite networks of resistors. *Am. J. Phys.*, 70:153, 2002. → pages 148
- [186] J. H. Asad, R. S. Hijjawi, A. Sakaji, and J. M. Khalifeh. Resistance calculation for an infinite simple cubic lattice application of green's function. *Int. J. Theor. Phys.*, 43:2223, 2004. → pages 148
- [187] J. H. Asad, R. S. Hijjawi, A. Sakaji, and J. M. Khalifeh. Remarks on perturbation of infinite networks of identical resistors. *Int. J. Theor. Phys.*, 44:471, 2005. → pages 148
- [188] V. L. Bulatov and P. E. Kornilovitch. Anomalous tunneling of bound pairs in crystal lattices. *Europhys. Lett.*, 71:352, 2005. → pages 148

- [189] R. Haydock, V. Heine, and M. J. Kelly. Electronic structure based on the local atomic environment for tight-binding bands. *J. Phys. C: Solid State Phys.*, 5:2845, 1972. → pages 163
- [190] R. Haydock, V. Heine, and M. J. Kelly. Electronic structure based on the local atomic environment for tight-binding bands: II. *J. Phys. C: Solid State Phys.*, 8:2591, 1975. → pages 163
- [191] A. S. Alexandrov and N. F. Mott. *Polarons and Bipolarons*. World Scientific, Singapore, 1995. → pages
- [192] A. S. Alexandrov. *Theory of Superconductivity: From Weak to Strong Coupling*. Institute of Physics Publishing, Bristol and Philadelphia, 2003. → pages
- [193] A. A. Ovchinnikov. Complexes of several spins in a linear heisenberg chain. *JETP Lett.*, 5:38, 1967. → pages 177
- [194] S. Pleutin. Excitonic strings in one-dimensional organic compounds. *Phys. Rev. B*, 61:4554, 2000. → pages 177
- [195] A. Kavokin. *Microcavities*. Oxford University Press, Oxford, UK, 2007. → pages 177
- [196] I. Carusotto and C. Ciuti. Quantum fluids of light. *Rev. Mod. Phys.*, 85:299, 2013. → pages 177
- [197] Pavlos L. Polariton condensates: Going soft. *Nature Mater.*, 13:227, 2014. → pages 177, 178
- [198] H. Deng, G. Weihs, D. Snoke, J. Bloch, and Y. Yamamoto. Polariton lasing vs. photon lasing in a semiconductor microcavity. *Proc. Natl Acad. Sci. USA*, 100:15318, 2003. → pages 178
- [199] D. G. Lidzey, D. D. C. Bradley, M. S. Skolnick, T. Virgili, S. Walker, and D. M. Whittaker. Strong excitonphoton coupling in an organic semiconductor microcavity. *Nature*, 395:53, 1998. → pages 178
- [200] J. D. Plumhof, T. Stöferle, L. Mai, U. Scherf, and R. F. Mahrt. Room-temperature boseeinstein condensation of cavity excitonpolaritons in a polymer. *Nature Mater.*, 13:247, 2014. → pages 178
- [201] K. S. Daskalakis, S. A. Maier, R. Murray, and S. Kéna-Cohen. Nonlinear interactions in an organic polariton condensate. *Nature Mater.*, 13:271, 2014. → pages 178

- [202] C. Ciuti, V. Savona, C. Piermarocchi, A. Quattropani, and P. Schwendimann. Role of the exchange of carriers in elastic excitonexciton scattering in quantum wells. *Phys. Rev. B*, 58:7926, 1998. → pages 178
- [203] F. Tassone and Y. Yamamoto. Exciton-exciton scattering dynamics in a semiconductor microcavity and stimulated scattering into polaritons. *Phys. Rev. B*, 59:10830–10842, 1999. → pages 178
- [204] H. Zoubi and G. C. La Rocca. Exciton-polariton kinematic interactions in organic microcavities. *Phys. Rev. B*, 72:125306, 2005. → pages 178
- [205] M. Litinskaya. Exciton polariton kinematic interaction in crystalline organic microcavities. *Phys. Rev. B*, 77:155325, 2008. → pages 178
- [206] E. R. Bittner and C. Silva. Estimating the conditions for polariton condensation in organic thin-film microcavities. *J. Chem. Phys.*, 136:034510, 2012. → pages 178
- [207] J. M. Raimond, M. Brune, and S. Haroche. Colloquium: Manipulating quantum entanglement with atoms and photons in a cavity. *Rev. Mod. Phys.*, 73:565, 2001. → pages 179
- [208] P. Cristofolini, G. Christmann, S. I. Tsintzos, G. Deligeorgis, G. Konstantinidis, P. G. Hatzopoulos, Z. Savvidis, and J. J. Baumberg. Coupling quantum tunneling with cavity photons. *Science*, 336:704, 2012. → pages 179
- [209] G. E. Astrakharchik, J. Boronat, I. L. Kurbakov, and Yu. E. Lozovik. Quantum phase transition in a two-dimensional system of dipoles. *Phys. Rev. Lett.*, 98:060405, 2007. → pages 179
- [210] J. Böning, A. Filinov, and M. Bonitz. Crystallization of an exciton superfluid. *Phys. Rev. B*, 84:075130, 2011. → pages 179
- [211] Ö. Eğecioğlu, C. K. Koc, and A. J. Laub. A recursive doubling algorithm for solution of tridiagonal systems on hypercube multiprocessors. *J. Comput. Appl. Math.*, 27:95, 1989. → pages 179
- [212] G. E. Blelloch. Prefix sums and their applications. Technical Report CMU-CS-90-190, School of Computer Science, Carnegie Mellon University, November 1990. → pages 181, 182
- [213] H. Nguyen. *Gpu Gems 3*. Addison-Wesley Professional, first edition, 2007. → pages 182